Stellenbosch University http://scholar.sun.ac.za

UNIVERSITEIT•STELLENBOSCH•UNIVERSITY
jou kennisvennoot • your knowledge partner

Probabilistic based evaluation of the structural reliability achieved for a typical building designed according to SANS 517:2009 and SANS 10162-2:2010

by

Frederik du Toit Oosthuizen

Thesis presented at the University of Stellenbosch in partial fulfilment of the requirements for the degree of

Master of Science in Structural Engineering

Department of Civil Engineering
University of Stellenbosch
Private Bag X1, 7602 Matieland, South Africa

Study leaders:

Prof. P.E. Dunaiski and Dr. C. Barnardo

December 2011

Stellenbosch University http://scholar.sun.ac.za

Copyright © 2011 University of Stellenbosch

All rights reserved.

Stellenbosch University http://scholar.sun.ac.za

DECLARATION

By submitting this thesis electronically, I declare that the entirety of the work contained therein is my own, original work, that I am the sole author thereof (save to the extent explicitly otherwise stated), that reproduction and publication thereof by Stellenbosch University will not infringe any third party rights and that I have not previously in its entirety or in part submitted it for obtaining any qualification.

Name: Frederik du Toit Oosthuizen

St.No: 14859890

Signed: .....

Date: 22 September 2011

Stellenbosch University http://scholar.sun.ac.za

Synopsis

This study aims to perform a quantitative probabilistic based evaluation of the reliability achieved in the design of Light Steel Frame Buildings (LSFB) when designed according to the loading code, SANS 517:2009 and the new design code for cold formed steel sections, SANS 10162-2:2010.

The evaluation was done as follows: A specific structure, chosen and designed according to the specifications given in SANS 517:2009, was modelled in a structural analysis program. From the analyses done it was possible to identify the most critical element for given failure modes. Spread sheets according to SANS 10162-2:2010 were developed to calculate the resistance or design values for the different failure modes.

By using a First Order Reliability Method (FORM), the reliability index for each failure mode could be calculated and evaluated in three different ways.

Firstly, the reliability margin implied by the design load was evaluated. It was assumed that the resistance of the profile had a deterministic value while the loads applied to the structure were taken as probabilistic, i.e. following their known distribution functions. From this evaluation it was found that the necessary level of reliability was achieved for all failure modes.

Secondly, the reliability margin implied by the resistance of the profile was evaluated. The resistance of the profile was taken as probabilistic with a distribution function that could be determined from the known distribution functions of the profile parameters responsible for the capacity of the profile. The loading was assumed to have a single deterministic value. From this evaluation it could be seen that a very low level of reliability was achieved for the failure modes of shear working in on the strong axis of the profile as well as interaction between bending and axial load. This is due to the strong dependence of this failure mode to the thickness of the profile, to which no partial factor is applied in the design process.

Thirdly, the reliability margin implied by both the resistance and loads was evaluated. In a real life situation both loads and resistances would have variability. The resistance and loading values were taken as probabilistic with their known distribution functions. From this evaluation it was

Stellenbosch University http://scholar.sun.ac.za

found that the necessary level of reliability was only achieved for shear working in on the weak-axis and axial load. All other failure modes achieved a level of reliability slightly lower than the target level of reliability for South Africa.

The stiffening effect of wall cladding elements were not taken into account in the analysis. The reliability of connections was also not evaluated.

It can be concluded that the element reliability achieved through the use of above-mentioned codes seems to be slightly less that desired. There could be an argument for recalibrating the partial factors to achieve the desired level of element reliability. However, the cladding elements provide significant additional stiffness to the structure and there is no immediate cause for stiffness concern. Future studies should aim to quantify the contribution that the cladding elements make to the overall structural reliability. The influence of connections reliability should also be investigated.

Stellenbosch University http://scholar.sun.ac.za

Oorsig

Die studie poog om ‘n kwantitatiewe probabilisties-gebaseerde beoordeling van die betroubaarheidsindeks vir Ligte Staalraam Strukture (LSS) te bepaal wanneer dit ontwerp word volgens die belastingskode, SANS 517:2009 en die nuwe ontwerpskode vir koudgevormde staal profiele, SANS 10162-2:2010.

Die beoordeling is as volg gedoen. ‘n Spesifieke strukturele model is gekies, ontwerp volgens die spesifiekasies in SANS 517:2009 en toe gemodelleer in ‘n struktuur analise program. Vanuit die analises was dit moontlik om die mees kritieke element te vind vir gegewe falings modusse. Sigblaaie, volgens SANS 10162-2:2010, is ontwikkel om die weerstand van die profile te bereken vir die falings modusse.

Dit was moontlik om die betroubaarheidsindeks op drie verskillende maniere te bereken deur gebruik te maak van ‘n Eerste Orde Betroubaarheids Metode (EOBM).

Eerstens is die betroubaarheids speling wat deur die belasting geimpliseer was, bepaal. Daar is aanvaar dat die weerstand van die profiel ‘n deterministiese waarde het terwyl die aangewende belasitng as probabilisties geneem is met hul bekende verdelingsfunksies. Uit hierdie beoordeling is gevind dat die nodige vlak van betroubaarheid bereik word vir alle falings modusse.

Tweedens is die betroubaarheids speling wat deur die weerstand geimpliseer was, bepaal. Daar is aanvaar dat die weerstand van die profile ‘n probabilistiese verdeling het wat bepaal is uit bekende verdelingsfunksies van die profiel parameters verantwoordelik vir die kapasiteit van die profiel. Daar is aanvaar dat die belasting ‘n enkele deterministiese waarde het. Uit hierdie beoordeling is gevind dat daar ‘n baie lae vlak van betroubaarheid is vir skuif in die rigting van die sterk as, asook interaksie tussen aksiaal-las en momente. Dit is te danke aan die falings modus se sterk afhanklikheid van die dikte van die profiel. Daar word egter geen parsiële factor aan die dikte toegeken in die ontwerp proses nie.

Derdens is die betroubaarheids speling wat deur beide die weerstand en belasting geimpliseer was, bepaal. In die werklikheid sal beide belasting en weerstand ‘n vlak van onsekerheid hê. Die weerstand en belasting is as probabilistiese waardes geneem met hul bekende

Stellenbosch University http://scholar.sun.ac.za

verdelingsfunksies. Uit hierdie beoordeling is gevind dat slegs die falings modus vir skuif in die rigting van die swak as en aksiaal-las die nodige vlak van betroubaarheid bereik. Al die ander modusse het steeds ‘n redelike hoë vlak van betroubaarheid. Dit is egter steeds laer as wat voorgeskryf word vir Suid-Afrika.

Die verstywings-effek van die bekleding is nie in hierdie ondersoek in ag geneem nie. Die betroubaarheid van die verbindings is ook nie bepaal nie.

‘n Gevolgtrekking kan dus gemaak word dat die element-betroubaarheid wat bereik word deur die bo-genoemde kodes effens laer is as die gewensde. ‘n Argument kan ontstaan vir die herkalibrasie van die parsiële faktore om die gewensde vlak van betroubaarheid te bereik, maar die bekleding bied ‘n noemenswaardige addisionele styfheid aan die struktuuur. Daar is dus geen onmiddellike kommer oor die styfheid van hierdie strukture nie. Verdere studies moet poog om die bydra van hierdie bekledingselemente tot die betroubaarheid van die struktuur te kwantifiseer. Die invloed van die konneksies tot die betroubaarheid van die struktuur sal ook ondersoek moet word.

Stellenbosch University http://scholar.sun.ac.za

LIST OF SYMBOLS AND ABBREVIATIONS

A_e = effective area

c = relation to skewness

c = shape parameter for Beta distribution

c_{pi} = internal pressure coefficient

C_{mx}, C_{my} = Coefficients for unequal end moments

c_r = roughness factor

c_a = aerodynamic shape factor

c_g = gust factor

c_d = dynamic factor

d = shape parameter for Beta distribution

DL = dead load

DSM = Direct Strength Method

$\mathbf{D}$ = vector for partial derivatives

E = demand of loading

EWM = Effective Width Method

f_n = critical stress

f_y = yield stress

f_{od} = elastic distortional buckling stress of the cross-section

$G(\mathbf{X})$ = performance function

g = auxiliary parameter for Beta distribution

JCSS = Joint Committee for Structural Safety

k = auxiliary parameter for Gamma distribution

LLF = live load on floor

LLR = live load on roof

LSFB = Light Steel Frame Buildings

Stellenbosch University http://scholar.sun.ac.za

L_{ex} = effective length in the x-direction

L_{ey} = effective length in the y-direction

L_{ez} = effective length in the z-direction

MC = Monte Carlo

M_c = critical moment

M_x^*, M_y^* = Applied moments about x- and y-axis respectively

M_{bx}, M_{by} = Nominal member moment capacity about the x- and y-axis respectively

m = sample mean

N_c = nominal member capacity of member in compression

N_s = nominal section capacity of member in compression

P_f = probability of failure

P_t = target value of failure

P(A) = probability of event A occurring

r_i = profile corner radius

R = resistance of structure

s^2 = sample variance

SLS = Serviceability Limit State

t = profile thickness

ULS = Ultimate Limit State

u' = adapted standardised variable

u_i^* = standardised design point

$v_{b.0}$ = basic characteristic wind speed

w = coefficient of variation for a population

WLW = Wind loads on walls

WLR = wind loads on roof

x_p = fractile value

x^* = design point of the performance function

Stellenbosch University http://scholar.sun.ac.za

X = actual variable in a sample

x_{mod} = mode for Gumbel distribution

α = coefficient of scewness

α_{nx}, α_{nx} = moment amplification factor

β = Reliability index

ε = kurtosis

μ = mean

σ = standard deviation

σ^2 = variance

$\phi(x)$ (also denoted as $\phi_X(x)$) = distribution function

$\varphi(x)$ = probability density function

λ = auxiliary parameter for Gamma distribution

$\Gamma(k)$ = gamma function of the parameter k

γ_m = material factor

γ_L = load factor

Stellenbosch University http://scholar.sun.ac.za

ACKNOWLEDGEMENTS

To be able to complete a thesis takes a lot of time, energy, perseverance, the ability to compile the findings, good research material and brilliant study leaders were needed.

First of all I would like to give thanks to my Heavenly Father for the ability to compile my findings in the form of a thesis.

Secondly I would like to thank people like Prof. Milan Holicky and Prof. Gregory Hancock for their excellent books that could be used as the foundation for my research. Barend Oosthuizen, thank you for your expert advice on Light Steel Frame Buildings in general.

Without the help and advice from my two study leaders, Prof P.E. Dunaiski and Dr C. Barnardo, this research would not be possible. Thank you for all the hours that we could spend together to ensure that the outcome of research is something that will be of great use in the future. It was an honour and privilege to have you as study leaders and mentors.

As we all know time is precious and one never knows when your time on earth has come to an end. I would like to esspecially thank Prof. Dunaiski who played an enormous role in this research, even in the last few months of his life. He was never to tired or sick to listen and to give advice. His kindness and silent strength will be missed by all. I therefore dedicate my written works to Prof. P.E Dunaiski. May you rest in peace.

Stellenbosch University http://scholar.sun.ac.za

CONTENTS

Stellenbosch University http://scholar.sun.ac.za

Stellenbosch University http://scholar.sun.ac.za

Stellenbosch University http://scholar.sun.ac.za

Stellenbosch University http://scholar.sun.ac.za

Stellenbosch University http://scholar.sun.ac.za

LIST OF FIGURES

Stellenbosch University http://scholar.sun.ac.za

Stellenbosch University http://scholar.sun.ac.za

Stellenbosch University http://scholar.sun.ac.za

Stellenbosch University http://scholar.sun.ac.za

LIST OF TABLES

Stellenbosch University http://scholar.sun.ac.za

Stellenbosch University http://scholar.sun.ac.za

1. Introduction

A new and exciting field in steel construction in South Africa has emerged. Very thin profiles of less than one millimetre in wall thickness are used in the construction of Light Steel Frame Buildings (LSFB). The main advantage of this construction method is that all the profiles for a specific structure can be manufactured and assembled in a factory and then be transported to the construction site. Furthermore it is much faster to erect a LSFB than the conventional brick and mortar or concrete building.

This type of building construction has been used in Australia and New Zealand with great success.

With the fast growing market for LSFB structures in South Africa it was necessary to develop a new loading code, SANS 517:2009, for these structures. However these profiles still need to be designed according to the cold formed steel design code, SANS 10162:2, in South Africa. It was therefore necessary to update and revise the old SANS 10162:2.

Seeing that the design programs and machines used to construct these profiles are developed in Australia and New Zealand it was decided to adopt the AS/NZ 4600:2005 design code as the new SANS 10162-2:2010 design code for South Africa. In practice LSFB are designed using computer software. It is safe to say that almost all of the LSFB in South Africa are designed by the SFS (Steel Frame Systems) or Frame Master programs. These programs use the AS/NZS 4600 to determine the profile sizes for a specific structure.

Looking at the South African loading code for cold formed steel sections (SANS 517:2009) and the Australian loading code it is clear that there are some differences in the loading conditions. With this in mind the question arises, is it possible to use the same design code for design of profiles and structural elements of LSFB in South Africa than used in Australia?

The research will therefore focus on a probabilistic based evaluation of the reliability index β of the South African loading code for cold formed steel sections, SANS 517:2009, and the new SANS 10162-2:2010.

Stellenbosch University http://scholar.sun.ac.za

2. LSFB in South Africa

2.1 Background

LSFB in South Africa are a fairly new concept. The aim is that 10% of the steel production in South Africa changes to LSFB in the near future. At the moment this has not yet been reached.

In general it is much easier to erect a LSFB in comparison to a conventional brick and mortar building. All the profiles are cut to the correct length in the factory and holes are punched where necessary. If the structure is small it is even possible to erect the structure in the factory and transport it as a whole to the site as shown in Figure 1. LSFB are therefore ideal not only in rural areas where materials can be hard to find, but anywhere where time is a factor.

(SASFA, 2010)

Figure 1: Easy transportation and erection of LSFB

2.2 Terminology and elements used in LSFB

In this section a look will be taken at the different terminologies that are used in LSFB as well as the general structural elements in a typical LSFB. The focus will only be on the steel in the

Stellenbosch University http://scholar.sun.ac.za

building and not on the foundations and wall members. The steel structure will consist of the following elements:

- Wall panels
- Floor joists
- Lintels
- Roof trusses
- Bracing
- Ceiling framework

The steel members will be C sections or lipped channels in most cases. It will be manufactured from high strength galvanised steel sheets. The typical steel elements in a steel framed house can be seen in Figure 2 and Figure 3.

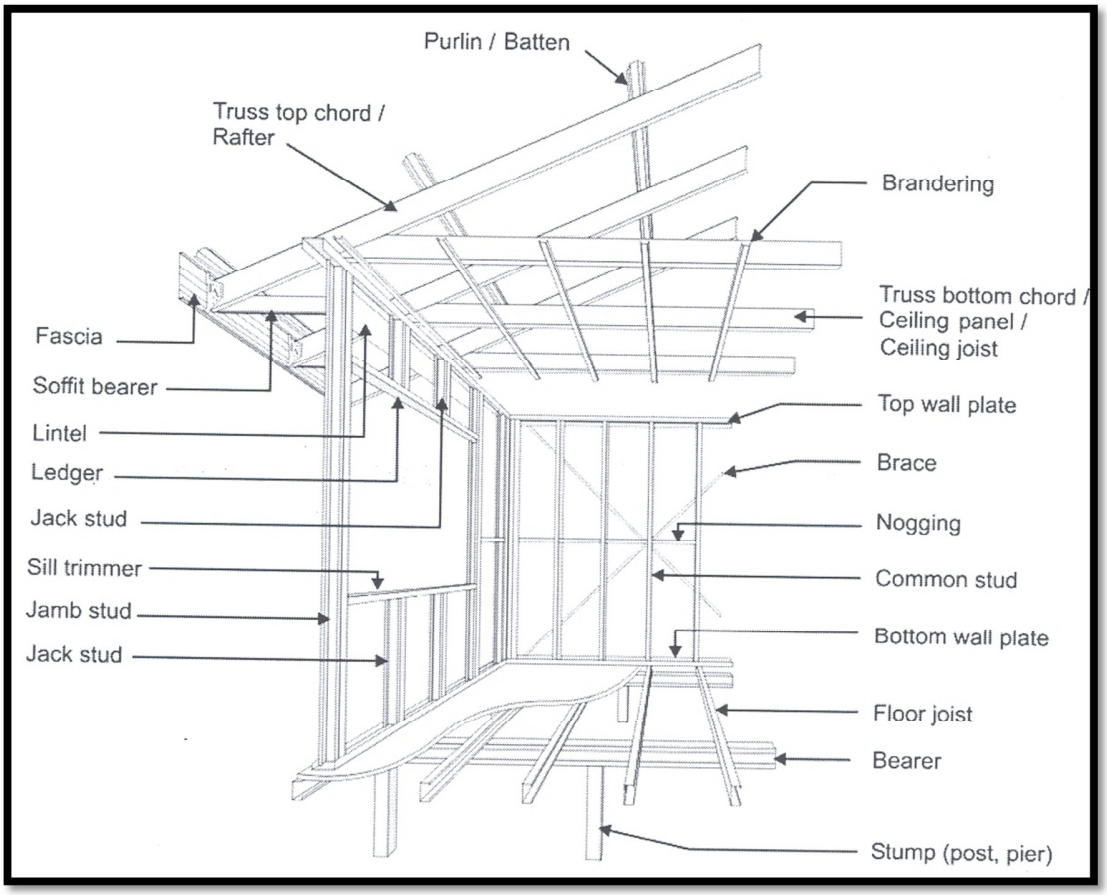

Figure 2: Typical elements of a steel framed house **(SASFA, 2010)**

Stellenbosch University http://scholar.sun.ac.za

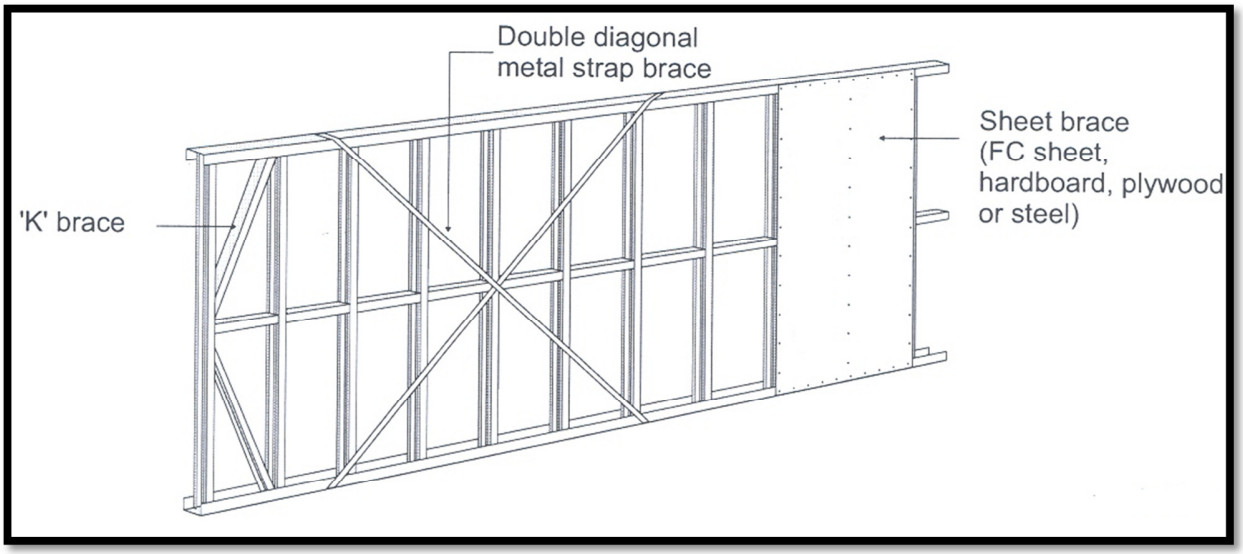

Figure 3: Bracing systems in a steel framed house **(SASFA, 2010)**

Bracing systems can also be present in the roofing structure as shown in Figure 4.

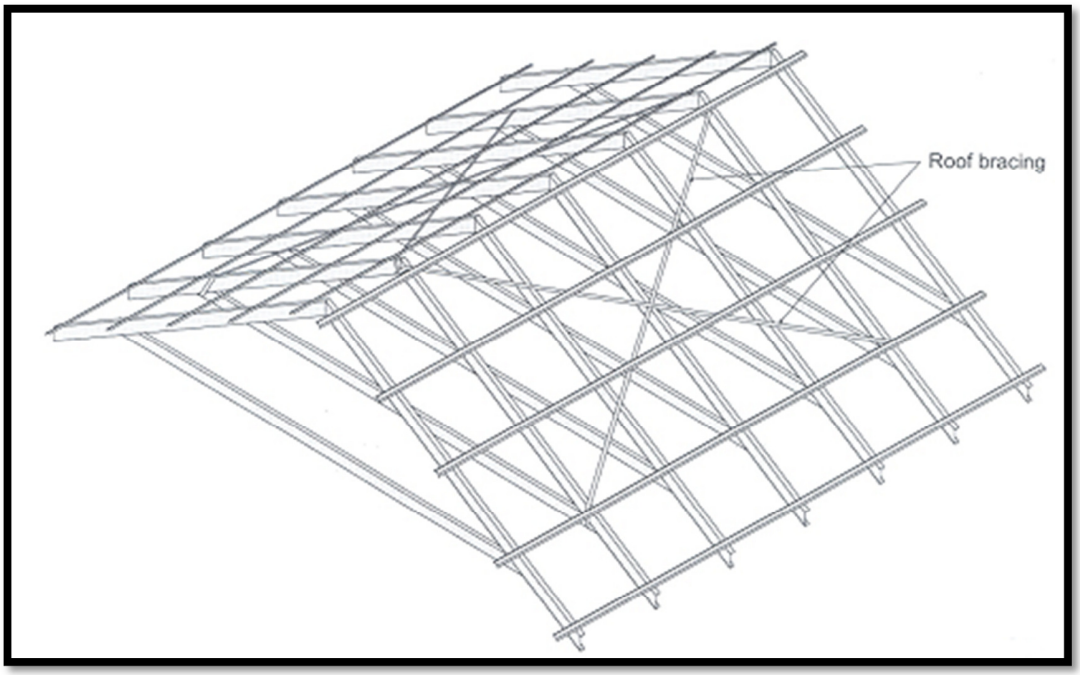

Figure 4: Bracing on roof structure **(SASFA, 2010)**

Furthermore, bearers will be in place in a typical LSFB. A typical layout can be seen in Figure 5.

Stellenbosch University http://scholar.sun.ac.za

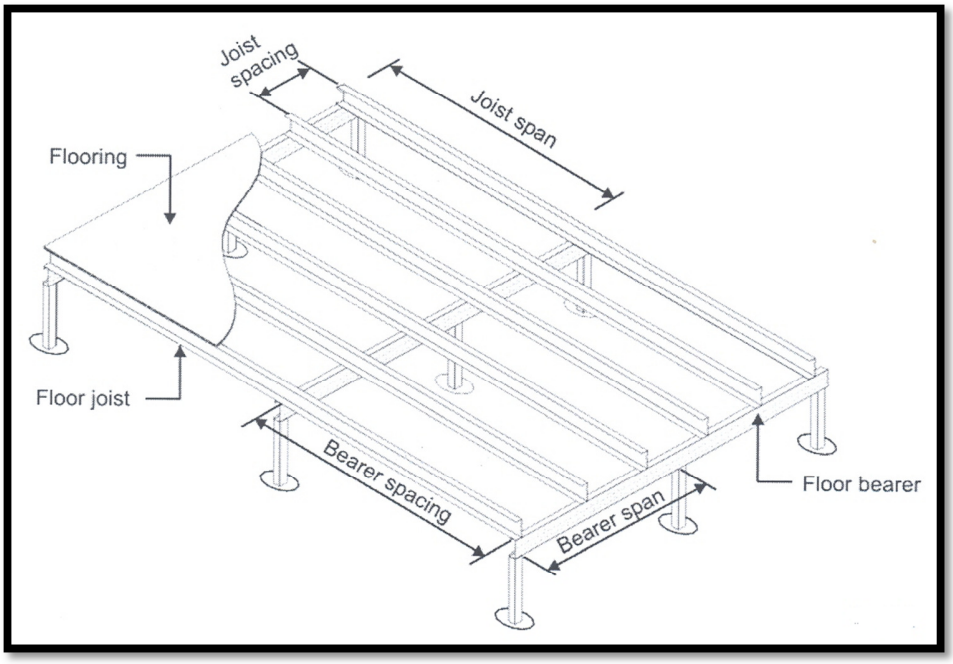

Figure 5: Typical layout of bearers in a LSFB **(SASFA, 2010)**

The typical elements present in suspended floors can be seen in Figure 6.

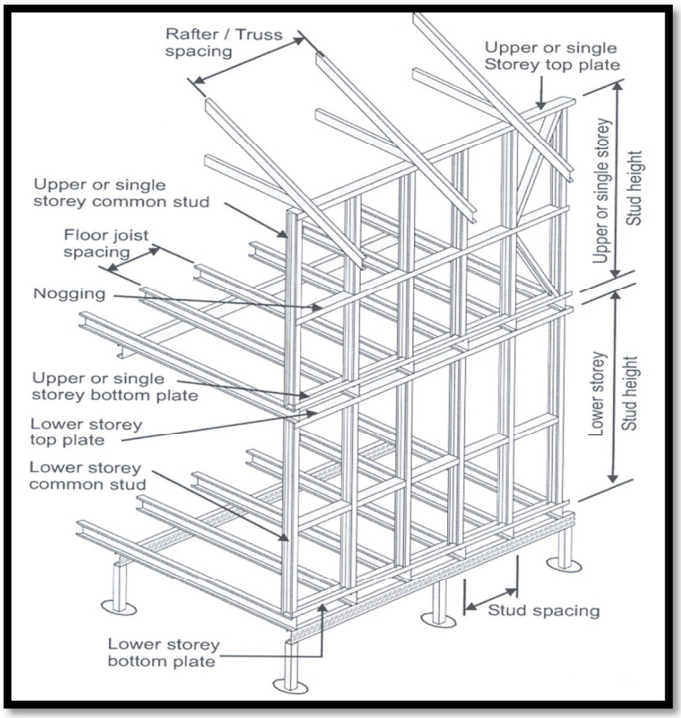

Figure 6: Typical elements in suspended floors **(SASFA, 2010)**

Stellenbosch University http://scholar.sun.ac.za

The element of importance in the roof structure is shown in Figure 7 and Figure 8.

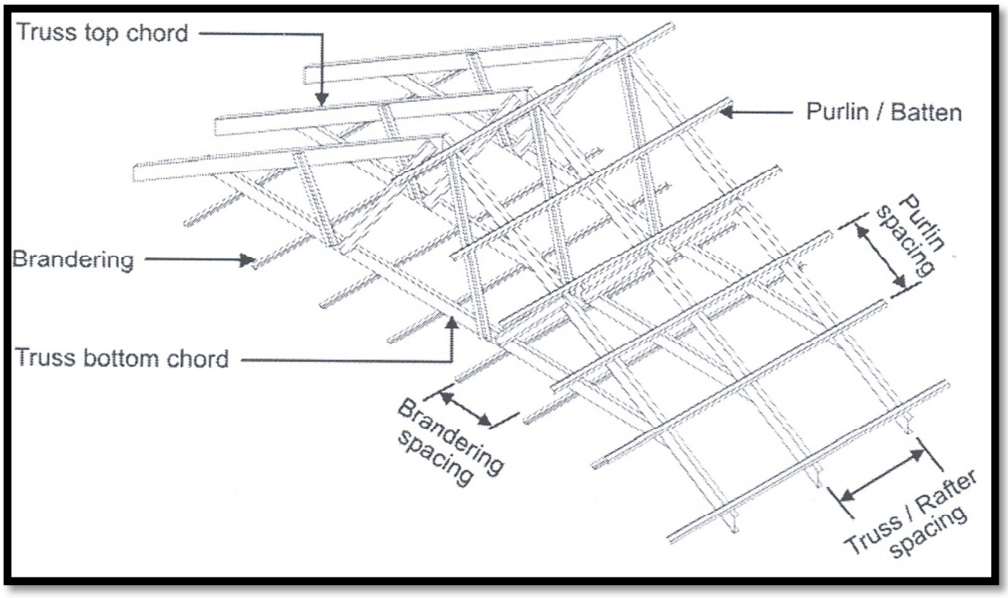

Figure 7: Typical roof elements **(SASFA, 2010)**

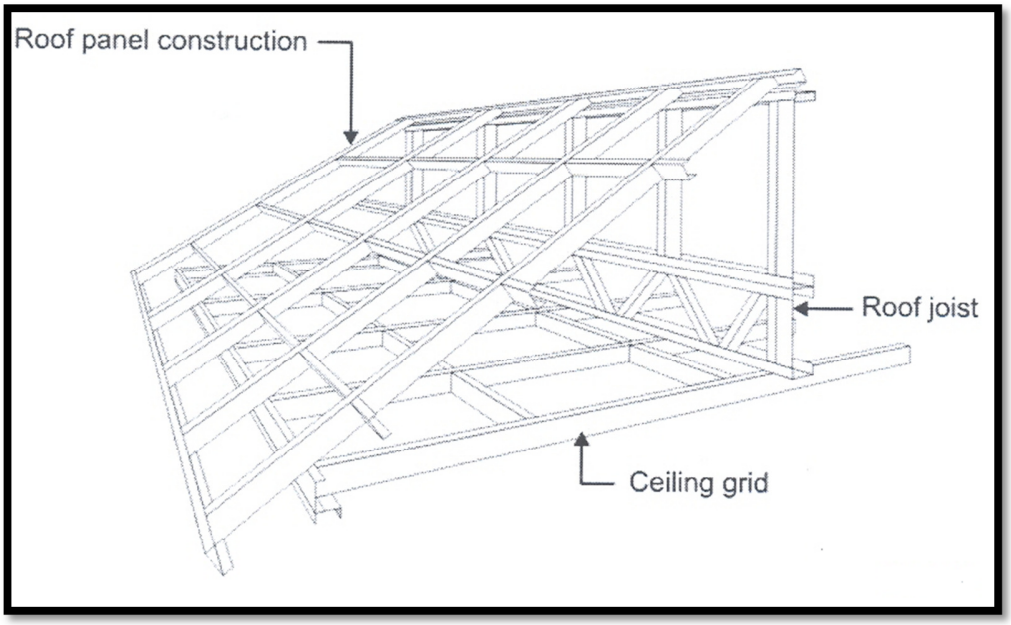

Figure 8: Typical roof elements **(SASFA, 2010)**

All steel used for the rolling of the profiles is galvanised steel sheets coated with zinc or aluminium–zinc. It has the following material properties:

Stellenbosch University http://scholar.sun.ac.za

- Yield strength: 300 – 550 MPa
- Elongation: 10 % min on a 50 mm tensile sample (SANS 0162:2, 1993)

2.3 General design procedures

The actions induced on LSFB will be applied according to SANS 517:2009. This code specifications focus on the actions induced on the structure. Appropriate load combinations for both ultimate limit state (ULS) and serviceability limit state (SLS) are given.

The member resistance calculations will be done in accordance to the new code, SANS 10162-2:2010 (SASFA, 2010)

According to SASFA, 2010, there are 4 golden rules in the design of LSFB:

1. A clear path must be discernable for every force from where it acts to where it meets the foundation
2. The importance of "in-line" construction, i.e. the wall studs on different floors must line up to ensure that forces are transferred to the foundation of the building
3. The roof, ceilings and floors are designed as bracing diaphragms. Walls are simply supported in between these diaphragms
4. Everything is tied down against wind uplift

In general, design procedures can be divided into three sub systems. These systems can then be designed separately (SASFA, 2010). The systems are divided as follows:

- Roofs
- Floors
- Walls

Each of these sub systems will be discussed in the following sections.

2.3.1 Roof members

In general the following roof members will require design:

- Purlins
- Trusses, rafters or panels
- Roof beams/ joists

Stellenbosch University http://scholar.sun.ac.za

- Ceiling panels or brandering

All these components will act as a unit to withstand the loads imposed on the roofing structure. It is important to know that under wind load the roof will provide lateral restraint to the top of the wall frames. This is referred to as diaphragm action. (SASFA, 2010)

There can be distinguished between the following roofing systems:

- Truss systems
- Panel systems
- Raftered systems

In this thesis a truss system will be used in the design of the structural model. The different truss systems and connections will be discussed in detail. A general overview of the other roofing systems will be given.

2.3.1.1 Truss Systems

A typical layout of a truss system can be seen in Figure 7 and in Figure 9. Figure 9 shows the different types of trusses used in LSFB.

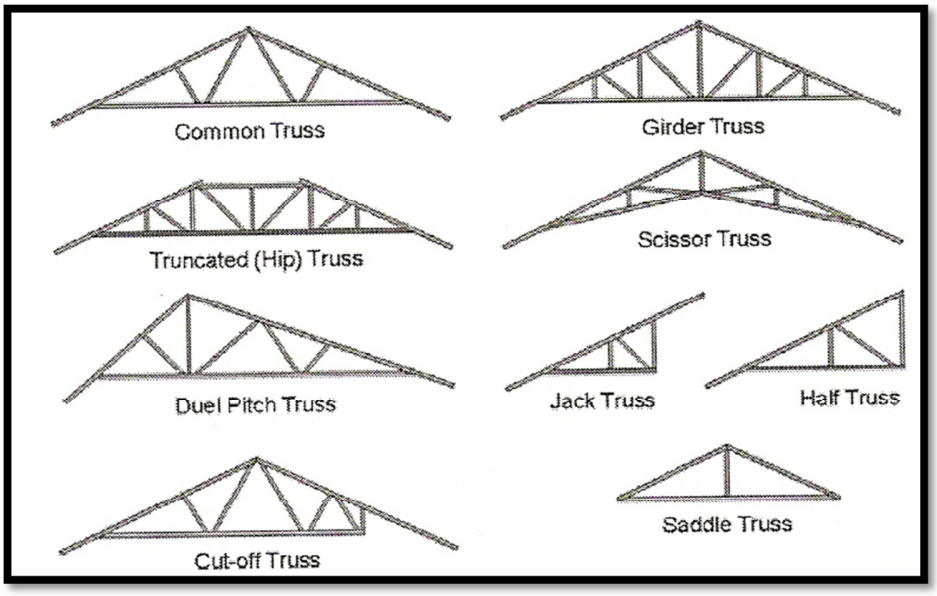

Figure 9: Different types of truss systems **(SASFA, 2010)**

For the design of the structural model a combination of a Common and Girder truss system will be used.

Stellenbosch University http://scholar.sun.ac.za

The typical connections used in a truss system are shown in Figure 10.

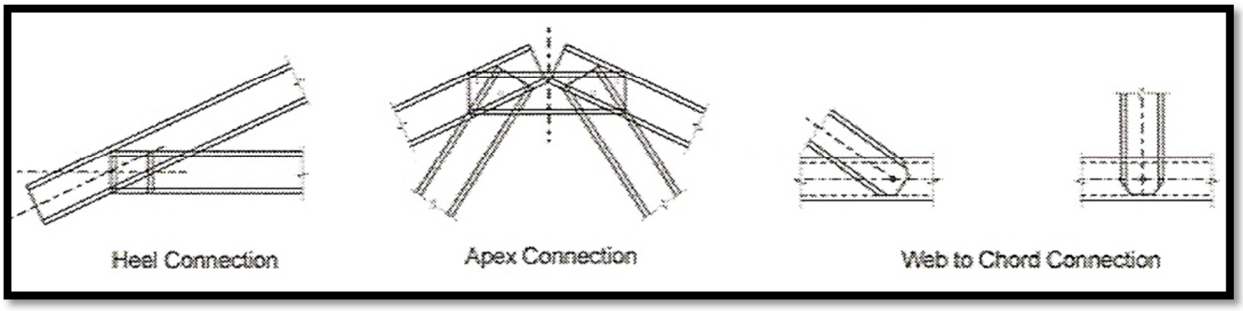

Figure 10: Typical connections in a truss system **(SASFA, 2010)**

The most critical connections will occur at the apex and heel of the truss. The connections between the top chord to the roofing sheets and the bottom chord to the ceiling are critical for restraining the top and bottom chords laterally. Most of the time 2 screws per connection will be sufficient. (SASFA, 2010)

In the case of a non-load bearing wall, the connections must restrain the wall laterally without transmitting vertical forces between the roof and wall. A typical connection between a truss and a non-load bearing wall can be seen in Figure 11.

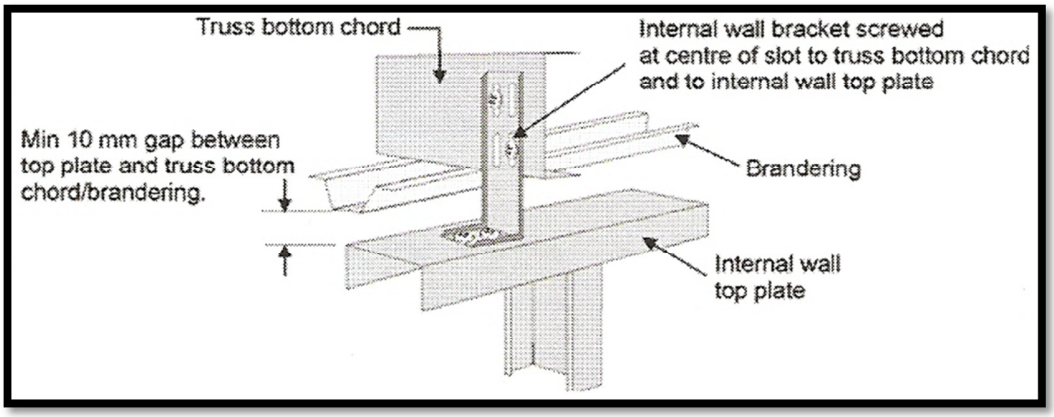

Figure 11: Non-load bearing connection **(SASFA, 2010)**

Stellenbosch University http://scholar.sun.ac.za

In the case of load bearing connections the following need to be taken into account:

- All vertical forces must be transmitted from roof to wall panels (including uplift forces)
- The connection must also be able to transmit all horizontal forces induced by wind loads
- In the case of wind loads the horizontal and vertical forces will act at the same time. The connection must therefore be capable of withstanding a combination of forces.

(SASFA, 2010)

A typical tie down connection can be seen in Figure 12.

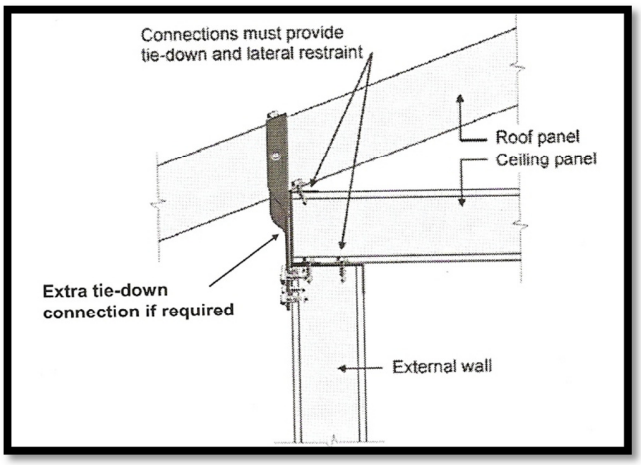

Figure 12: A typical tie down connection **(SASFA, 2010)**

2.3.1.2 Panel System

A presentation of a typical panel system is given in Figure 13.

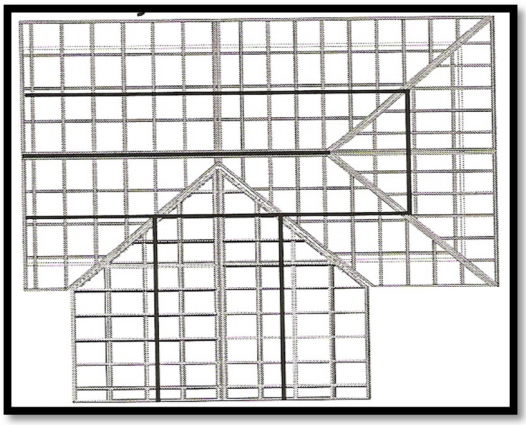

Figure 13: A typical panel system **(SASFA, 2010)**

Stellenbosch University http://scholar.sun.ac.za

2.3.1.3 Raftered System

Figure 14 shows a typical raftered system.

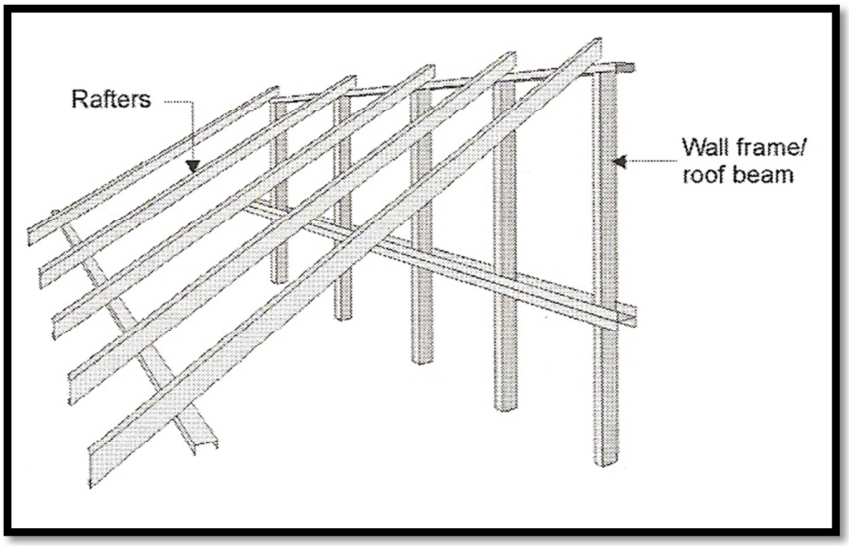

Figure 14: A typical raftered system **(SASFA, 2010)**

2.3.2 Wall elements

Typical wall elements as found in LSFB can be seen in Figure 15.

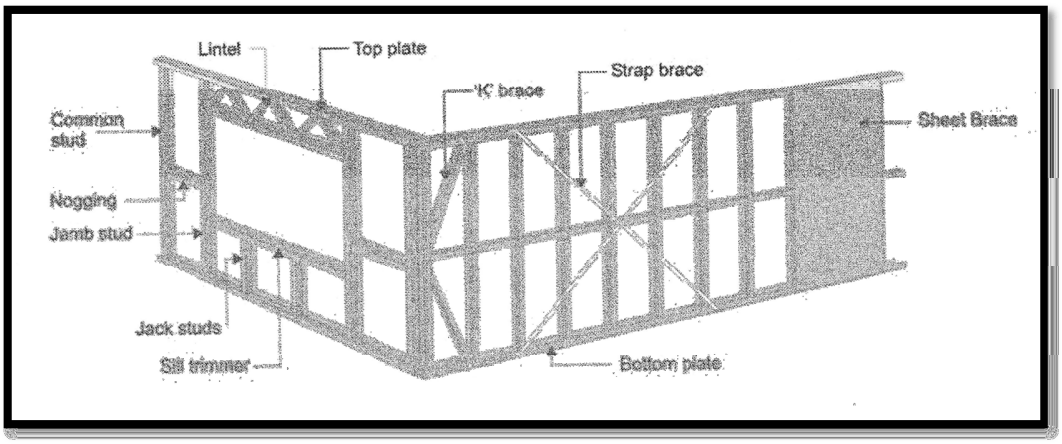

Figure 15: Wall elements used in LSFB. **(SASFA, 2010)**

Walls in a LSFB can be divided into load bearing or non-load bearing. Nogging as shown in Figure 15 will provide lateral support to the studs used. The maximum allowed stud spacing is 600 mm.

Stellenbosch University http://scholar.sun.ac.za

2.3.2.1 Load bearing wall studs

When looking at load bearing wall studs, the following loads must be resisted:

- Axial load by gravity and wind forces
- Strong-axis bending moment and shear caused by horizontal wind
- Additional axial force caused by the bracing system.

(SASFA, 2010)

2.3.2.2 Non-load bearing wall studs

In the case of non – load bearing wall studs, all strength and serviceability requirements are the same as those in the case for load bearing wall studs. It will however carry no gravitational load except its own weight. The top wall will be tied laterally, but in such a way that the connection does not transfer any vertical force from above. (SASFA, 2010)

2.3.2.3 Noggings

The purpose of a nogging is to:

- Provide lateral restraint to wall studs
- Provide fixing for cladding material
- It must be able to withstand an imposed load of 1 kN at midspan

(SASFA, 2010)

2.3.2.4 Lintels and wall plates

Wall plates are necessary where no in – line construction is used; this is to ensure that the vertical loads are transferred to the studs. Lintels are used over openings (doors, windows) to transfer vertical loads to jamb studs. The load bearing capacity of lintels is governed by connections. (SASFA, 2010)

Stellenbosch University http://scholar.sun.ac.za

2.3.3 Floor elements

Figure 16 shows the layout of typical floor elements in a LSFB.

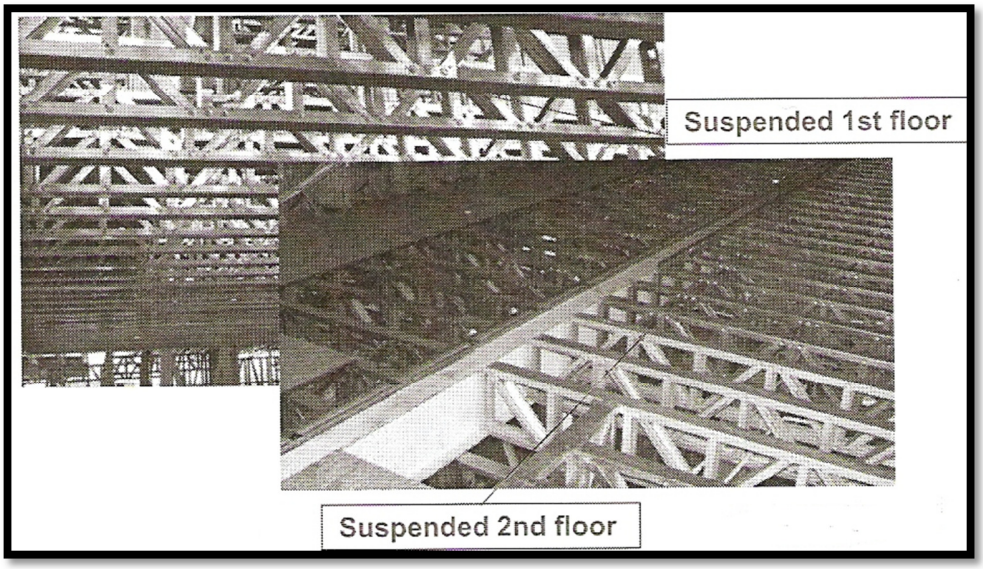

Figure 16: Suspended floor joists (SASFA, 2010)

In general slender floor joists have to be braced to prevent toppling or rolling over. There can be distinguished between two types of bracing as shown in Figure 17. Blocking or bridging will be used over supports and strapping for span (midspan) longer than 4 m.

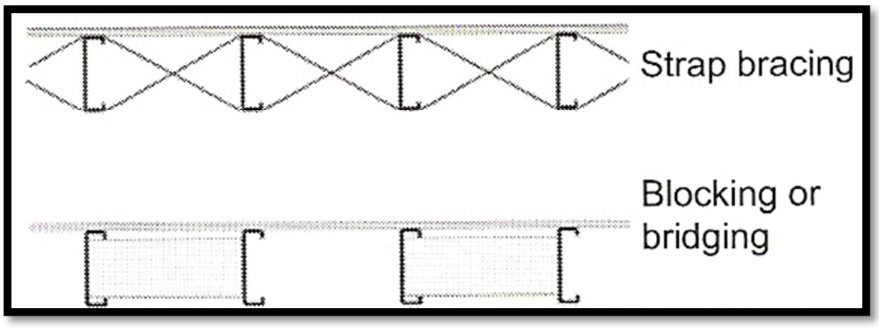

Figure 17: Types of bracing **(SASFA, 2010)**

Some other general design considerations that need to be taken into account are:

- Span over depth rule: depth ≥ span/12

Stellenbosch University http://scholar.sun.ac.za

- To reduce the force in the top and bottom cord, increase the depth
- In the case of a suspended floor, floor boards will provide lateral support to the top chord and the ceiling to the bottom chords
- The number of connections is in most cases the most critical design consideration

2.3.4 Bracing

For the chosen structural model only wall bracing will be required. A general overview of the types of wall bracing and their applications will be given. In general, wall bracing is required to transfer all horizontal loads from the roof, walls and floors to the appropriate floor and foundation.

Different types of wall bracing as shown in Figure 3 include:

- K-bracing
- Cross bracing
- Sheet bracing

The design of wall bracing must conform to the following:

- The forces will be determined according to SANS 517:2009
- Bracing must be provided in two orthogonal directions
- Braced panels must be effectively attached to the roof and floor structures to ensure diaphragm action

(SASFA, 2010)

2.4 General geometric limitations in LSFB

SANS 517:2009 provides certain geometric limitations for the design of LSFB. The main limitations can be seen in Figure 18.

Stellenbosch University http://scholar.sun.ac.za

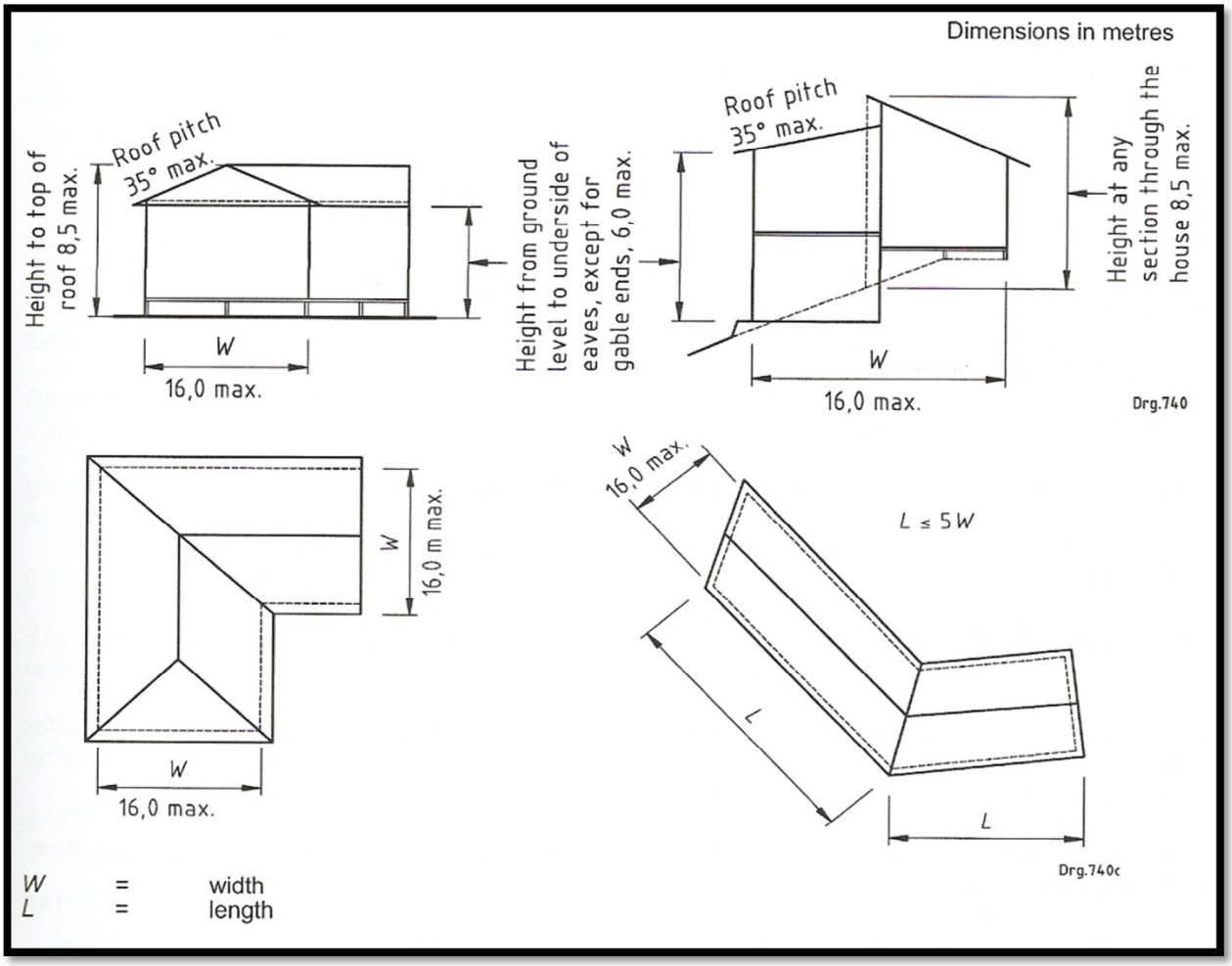

Figure 18: Geometric limitations on LSFB (SANS, 2009)

Stellenbosch University http://scholar.sun.ac.za

3. Design methods for cold – formed sections

The SANS 10162-2:2010 code is used in South Africa for the design of cold-formed steel sections. The code provides two design methods that can be used. These are the Effective Width Method (EWM), where the effective section properties need to be calculated, and the Direct Strength Method (DSM), (Schafer, 2006). The EWM can be seen as the conventional method that has been used for years. Dr. Bejamin Schafer of Johns Hopkins University was greatly involved in the development of the new DSM to calculate the capacity of cold formed steel sections. The DSM was formally adopted in the North American Design Specifications in 2004(AISI 2005) and in AS/NZS 4600:2005. Up to now this method has only been adopted in North America and Australia/New Zealand. DSM forms an alternative design method to the standard effective width method (EWM). The direct strength of a member will be calculated by using the elastic buckling solutions for the entire member cross section. The DSM provides two main advantages; firstly it provides a direct computation of capacity for complex shapes. Secondly it takes into account the interaction between local and overall modes. The elastic buckling stress is determined by using a computer aided numerical solution. (Cao Hung Pham, Gregory J Hancock, March 2009)

Software such as THIN-WALL and CSFUM can be used to calculate the elastic buckling stress. For this research CSFUM will be used.

The DSM will be used in conjunction with the EWM to determine the capacities of the profiles as obtained from the structural model. This will ensure that an accurate decision can be made about the capacity of a specific profile. A basic introduction into the EWM and DSM will be given. The aim of this section is therefore not to provide an extensive knowledge of the EWM or DSM.

3.1 The Effective Width Method (EWM)

The EWM is seen as the conventional design method used in SANS 10162-2:2010. The profiles used in cold formed steel design are class 4 members in axial load and bending. It is therefore necessary to calculate the effective area of these profiles. The basic idea of the EWM is therefore that local plate buckling leads to the reduction in the effective area of the plates that make up a profile. This reduction from the gross cross-sectional area to the effective cross-sectional area can be seen in Figure 19.

Stellenbosch University http://scholar.sun.ac.za

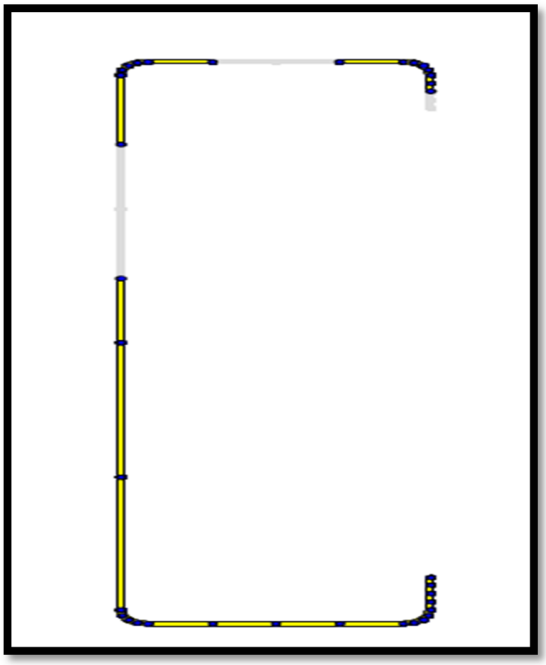

Figure 19: Reduction in cross-section due to local plate buckling **(Schafer, September 2006)**

Figure 19 represents a C-profile in bending. The area shown in yellow and dark blue is the effective cross-sectional area of the profile when subjected to a certain bending moment. Only the effective cross-sectional area can withstand a load. The ineffective areas shown in light blue can therefore not be used in the capacity calculation of the profile. Furthermore the neutral axis of the profile will shift due to local buckling and change in effective cross-sectional area. Obvious means are provided to incorporate local-global interaction where the reduced cross-sectional properties will influence global buckling. However, with the EWM the following occurs:

- Ignoring inter element equilibrium and compatibility in determining elastic buckling behaviour
- Cumbersome iterations to determine even the basic member strength.

The EWM is therefore a useful design method, but only for simple profiles. As soon as the profile gets more complicated it becomes more and more difficult to make use of the EWM. (Schafer, September 2006)

Stellenbosch University http://scholar.sun.ac.za

3.2 The Direct Strength Method (DSM)

As mentioned, the effective width or section of a profile is the fundamental concept behind the EWM. In the case of the DSM the accurate prediction of the member's elastic stability is the fundamental concept. The basic idea behind the DSM works as follows: the engineer determines all the elastic instabilities for the whole structural element such as local -, distortional-and overall buckling. Furthermore the load that causes the section to yield can be determined. It is then possible to determine the member capacity directly. (Schafer, September 2006)

A short explanation of each of the buckling modes that will occur will be explained below.

Local buckling: Mode of buckling involving plate flexure alone without transverse deformation of the lines of intersection of adjoining plates. This is the first buckling mode shown in Figure 20.

Distortional buckling: Mode of buckling involving change in the cross-sectional shape of a profile. This excludes local buckling. This is the second buckling mode shown in Figure 20.

Flexural/lateral torsional buckling: Mode which involves rigid body deformation of the cross section, without distortion (Schafer, October 2006). This is the final buckling mode shown in Figure 20.

The half-wavelength can be seen as the unsupported length of a profile where the certain buckling mode will occur.

Stellenbosch University http://scholar.sun.ac.za

For an applied moment M_y, the stress distribution in the profile will be as shown in red and blue below. All results are given in reference to this stress distribution

Relationship between the critical moment M_{cr} and yield moment M_y where a certain buckling mode will occur

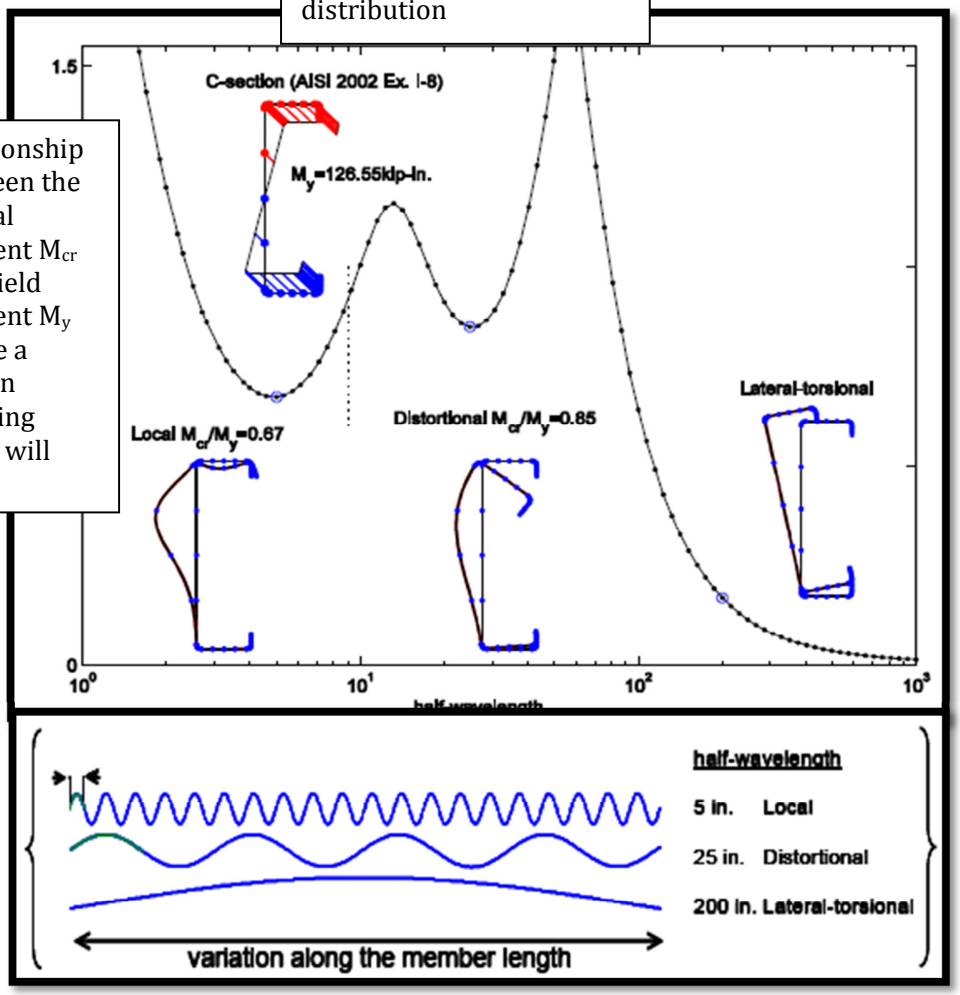

Different mode shapes are given. Each mode shape is crucial to DSM. In this section *local buckling* only involves rotation at internal folds i.e. plate flexure alone, *distortional buckling* involves rotation and translation of internal fold lines i.e. change in cross – sectional shape and *lateral torsional buckling* involves rigid body deformation of the cross section, without distortion

Half wave length shows how a cross – sectional mode shape varies along its length

Figure 20: Presentation of different failure modes **(Schafer, October 2006)**

3.2.1 Software to determine elastic instabilities – CSFUM

As discussed, the DSM uses the elastic buckling solutions on gross properties to determine member strength. To calculate all elastic buckling coefficients by hand will be almost impossible. This is made much easier with the aid of a computer program such as CSFUM. The program

Stellenbosch University http://scholar.sun.ac.za

makes use of the finite strip method. A thin walled member can be divided transversely into a number of strips using n nodal lines. It can then further be subdivided longitudinally into m sections. Each section knot will therefore have four degrees of freedom, corresponding to the two out-of-plane deformations, v and θ_z, and two in-plane displacements, u and w. (Lau & Hancock, 1986). This can be seen in Figure 21.

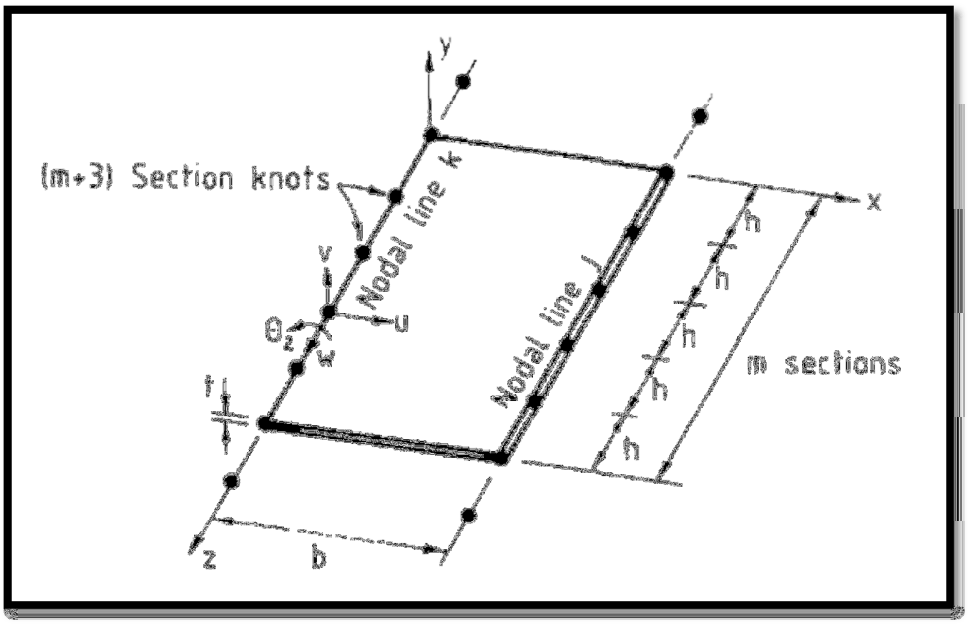

Figure 21: A spline strip (Lau & Hancock, 1986)

The finite strip method used here is therefore very similar to Finite Element Modelling (FEM). By integrating over the chosen fine strip it is possible for the program to determine all the buckling modes as shown in Figure 20. With the critical moments known for each buckling mode it is possible to determine the corresponding critical stress. A detailed description of the program and its user manual can be seen in Appendix A: User manual for the use of CSFUM.

Stellenbosch University http://scholar.sun.ac.za

4. Structural reliability

"The theory of structural reliability becomes a powerful tool when used for the development of new standards…."

"Recently revised national and international standards for structural design are systematically based on probabilistic concepts….." (Holicky, 2009)

This study aims to perform a quantitative probabilistic based evaluation of the reliability achieved in the design of Light Steel Frame Buildings (LSFB) when designed according to the loading code, SANS 517:2009 and the new design code for cold formed steel sections, SANS 10162-2:2010. This evaluation will be based on structural reliability. It is therefore of utmost importance that a thorough understanding of structural reliability is in place. This section will provide all the necessary information and explanations to ensure a good understanding of structural reliability.

4.1 Basic concepts

When a structure is designed, a deterministic design approach is normally followed. The deterministic design procedure is based on factorised characteristic values for the different loads, material properties and geometric parameters present in the specific structure.

However, in real life a certain statistical variability of load effects, material properties and geometry occurs. Furthermore other uncertainties such as the ability of the theoretical model to compare to the real behaviour of the structure must also be taken into account. It is possible to distinguish between statistical variability and uncertainties or unknowns.

The statistical variability can be expressed in terms of a certain cumulative distribution function with know statistical parameters. Certain other uncertainties and unknowns will also be present. There is no way to know how these uncertainties will influence the outcome of the design.

The following types of uncertainties can be identified:

- Vagueness due to performance requirements

Stellenbosch University http://scholar.sun.ac.za

- Errors in the design or operation of the structure
- Lack of knowledge into the behaviour of new materials

Some way must be found to incorporate these uncertainties and statistical variability into the design.

When performing a reliability analysis these uncertainties are explicitly accounted for. A reliability index β, which can be seen as the smallest number of standard deviations (that describe the system uncertainty) between the mean state of the system and a random failure event, can be calculated. This is then also directly related to the probability of failure of the system.

$$\beta = \Phi'(p_f) \quad (1)$$

therefore

$$p_f = \Phi(-\beta) \quad (2)$$

Holicky provides the following definition for reliability: "Reliability is the ability of a structure to comply with given requirements under specific conditions during the intended life for which it is designed". Furthermore it can be said that probability describes the occurrence of a random event. From a probabilistic point of design the probability of failure p_f does not exceed a specific target value of failure p_t.

$$p_f \leq p_t \quad (3)$$

The probability of failure p_f can be assessed by using a computational structural model. This model will be defined through basic quantities $\mathbf{X}[X_1, X_2, \ldots, X_n]$ for actions, mechanical properties and geometric data. The limit state of a structure can be defined by a performance function $g(\mathbf{X})$. For a safe structure, the limit state will be positive i.e.

$$g(\mathbf{X}) \geq 0 \quad (4)$$

Thus, for the ultimate limit state and serviceability limit state, p_f can be expressed as follows:

$$p_f = P\{g(\mathbf{X}) < 0\} \quad (5)$$

Stellenbosch University http://scholar.sun.ac.za

It is important to note that this simple procedure is only applicable if the quantities are not time dependent. A more complicated procedure will have to be followed if time dependent variables are taken into account.

In the Eurocode, EN1990, three different structural classes are given with different target levels of reliability associated to each of them. These classes can be defined as follows:

Class 3: High consequence for the loss of human life or the social, environmental and economical consequences are very high. The target level of reliability for this structural class is given as $\beta_t = 4.3$

Class 2: Medium consequence for the loss of human life with a considerable social, environmental and economical consequence. The target level of reliability for this structural class is given as $\beta_t = 3.8$

Class 1: Low consequence for the loss of human life with negligible social, environmental and economical consequences. The target level of reliability for this structural class is given as $\beta_t = 3.3$

In general, class 2 reliability is considered for residential and office buildings.

(Holicky, 2009)

In South Africa four structural classes can be found. For class 2, which corresponds to EC1990's class 2(residential and office buildings up to 4 storeys high), $\beta_t = 3$ is assigned. This corresponds to a target probability of failure of $p_f \approx 10^{-4}$

4.2 Probabilistic models of random variables

In this section a description of the most important probabilistic models of random variables used in structural reliability will be given.

4.2.1 Random variable

According to Holicky a random variable is defined as a variable that attains one and only one value x, which is unknown in advance when a certain set of conditions is released. Furthermore it

Stellenbosch University http://scholar.sun.ac.za

can be set that a random variable is an indicator of random events caused by specific experiments. (Holicky, 2009)

There can be differentiated between discrete (distinct values within a given interval) and continuous (any value within a given interval) random variables. In general continuous random variables are more often used in structural reliability than discrete random variables.

A population can be described as the totality of all the possible x values for the considered random variable X. The totality will be described by a distribution of probabilities i.e. by a function that determines the probability X contains a specific value x.

The cumulative distribution function $\Phi(x)$ will give each x value a probability that the random variable X will be smaller or equal to x.

$$\Phi(x) = P(X \leq x) \qquad 6$$

By getting the derivative of the cumulative distribution function it is possible to determine the probability density function $\varphi(x)$ for a continuous random variable.

$$\varphi(x) = \frac{d\Phi(x)}{dx} \qquad 7$$

The relationship between the probability density function and the cumulative distribution function for a specific interval between a and b with a continuous random variable X can be seen in Figure 22.

Stellenbosch University http://scholar.sun.ac.za

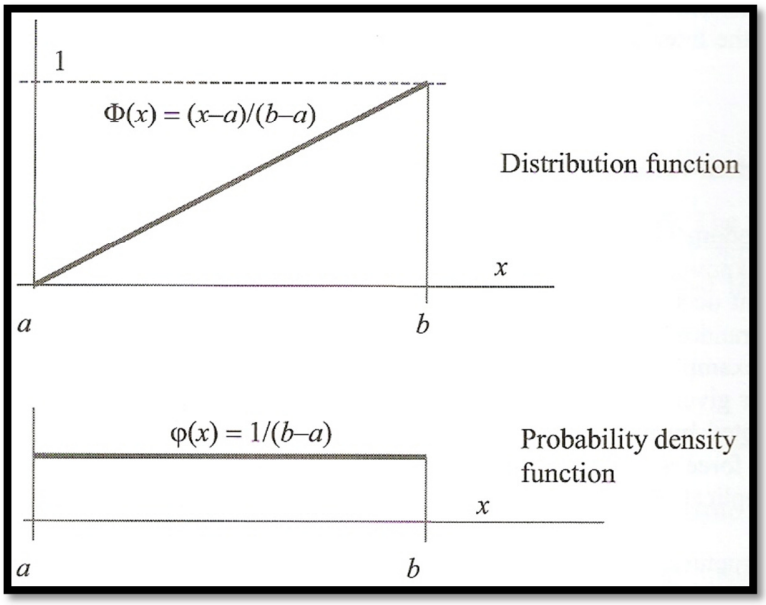

Figure 22: Probability density and distribution function for a uniform distribution **(Holicky, 2009)**

It is important to note that the integral of the probability density function within the chosen domain equals 1, thus:

$$\int_a^b \varphi(x)dx = 1 \qquad 8$$

This means that the sum of the probability for all possible values in a chosen domain will be equal to 1.

Various other parameters may be used to describe the random variable X. Moment parameters are the most frequent used. The fundamental moment parameter, the mean for a specific population can be described by the following equation:

$$\mu = \int x\varphi(x)dx \qquad 9$$

For a random variable X it is possible to measure the dispersion relative to the mean μ. The dispersion is given by the moment of second order. This is called the variance σ^2 where

$$\sigma^2 = \int(x-\mu)^2\varphi(x)dx \qquad 10$$

The square root of the variance denotes the standard deviation σ.

The coefficient of skewness is defined by getting the central moment to the third order

$$\alpha = \frac{1}{\sigma^3}\int(x-\mu)^3\varphi(x)dx \qquad 11$$

Stellenbosch University http://scholar.sun.ac.za

Furthermore it is possible to give definition to the concentration of values around the mean. This is called the kurtosis and is defined on the basis of the central moment of the fourth order

$$\varepsilon = \frac{1}{\sigma^4}\int (x-\mu)^3 \varphi(x) dx \; - 3 \qquad 12$$

An illustration of a Log – Normal distribution with a mean $\mu = 1$, a standard deviation $\sigma = 0.2$ and a skewness of 1 can be seen in Figure 23.

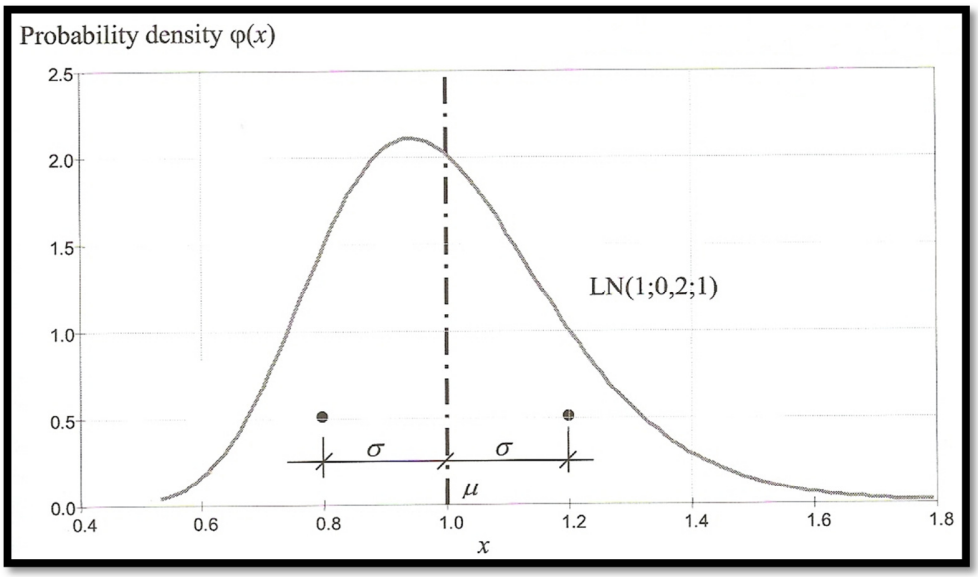

Figure 23: Illustration of a Log-Normal distribution with $\mu = 1$, $\sigma = 0.2$ and skewness $= 1$ (Holicky, 2009)

A dimensionless parameter is introduced to measure the relative dispersion. This parameter is called the coefficient of variation and can be defined as follows:

$$\text{COV} = \frac{\sigma}{\mu} \qquad 13$$

It is important to note that the standard deviation should be used as a measure of dispersion in the cases where the mean is close to zero. Typical values for the coefficient of variance will be between 0.03 – 0.3 for common material properties. For actions it could be anything from 0.05 – 1.

(Holicky, 2009)

Stellenbosch University http://scholar.sun.ac.za

4.2.2 Sample characteristics

A sample is obtained by executing the same test with specific conditions for a number of n times. In general there can be distinguished between three sample sizes: a very small sample ($n \leq 10$), a small sample ($10 \leq n \leq 30$) and a large sample ($n > 30$).

In any sample taken there will be some data that can be seen as outliers i.e. extreme and inaccurate values. An easy way to spot outliers is by setting up a histogram. It is therefore important to find a way to be able to spot these outliers and neglect them from the calculations.

With the corrected sample it is then possible to calculate accurate parameters as discussed in the previous section. For a specific sample of size n, these parameters can be calculated as follows:

Sample mean:

$$m = \frac{1}{n}\sum_i x_i \qquad 14$$

with $i = 1, 2 \ldots n$

Sample variance:

$$s^2 = \frac{1}{1-n}\sum_i (x_i - m)^2 \qquad 15$$

Sample skewness:

$$\propto = \frac{n}{(n-1)(n-2)s^3}\sum_i (x_i - m)^3 \qquad 16$$

The square root of the sample variance i.e. $\sqrt{s^2} = s$ denotes the sample standard deviation.

The sample coefficient of variation can be expressed as follows:

$$v = \frac{s}{m} \qquad 17$$

The sample parameters are unbiased point estimators for the population parameters.

(Holicky, 2009)

Stellenbosch University http://scholar.sun.ac.za

4.2.3 The Normal distribution

The normal distribution is the most important distribution for a continuous random variable. It is frequently found in structural reliability to describe loads such as self-weight, mechanical properties and geometric properties. A normal distribution will be symmetrical with an interval from $-\infty < x < \infty$. The distribution has a skewness of zero and is therefore only dependent on two parameters: the mean μ and the standard deviation σ.

The probability density function for a normal random variable, with μ_x and σ_x, is given by the following equation:

$$\varphi(x) = \frac{1}{\sigma_x\sqrt{2\pi}} e^{\left[-\frac{1}{2}\left(\frac{x-\mu_x}{\sigma_x}\right)^2\right]} \quad 18$$

No analytical formula is available for the cumulative distribution function $\Phi(x)$. Numerical tables are available for the probability density functions as well as for the distribution function. These tables give a probability density function $\varphi(u)$ and a cumulative distribution function $\Phi(u)$ where U is the standardised variable derived from the following equation:

$$U = \frac{X-\mu_x}{\sigma_x} \quad 19$$

The mean and standard deviation used in equation 19 will still be the actual values obtained from the variable X.

By substituting equation 19 into 18 it is possible to find the expression for the probability density function of the standardised random variable U.

$$\varphi(u) = \frac{1}{\sqrt{2\pi}} e^{\left(-\frac{u^2}{2}\right)} \quad 20$$

(Holicky, 2009)

4.2.4 The Log-normal distribution

A log-normal distribution differs from a normal distribution in the way that it is defined on intervals from either $x_0 < x < \infty$ or from $-\infty < x < x_0$. It will have a skewness α_x which means that a log-normal distribution will be an asymmetric distribution. Furthermore it entails that there will be three significant parameters in a log-normal distribution. These parameters are the mean

Stellenbosch University http://scholar.sun.ac.za

μ_x, the standard deviation σ_x and the skewness α_x. When the skewness is unknown, the upper or lower bounds of x_0 can be used.

A random variable X will have a log-normal distribution if the transformed random variable $Y = \ln|X - x_0|$ has a normal distribution. The lower or upper bound can be expressed as

$$x_0 = \mu_x - \frac{\sigma_x}{c} \qquad 21$$

Where c is a relation to the skewness α_x that can be presented by the following expression:

$$\alpha_x = c^3 + 3c \qquad 22$$

From equation 22 it is then possible to get an explicit relation for c as shown

$$c = \left[\left(\sqrt{\alpha_x{}^2 + 4} + \alpha_x\right)^{\frac{1}{3}} - \left(\sqrt{\alpha_x{}^2 + 4} - \alpha_x\right)^{\frac{1}{3}}\right] 2^{\frac{-1}{3}} \qquad 23$$

It is possible to obtain expressions for the probability density function and the cumulative distribution function by using an adapted standardised variable u'. This value can be obtained from the standardised random variable U as shown in the following expression:

$$u' = \frac{\ln\left(\left|u+\frac{1}{c}\right|\right)+\ln\left(|c|\sqrt{1+c^2}\right)}{\sqrt{\ln(1+c^2)}}\ \mathrm{sign}(\alpha_x) \qquad 24$$

The probability density function $\varphi_{LN,U}(u)$ and the distribution function $\Phi_{LN,U}(u) = \Phi_{LN,X}(x)$ for the log-normal distribution is as shown by the following expression:

$$\varphi_{LN,U}(u) = \frac{\varphi(u')}{\left(|u+\frac{1}{c}|\right)\sqrt{\ln(1+c^2)}} \qquad 25$$

$$\Phi_{LN,U}(u) = \Phi_{LN,X}(x) = \Phi(u') \qquad 26$$

The probability density function and the cumulative distribution function of the standardised function will be denoted by $\varphi(u')$ and $\Phi(u')$ respectively.

A very popular log-normal distribution is when it is possible to have the lower bound at zero. This means that the distribution will only be dependent on two variables – the mean μ_x and the standard deviation σ_x. If this is the case it can be seen that the coefficient of variation w_x will be equal to the coefficient c. With this in mind it is possible to find the following expression for the skewness α_x.

$$\alpha_x = 3w_x + w_x^3 \qquad 27$$

Stellenbosch University http://scholar.sun.ac.za

From equation 27 it can be seen that a log-normal distribution with a lower bound a zero will always have a positive skewness with a relative high value of above 0.5 typically. It is important to note that a log-normal distribution with a lower bound at zero can lead to unrealistic theoretical models, seeing that it will influence the occurrence of deviations from the mean. A comparison between the normal and 2 parameter log-normal distribution can be seen in Figure 24.

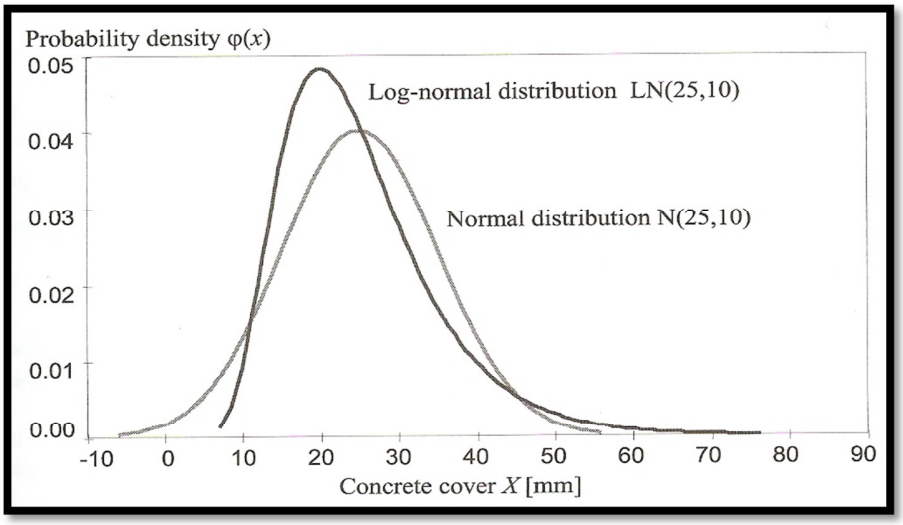

Figure 24: Comparison between normal and 2 parameter Log-normal distribution for concrete cover (Holicky, 2009)

The log-normal distribution is widely used in structural reliability. This is due to the fact that this distribution can be used for one-sided limited asymmetric random variables. These variables include actions, material properties and geometric data.

(Holicky, 2009)

4.2.5 The Gamma distribution

Like the log-normal distribution, the Pearson's distribution of type III is a one-sided limited distribution. The gamma distribution is a special case of the Pearson's distribution with its lower bound set at zero. The probability density function will therefore be dependent on only two parameters, the mean μ and the standard deviation σ. The expression for the probability density

Stellenbosch University http://scholar.sun.ac.za

function will get very complicated if it should be given in terms of μ and σ. Two additional parameters will be introduced to simplify the expression:

$$\varphi(x) = \frac{\lambda^k x^{k-1} \exp(-\lambda x)}{\Gamma(k)} \qquad 28$$

where:

$$\lambda = \frac{\mu}{\sigma^2} \text{ and } k = \left(\frac{\mu}{\sigma}\right)^2$$

The gamma function Γ is in terms of the parameter k. From equation 28 it is possible to obtain the moment parameters of the gamma distribution as shown below

$$\mu = \frac{k}{\lambda}, \sigma = \frac{\sqrt{k}}{\lambda}, \alpha = \frac{2}{\sqrt{k}} = \frac{2\sigma}{\mu} = 2w, \varepsilon = \frac{3\alpha^2}{2} \qquad 29$$

The shape of the bell curve for the gamma distribution will be influenced by the value of k. If $k < 1$, the skewness will be $\alpha < 2$. When $k \to \infty$, the gamma distribution will act as a normal distribution with parameters μ and σ, the question can arise, what is the difference between the gamma distribution and the 2 parameter log-normal distribution? The difference is that the skewness of the gamma distribution will be equal to $\alpha = 2w$. As can be seen, this is noticeably lower than the skewness for the log – normal distribution ($\alpha_x = 3w_x + w_x^3$). For a variable that does not have a great skewness, it will be more convenient to use the gamma distribution. This is the case for some geometric quantities.

A summary of the probability density functions for all the distributions as described above can be seen in Figure 25.

Stellenbosch University http://scholar.sun.ac.za

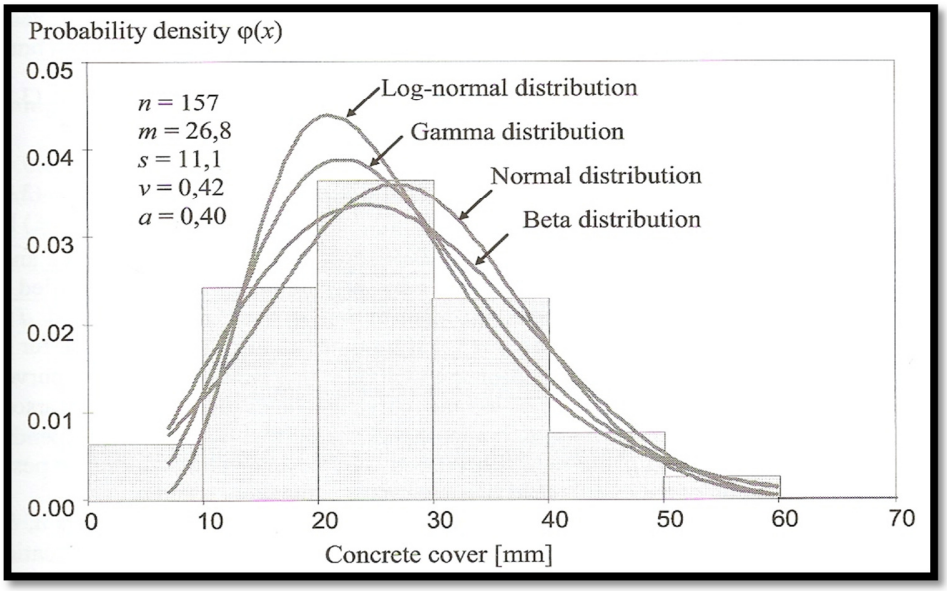

Figure 25: Histogram and different distribution functions for concrete cover (Holicky, 2009)

It is often a very complex task to determine which theoretical model to use for a specific property. Some practical guidelines will be provided at a later stage of this thesis.

(Holicky, 2009)

4.2.6 The Beta distribution

Like the gamma distribution, the beta distribution forms part of the Pearson's distribution. The beta distribution is therefore also called the Pearson's distribution of type I. The beta distribution depends on four parameters. In general it is used in the cases where the field of the random variable is limited. The beta distribution is difficult to use because the user has to estimate the four parameters, which is not always possible.

The general expression for the beta distribution can be written as follows:

$$\varphi(x) = \frac{(x-a)^{c-1}(x-b)^{d-1}}{B(c,d)(b-a)^{c+d-1}} \qquad 30$$

c and d can be defined as shape parameter. The lower and upper bound are given as

$$a = \mu - cg\sigma\,,\ b = \mu + dg\sigma\,,\ g = \sqrt{\frac{c+d+1}{cd}} \qquad 31$$

32

Stellenbosch University http://scholar.sun.ac.za

Parameter g can be said to be an auxiliary parameter. From equation 31 it is possible to derive expressions for c and d

$$c = \frac{\mu - a}{b - a}\left(\frac{(\mu - a)(b - \mu)}{\sigma^2} - 1\right) \text{ and } d = \frac{b - \mu}{b - a}\left(\frac{(\mu - a)(b - \mu)}{\sigma^2} - 1\right) \quad 32$$

For the beta distribution it is possible to write an expression for the moment parameters in term of a, b, c and d as shown below

$$\mu = \frac{a + (b - a)c}{(c + d)} \text{ and } \sigma = \frac{(b - a)}{(cg + dg)} \quad 33$$

furthermore:

$$\propto = \frac{2g(d - c)}{(c + d + 2)} \text{ and } \varepsilon = \frac{3g^2(2(c + d))^2 + cd(c + d - 6))}{(c + d + 2)(c + d + 3)} - 3 \quad 34$$

From the equations above it is possible to see that for the beta distribution, the skewness and kurtosis will only be dependent on the parameters c and d. (Holicky, 2009)

4.2.7 The Gumbel and other distributions of extreme values

The maximum and minimum values in a specific population are referred to as extreme values. These values and their distributions are of great importance in structural reliability. It is important to note that all these distributions will have two versions, the one version being the distribution of the minimal values and the other for the maximal values. These distributions will follow an exponential shape. The Gumbel (also referred to as the extreme values distribution of type 1) will be described below.

The cumulative distribution function of the Gumbel distribution can be expressed by the following equation:

$$\Phi(x) = \exp(-\exp(-c(x - x_{mod}))) \quad 35$$

The cumulative distribution function will depend on two parameters: the mode x_{mod} and the parameter c, where $c > 0$.

The density function can be expressed by the following equation:

$$\varphi(x) = c \exp(-c(x - x_{mod}) - \exp(-c(x - x_{mod}))) \quad 36$$

Stellenbosch University http://scholar.sun.ac.za

The parameters c and x_{mod} can be calculated by using the expressions:

$$x_{mod} = \mu - 0.577\sigma\frac{\sqrt{6}}{\pi} \quad 37$$

$$c = \frac{\pi}{\sigma\sqrt{6}} \quad 38$$

For the Gumbel distribution, the skewness and kurtosis will be constant values of 1.14 and 2.4 respectively.

The cumulative distribution function $\Phi(x)$ of an original random variable, with a mean μ and standard deviation σ, can easily be transformed to a cumulative distribution function $\Phi_N(x)$ for a population that is N times bigger than the original population. This feature is shown below.

$$\Phi_N(x) = (\Phi(x))^N \quad 39$$

It can be seen as one of the greatest advantages of the Gumbel distribution, because it allows easy transformation of the distribution of extreme value events to describe different return periods.

(Holicky, 2009)

4.2.8 Multivariate random variables

Sometimes it happens that two variables have to be investigated at the same time or for the same entity. Every time a new random event is realised and given that variable X takes on a specific value x and that variable Y takes on a specific value y, it can be said that X and Y will form a pair of joint random variables. An example of such a pair of joint random variables could be when the ductility and displacement is studied of a certain steel element under a specific load. It is possible to investigate more than two variables. This will be denoted as a vector **X** $[X_1, X_2 \ldots X_n]$. The realizations will be given as a vector **x** $[x_1, x_2 \ldots x_n]$.

All the possible outcomes of the realizations x and y of a pair of joint random variables X and Y are called the two-dimensional population. A two-dimensional random variable will therefore be the pair of random joint variables X and Y.

The two-dimensional cumulative distribution function can be written as $\Phi(x,y)$.

The cumulative distribution function shows the probability that the random variable X is less than or equal to x and the probability that random variable Y will be less than or equal to y, i.e.

Stellenbosch University http://scholar.sun.ac.za

$$\Phi(x,y) = P(X \leq x, Y \leq y) \quad 40$$

The probability density function is the derivative of the distribution function. In the case of joint random variables the probability density function does not always exist.

$$\varphi(x,y) = \frac{\partial^2 \Phi(x,y)}{\partial x \, \partial y} \quad 41$$

A very special case of the cumulative distribution function $\Phi(x,y)$ occurs where the variable X has no constraint on the variable Y. $\Phi_X(x)$ is called the marginal distribution function. It can be expressed as follows:

$$\Phi(x,\infty) = P(X \leq x; Y \leq \infty) = \Phi_X(x) \quad 42$$

The marginal distribution functions for the variable Y, $\Phi_Y(y)$, can be defined in a similar way.

Just like in the case of the one-dimensional variables it is possible to describe the two-dimensional variables by various moment parameters and distributions. It is therefore possible to determine μ_x, μ_y, σ_x and σ_y. Furthermore it is possible to determine the joint moments for both variables X and Y. The most important one will be the covariance σ_{xy}. It can be expressed as shown below.

$$\sigma_{xy} = \int \varphi(x,y)(x-\mu_x)(y-\mu_y)dxdy \quad 43$$

The covariance will form the basis for the correlation coefficient ρ_{xy}.

$$\rho_{xy} = \frac{\sigma_{xy}}{\sigma_x \sigma_y} \quad 44$$

The correlation coefficient will always hold the values $-1 \leq \rho_{xy} \leq +1$. The value of ρ_{xy} will be 0 if the variable X and Y are independent.

(Holicky, 2009)

4.2.9 Fractiles in probability density functions

Fractiles of a random variable X forms a very important part of structural reliability. A definition of a fractile can be presented in Figure 26.

Stellenbosch University http://scholar.sun.ac.za

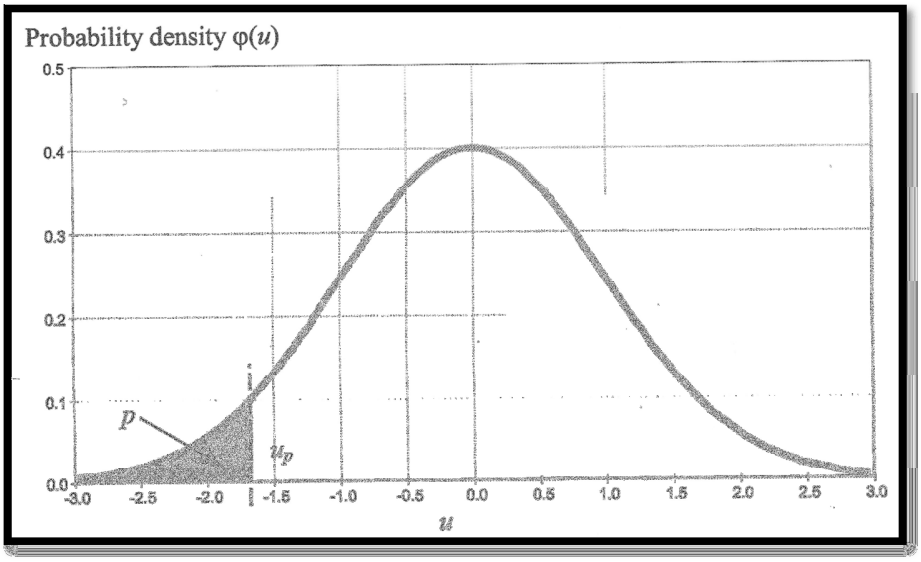

Figure 26: Presentation of a fractile for a standardised normal distribution (Holicky, 2009)

From the figure it can be seen that the fractile p, indicated by x_p represents a value of the random variable X where the values less than or equal to x_p will occur with the probability p. the fractile x_p can therefore be defined as

$$P(X \leq x_p) = \Phi(x_p) = p \qquad 45$$

As can be seen in Figure 26, the fractile p is represented by u_p and not x_p as defined above. This is due to the fact that that a standardised random variable U has been used. The fractiles of the standardised random variable U, u_p, can easily be found in tables. Figure 27 illustrates a typical standardised random variable U with its probability density function φ(u). In this case the probability $p = 0.05$ and the fractile $u_p = \mp 1.645$ can also be seen.

(Holicky, 2009)

Stellenbosch University http://scholar.sun.ac.za

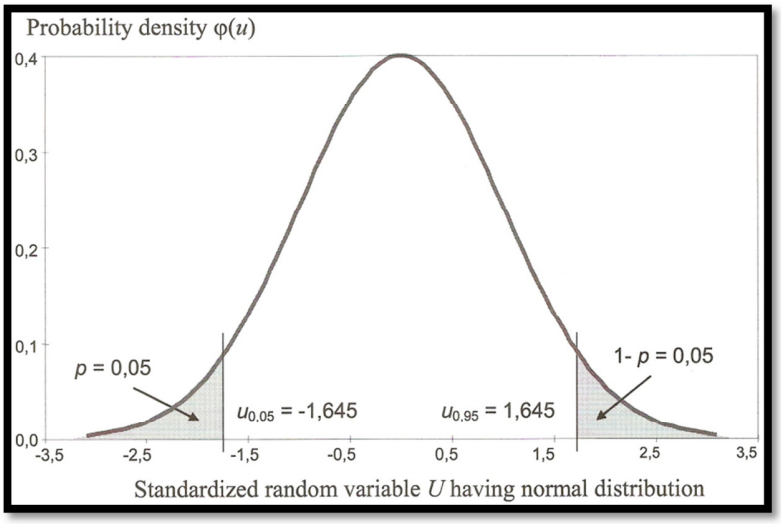

Figure 27: Presentation of probability p and fractile u_p (Holicky, 2009)

Stellenbosch University http://scholar.sun.ac.za

5. The reliability theory

The reliability of any engineering system is of great importance to the designer as well as the user of the system. Seeing that the aim of this research is to perform a probabilistic based evaluation of the codes mentioned in Chapter 1, it is essential that the theory behind structural reliability and its applications are discussed.

5.1 Basic concepts and problems in reliability

The basic requirement for a structure or system to be reliable is that the resistance or supply must be bigger than the load or demand on the system. The engineer therefore has to design the structure in such a way that it can withstand the lifetime maximum load or demand. In the past this objective was achieved by using partial load factors or margins of safety and by adopting conservative assumptions. (Alfredo H - S. Ang, Wilson H. Tang, n.d.). This is still used in the design of structures today, but with the partial factors calibrated to achieve a certain target reliability level.

The problem with the conventional way of design is the fact that it is sometimes difficult to quantify the uncertainties in the design and it lacks the logical basis for addressing these uncertainties. (Alfredo H - S. Ang, Wilson H. Tang, n.d.)

In the case of reliability based design it is still a very difficult task to determine the maximum resistance and load effect that will realize in the life of the structure. The only way that these values can be quantified is to make an estimation or prediction based on statistical models. With these statistical models it will be possible to describe a specific range (population) to which the possible resistance and demand belong. The following variables will be defined:

E = Demand or load effect

R = Resistance of structure

It is clear to see that the objective of reliability is to ensure that $R > E$, throughout the useful life of the structure. (Alfredo H - S. Ang, Wilson H. Tang, n.d.)

Stellenbosch University http://scholar.sun.ac.za

It can also be said that the limit state for structural reliability will be reached if R – E = 0. In reliability it is necessary to accept that the limit state of a structure may be exceeded. It is therefore essential to be able to assess the probability of failure p_f. The probability of failure can be expressed as

$$p_f = P(E > R) \quad (46)$$

Both the demand and resistance can be described by an appropriate cumulative distribution function, $\Phi_E(x)$ and $\Phi_R(x)$, and the corresponding probability density function $\varphi_E(x)$ and $\varphi_R(x)$. The general point of the considered variable X, used to describe E and R, is denoted by x. An example of the probability density functions for both variables and their mutual location with certain moment parameters can be seen in Figure 28.

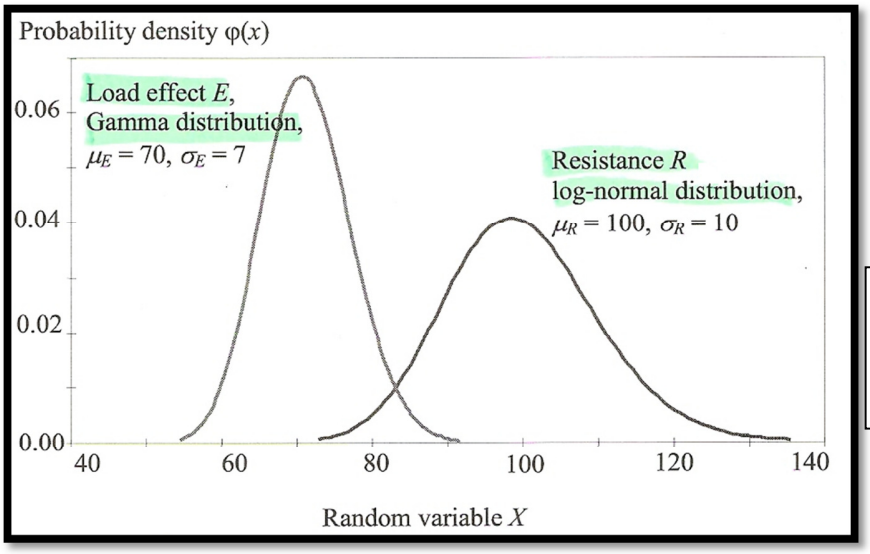

Unfavourable conditions can occur in the area where E and R overlap

Figure 28: Presentation of the probability density functions for E and R (Holicky, 2009)

From Figure 28 it can be seen that a small part exists where the probability density function of the demand E overlaps with the probability density function of the resistance R. This is the area where a possible failure in the structure can occur. It is therefore obvious that the parameters of the variables E and R must satisfy certain criteria to ensure that the probability of failure $p_f = P(E > R)$ stays within reasonable limits.

Figure 28 forms the fundamental concept behind the reliability concept for this research. The chosen structural model will therefore have a resistance that will be a function of variables such

Stellenbosch University http://scholar.sun.ac.za

as material properties and geometric parameters. The structure will have to withstand an applied load that will be a function of variables such as dead-, live- and wind load. From the considered variables it will be possible to set up figures for the chosen structural model as shown in Figure 28. With these figures it will then be possible to determine the probability of failure p_f and other values that will still be discussed in detail in the chapters to follows.

(Holicky, 2009)

5.2 One random variable cases

If either the load E or the resistance R of a specific case have a very low variability compared to the other it may be safe to assume that the variable is non-random i.e. a deterministic variable with a fixed value. An illustration of a case where the load E will be taken as deterministic and the resistance R as a random variable with a log-normal distribution can be seen in Figure 29. The same figure can be applied to a situation where the load will have a random variable with a certain distribution function and the resistance a deterministic value.

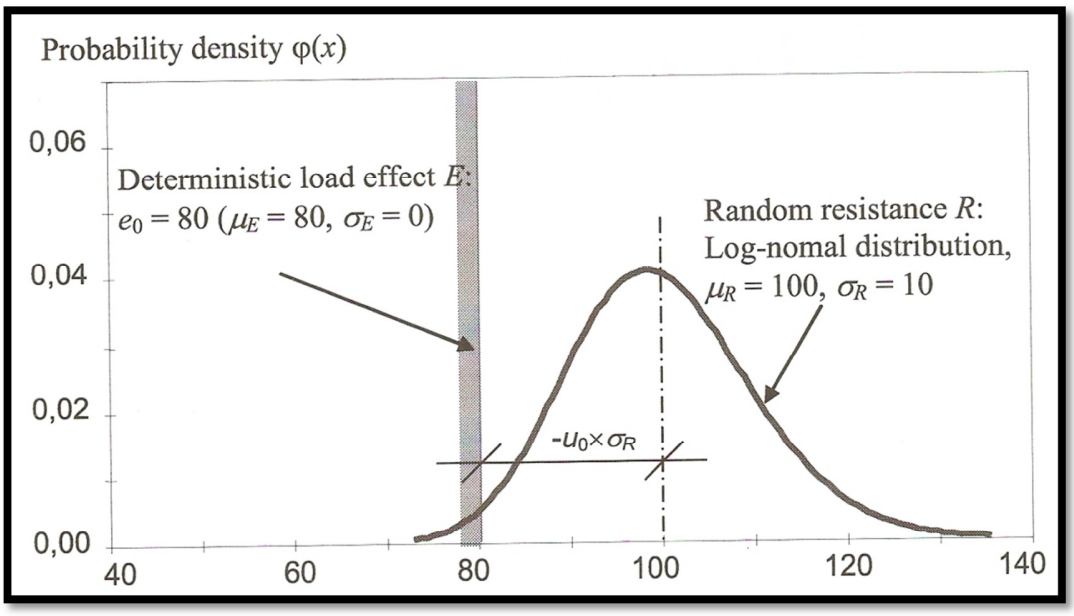

Figure 29: Deterministic load effect E with a random resistance R (Holicky, 2009)

From Figure 29 it can be seen that the probability of failure for this specific case will occur if the resistance is on the left hand side of the load effect. It can therefore be assessed directly from the

Stellenbosch University http://scholar.sun.ac.za

cumulative distribution function $\Phi_R(x)$ as in the case of a fractile. Let's assume the value e_0 is a fractile of resistance R. with this in mind it is then possible to calculate the probability of failure p_f for the specific case as

$$p_f = P(R<e_0) = \Phi_R(e_0) \quad 47$$

From the standardised tables available to assess the cumulative distribution function $\Phi_R(e_0)$ of a random variable U, the value of u_0 can be computed using equation 47.

$$u_0 = (e_0 - \mu_R)/\sigma_R \quad 48$$

The distance of u_0 is therefore the safety or reliability index β.

The probability of failure can therefore be written as

$$P_f = R(R<e_0) = \Phi_U(-\beta) \quad 49$$

Equation 47 will only be applicable in the case of normal distributions. In the case of different distributions it is necessary to standardize the random variables. β is now defined as a negative value of the standardised random variable corresponding to the probability of failure p_f.

$$\beta = -\Phi_U^{-1}(p_f) \quad 50$$

The reliability index as defined above forms the basis of structural reliability and is used in most cases to measure reliability of a structure.

(Holicky, 2009)

5.3 Two random variables both with normal distributions

When both the load E and the resistance R are random variables, the simplest case is to assume that both will follow a normal distribution. However, this is almost never the case. Looking back at Chapter 5.1 it can be seen that the performance function can be written as follows:

$$G = R - E \quad 51$$

Furthermore it is possible to determine the mean μ_G and the standard deviation σ_G of the performance function G in terms of R and E as shown bellow

$$\mu_G = \mu_R - \mu_E \quad 52$$

$$\sigma_G^2 = \sigma_R^2 + \sigma_E^2 + 2\rho_{RE}\sigma_R^2\sigma_E^2 \quad 53$$

Stellenbosch University http://scholar.sun.ac.za

The coefficient of correlation between R and E can be represented by ρ_{RE}. In most of the cases the load and resistance of a structure are independent or mutually independent. It is then safe to assume that $\rho_{RE} = 0$. From equation 49 it is possible to express the probability of failure p_f as shown below

$$p_f = P(E > R) = P(G < 0) = \Phi_G(0) \quad 54$$

This reduces the complexity of the problem to the determination of the cumulative distribution function for $\Phi_G(0)$. The variable G can again be standardised to the random variable U. This means that u_0 as described in equation 48 can be written as

$$u_0 = (0 - \mu_G)/\sigma_G = -\mu_G/\sigma_G \quad 55$$

The probability of failure p_f can be given as

$$p_f = P(R < E) = \Phi_G(0) = \Phi_U(u_0) \quad 56$$

If it is assumed that both the load and resistance have normal distributions, equations 52, 53 and 55 it is possible to determine the expression for the reliability/safety index β.

$$\beta = \frac{\mu_G}{\sigma_G} = \frac{\mu_R - \mu_E}{\sqrt{\sigma_R^2 + \sigma_E^2 + 2\rho_{RE}\sigma_R^2\sigma_E^2}} \quad 57$$

In most cases either the load E or resistance R will not be a normal distribution. The equations shown in this section so far therefore have to undergo some modifications. By making use of numerical integration it is possible to transform the variable or variables into normal distributions. Numerical integration is done by computer software in most cases. This will be explained in more detail in the next section.

(Holicky, 2009)

Stellenbosch University http://scholar.sun.ac.za

5.4 Random variables with general distributions

The case where the random variables follow general distributions is by far the most common case in structural reliability. The probability of failure p_f for such a case can be determined by integration. A graphical explanation can be seen in Figure 30.

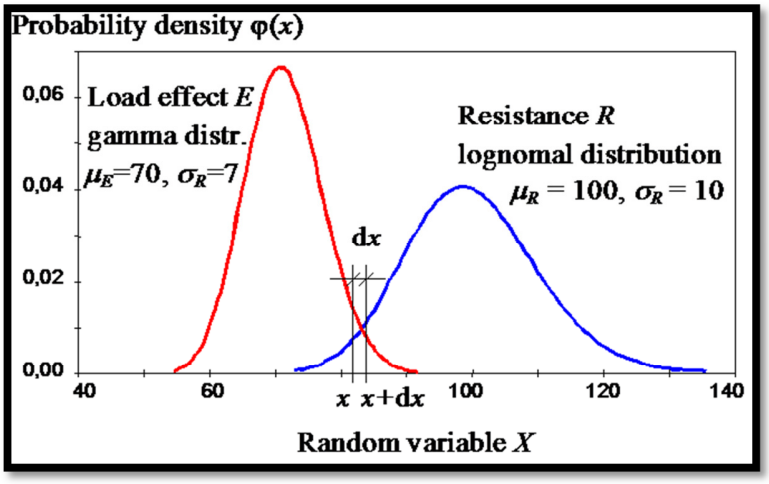

Figure 30: Variables E and R with general distribution functions (Holicky, 2009)

From Figure 30 the following can be said:

If event A denotes the occurrence of a certain load E in the differential interval $< x, x + dx >$, the probability of occurrence of event A can be expressed as follows:

$$P(A) = P(x < E < x + dx) = \varphi_E(x)dx \quad 58$$

If an event B denotes the occurrence of a resistance R in interval $<-\infty, x >$, the probability occurrence of event B is:

$$P(B) = P(R < x) = \Phi_R(x) \quad 59$$

The probability of failure dp_f is given by the simultaneous occurrence of the events A and B, i.e. the probability of A intersecting B, $(A \cap B)$. The probability of failure can therefore be represented by the following expression:

$$dp_f = P(A \cap B) = P(A)P(B) = P(x < E < x + dx)P(R < x) = \varphi_E(x)\Phi_R(x)dx \quad 60$$

Note that equation 60 will only be applicable if events A and B are mutually independent, i.e. if the load E is independent from the resistance R.

Stellenbosch University http://scholar.sun.ac.za

The integration over the interval, $-\infty < x < \infty$ where both variables E and R occur simultaneously leads to the following expression for the total probability of failure:

$$\rho_f = \int_{-\infty}^{\infty} \varphi_E(x)\Phi_R(x)dx \quad 61$$

As indicated in the previous section the integration process described in equation 61 has to be carried out numerically or by using a simulation method such as the Monte Carlo (MC) simulation. (Holicky, 2009)

5.5 Multivariate cases

In all previous sections discussed so far a maximum of two variables were taken into consideration at a time. This section will focus on the case where n variables have to be taken into consideration on a specific interval. The random variables $X_1, X_2 \ldots X_n$ now will be denoted in vector form $\mathbf{X}$ $[X_1, X_2 \ldots X_n]$ with their realisations $x_1, x_2 \ldots x_n$ in vector form as $\mathbf{x}$ $[x_1, x_2 \ldots x_n]$. The performance function is then generalised as follows:

$$G(X_1, X_2 \ldots X_n) = G(\mathbf{X}) \quad 62$$

The safe domain can be described as the domain where the supply exceeds demand, i.e. where the performance functions takes on a positive value.

$$G(X_1, X_2 \ldots X_n) = G(\mathbf{X}) > 0 \quad 63$$

The unsafe domain is the domain where the performance function takes a negative value

$$G(X_1, X_2 \ldots X_n) = G(\mathbf{X}) < 0 \quad 64$$

The limit state of the performance function is given by

$$G(X_1, X_2 \ldots X_n) = G(\mathbf{X}) = 0 \quad 65$$

For the case of non-linear performance functions the probability of failure can be expressed as

$$p_f = P(G(\mathbf{X}) \leq 0) = \int_{G(\mathbf{X})\leq 0} \varphi(\mathbf{X})d\mathbf{X} \quad 66$$

$\varphi(\mathbf{X})$ is the joint probability density function of all the random variables X

A way must be found to compute the probability of failure as shown in equation 66. In the case of the research done for this thesis an approximate analytical method will be used, such as FORM and SORM.

(Holicky, 2009)

Stellenbosch University http://scholar.sun.ac.za

5.6 Approximate analytical methods: FORM and SORM

The First Order Reliability Method (FORM) forms the basis of structural reliability analysis in computer packages dedicated to determine structural reliability. If a case of multivariate variables, **X** is considered. The steps of the FORM method can be summarized as follows (Holicky, 2009).

The variables **X** must be transformed into standardised normal variables **U**, with the performance function $G(\mathbf{X}) = 0$ transformed to $G'(\mathbf{U}) = 0$

- The failure surface $G'(U) = 0$ is approximated at a chosen point by a tangent hyper plane
- The point on the surface $G'(U) = 0$ closest to the origin is found by iteration
- The reliability index β can then be described as the distance of the design point from the origin and then the failure probability P_f is given as $P_f = \Phi(-\beta)$

The first step of FORM is to transform the original value **X** into the space of standardised normal variables **U** as shown in Figure 31 (a) and (b). The transformation at a specific point **x*** (design point) is based on the following two conditions:

- Equal distribution functions

$$\Phi_X(x^*) = \Phi_U\left(\frac{x^* - \mu_X^e}{\sigma_X^e}\right) \quad 67$$

- Equal probability increments

$$\varphi_X(x^*) = \frac{1}{\sigma_X^e}\varphi_u\left(\frac{x^* - \mu_X^e}{\sigma_X^e}\right) \quad 68$$

From equation 67 and 68 the mean and standard deviation of the equivalent normal distribution can then be calculated:

$$\mu_X^e = x^* - \sigma_X^e\left[\Phi_U^{-1}(\Phi_X(x^*))\right] \quad 69$$

$$\sigma_X^e = \frac{1}{\varphi_X(x^*)}\varphi_U\left[\Phi_U^{-1}(\Phi_X(x^*))\right] \quad 70$$

This is used to approximate the reliability index β associated to the design point.

Stellenbosch University http://scholar.sun.ac.za

A presentation of a FORM analysis is shown in Figure 31.

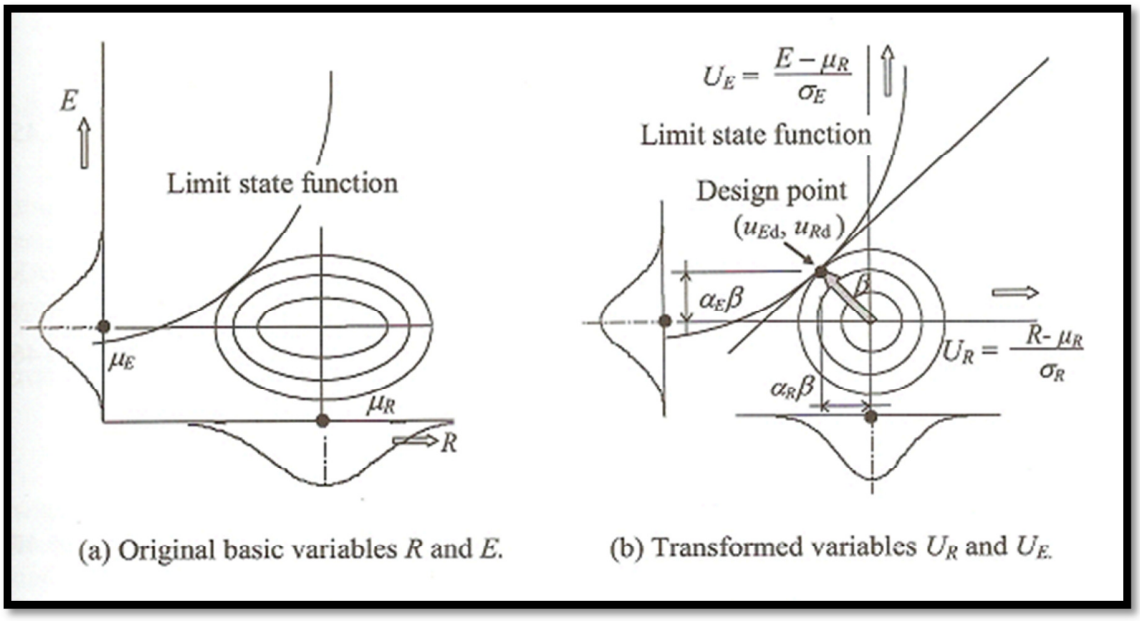

Figure 31: Presentation of a FORM analysis (Holicky, 2009)

To perform a FORM analysis, as described above, by hand is only possible for very simple cases and even then it is still extremely time consuming. In most cases computer programs are used to perform a FORM analysis. In the research done for this thesis a computerised FORM analysis will be done.

Holicky provides the following ten steps for the computation iteration procedure of the FORM method:

1. The limit state function $G(\mathbf{X}) = 0$ is defined with its theoretical models and basic variables $\mathbf{X} = [X_1, X_2 \ldots X_n]$
2. An initial assessment of the design point $\mathbf{x^*} = \{x_1^*, x_2^* \ldots x_n^*\}$ is made by taking the mean values of n - 1 basic variables and the last one is determined from the limit state function $G(x^*) = 0$
3. At the point $\mathbf{x^*} = \{x_1^*, x_2^* \ldots x_n^*\}$ the equivalent normal distributions are found for all the basic variables using equations 66.

Stellenbosch University http://scholar.sun.ac.za

4. It is now possible to determine the corresponding standardised design point $\mathbf{u^*} = \{u_1^*, u_2^* \ldots u_n^*\}$ of the standardised random variable $\mathbf{U} = \{U_1, U_2 \ldots U_n\}$ by using the following expression:

$$u_i^* = \frac{x_i^* - \mu_{x_i}^e}{\sigma_{x_i}^e} \quad 71$$

5. Partial derivatives of the standardised variables $\mathbf{U} = \{U_1, U_2 \ldots U_n\}$ at the design point can be evaluated. Let the vector denote **D**

$$\mathbf{D} = \begin{bmatrix} D_1 \\ D_2 \\ D_n \end{bmatrix} \text{ where } D_i = \frac{\partial G}{\partial U_i} = \frac{\partial G}{\partial X_i} \sigma_{X_i}^e \quad 72$$

6. The reliability index β is estimated as

$$\beta = -\frac{\{D\}^T\{u^*\}}{\sqrt{\{D\}^T\{D\}}} \text{ where } \{u^*\} = \begin{Bmatrix} u_1 * \\ u_2 * \\ u_n * \end{Bmatrix} \quad 73$$

7. Sensitivity factors are determined as

$$\{\alpha\} = \frac{\{D\}}{\sqrt{\{D\}^T\{D\}}} \quad 74$$

8. A new design point can now be determined for n -1 standardised and original basic variables from the following expressions

$$u_i * = \alpha_i \beta_i \quad 75$$

$$x_i * = \mu_{X_i}^e - u_i^* \sigma_{X_i}^e \quad 76$$

9. The remaining basic variable can be determined from the limit state function $G(\mathbf{x^*}) = 0$
10. Steps 3 to 9 can be repeated until the reliability index β and the design point $\{\mathbf{x^*}\}$ have the required accuracy

(Holicky, 2009)

5.7 The Monte Carlo simulation

By performing a large number of experiments on a specific topic, for example a profile parameter such as the yield stress of a profile, it is possible to obtain the distribution function that will be

Stellenbosch University http://scholar.sun.ac.za

followed by this parameter and to determine other statistical parameters such as the COV, μ and σ. These values can then be used in further calculations.

The Monte Carlo (MC) simulation was developed as a mathematical substitution for experiments (Cardoso et al., 2008). For each iteration a realisation is generated of each input parameter from its distribution function and the realisations are propagated through the assumed model to obtain a realisation of the desired output parameters. With the statistical parameters known, from previous experiments and tests, it is now possible to have a software application such as @RISK that will perform a MC simulation for a user defined amount of iterations. It can be used when a parameter is a function of other parameters for which statistical descriptions are available. In such a case, from the iterations performed on the estimate of the distribution function for the parameter under investigation will be obtained. The MC simulation only became effective with the birth of computers with large processing capability.

Stellenbosch University http://scholar.sun.ac.za

6. Choosing a structural model

As mentioned, this study aims to perform a quantitative probabilistic based evaluation of the reliability achieved in the design of Light Steel Frame Buildings (LSFB) when designed according to the loading code, SANS 517:2009 and the new design code for cold formed steel sections, SANS 10162-2:2010.

To achieve this research outcome a representative light steel frame building must be designed according to the two codes mentioned above. The designed building will serve as the structural model that will be used in this research. The chosen structural model has to be within the limits specified in the SANS 517:2009. The most important geometric limitations can be found in Chapter 2.4. Furthermore the loads and load combinations applied on the structural model will be obtained from SANS 517:2009. It must be ensured that all the structural members that where discussed in Chapter 2.2 are present in the chosen structural model. With the different structural elements present it is possible to define the most critical failure modes that will be present in the model:

- Axial load
- Shear
- Tension
- Combination of bi-axial bending and axial loading

Before a probabilistic based evaluation of the reliability achieved by the structural model can be performed it must be ensured that no structural element in the model will fail when designed according to a deterministic design approach. The loads on the chosen structural model are known. From these loads it is therefore possible to choose a profile that has the capacity to withstand the applied loads for all the failure modes defined above. In practice when a LSFB in constructed, it is common practice to construct the whole structure from one specific profile. This enables easy erection on sight and ensures that all the profiles fit into each other. For the chosen structural model, the same approach was used where one specific profile was chosen for the whole structure. SANS 10162-2:2010 will be used to determine the capacity for the chosen profile used in the model. However, the smallest available section that achieves the necessary resistance for the loads induced on the structure was chosen. This was done for economic reasons and to represent the weakest structure that would still be acceptable according to the codified design requirements. Once the structure is classified as safe from a deterministic

Stellenbosch University http://scholar.sun.ac.za

(codified requirements) point of view, the probabilistic based evaluation of the reliability achieved for all the different failure modes can be evaluated.

The probabilistic based evaluation will be done as follows: The reliability index achieved for each failure mode will be calculated by choosing the most critical element for each failure mode.

It is therefore assumed that the element reliability of these few critical elements provide an acceptable indication of the overall structural reliability. This assumption is based on the fact that it is very unlikely that the structure will fail if none of its structural elements fail. However, this does not mean that structure will have the necessary structural stability. A second order analysis will be performed to ensure that the necessary level of structural stability is achieved, but no probabilistic based evaluation on the stability of the structure as a whole will be performed.

6.1 Basic layout of structural model

The basic layout of the chosen model is as follows. The chosen model was designed as a human dwelling. The dimensions of the structure are 6 m x 12 m with an eaves height of 5.3 m. The roof is dual pitched, spanning over the 6 m span, with a slope of 15 degrees. The total height of the structure will therefore be 6.1m. It was decided that there will be two large rooms and a small room for a bathroom on the ground floor. The first floor will consist of the main bedroom with an en-suite bathroom. There will be two more bedrooms and a bathroom. The whole structural model will be constructed from one profile size, the S8995 profile. The profile parameters of the chosen profile can be found in APPENDIX B: Profile parameters for the S8995 profile. A three-dimensional presentation of the final structural model used in the research done can be seen in Figure 32. Detailed drawings and layouts of the model can be found in APPENDIX C: Detailed drawings and layouts for structural model.

Stellenbosch University http://scholar.sun.ac.za

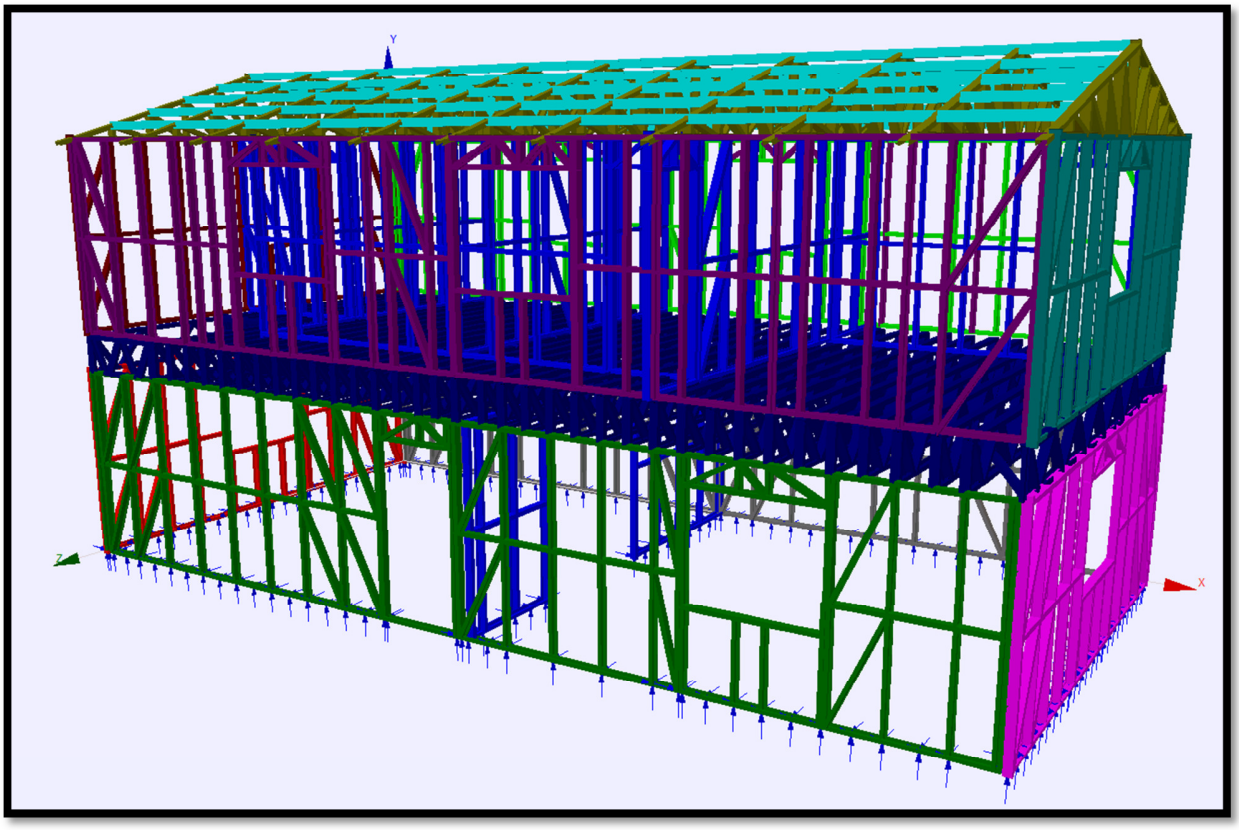

Figure 32: 3 – D presentation of the structural model

6.2 Support used in structural model

It is important to note that the foundation of the structural model will be built from concrete. However, this is not part of the research done and was therefore modelled as rigid supports, as shown in Figure 32. The supports modelled must still represent the real life situation. Each node at the bottom of the structure was therefore fixed in the X, Y and Z directions against translations. This is realistic since the bolt-spacing in practice correspond approximately to the distances between supports.

Stellenbosch University http://scholar.sun.ac.za

6.3 Loads acting on structural model

The loads acting on the structural model can be divided into three categories namely: live loads (LL), permanent or dead loads (DL) and wind loads (WL). These three categories will act on the structure in different combinations and at different times. All the different characteristic values for each category as well as the load combinations for each load case will be given and discussed in this section.

6.3.1 Determination of live loads (LL)

Live loads on the structure can be divided into two parts namely, the load on the roof of the structure and the load on the first floor of the structure. By referring to clause 5.3.2 of SANS 517:2009, the following characteristic loads can be obtained

a) For roofs, not accessible except for normal maintenance:

0.25 kPa for contributory areas $> 15m^2$

b) For general floor areas:

Uniformly distributed load of 1.5 kPa

6.3.2 Determination of dead loads (DL)

Dead loads will consist of the self-weight of the structural model as well as additional loads added on the structure due to services etc. The structural analysis program used includes the self-weight of the structure automatically. It is therefore only necessary to determine the characteristic value for the dead load such as the ceiling below the first floor as well as other services. It was assumed sufficient to allow for a dead load due to services and ceiling weight a distributed load of 0.2 kPa.

The following question arises. Due to the fact that only a part of the dead load (0.2 kPa) on the structure will be applied as a probabilistic load, how will this influence the overall probabilistic based evaluation of the different failure modes? Seeing that these structures have a very low dead load compared to the wind load and live load induced on it, it can be assumed that the dead

Stellenbosch University http://scholar.sun.ac.za

load will have a very small influence on the final reliability index for the different failure modes. This assumption was confirmed by performing a linear structural analysis on the structural model with and without dead load. The obtained element forces for both analyses done were compared and it was seen that there was a difference of less than 1 %. This simplification in the evaluation process will therefore have a negligible influence on the final reliability indices obtained.

6.3.3 Determination of wind loads (WL)

Calculating the wind load is much more complicated than calculating any of the other loads acting on the structure. The basic values obtained from clause 5.3.3 of SANS 517:2009 that were used to do the wind load calculations for the chosen structure are as follows:

- A terrain roughness factor $c_r = 0.98$ for a structure in a more exposed situation was assumed
- An imaginary site altitude of 500 m above sea level was chosen. This is representative of the Stellenbosch area
- Air density $\rho = 1.12$ kg/m^3, obtained from the code for an elevation of 500 m above sea level
- WLW = wind load on walls of structure
- WLR = wind load on roof of structure
- Fundamental basic wind speed $v_{b,0}$ as obtained from Figure 11 in SANS 517:2009 as 28 m/s.

Before it is possible to calculate the wind pressure (in kPa) on the building, the different wind pressure zones with their external pressure coefficients (c_{pe}) and internal pressure coefficient (c_{pi}), according to SANS 517:2009 clause 5.3.3.3, must be summarised for each relevant wind load condition on the chosen structural model. Three wind load conditions need to be investigated to obtain the worst combination of wind loads on the chosen structure. These conditions were as follow:

Stellenbosch University http://scholar.sun.ac.za

Wind load condition 1 (WLC1)

For WLC1, the wind will blow onto the structure from the side as shown in Figure 33 and Figure 34 for the walls and roof respectively.

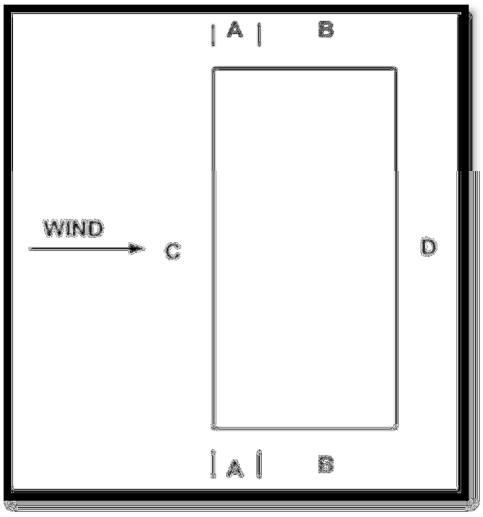

Figure 33: Wind pressure zones on the walls of structural model

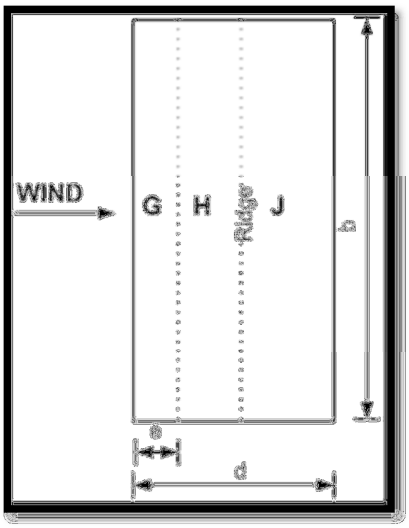

Figure 34: Wind pressure zones on the roof of structural model

Stellenbosch University http://scholar.sun.ac.za

For across wind situations the pressure changes rapidly between positive and negative values on the windward face of the roof, depending on the pitch. (SANS, 2009). Different values for zone G, H and J are therefore given. The designer has to determine the worst combination of pressure coefficients for these zones. The summarised pressure coefficients for WLC1 with the chosen pressure coefficients for zones G, H and J are shown in Table 1.

Table 1: Pressure coefficients (dimensionless) for each zone for WLC1

Zone	Coeff
A	-1.2
B	-0.8
C	0.8
D	-0.5
G	-0.8
H	-0.3
J	-0.4

Furthermore, the internal pressure coefficient (c_{pi}) for WLC1 is 0.2

Wind load condition 2 (WLC2)

For WLC2, the wind will blow onto the structure from the side as shown in Figure 35 and Figure 36 for the walls and roof respectively.

Stellenbosch University http://scholar.sun.ac.za

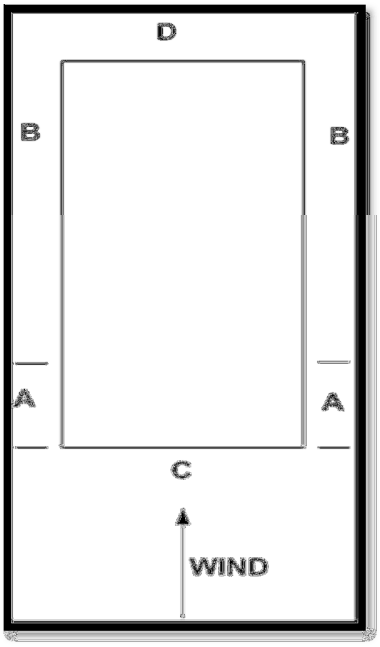

Figure 35: Wind pressure zones on the walls of structural model

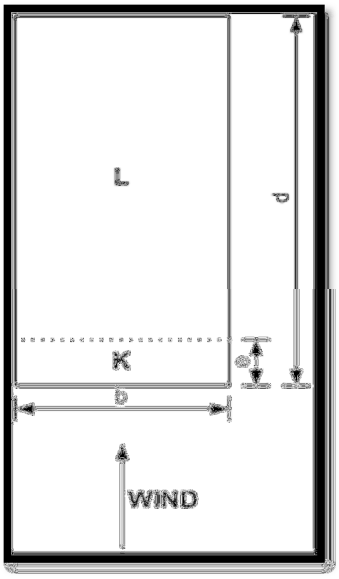

Figure 36: Wind pressure zones on the roof of structural model

If the wind is blowing in the longitudinal direction of the structure, only two pressure zones are present on the roof of the structure. These zones are zone K and L. The worst pressure coefficients obtained from SANS 517:2009 for these zones are used.

Stellenbosch University http://scholar.sun.ac.za

The summarised pressure coefficients for WLC2 are shown in Table 2.

Table 2: Pressure coefficients (dimensionless) for each zone for WLC2

Zone	Coeff
A	-1.2
B	-0.8
C	0.8
D	-0.5
K	-1.3
L	-0.6

Furthermore, the internal pressure coefficient (c_{pi}) for WLC2 is 0.2

Wind load condition 3 (WLC3)

For WLC3, the wind will blow onto the structure from the side as shown in Figure 37 and Figure 38 for the walls and roof respectively. The summarised pressure coefficient for WLC1 is shown in Table 3. It must be noted that the wind pressure zones on the walls for WLC3 in the same as for WLC1. The only difference will be in the values of the pressure coefficients on the roof for WLC3.

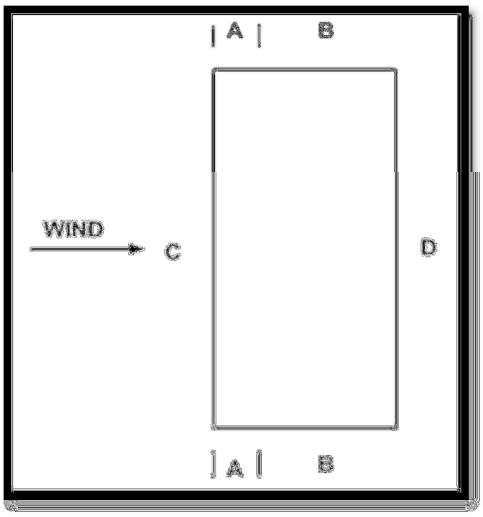

Figure 37: Wind pressure zones on the walls of structural model

Stellenbosch University http://scholar.sun.ac.za

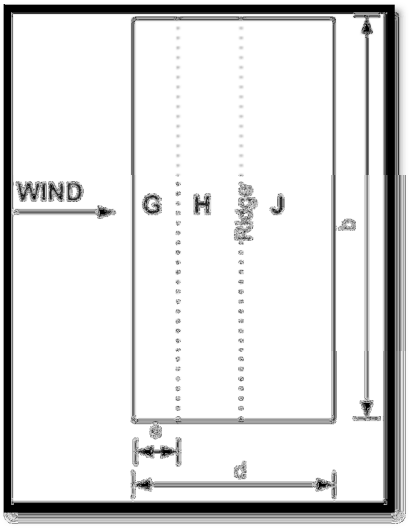

Figure 38: Wind pressure zones on the roof of structural model

For across wind situations the pressure changes rapidly between positive and negative values on the windward face of the roof, depending on the pitch. (SANS, 2009). Different values for zone G, H and J are therefore given. The designer has to determine the worst combination of pressure coefficients for these zones. A different combination of these coefficients was therefore used for WLC 3 than what was used for WLC1. The summarised pressure coefficients for WLC3 with the chosen pressure coefficients for zones G, H and J are shown in Table 3.

Table 3: Pressure coefficients (dimensionless) for each zone for WLC3

Zone	Coeff
A	-1.2
B	-0.8
C	0.8
D	-0.5
G	0.2
H	0.2
J	0

Furthermore, the internal pressure coefficient (c_{pi}) for WLC3 is -0.3. With the internal and external pressure coefficients calculated for each wind load condition it is now possible to

Stellenbosch University http://scholar.sun.ac.za

calculate the wind loads on the chosen structural model. The detailed wind load calculations can be seen in Appendix D: Detailed wind load calculations.

6.4 Load combinations acting on structural model

In general there can be distinguished between two design situations namely, ultimate limit state (ULS) and serviceability limit state (SLS). Is this research, the focus will be on the ULS. It is therefore of utmost importance that the worst combinations of the different loads described above act on the structure simultaneously. The following four different load combinations were deemed to achieve this. They were applied on the structural model with partial factors according to SANS 517:2009.

Load Combination 1

ULS: 0.9DL + 1.3WLR1 + 1.3 WLW1

Where:

DL = dead load

WLR1 = wind load on roof for wind condition 1

WLW1 = wind load on walls for wind condition 1

Load Combination 2

ULS: 0.9DL + 1.3 WLR2 + 1.3 WLW3

DL = dead load

WLR2 = wind load on roof for wind condition 2

WLW3 = wind load on walls for wind condition 3

Load Combination 3

ULS: 1.2DL + 1.6LL + 1.3 WLR3 + 1.3 WLW3

DL = dead load

LL = Live load

Stellenbosch University http://scholar.sun.ac.za

WLR2 = wind load on roof for wind condition 2

WLW3 = wind load on walls for wind condition 3

Load Combination 4

ULS: 1.2DL + 1.6LL

DL = dead load

LL = live load

6.5 Analysis of the structural model in a structural analysis program

Once all the loads and load combinations had been defined, a structural analysis on the chosen structural model was performed. The chosen structural model was analysed as a whole. This ensured that the full three-dimensional stability of the structure was investigated. To be able to investigate the stability of the structure it was necessary to perform a buckling as well as a Second order analysis. From the results obtained it was possible to detect any structural elements that will fail in stability. When looking at the bucking analysis, it can be said that the element or structure will buckle if the load factor obtained for any mode shape is smaller than 1. The buckling result for the mode under consideration is shown in the top left corner of each figure. For mode 1 buckling it can be seen that Load combination 4 presents the worst case with a load factor of 1.75. Other mode shapes are not shown here, but load factors above 1 were obtained for all mode shapes and load combinations. The chosen K-Bracing and element size for the structural model is therefore enough for overall structural stability and no structural element on its own will buckle.

The results of the buckling analysis done for each load combination as described in Chapter 6.4 can be seen in Figure 39 to Figure 42, each time for mode one only.

Stellenbosch University http://scholar.sun.ac.za

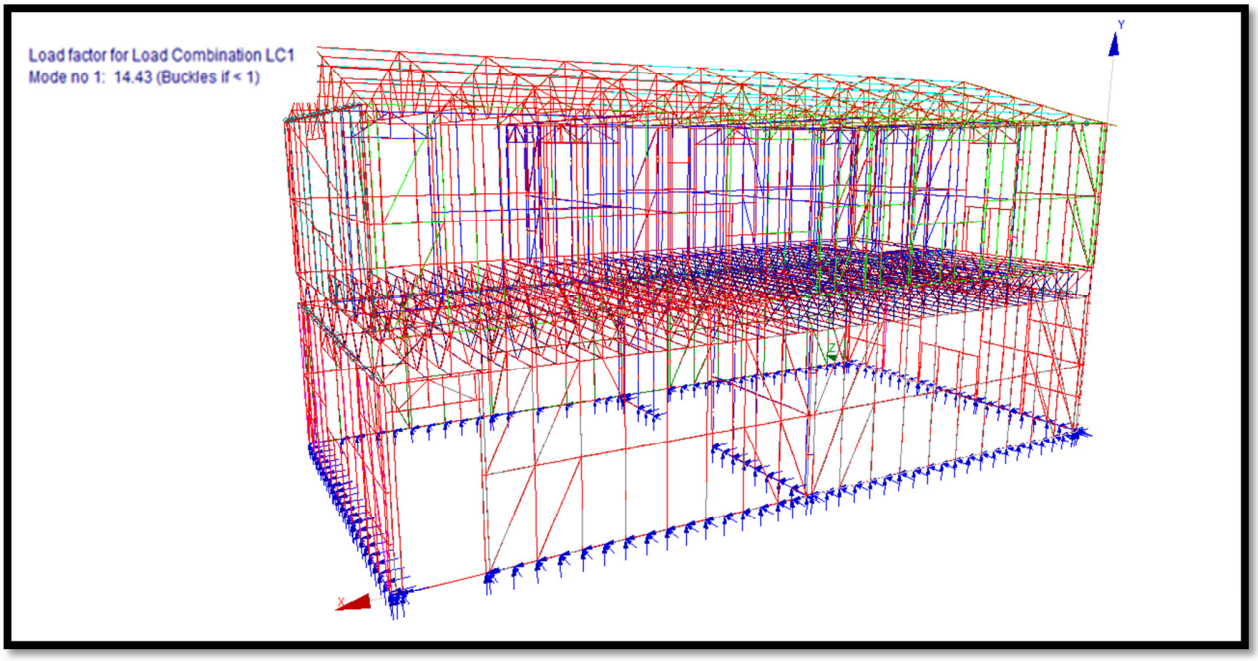

Figure 39: Buckling analysis for Load Combination 1

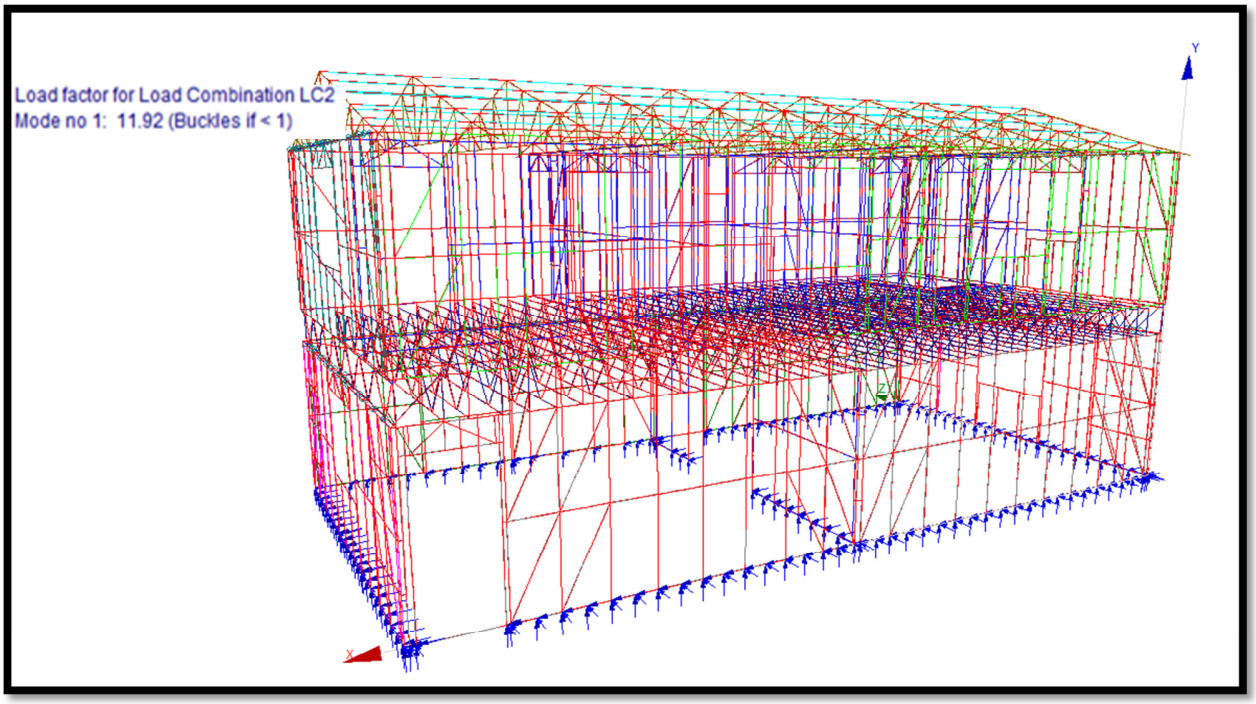

Figure 40: Buckling analysis for Load Combination 2

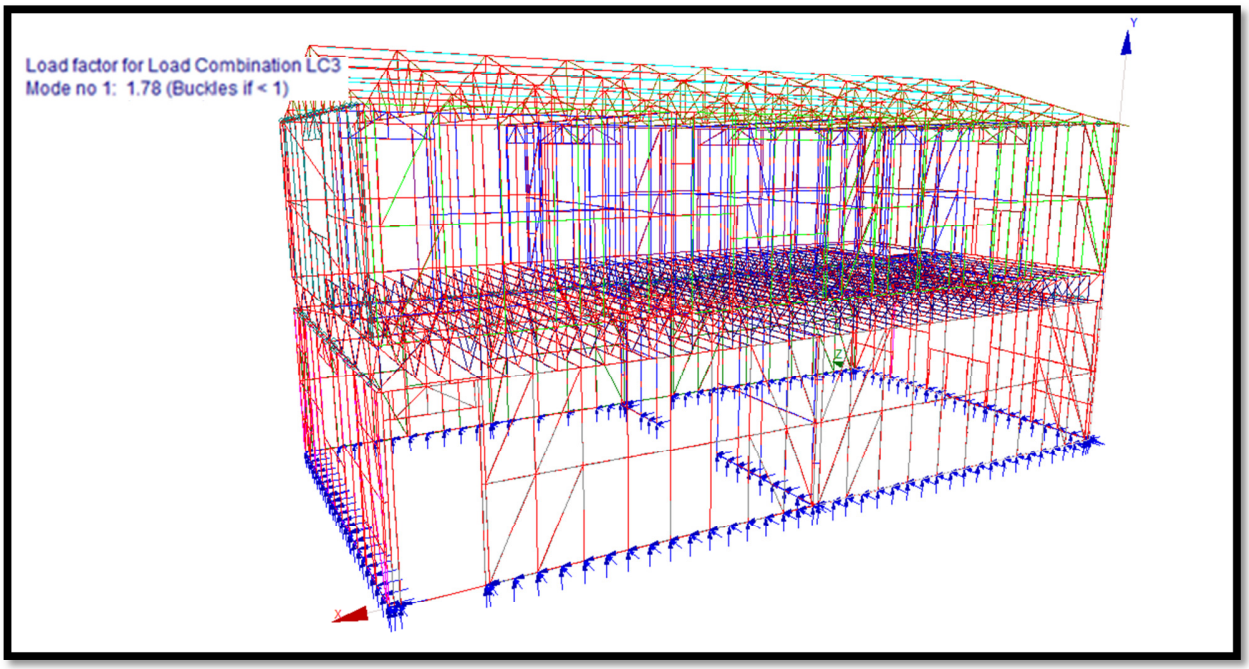

Figure 41: Buckling analysis for Load combination 3

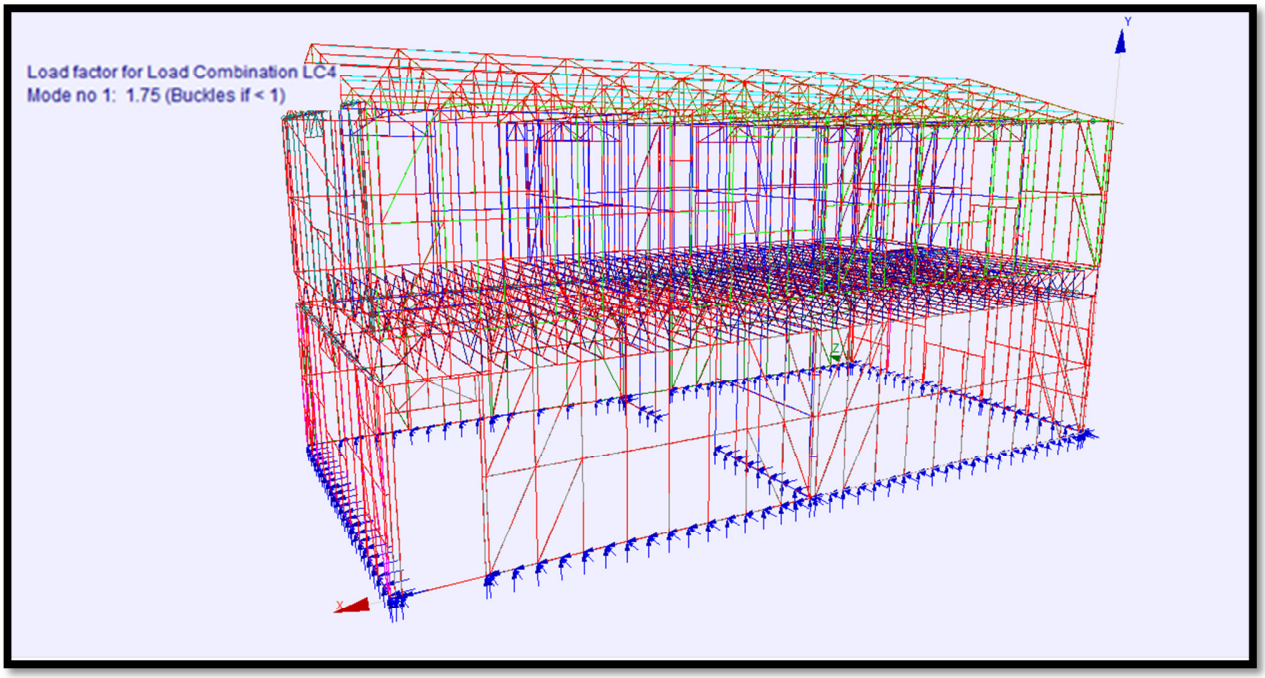

Figure 42: Buckling analysis for Load Combination 4

Stellenbosch University http://scholar.sun.ac.za

The second order analysis was done to ensure that convergence of the stiffness matrices take place. Furthermore it provides another check to ensure that the necessary level of element stability is achieved. A second order analysis can also be used to determine all the element forces (shear, moments and axial loads) as well as the displacements of each element and the structure as a whole. Without a powerful computer it is very time consuming to perform a three-dimensional second order analysis for the chosen structural model. Linear analyses were therefore done to determine the element forces and displacements as discussed above. The values obtained from the linear analyses were compared to the values from the second order analyses. It was seen that the element force values obtained for these two analyses differed less than 1 %. If the element force values from the two different analyses are the same, linear analyses can be used to obtain the element forces for the different load combinations.

6.6 Structural elements used in chosen structural model

In many cases LSFB will be constructed from one profile size only. This was also done for the chosen structural model. By performing a structural analysis on the model shown in Figure 32, it was possible to obtain element forces. By applying a deterministic design approach it was possible to choose a profile size that had the capacity to withstand the element forces for all the different failure modes. Therefore, no element in the chosen structural model will fail deterministically. However, it had to be ensured that the chosen profile's capacity was just higher than the applied load. The most critical element for each failure mode will therefore be the element that is the closest to failure. This ensured that the chosen structural model was as economic as possible. It would also provide a better estimate of the actual level of reliability achieved by the chosen model. With all these factors taken into account it was decided that a S8995 profile would be used for the design of the chosen structural model. All the profile parameters for the S8995 profile can be found in APPENDIX B: Profile parameters for the S8995 profile.

6.7 Obtaining element forces by performing linear analyses

In Chapter 6 the different failure modes that will be investigated were defined. The most critical element for each failure mode needs to be identified. With the most critical element known for

Stellenbosch University http://scholar.sun.ac.za

each failure mode, it is possible to evaluate the structural safety of the chosen structural model. Seeing that there are more than 4000 elements in the chosen structural model, it will be unpractical to provide all the data obtained from the linear analyses here. This was summarised in Excel, for each failure mode, and used to select the most critical element for each failure mode. The different failure modes with the most critical element will be discussed in detail below.

6.7.1 Axial loads

The first failure mode that can be identified is the failure of a specific element due to axial loads only. This failure mode is not only governed by the force in a specific element, but also by the effective length of that element. It is therefore possible that a very slender element with a low axial force will be more critical than a short element with a large axial force. It is important to note that the structural analysis program used will give axial compression as a positive value and axial tension as a negative value. By thoroughly analysing and processing the data obtained from the structural analysis, in Excel, it was possible to identify the most critical element. It was found that the most critical axial load, for a given effective length, present in any element in the chosen structural model is 15.76 kN. This axial force is present in element 727 – 728 – which is a "wall column", shown Figure 43. The element will have effective lengths as follows:

$L_{ey} = 600$ mm

$L_{ez} = 600$ mm

$L_{ex} = 2400$ mm

The axial load envelope for the critical element can be seen in Figure 44.

Stellenbosch University http://scholar.sun.ac.za

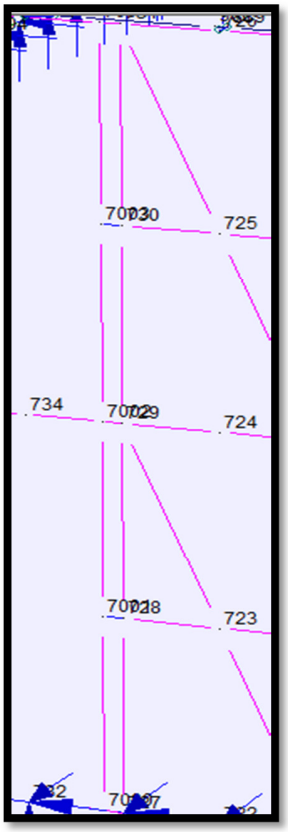

Figure 43: Most critical element for axial loads

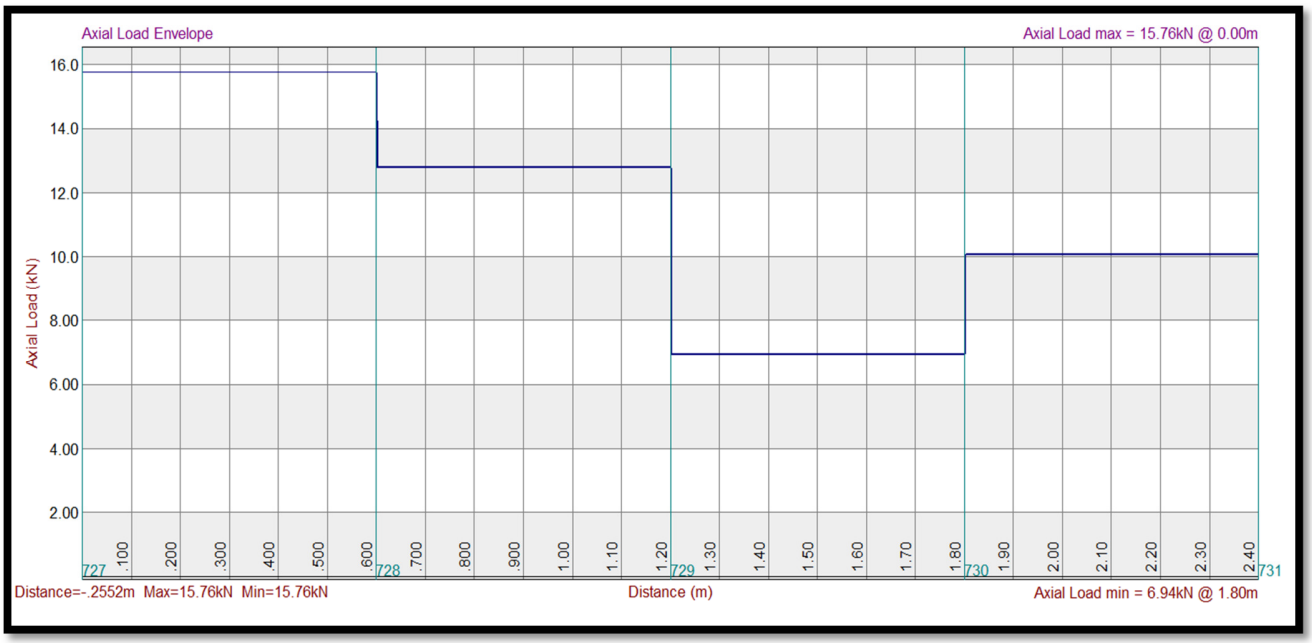

Figure 44: Axial load envelope of the critical element in axial load

Stellenbosch University http://scholar.sun.ac.za

6.7.2 Strong-axis shear

The second failure mode observed was strong-axis shear. The thickness and dimensions of a profile will govern the shear capacity of that profile. For the chosen structural model all the elements have the same profile parameters. The biggest shear value obtained from the structural analysis is therefore the most critical, given that the shear value obtained is representative of the real life situation. With this in mind, element 854 – 863 was identified as the critical element for strong-axis shear, with a value of 8.05 kN. This element is found in the floor joist between a wall panel of the first and second floor on the 6 m side of the building. If the wind would blow onto the structure in a longitudinal direction, this floor joist will have a great shear load on it, induced by the wall panels. The element is shown in Figure 45. The shear envelope for the most critical element 854-863 can be seen in Figure 46. As mentioned the shear capacity of a profile is determined by the thickness of the web or flange of the profile. The effective length of the profile will therefore have no influence on it s shear capacity.

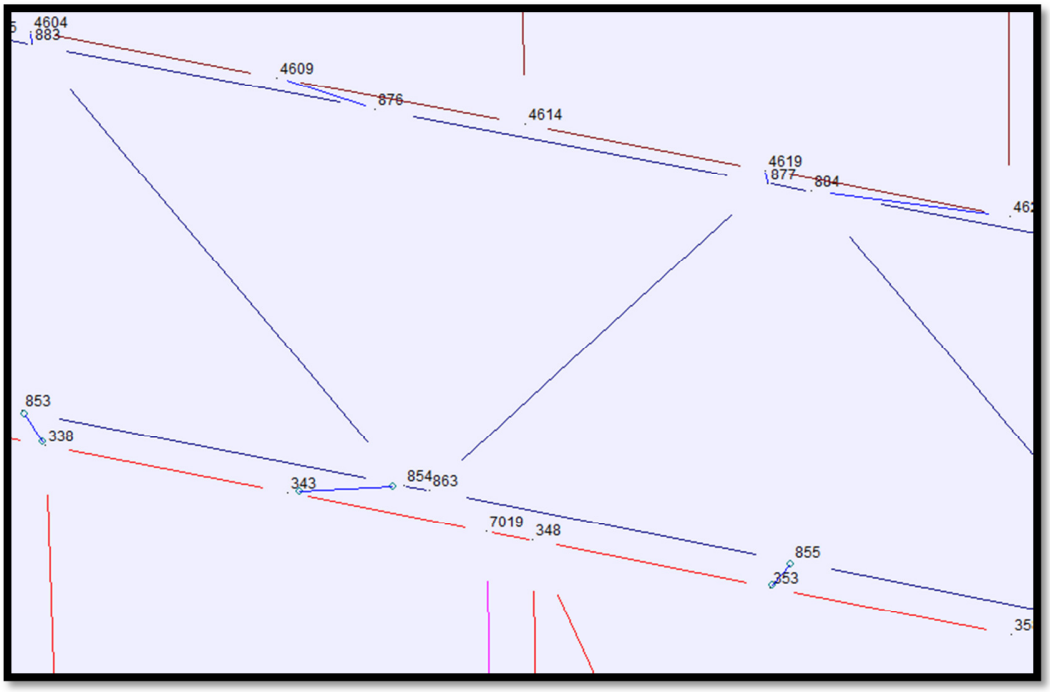

Figure 45: Most critical element for strong – axis shear

Stellenbosch University http://scholar.sun.ac.za

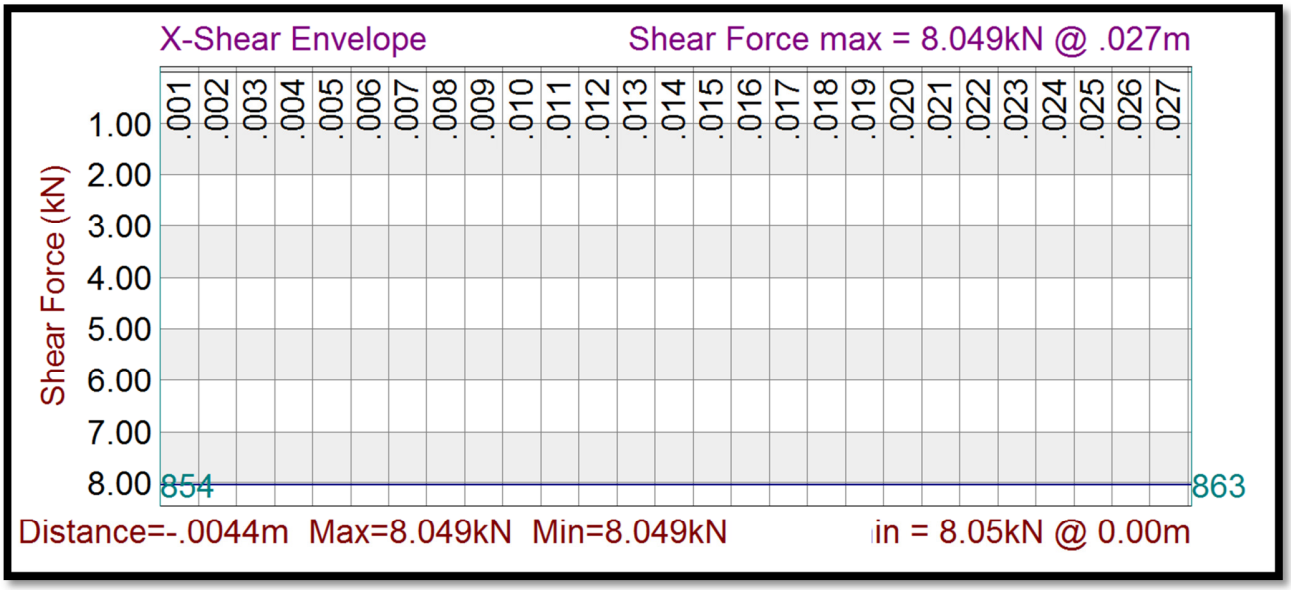

Figure 46: Shear envelope for the most critical element in strong-axis shear

6.7.3 Weak-axis shear

The third failure mode that had to be investigated was the failure of a profile in weak-axis shear. The weak-axis shear capacity of the profile will be provided by the width and thickness of the flanges of the profile. Element 3000 – 3005 -3010 – 3015 -– 3050 with a shear value of 4.458 kN was identified as the critical element for weak – axis shear. This element is found at the bottom of the wall panel (bottom wall beam) for the second floor. It is therefore connected to the floor joists between the two floors. As in the case of strong-axis shear, the effective length of the profile does not have an effect on the capacity of the profile. Figure 47 shows the critical element. The shear envelope for weak-axis shear is shown in Figure 48.

Stellenbosch University http://scholar.sun.ac.za

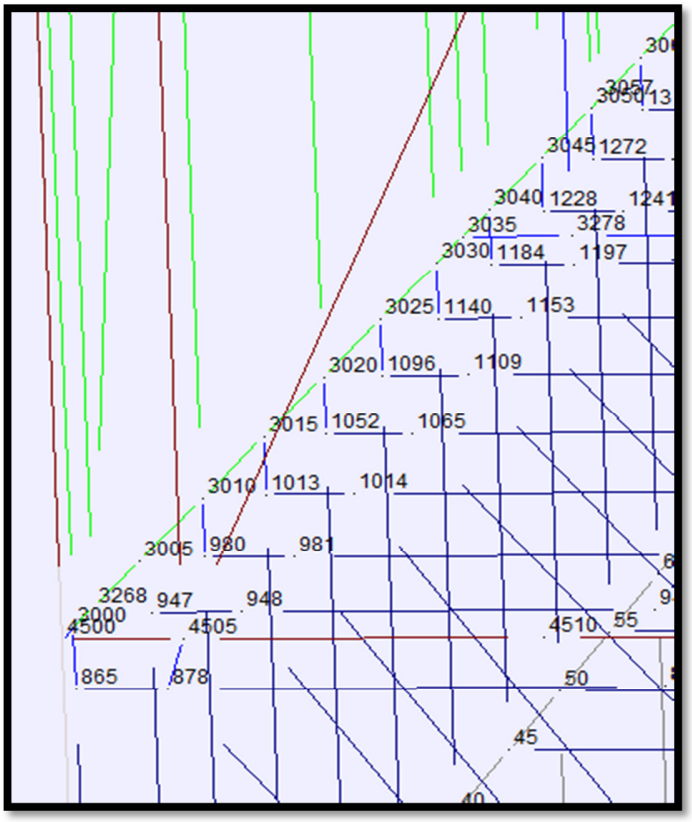

Figure 47: Critical element for weak – axis shear

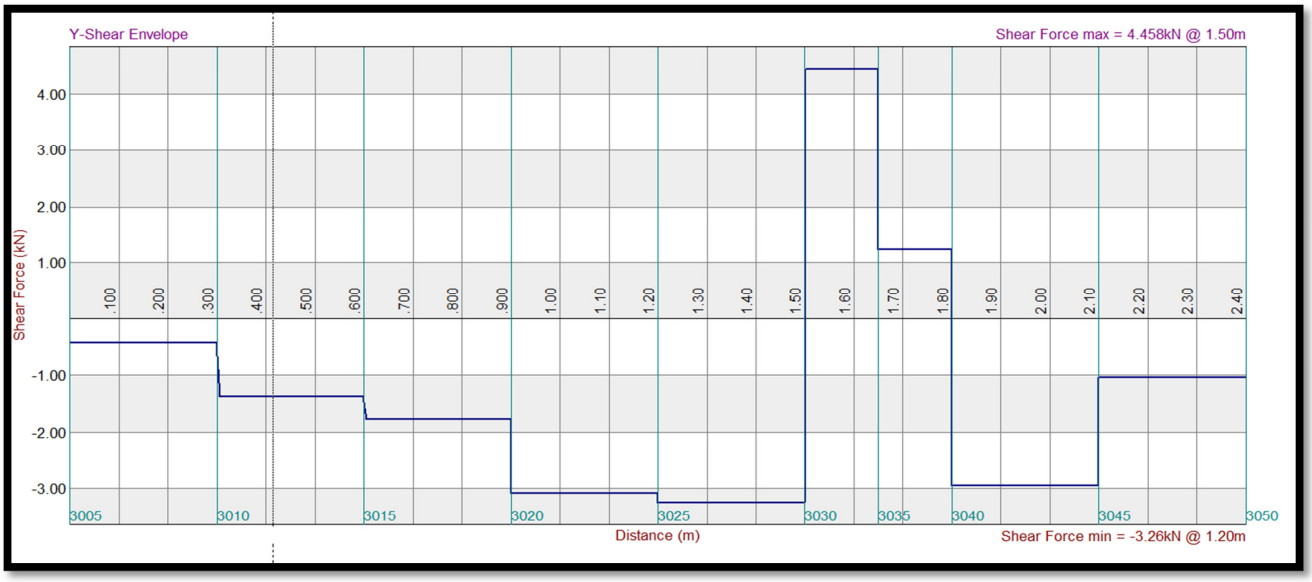

Figure 48: Shear envelope for the most critical element in weak-axis shear

Stellenbosch University http://scholar.sun.ac.za

6.7.4 Tensile force

The fourth failure mode that was investigated was the failure mode of an element in tension. The capacity of an element in tension normally depends on the capacity of the connections used in that element. For this chosen structural model it is no different. It can therefore be said that by identifying the element with the biggest tension force (and by still considering the shear force in that element), often the biggest load on a connection is also identified. As mentioned earlier, the structural analysis program used will give a tension force as a negative value. The tension capacity of the profile will therefore be dependent on the thickness and yield stress of the profile as well as the type of connection used. All the profiles used in the structural model have the same profile parameters. From the analysis performed it was identified that element 707 – 713 – 719 – 731 had the largest tension force of 16.93 kN. This element is a bracing element found in one of the walls of the ground floor. It can be seen that this element has a connection to the beam running on the concrete floor. The critical element is shown in Figure 49. The tension envelope for the critical element is shown in Figure 50.

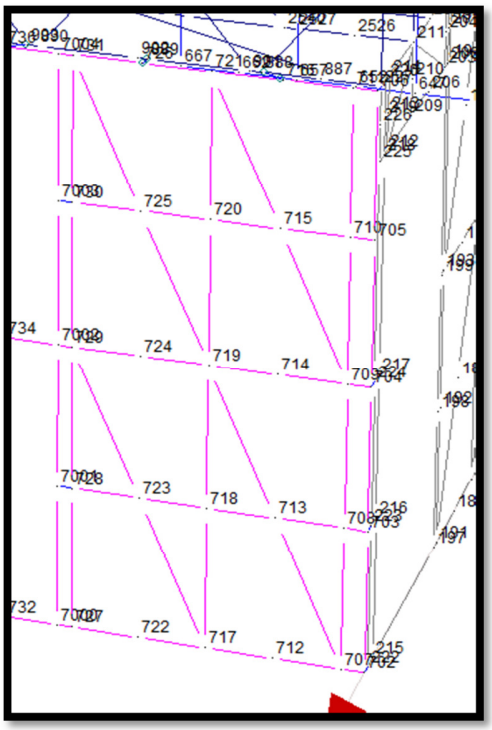

Figure 49: Critical element for the failure mode of tension

Stellenbosch University http://scholar.sun.ac.za

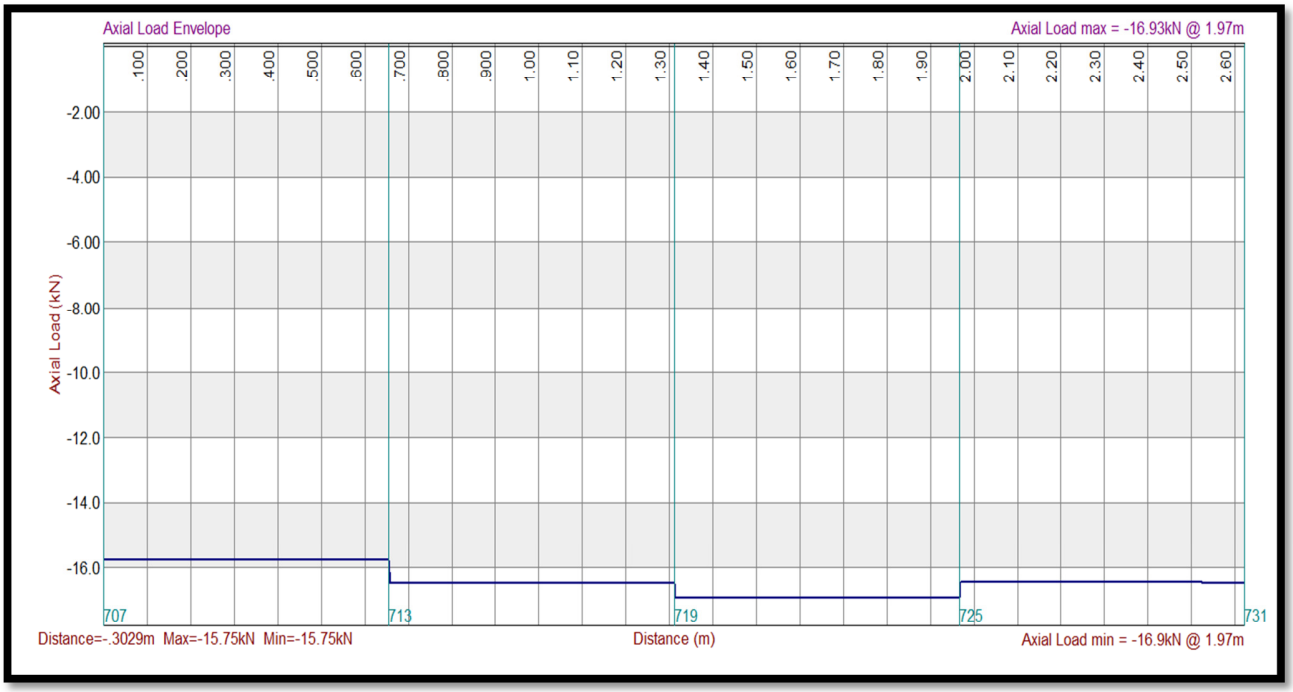

Figure 50: Tension envelope for critical element

6.7.5 Bi-axial bending with axial force

The fifth failure mode that was investigated is the failure mode where a structural element is subjected to bi-axial bending as well as an axial load. It is safe to say that all structural elements in the chosen structural model will be subject to either a moment in one direction and an axial force or bi-axial bending. Some of the elements will be subjected to bi-axial bending as well as an axial load. It is believed that these elements will be the most critical elements. It is of utmost importance that the effective length of a specific element is taken into account when deciding if the element can be seen as critical or not. A slender element with small loads can be more critical than a short element with bigger loads. It is therefore necessary to find the element with the most critical combination of effective length, bi-axial bending as well as an axial load for the specific failure mode. A spread sheet was developed to calculate the biggest combination between the three forces induced on certain structural members. From the structural analysis and spread sheet it was possible to identify element 7000 – 7001--7004 as the most critical element for the specified failure mode. This element is a wall column on the ground floor of the structural model.

Stellenbosch University http://scholar.sun.ac.za

The element forces in the element are as follow:

Axial = 12.54 kN

M_x = 0.267 kNm

M_y= 0.163 kNm

The element has effective lengths as follows:

L_x = 2400 mm

L_y = 600 mm

L_z = 600 mm

For the failure mode there will be a total of three envelopes present as shown in Figure 52 to Figure 54.

The critical element is shown in Figure 51.

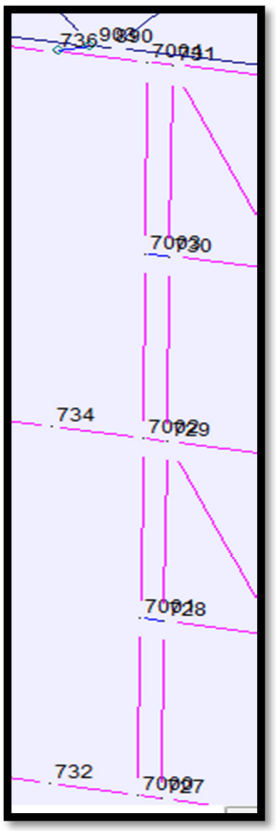

Figure 51: Critical element for the failure mode of bi-axial bending and axial load

Stellenbosch University http://scholar.sun.ac.za

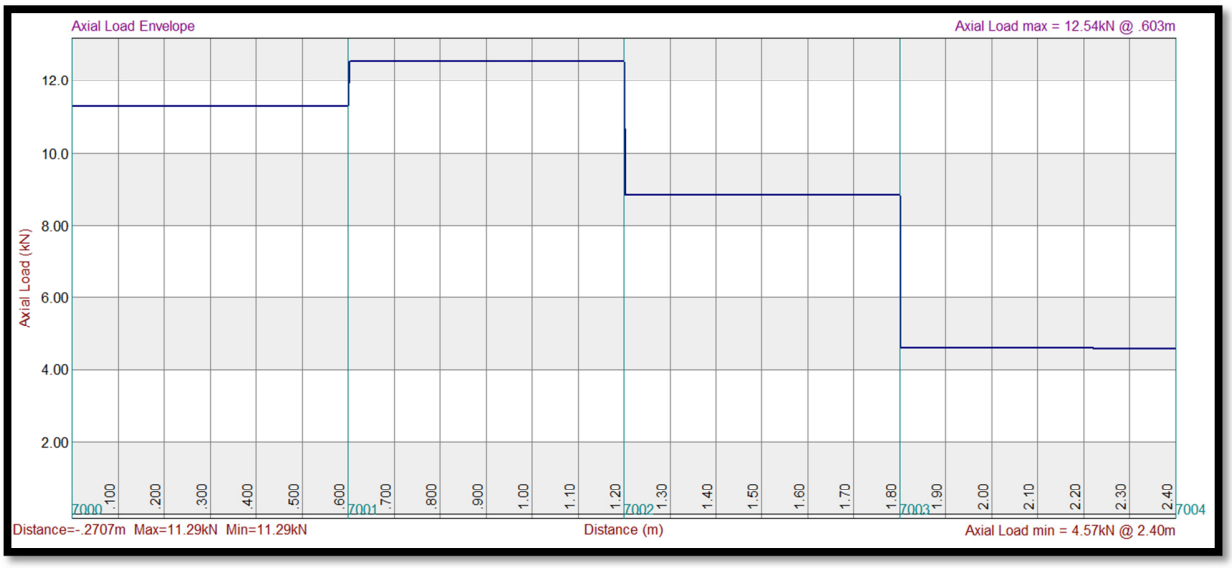

Figure 52: Axial load envelope for critical element

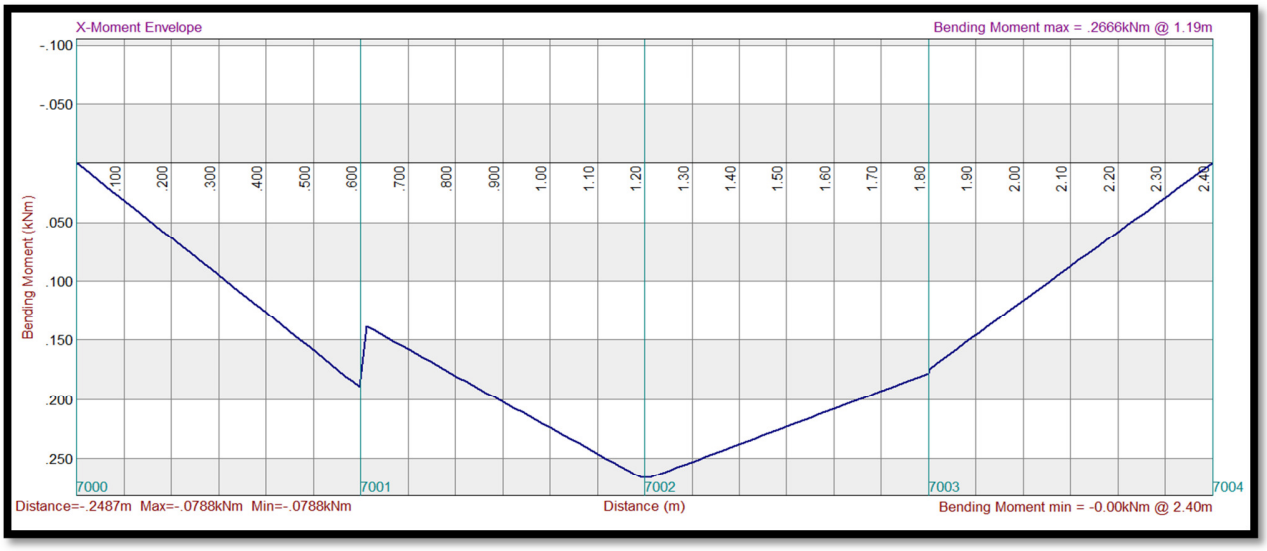

Figure 53: Envelope for strong-axis bending of critical element

Stellenbosch University http://scholar.sun.ac.za

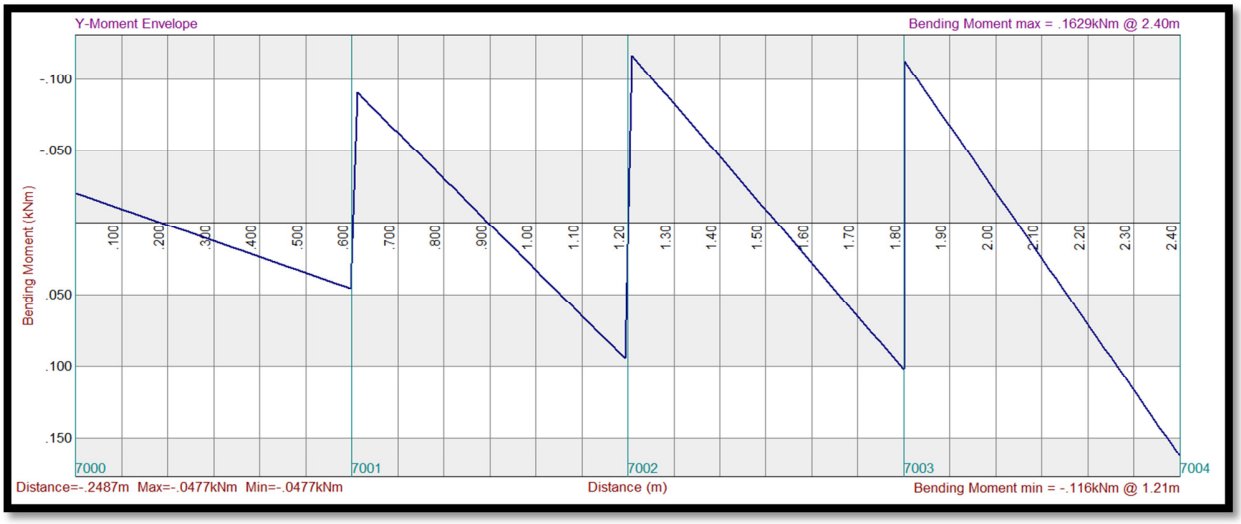

Figure 54: Envelope for weak-axis bending of critical element

6.8 Concluding remarks

The chosen structural model as described in Chapter 6.1 to Chapter 6.7 is based on a deterministic design approach. The loads that act on the structure were obtained from the relevant design codes and were seen as deterministic. By referring to Chapter 6.5, it can be seen that the analysis was done, using deterministic factored characteristic load values from the relevant code, SANS 517:2009.

This typical structure was designed to fulfil code requirements. The aim is now to evaluate the implied reliability achieved for this structure, as a first indication of the sufficiency of the codes' design provisions. This is discussed in Chapter 8.

Stellenbosch University http://scholar.sun.ac.za

7. Development of Excel spread sheets to perform resistance calculations

The resistance or capacity calculation for any thin walled cold formed section needs to be done according to the new SANS 10162-2:2010, which is based on the Australian design code AS/NZ 4600: 2005. The equations found in these codes to calculate the resistance of a certain profile is based on a resistance model with further model uncertainty. Included in these equations are the different characteristic material properties of the profile as well as material partial factors. The resistance calculations of cold formed steel members are often very time consuming. This is due to the fact that the effective area of the profile that can be used in the resistance calculations is often less that the cross – sectional area of the profile. It is therefore necessary to first determine the effective area before the actual resistance calculations can be done. This is done using the Effective Width Method (EWM), which is discussed in Chapter 3.1. Spread sheets were developed to perform the necessary resistance calculations.

When referring back to Chapter 3.2, it can be seen that there are several buckling modes that are possible for a certain profile. Before the correct resistance value for a certain failure mode can be calculated, the correct buckling mode for the specific effective length of the profile under consideration must be found. This can be done by using the CSFUM software package as discussed in Chapter 3.2.1 and Appendix A: User manual for the use of CSFUM.

The resistance calculations for the failure modes as described in Chapter 6.7 will be discussed below.

7.1 Axial load calculations

The first resistance that needs to be calculated is the resistance of the S8995 profile due to axial load only. Looking at the critical structural element for axial loading as discussed in Chapter 6.7.1, it can be recalled that the effective lengths are as follows:

$L_{ey} = 600$ mm

$L_{ez} = 600$ mm

Stellenbosch University http://scholar.sun.ac.za

$L_{ex} = 2400$ mm

Using the CSFUM software it is possible to determine the generated stress distribution for the structural element under consideration as shown in Figure 55.

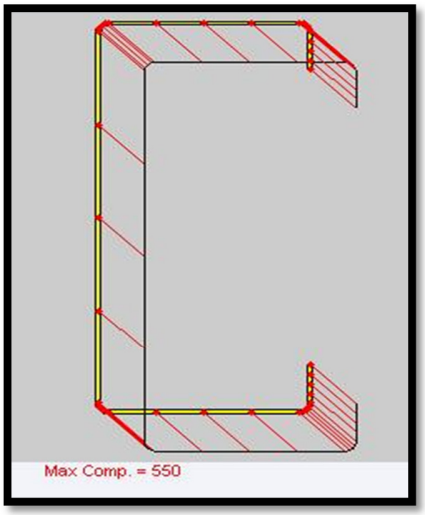

Figure 55: Generated stress distribution for axial load

By performing a finite strip analysis (Schafer, September 2006) with CSFUM it is possible to determine the half wave lengths where each of the buckling modes as described in Chapter 3.2 occurs.

Stellenbosch University http://scholar.sun.ac.za

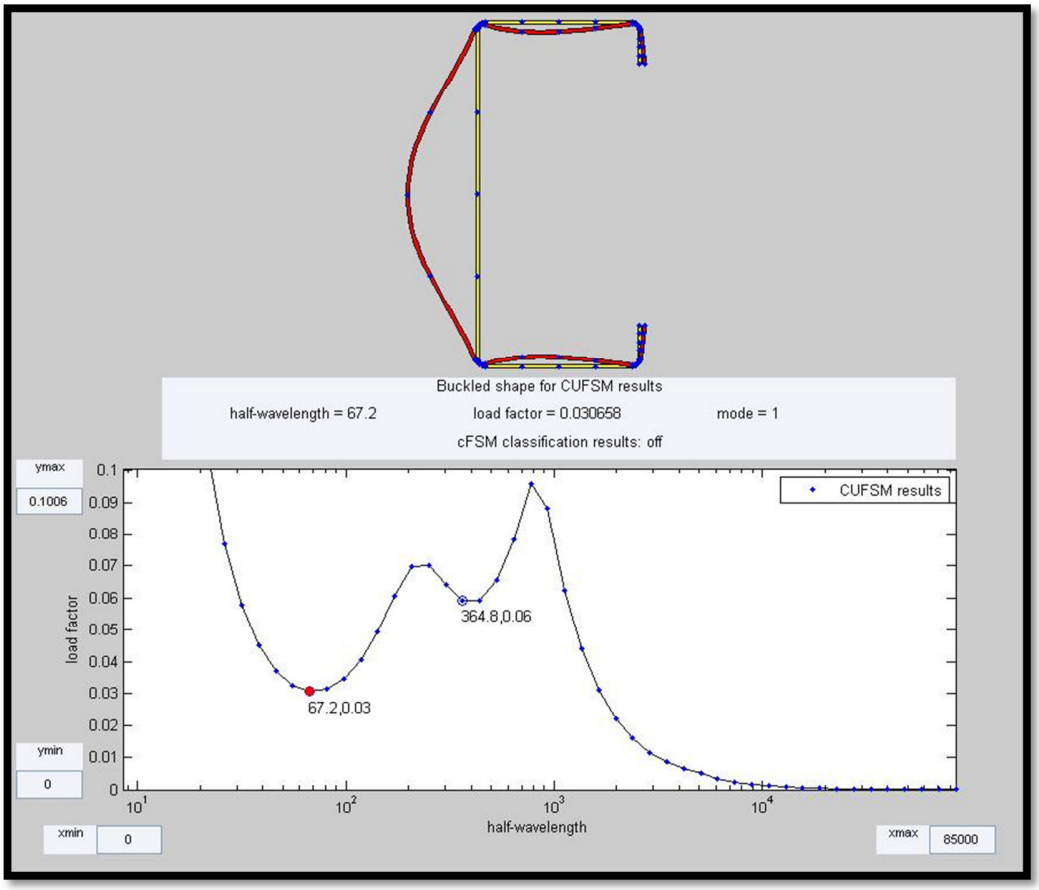

Figure 56: Buckling modes of the S8995 profile under pure axial load

Looking at Figure 56, it can be seen that the local buckling mode occurs at a half wave length of 67.2 mm. The distortional buckling mode will occur at a half wave length of 364.8 mm. Also from Figure 56, it is clear that local buckling will occur at a lower axial load than distortional buckling. The resistance calculations must therefore be based on local buckling failure.

Detailed resistance calculations for axial load can be seen in Appendix E: Detailed axial load calculations. A summary of the values will be given below.

For the critical stress f_n

$f_n = 282.4$ MPa

$A_e = 117.39$ mm^2

$N_c = 33.15$ kN

Stellenbosch University http://scholar.sun.ac.za

For the yield stress f_y

$f_y = 550$ MPa

$A_e = 91.92$ mm^2

$N_s = 50.57$ kN

By multiplying the smallest of N_c (Nominal member capacity) and N_s (Nominal section capacity) with the reduction factor $\phi = 0.9$. The axial resistance of the S8995 with the given effective lengths is obtained as 29.84 kN.

Note that all the calculations given in Appendix E: Detailed axial load calculations are based on the critical stress $f_n = 282.4$ MPa. The critical stress is based on the effective length of the element under consideration, obtained from clause 3.4.1 of SANS 10162-2010.

7.2 Strong-axis shear calculations

The shear capacity of the chosen profile, S8995, was calculated according to clause 3.3.4 of SANS 10162-2:2010. A spread sheet with the detailed design of the profile shear capacity can be found in Appendix F: Detailed calculation of shear capacity. The shear capacity of the profile about the strong axis is dependent on the thickness and width of the web of the profile under investigation.

The characteristic shear capacity about the strong axis was calculated to be 9.31 kN. By multiplying this value with the reduction factor $\phi = 0.9$, the design capacity of the S8995 profile was calculated to be 8.38 kN.

7.3 Weak-axis shear calculations

The same clause and spread sheet was used to calculate the design capacity of the S8995 profile for shear force about the weak axis than what was used in Chapter 7.2. The only difference is that the shear force resistance about the weak axis will be provided by the flanges of the profile. The characteristic shear capacity was calculated to be 10.11 kN. By multiplying this value with the reduction factor $\phi = 0.9$, the design capacity of the S8995 profile was calculated to be 9.1 kN.

Stellenbosch University http://scholar.sun.ac.za

7.4 Tension capacity calculations

As mentioned in Chapter 6.7.4, the tension capacity of the S8995 profile was determined by the capacity of the connection. Element 707 – 731 had the biggest tensile force in the chosen structural model. This element serves as a K-bracing component in the chosen model. To ensure that the connection had the necessary capacity a combination of screwed and bolted connections were used for this connection. A presentation of the connection is showed in Figure 57.

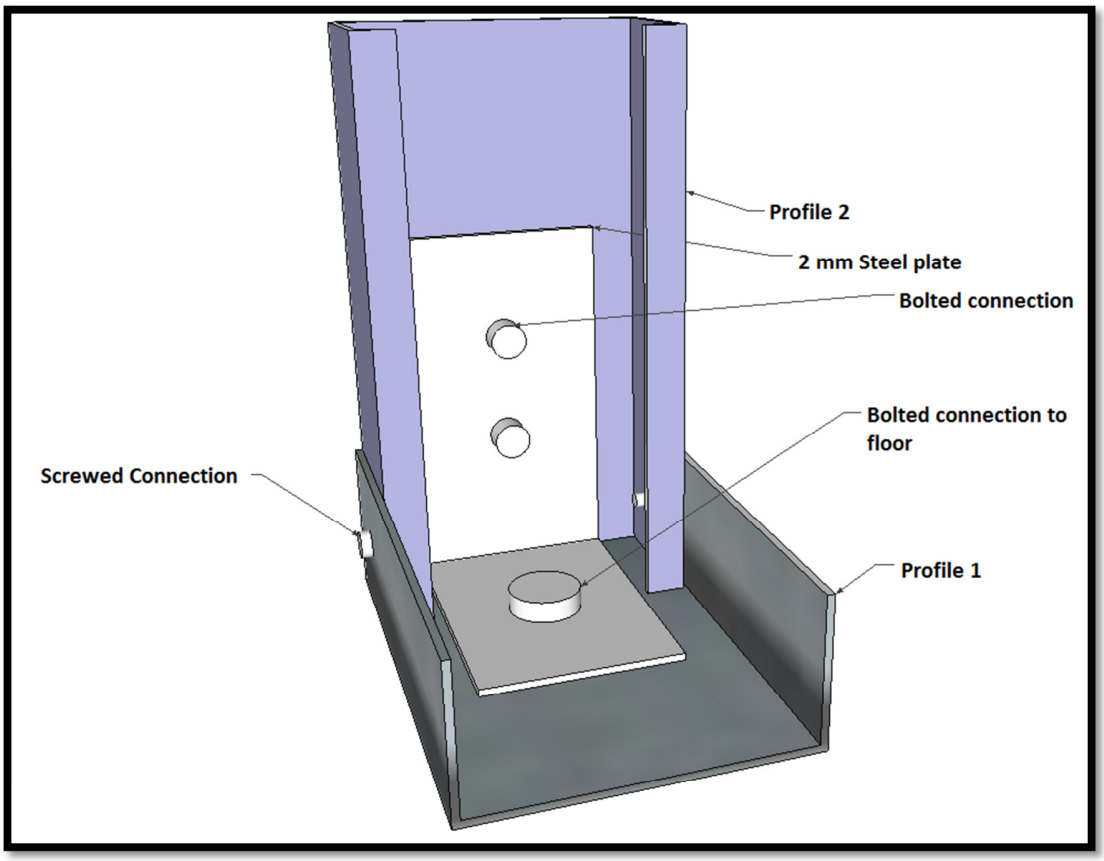

Figure 57: Combination of connections used

Mr Andries van der Merwe from the University of Stellenbosch developed spread sheets to determine the capacity of connections between cold formed steel sections in 2010 (Van der Merwe, 2010). These spread sheets will be used to calculate the capacity of a specific chosen connection in the structural model. A combination of the capacity of a screwed and bolted

Stellenbosch University http://scholar.sun.ac.za

connection has to be used to determine the end capacity of the connection shown in Figure 57. The capacity of the bolted connection on its own will be 13.19 kN and that of the screwed connection 4.71 kN. The end capacity of the connection was calculated to be 17.9 kN. Detailed calculations can be found in Appendix G: Detailed Tensile capacity calculations.

It must be noted that for this research only the type of connection shown in Figure 57 will be investigated and evaluated. Seeing that many types of different connections are found in a LSFB, the results obtained in Chapter 10 for this specific connection is not necessarily representative of all cold formed connections.

7.5 Moment capacity about the strong axis

The fifth resistance calculation that was done is the bending resistance of the S8995 profile about the strong axis. Looking at the critical structural element for strong axis bending as discussed in Chapter 6.7.5, it can be recalled that the effective lengths are as follow

$L_{ex} = 2400$ mm

$L_{ey} = 600$ mm

$L_{ez} = 600$ mm

Using the CSFUM software it is possible to determine the generated stress distribution for the structural element under consideration when in bending around the strong axis as shown in Figure 58.

Stellenbosch University http://scholar.sun.ac.za

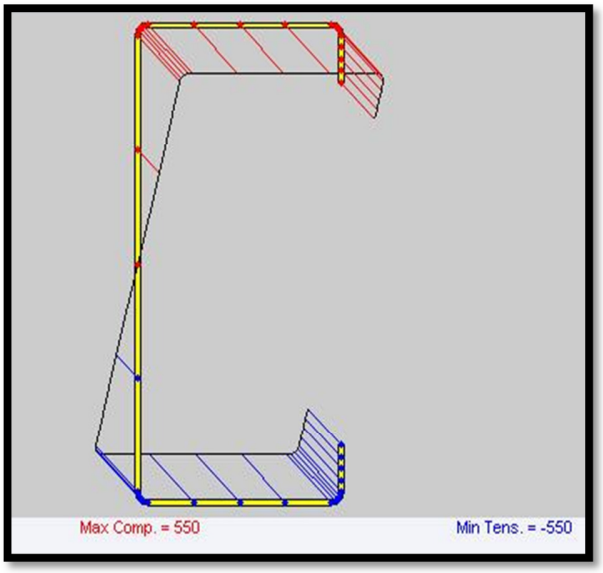

Figure 58: Generated stress distribution for bending about the strong axis

By performing a finite strip analysis with CSFUM it is possible to determine the half wave lengths for each of the buckling modes as described in Chapter 3.2.

Stellenbosch University http://scholar.sun.ac.za

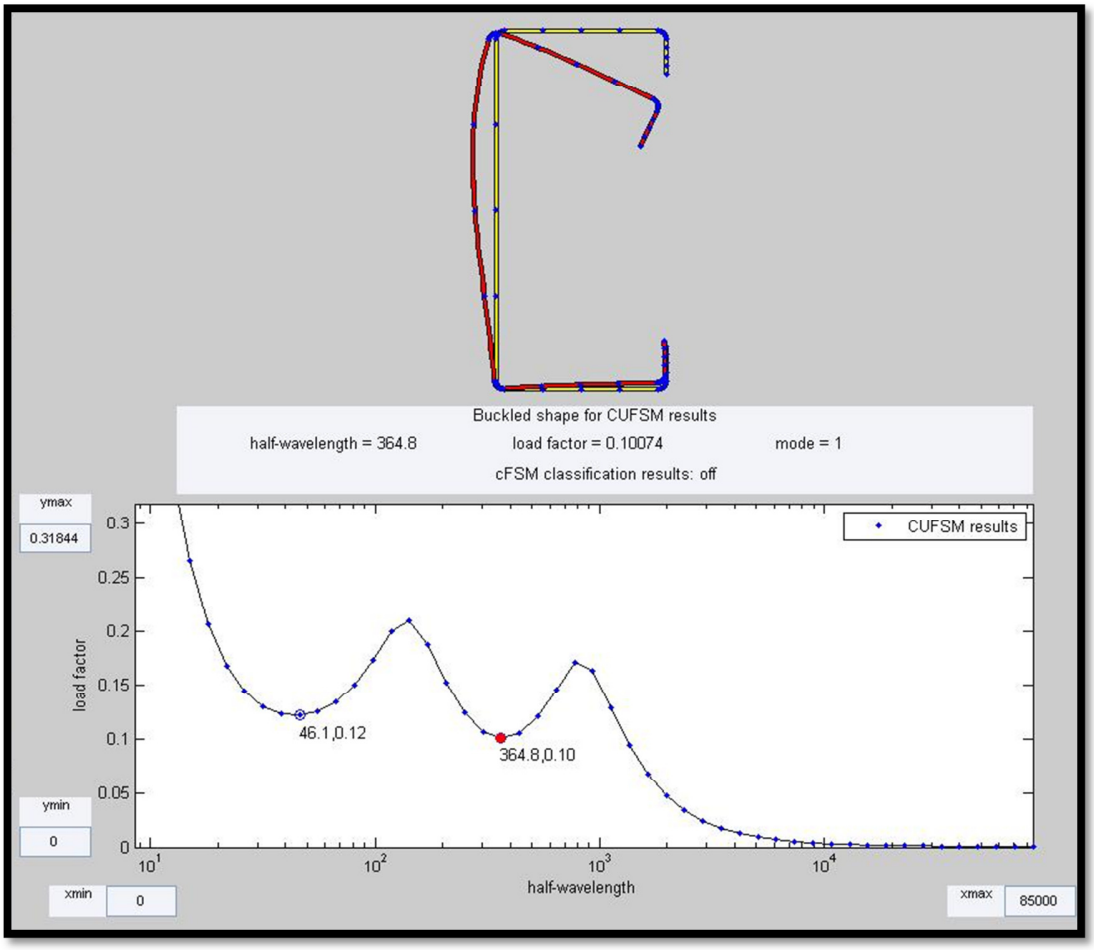

Figure 59: Buckling modes of the S8995 profile under bending about the strong axis

When looking at Figure 59, it can be seen that the local buckling mode occurs at a half wave length of 46.1 mm. The distortional buckling mode will occur at a half wave length of 364.8 mm. Although the local buckling mode occurs at a shorter half wave length than the distortional buckling mode, it can be seen that the distortional buckling mode will occur at a lower applied moment. The resistance calculations must therefore be based on distortional buckling failure.

Detailed moment capacity calculations for moments about the strong axis can be found in Appendix H: Detailed calculation of moments about the strong axis. A summary of the values are given below.

For the yield stress f_y

Stellenbosch University http://scholar.sun.ac.za

$f_y = 550$ MPa

$f_{od} = 355.87$ MPa

$M_c = 1.84$ kNm

The distortional buckling stress f_{od}, is calculated according to Appendix D of SANS 10162-2:2010. By multiplying M_c with the reduction factor of $\phi = 0.9$, the moment resistance of the S8995 with the given effective lengths was calculated as 1.66 kN.

7.6 Moment capacity about the weak axis

The critical element discussed in Chapter 6.7.5 will have bi-axial element forces. It is therefore necessary to determine the resistance of the S8995 profile against bending about the weak axis.

The generated stress distribution for the specific element that was obtained by using CSFUM software is shown in Figure 60. It can now be observed that there is a difference between the maximum compression and tension force. The change from compression to tension zone will take place through the centre line (neutral axis) in the Y-direction. Seeing that this line will be closer to the web of the profile, the stress distribution as shown is expected.

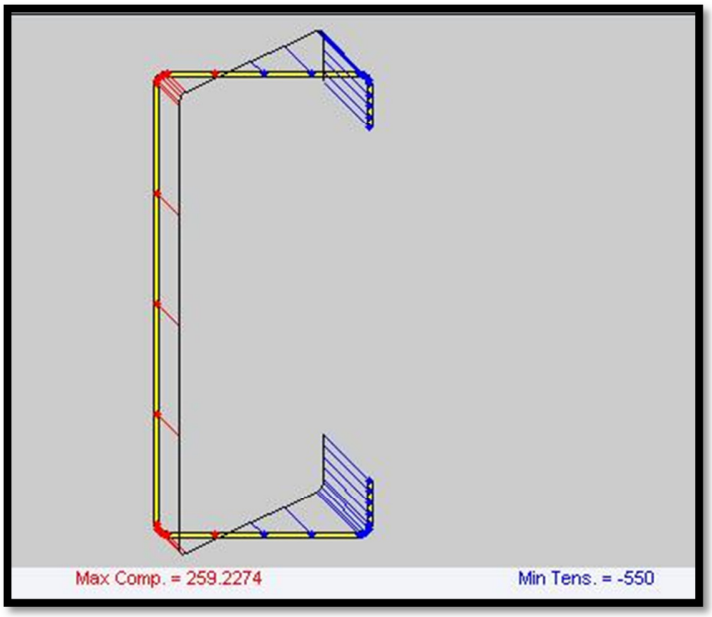

Stellenbosch University http://scholar.sun.ac.za

Figure 60: Stress distribution for bending about weak axis

By using the CSFUM software to perform a finite strip analysis it is possible to determine the half wave lengths where the different buckling modes will occur. These different buckling modes are shown in Figure 61.

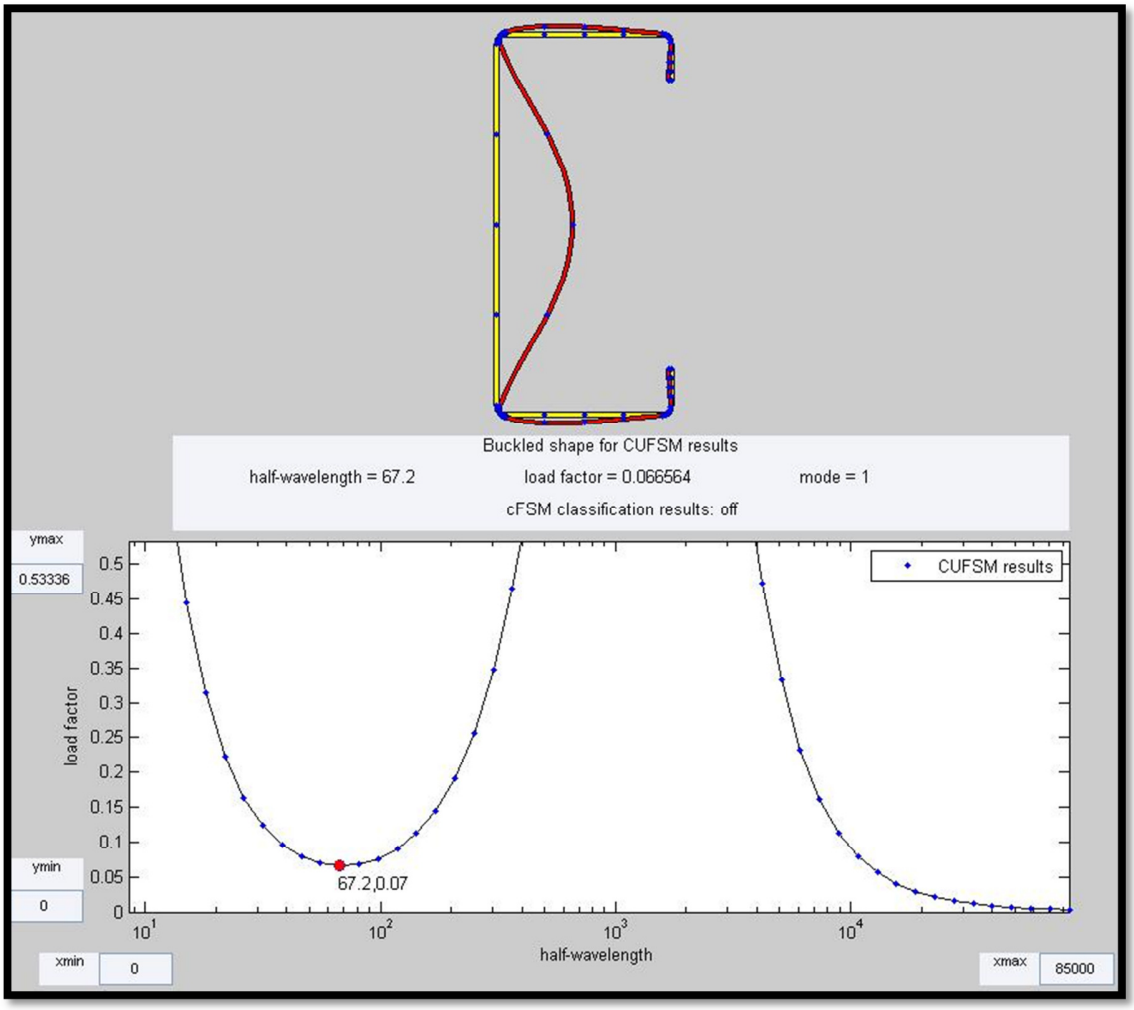

Figure 61: Buckling modes of the S8995 profile under bending about the weak axis

When looking at Figure 61, it can be seen that the local buckling mode will occur at a half wave length of 67.2 mm. The resistance calculations of the S8995 profile about the weak axis therefore

Stellenbosch University http://scholar.sun.ac.za

need to be based on local buckling failure. The effective lengths of the profile under consideration will be the same as discussed in Chapter 7.5.

Detailed moment calculations about the weak axis can be found in Appendix I: Detailed calculation of moments about the weak axis. In the calculations done, it was found that yielding of the tension flange occurs for the first time at an f_n value of 404 MPa. The calculated resistance moment for f_n is shown.

For $f_n = 404$ MPa

$M_{cy} = 0.715$ kNm

All the calculations, found in Appendix I: Detailed calculation of moments about the weak axis, will be done with $f_n = 404$ MPa. By multiplying the characteristic moment capacity with the reduction factor $\phi = 0.9$, it is possible to obtain the design value for bending about the weak axis as is obtained 0.644 kNm.

7.7 Interaction between axial loads and bending moments

For bi-axially loaded elements an expression must be found where the relationship between the interactions of bending and axial load is expressed. Clause 3.5.1 of SANS 10162-2:2010 provides such expressions which shall be satisfied by a member both in bending and under an axial load. These expressions are shown below

$$\frac{N^*}{\emptyset_c N_c} + \frac{C_{mx} M_x^*}{\emptyset_b M_{bx} \alpha_{nx}} + \frac{C_{my} M_y^*}{\emptyset_b M_{by} \alpha_{ny}} \leq 1 \qquad 77$$

$$\frac{N^*}{\emptyset_c N_s} + \frac{M_x^*}{\emptyset_b M_{bx}} + \frac{M_y^*}{\emptyset_b M_{by}} \leq 1 \qquad 78$$

Using equations 77 and 78 it is possible to determine if the element under investigation has sufficient resistance to withstand the combination of element forces applied to it.

Stellenbosch University http://scholar.sun.ac.za

7.8 Concluding remarks

In the deterministic design approach, the applied *structural* loading is taken as single deterministic values obtained from characteristic load values multiplied by partial factors. The *element* loadings are then correspondingly deterministic values that come from the structural analysis.

The element loading is then compared to the deterministic element capacity which is calculated from resistance equations using characteristic values and partial factors for material properties and geometry.

Loads, material properties and geometric design parameters are however not in practice single deterministic values. Instead, these are variables for which the actual value will be a realisation from a probability distribution.

The element reliability analysis attempted in Chapter 9 aims to evaluate the probability of failure for each critical element (which was deterministically designed according to code requirements) by taking into account the variability of the load process and the parameters that contribute to element resistance (geometry and material properties)

The development of the Excel spread sheets that were discussed this Chapter are based on a deterministic design approach. For the aim of the research done it is therefore necessary to develop probabilistic approaches to these spread sheets. To be able to obtain probabilistic design values for the different failure modes, distribution functions for the resistance (axial, moment, connections and shear) of the structural elements must be developed. The probabilistic design approach will be discussed in Chapter 9.

Stellenbosch University http://scholar.sun.ac.za

8. Probabilistic models and statistical parameters for loads acting on structural model

The deterministic design load in codified designs are typically specified as the characteristic value of the load, defined as a specified fractile of the underlying probability distribution of the load and adapted using partial factors to get the design value for the load. A detailed discussion of fractiles can be seen in Chapter 4.2.9. The fractile x_p for each relevant load is as follows:

Wind load

p = 0.98 according to clause 6.2.3 of SANS 10160-3:2009

The basic wind loads for which the structure is designed have a probability of exceedence of 0.02 (2 %).

Dead load

p = 0.5 (JCSS)

With p = 0.5, the mean μ will have the same value as p.

Live load

p = 0.95 (Varpasuo, August 2001)

The basic live loads for which the structure is designed have a probability of exceedence of 0.05 (5 %).

With this in mind, it is now possible to determine statistical parameters such as the mean μ, standard deviation σ and the coefficient of variation (COV) for the loads acting on the structural model. This section will focus on the determination of the relevant distribution functions as well as the statistical parameters of importance.

Stellenbosch University http://scholar.sun.ac.za

8.1 Distribution functions for loads applied to structural model

As mentioned in Chapter 6.3, the loads acting on the structural model can be divided into three categories namely: live loads (LL), permanent loads (DL) and wind loads (WL). Each of these loads will contribute to the overall load E(**X**) in the performance function G(**X**). E(**X**) can be written as:

$$E(\mathbf{X}) = WL(\mathbf{X}) + DL(\mathbf{X}) + LL(\mathbf{X}) \quad 79$$

It must be noted that the equation above assumes WL(**X**), DL(**X**), LLF(**X**) and LLR(**X**) to be probabilistic variables. It is thus without any partial load factors or load combinations as described in the loading code SANS 517:2009, since these are only applicable in deterministic design.

For each of the three loads mentioned, a distribution function with its statistical parameters as input to the reliability analysis that is to follow. The type of distribution with its COV for each type of load can be found in articles published by the Joint Commission for Structural Safety (JCSS). The mean and standard deviation for each type of load will be case specific. As mentioned in the previous section, the values obtained from the loading code (SANS 517: 2009) are certain fractile values. With this fact known it is possible to determine the mean μ value for each load, explained in (Holicky, 2009). If the mean μ is known, it is possible to calculate the standard deviation σ if the COV is known according to equation 13:

$$\text{Cov} = \frac{\sigma}{\mu}$$

8.1.1 Permanent loads

Permanent loads will consist of the self-weight and dead load of the structural model. According to the JCSS, permanent loads will follow a Normal distribution function with a COV of 0.1. It was assumed that the own weight of the structure is deterministic. Although this may be seen as a very crude assumption it was based on the fact that the total dead load has less than 1 % influence on the element forces in the chosen structural model in Chapter 6. It is therefore believed that this assumption will make no difference to the final evaluation of the reliability index for the different failure modes discussed in Chapter 6.7. The only additional dead load on the structural model will be that of the ceiling and services imposed on the first floor. It was

Stellenbosch University http://scholar.sun.ac.za

decided that a characteristic load of 0.2 kPa would be applied. The value of 0.2 kPa can therefore be seen as the fractile x_p of the theoretical model. In the case of dead loads, $x_p = \mu$. The mean μ is therefore 0.2 kPa.

With the mean and COV known, it is possible to calculate the standard deviation σ for the additional dead loads on the structure, using equation 14, as 0.02 kPa. The Normal distribution of the additional dead load is shown in Figure 62.

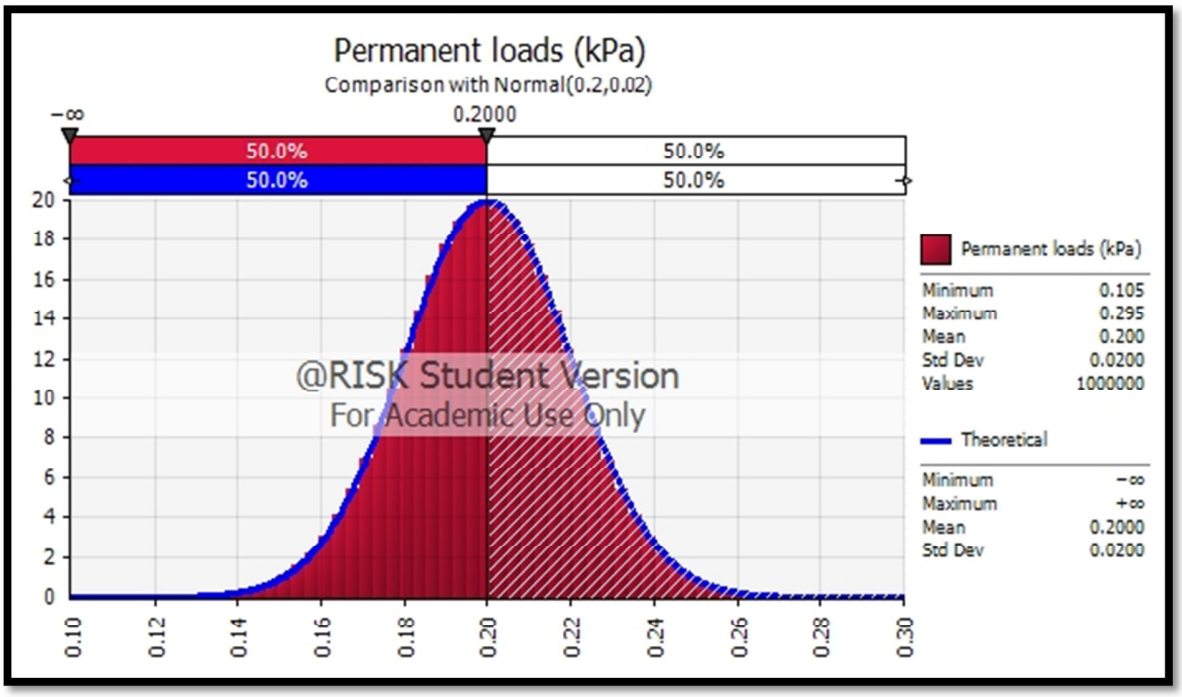

Figure 62: Normal distribution for permanent loads ($\mu = 0.2$ kPa, $\sigma = 0.02$ kPa)

8.1.2 Live loads

Live loads on the structural model will be seen as any type of loading that can be removed or added to the structure at any time. For the chosen structural model there will be an imposed load on the roof of 0.25 kPa. Furthermore there will be an imposed load of 1.5 kPa applied to the floor of the structural model. Both the live roof and floor loads are characteristic values according to the loading code for LSFB, SANS 517:2009 and can therefore be seen as the 95% fractile x_p of the theoretical model. According to JCSS live loads on structures will follow a Gamma distribution with a COV of 0.2. By referring back to Chapter 4.2.5, it can be seen that a Gamma distribution is

Stellenbosch University http://scholar.sun.ac.za

applied similarly as the Log-normal distribution with its lower bound at zero. The Gamma distribution differs from the Log-normal distribution by its skewness. The Gamma distribution will have a lower skewness of $\alpha = 2*COV$. It is therefore a more convenient distribution for describing variable actions with a small skewness, such as live loads. According to (Holicky, 2009) the fractile x_p can be expressed with the following equation when $0.2 \leq COV$

$$x_p = \frac{\mu}{\sqrt{1+COV^2}} \exp\left(u_p \sqrt{\ln(1+COV^2)}\right) \quad 80$$

Where $u_p = 1.746$ (Holicky, 2009)

Equation 80 can be rewritten to determine the mean μ as follows:

$$\mu = \frac{\left(x_p \sqrt{1+COV^2}\right)}{\exp\left(u_p \sqrt{\ln(1+COV^2)}\right)} \quad 81$$

From equation 81 it is therefore possible to calculate the mean for the floor load as $\mu = 1.083$ kPa and for the roof load as $\mu = 0.18$ kPa.

With the mean and COV known for both the floor load and the roof load it is now possible to determine the standard deviation σ for both loads from equation 13 as follows:

$\sigma_{floor} = 0.2166$ kPa

$\sigma_{roof} = 0.036$ kPa

The Gamma distribution for the floor and roof loads can be seen in Figure 63 and Figure 64 respectively.

Stellenbosch University http://scholar.sun.ac.za

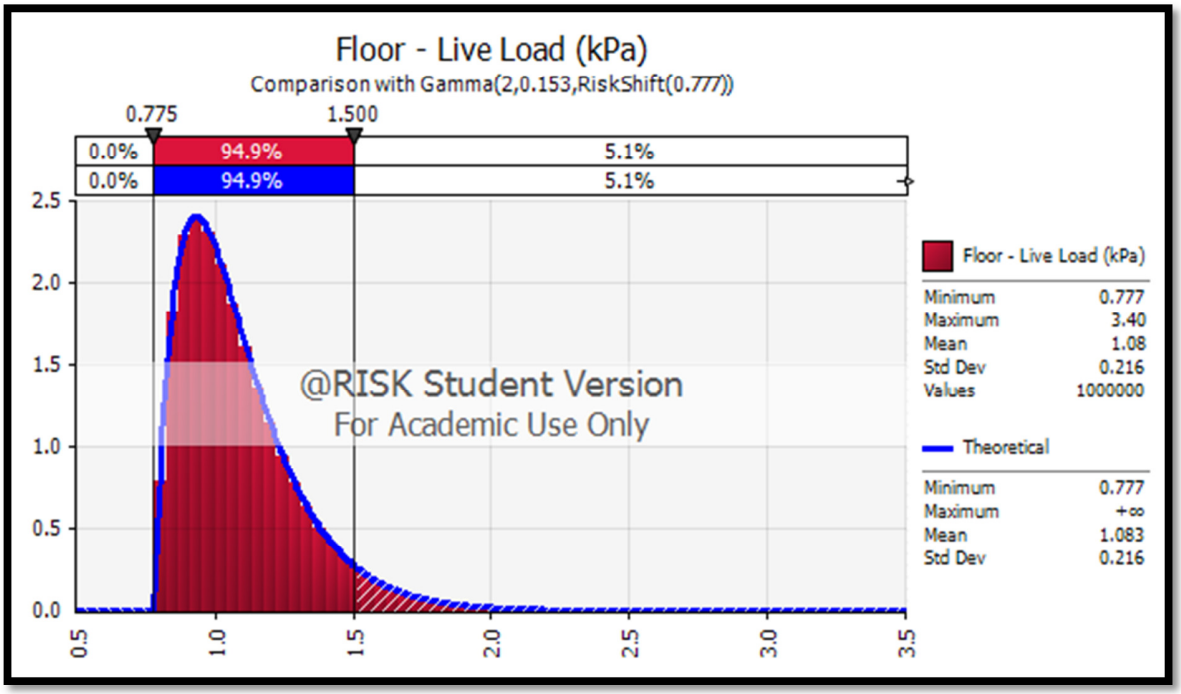

Figure 63: Gamma distribution for floor loads ($\mu = 1.083$ kPa, $\sigma = 0.216$ kPa)

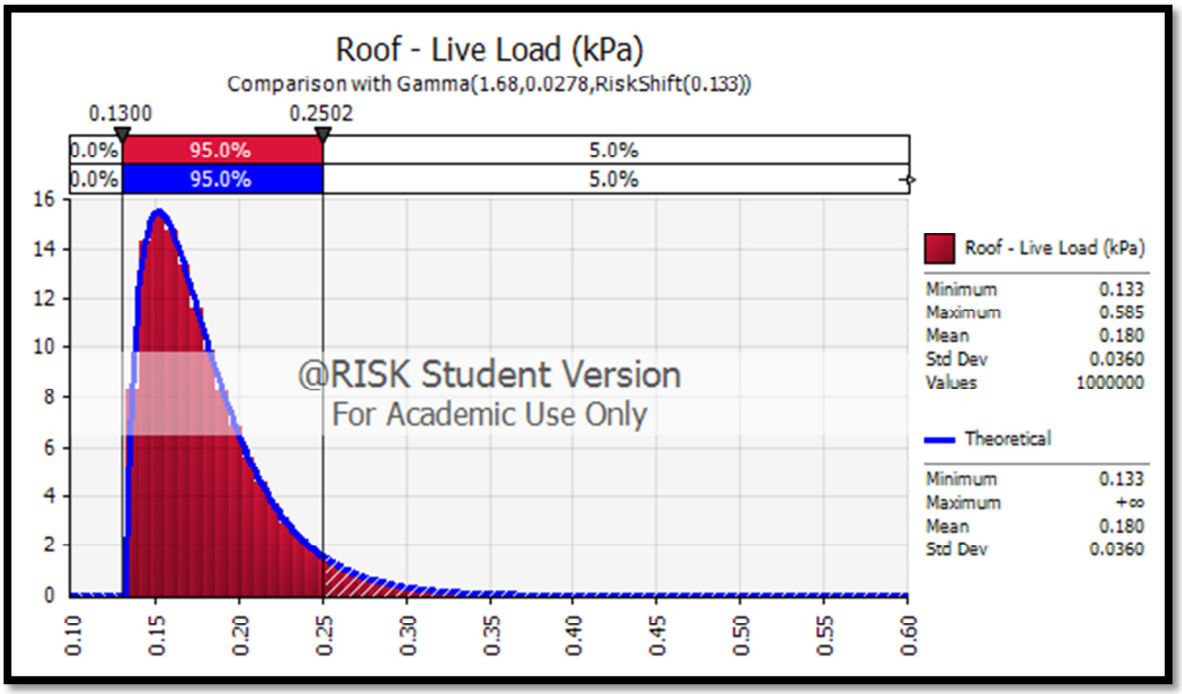

Figure 64: Gamma distribution for roof load ($\mu = 0.18$ kPa, $\sigma = 0.036$ kPa)

Stellenbosch University http://scholar.sun.ac.za

8.1.3 Wind loads

For LSFB the wind loads acting on the structures are the most critical load. Looking at the design code, SANS 517:2009, it is clear that any structure will have a number of wind pressure zones, influenced by a number of variables as described in Chapter 6.3.3. It will be assumed that all the variables will be deterministic, except for the basic characteristic wind speed, influencing the wind pressure. It is therefore necessary to determine the distribution function for the basic characteristic wind speed $v_{b,0}$. The distribution function obtained for the basic wind speed can then be applied to the rest of the wind force calculations to calculate the wind force for the structural model. From Chapter 6.3.3 it can be seen that the characteristic wind speed $v_{b,0}$ has a value of 28 m/s. Therefore the value of the 98% fractile x_p is 28 m/s. In the JCSS it is stated that wind loads will follow a Gumbel distribution with a COV of 0.37. According to (Holicky, 2009), the relationship between the mean μ and the fractile x_p can be represented by the following expression

$$x_p = \mu - (0.45 + 0.78\ln(-\ln(p)))\sigma \qquad 82$$

Where

$x_p = 28\ \text{m/s}$

$p = 0.98$

$\text{COV} = \frac{\sigma}{\mu}$

Therefore, rewriting the expression in terms of the mean μ

$$x_p = \mu - (0.45 + 0.78\ln(-\ln(p)))(0.37\mu) \qquad 83$$

Solving equation 83, brings the value of the mean basic wind speed $\mu = 14.289$ m/s

With the use of equation 14 it is possible to calculate the standard deviation σ for the basic wind speed to be 5.287 m/s. The Gumbel distribution for the basic wind speed is shown in Figure 65.

Stellenbosch University http://scholar.sun.ac.za

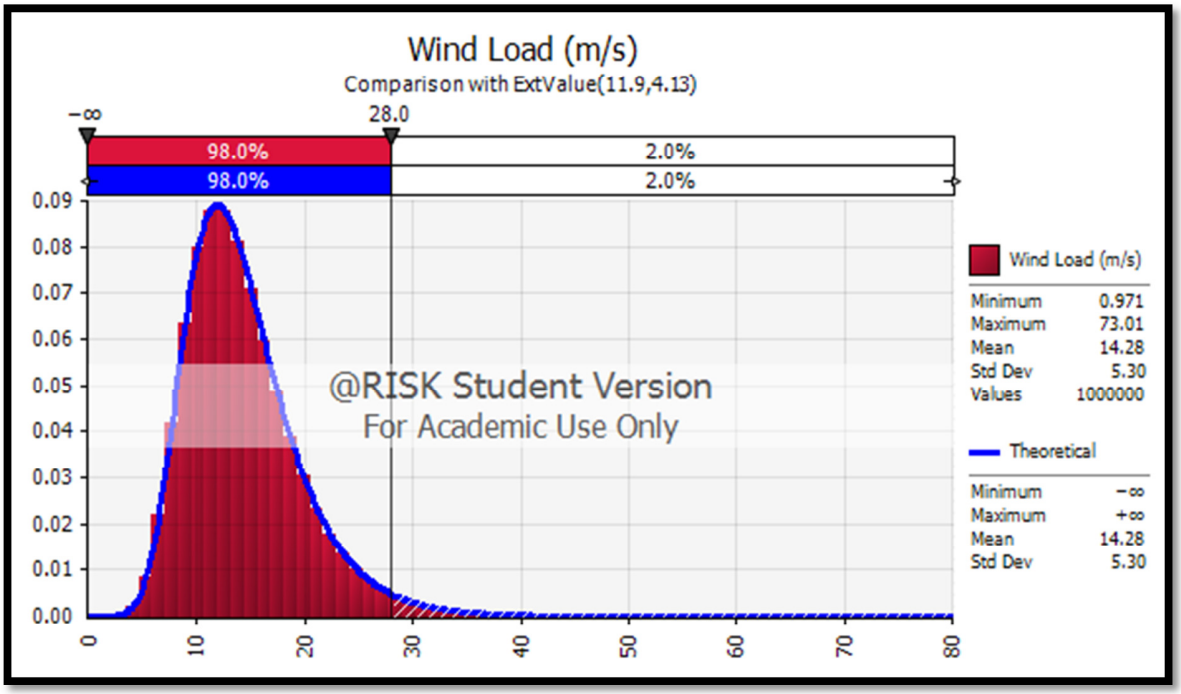

Figure 65: Gumbel distribution for basic wind speed ($\mu = 14.289$ m/s)

8.2 Concluding remarks

The distribution functions developed in Chapter 8.1.1 to Chapter 8.1.3 will serve as an important input to the FORM analysis that will be used in Chapter 10 to evaluate the reliability indices, of the critical elements.

Stellenbosch University http://scholar.sun.ac.za

9. Probabilistic models for the resistance of the structural elements

In Chapter 7 the development of Excel spread sheets to calculate the resistance of the S8995 profile for various failure modes were discussed. The profile parameters that influence the design capacity of a given profile can be summarized in the list below

- **Effective length of the profile**

  The dimensions of the chosen structural model are fixed and therefore it can be assumed that this parameter is deterministic.

- **Corner radius r_i**

  It can be said that the profile dimensions are mean values obtained from a certain amount of experiments done. From these experiments it is possible to fit a certain distribution function to each of the profile dimensions. The corner radius r_i of the profile will follow a Normal distribution (Chen & Young, 2006).

- **Profile thickness**

  The thickness of the profile will follow a Normal distribution (Schafer et al., 1998).

- **Yield stress of the steel used to form the profile**

  The yield stress of the profile will follow a log-normal distribution (Pham & Hancock, March 2009)

- **Width and height of profile**

  The width and height of the profile were taken as deterministic values. Although this may seem as a very crude assumption it was seen from the preliminary excel calculations that the thickness t and yield stress f_y of the profile had the biggest influence on the resistance capacity of the profile. Therefore the assumption made to use a deterministic value for all other profile parameters is reasonable, because their variability would have a small influence on the resistance capacity of the profile.

Stellenbosch University http://scholar.sun.ac.za

- **Modules of elasticity**

  It is assumed that the variability of the modules of elasticity for cold-formed sections will be very small. This value for this parameter is therefore assumed to be deterministic.

- **The boundary conditions of the profile**

  The boundary conditions of the profile under consideration could have a significant influence on the reliability index of all failure modes. However, further investigation and research will be necessary to quantify the variability of the boundary conditions. This investigation will not be done for this research. The variability of the boundary conditions is therefore not considered. From this assumption it is clear that an investigation into the connections of cold-formed sections needs to be conducted in future research. The evaluation of the tension capacity failure mode (governed by the connection) in this research is therefore very case specific and the results obtained can not be applied to connections of cold-formed sections in general.

From the capacity calculations performed in Chapter 7, it was observed that the capacity of cold-formed steel sections is mainly influenced by the thickness, yield stress and dimensions of the profile. It is therefore very important that these parameters are treated as probabilistic values, as they will have the biggest influence on the results obtained for the evaluation of the reliability index for each failure mode. The following three parameters will therefore be treated as probabilistic values:

- Yield stress (f_y)
- Corner radius properties (r_i)
- Profile thickness (t)

Deterministic design values were assigned to the other profile parameters.

The three chosen parameters will therefore each have a certain distribution function. From experiments done, statistical parameters such as the COV, μ and σ for each of these profile parameters are available from literature. The distribution functions are shown in Chapter 9.1 and serve as input to the FORM calculations that will be discussed in Chapter 10.

Stellenbosch University http://scholar.sun.ac.za

9.1 Distribution functions for chosen profile parameters

In this section the focus will be on the development of the distribution functions for the three chosen profile parameters as discussed above.

9.1.1 Yield stress (fy)

The yield stress of the S8995 profile will have a log-normal distribution with a COV of 0.031 (Pham & Hancock, March 2009)

The yield stress, f_y, value of 550 MPa that is used in the deterministic design approach is the 5% fractile of the distribution function for f_y (Pham & Hancock, March 2009). Thus 95% of profiles will have a yield stress exceeding this value.

The mean of the distribution function can be calculated by using the expressions developed in equation 80 and 81 in Chapter 8.1.2 for log-normal distributions. From these equations it is possible to obtain the mean $\mu = 578.56$ MPa for the yield stress. With the mean and COV known, the standard deviation σ can be calculated as 17.94 MPa from equation 13.

The distribution function is shown in Figure 66.

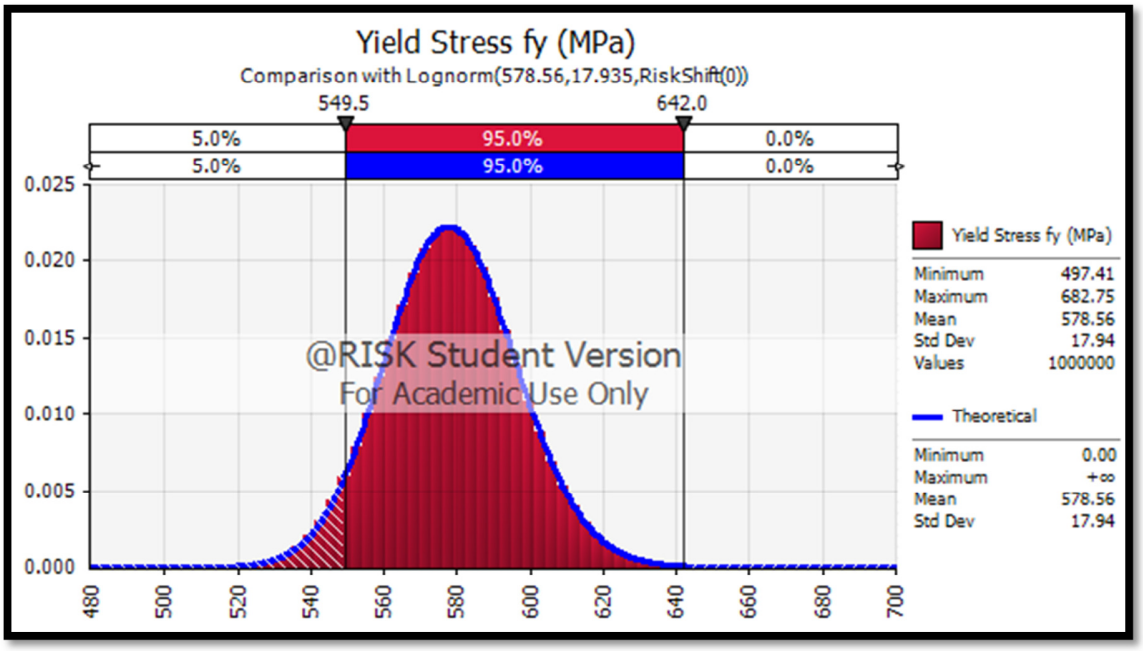

Figure 66: Log-Normal distribution for the yield stress ($\mu = 578.56$ MPa)

Stellenbosch University http://scholar.sun.ac.za

9.1.2 Corner radius (ri)

The corner radius for cold formed steel sections will follow a Normal distribution with a COV of 0.014 (Chen & Young, 2006). The characteristic value is equal to the 50 % fractile, i.e $\mu = x_p = 2$ mm. With the mean and COV known the standard deviation σ can be calculated to be 0.028 mm with equation 13. The Normal distribution for the corner radius is shown in Figure 67.

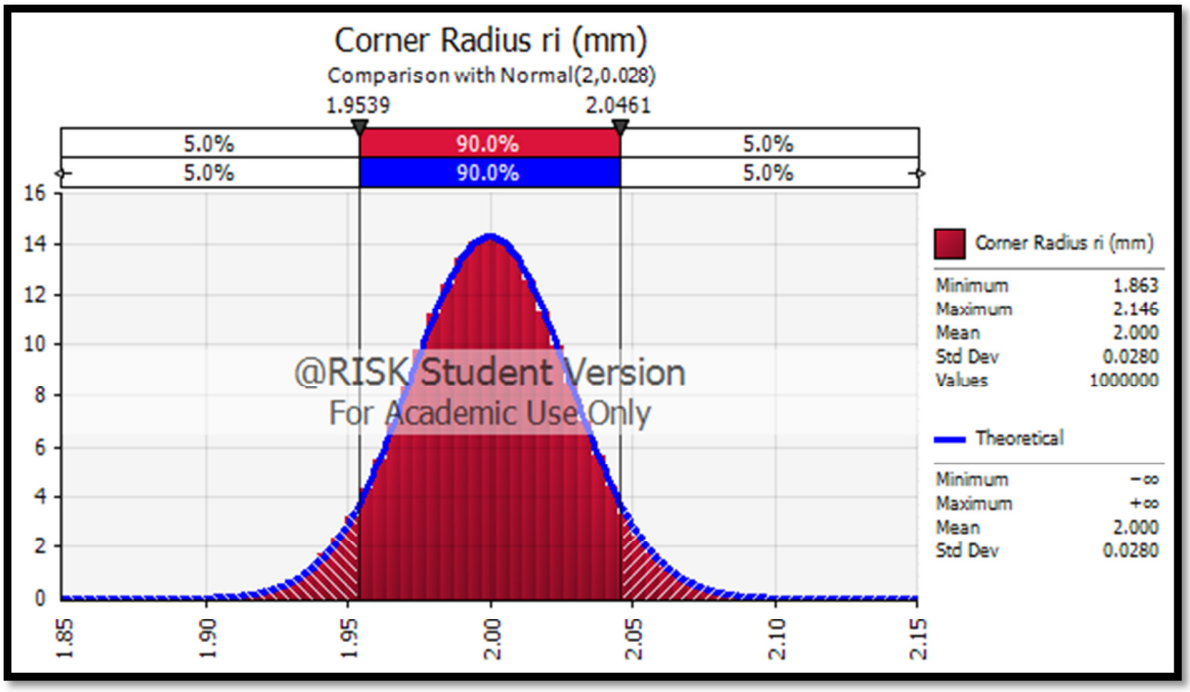

Figure 67: Normal distribution for the corner radius ($\mu = 2$ mm)

9.1.3 Thickness of profile (t)

As in the case of the corner radius, the thickness t of cold formed steel sections will also follow a Normal distribution with a COV of 0.053. (Schafer et al., 1998). The value of the mean μ will be equal to the deterministic design value $x_p = 0.95$ mm, resulting in a standard deviation 0.05035 mm.

Stellenbosch University http://scholar.sun.ac.za

The Normal distribution for the thickness of the profile can be seen in Figure 68 as shown on the next page.

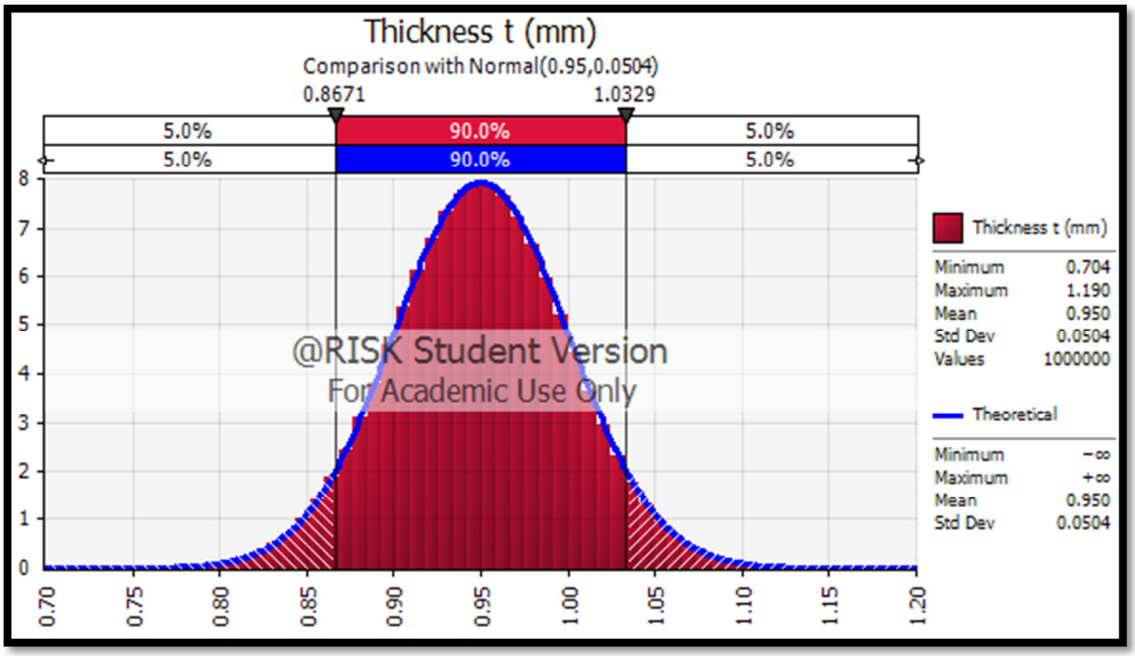

Figure 68: Normal distribution for the thickness (μ = 0.95 mm)

9.2 Distribution functions for resistance calculations

The design capacity of a profile against its different failure modes is dependent on the profile parameters. For three of these profile parameters a distribution function was assigned. The design capacity of the different failure modes therefore will now also follow a distribution function with statistical parameters such as μ, σ and COV. To estimate the distribution functions for the profile resistance to a given failure mode requires that the profile parameter uncertainty be propagated through the resistance model. For LSFB resistance calculations this is a highly non-linear process with complicated interactions. Analytical ways of obtaining the resistance distribution function is therefore unpractical. Monte Carlo simulation was used to propagate the input uncertainty through the Excel spread sheets that predict resistance, to obtain resistance distribution functions for each failure mode. This was done using the @RISK software package

Stellenbosch University http://scholar.sun.ac.za

which is an Excel based tool. The distribution functions that were obtained for each failure mode are shown for illustrative purposes. The reliability evaluations done in Chapter 10 will use the statistical parameters (such as the distribution type, μ and σ) of the resistance parameters (f_y, r_i and t). Seeing that the @RISK software is only capable to perform 100 000 MC simulations, it will imply that the tail end of the distribution functions shown in the next section will be inaccurate. However, it still gives a good idea of the distribution function for each resistance mode.

9.2.1 Distribution function for axial resistance

Three of the input parameters (f_y, t and r_i) were probabilistic. The @RISK software was used to propagate uncertainty associated to these parameters by implementing the MC simulation technique on the developed Excel spread sheets for calculating axial resistance. In this way it was possible to obtain the distribution function for axial load resistance of the S8995 profile.

Figure 69 shows the fitted Log-Normal distribution function, with $\mu = 33.53$ kN and $\sigma = 2.53$ kN, obtained from the MC simulations.

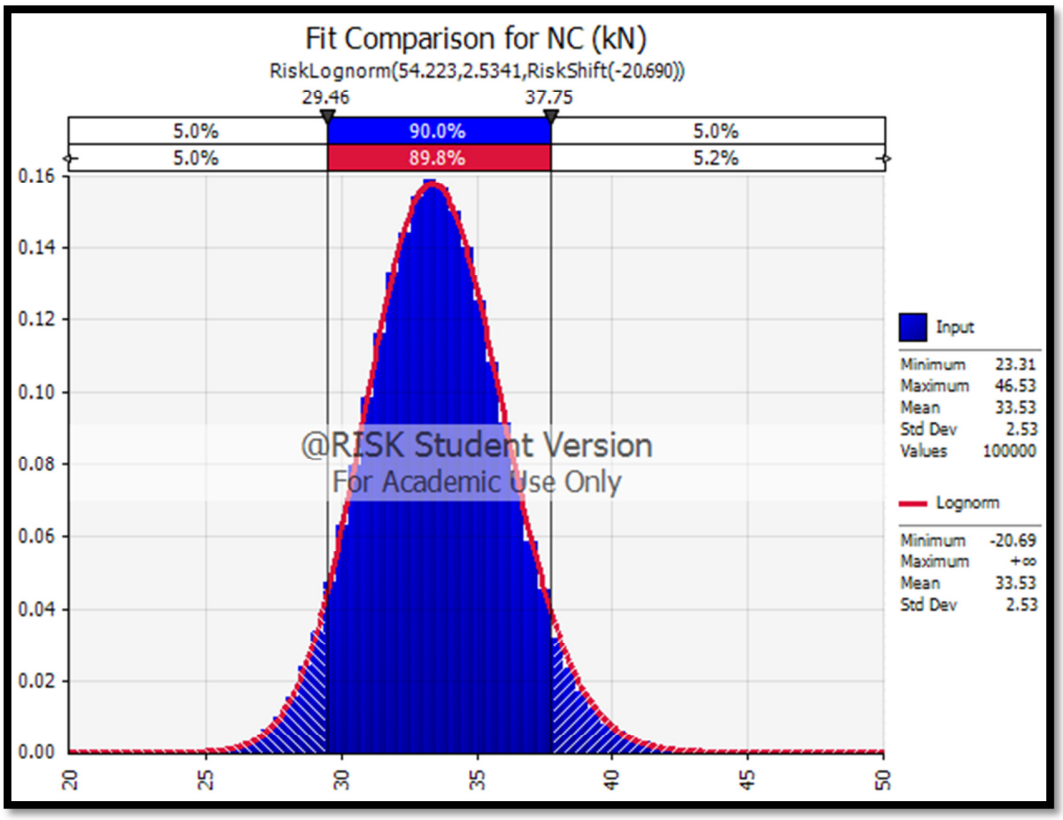

Stellenbosch University http://scholar.sun.ac.za

Figure 69: Fitted Log-normal distribution for the axial load capacity (μ = 33.53 kN, σ = 2.53 kN)

9.2.2 Distribution function for strong axis shear resistance

Applying the @RISK software to the developed spread sheets; it is possible to obtain a distribution function for the shear capacity about the strong axis of the S8995 profile. Figure 70 shows the MC output histogram for the predicted resistance. A Gamma distribution, with μ = 9.39 kN and σ = 1.49 kN, fits the output and can thus be used to describe this resistance.

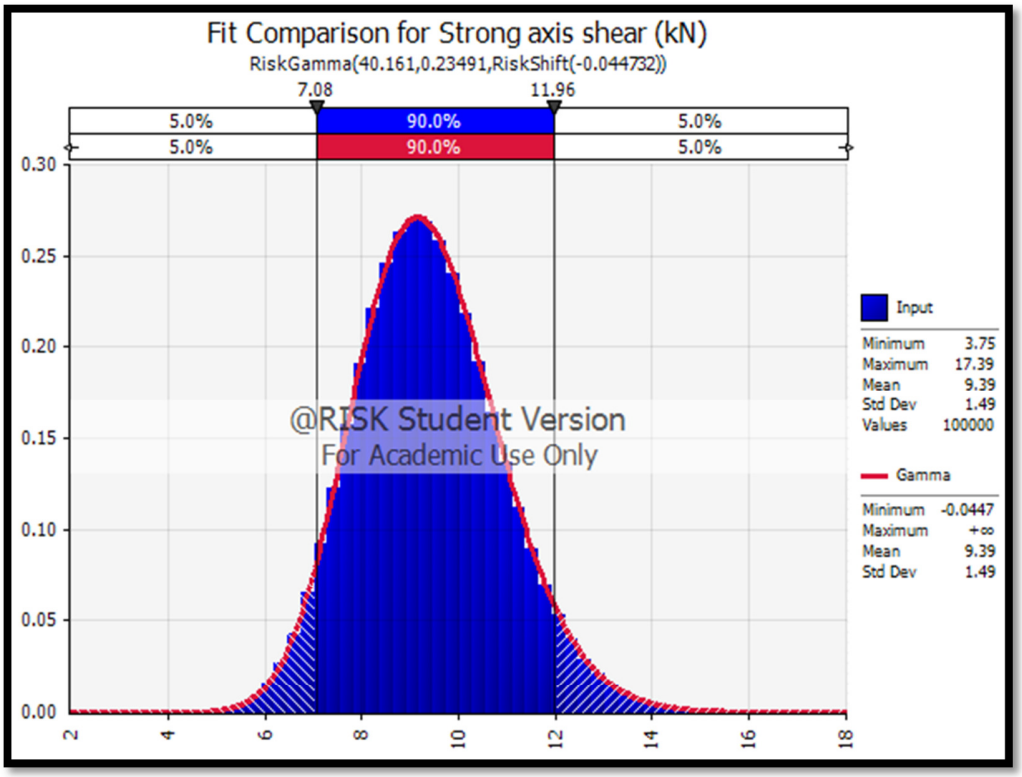

Figure 70: Fitted Gamma distribution for the shear capacity about the strong axis (μ = 9.39 kN, σ = 1.49 kN)

Stellenbosch University http://scholar.sun.ac.za

9.2.3 Distribution function for weak axis shear resistance

With the same steps used to obtain the distribution function for strong axis shear, it is possible to obtain the distribution function for weak axis shear as shown in Figure 71. Figure 71 shows the MC output histogram for the predicted resistance. A Gamma distribution, with $\mu = 10.19$ kN and $\sigma = 1.62$ kN, fits the output and can thus be used to describe this resistance.

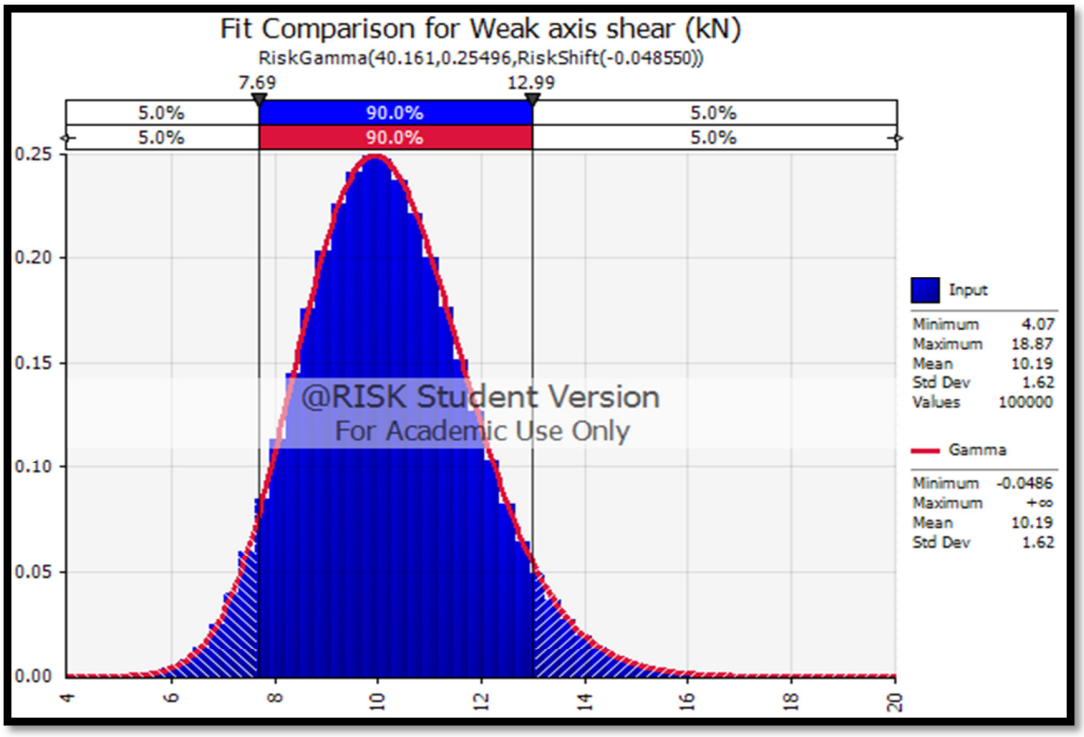

Figure 71: Fitted Gamma distribution for the shear capacity about the weak axis ($\mu = 10.19$ kN, $\sigma = 1.62$ kN)

9.2.4 Distribution function for tension resistance

By using MC simulation to propagate input uncertainty (t, r_i and f_y) through the developed Excel spread sheets the distribution function for tensile capacity of the specific chosen connection (shown in Figure 57) was obtained. A Log-normal distribution (with $\mu = 21.01$ kN and $\sigma = 1.05$ kN) fits the MC output as shown in Figure 72.

Stellenbosch University http://scholar.sun.ac.za

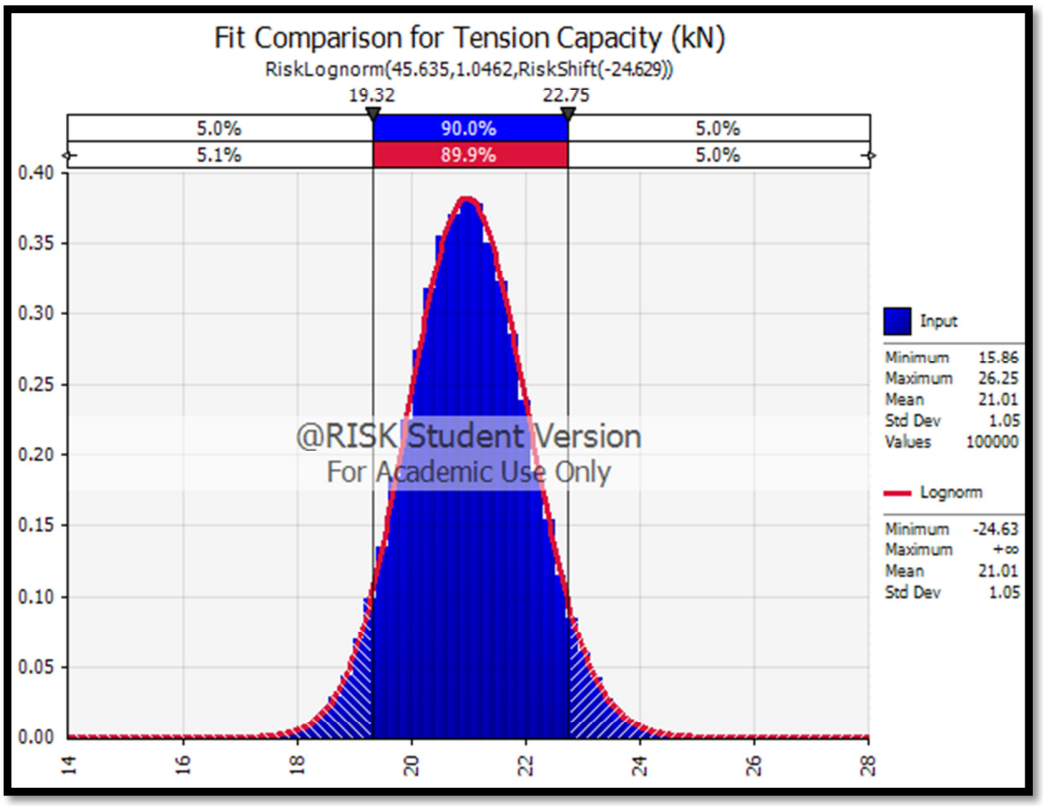

Figure 72: Fitted Log-normal distribution for tensile capacity ($\mu = 21.01$ kN, $\sigma = 1.05$ kN)

9.2.5 Distribution function for moment resistance about the strong axis

By using MC simulation to propagate input uncertainty (t, r_i and f_y) through the developed Excel spread sheets the distribution function for moment capacity about the strong axis was obtained. A Log-normal distribution (with $\mu = 1.898$ kNm and $\sigma = 0.103$ kNm) fits the MC output as shown in Figure 73.

Stellenbosch University http://scholar.sun.ac.za

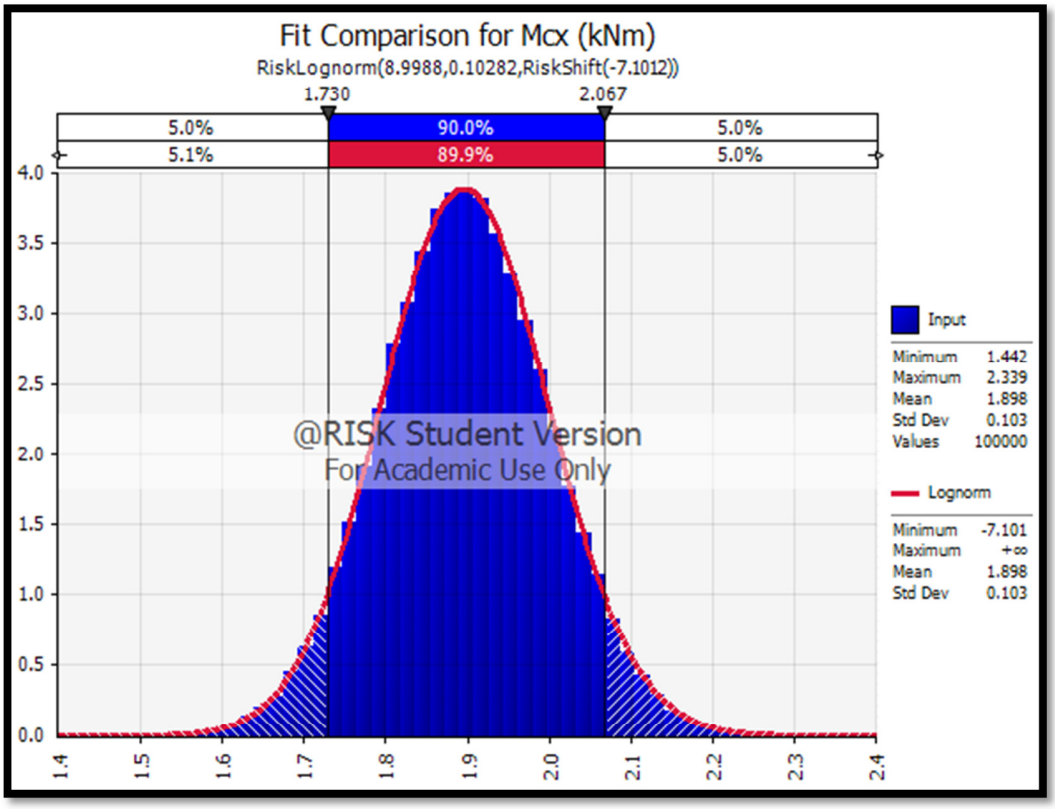

Figure 73: Fitted Log-normal distribution for moment capacity about the strong axis ($\mu = 1.898$ kNm, $\sigma = 0.103$ kNm)

9.2.6 Distribution function for moments resistance about the weak axis

By using MC simulation to propagate input uncertainty (t, r_i and f_y) through the developed Excel spread sheets the distribution function for moment capacity about the weak axis was obtained. A Log -normal distribution (with $\mu = 0.752$ kNm and $\sigma = 0.0474$kNm) fits the MC output as shown in Figure 74.

Stellenbosch University http://scholar.sun.ac.za

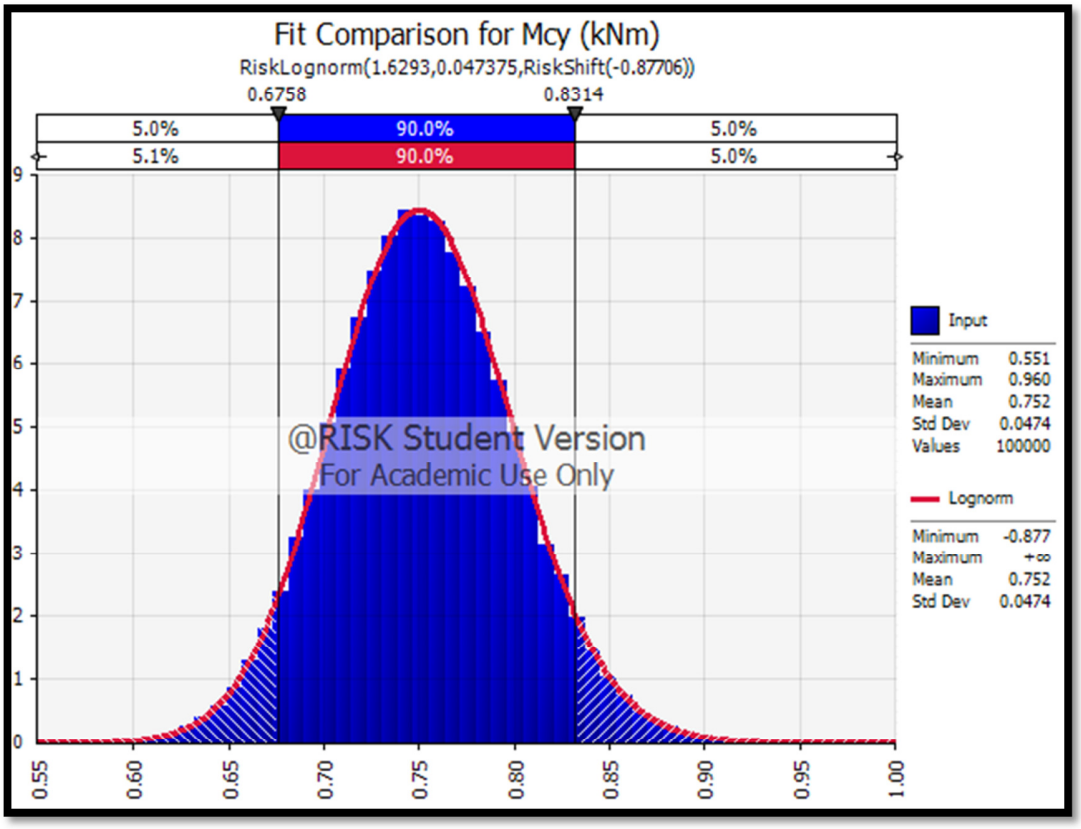

Figure 74: Fitted Log-normal distribution for moment capacity about weak axis ($\mu = 0.752$ kNm, $\sigma = 0.0474$kNm)

9.3 Concluding remarks

Chapter 8 focused on the distribution functions of the different loads induced on the chosen structural model. In Chapter 9 distribution functions were assigned to three profile parameters that were shown to govern resistance variability. MC simulations were used to propagate the uncertainty described by these distributions through the various element resistance models to obtain distribution functions for element (specifically the critical elements) resistance for each failure mode.

With the distribution functions known on both the loading and resistance side of the performance function G(**X**), the foundation for the probabilistic based evaluation of β for the typical structure, designed according to the loading code, SANS 517:2009, and the design code, SANS 10162-2:2010, has been laid. It is now possible to perform these evaluations for the different failure modes.

Stellenbosch University http://scholar.sun.ac.za

10. Probabilistic based evaluation of β, using a FORM

The probabilistic evaluation of a specific code can be divided into two different categories. The first category can be seen as the evaluation of the achieved reliability index β. The second category entails the evaluation or calibration of the partial material or load factors (γ_m, γ_L) to obtain a certain target reliability value β_t. (Faber, 2009) . For this research the focus will be on the first category, specifically to assess the achieved element reliability of a typical structure designed according to SANS 517:2009 and SANS 10162-2:2010. The β value, based on the element performance function G(**X**) can be evaluated using distribution functions of input variables obtained in previous chapters. For each element in the chosen structural model a specific G(**X**) will exist for each failure mode. G(**X**) will be a combination of the capacity of the element against the specific failure mode, discussed in Chapters 7 and 9, and the loads induced on that element, discussed in Chapters 6 and 8. For each element this combination will differ. In Chapter 6.7 the most critical elements for different failure modes were identified. The evaluation of β will therefore be performed on these elements only. It must thus be noted that the reliability evaluations performed in this Chapter are on individual structural members and not on the structural system as a whole.

10.1 FORM used to evaluate β

In real life a certain element can either have a larger or smaller capacity than what was determined in the deterministic design approach due to variability of material and geometry properties. Furthermore, the loads acting on that element can also differ from the design loads.

The FORM method described in Chapter 5.6 was used to perform the evaluation done in this research. This method was used to evaluate each individual failure mode. Excel spread sheets were developed to perform the FORM calculations for each failure mode. The evaluation of each failure mode was done in three different ways:

Firstly the reliability margin implied by the design load was evaluated. It was assumed that only the loads acting on the structure were probabilistic, i.e. that the loads follow their known distribution functions. This allows evaluating the probability that the load effect will exceed the deterministic design resistance. On the resistance side, deterministic values were used.

Stellenbosch University http://scholar.sun.ac.za

Secondly the reliability margin implied by the section resistance was evaluated. The design load was set as the deterministic value obtained from code provisions of characteristic load values, scaled by the partial and combination factors as described in Chapter 7. The variability of profile parameters (f_y, t and r_i) were described by their distribution functions and the probability that the section will fail to carry the design load due to section variability was thus evaluated.

The first two evaluations done can be represented by Figure 29 in Chapter 5.

Lastly, the total reliability margin implied by the codified design provisions was evaluated for each failure mode. This was done by describing both the load and the resistance probabilistically, using the distribution functions discussed in Chapter 8 and 9. The probability of failure, i.e. of the load exceeding resistance was computed and described in terms of the reliability index β.

This evaluation of β will reflect what level of reliability for LSFB can be expected when using the loading code, SANS 517:2009, and the design code, SANS 10162:2 – 2010 to design such typical buildings.

The basic principles behind the FORM for all three types of evaluations done will stay the same. Therefore an example of the FORM for the first type of evaluation done on the axial load failure mode will be shown below. It will be shown and discussed how the different steps of the FORM shown in Chapter 5.6 were incorporated into the spread sheets to evaluate β for each failure mode. The spread sheet for the axial load failure mode is shown in Figure 75 and the 10 steps of the FORM can be summarized as follows, for this specific case:

1. Obtain the expression for the reliability margin G(**X**) for the axial load failure mode

$$G(\mathbf{X}) = R(\mathbf{X}) - E(\mathbf{X}) \qquad 84$$

Where the expression for E(**X**) is described in equation 79 and R(**X**) is taken as a single deterministic value, obtained from characteristic input values for resistance parameters. Seeing that E(**X**) consists out of dead loads (DL), live loads (LL) and wind loads (WL), all the combinations of these loads were modelled on the chosen structural model in the structural analysis program. Thus, the vector {**X**} of variables in this case is {DL, LLF, LLR, WL}^{T}, and even though R(**X**) is shown as a function of **X**, in this example it is not. By performing a linear analysis it was then possible to obtain the axial load in the critical (discussed in Chapter 6) element. This force can then be compared to the resistance value of the element (obtained in Chapter 7).

Stellenbosch University http://scholar.sun.ac.za

The limit state function $G(\mathbf{X}) = 0$ can be found in B3 of Figure 75.

2. The initial assessment of the design point $\mathbf{x^*} = \{x_1^*, x_2^* \ldots x_n^*\}$ is made by taking the original design values of n – 1 variables for the loads (discussed in Chapter 6.3) acting on the structural model. The design point value for the last variable is determined from the limit state function, i.e. to ensure that the design point vector describes a state of variable realisations that would set the element on the limit state. This can be seen in H9 – H12 of Figure 75.

3. At the point $\mathbf{x^*} = \{x_1^*, x_2^*, \ldots x_n^*\}$ equivalent normal distributions are found for all the basic variables with equation 69 and 70. This can be seen in B11 and B14 of Figure 76 respectively. It must be noted that dead load (DL) applied to the chosen structural model has a Normal distribution. The mean, μ and standard deviation, σ, will therefore be equal to the mean, μ^e and standard deviation, σ^e, of the equivalent normal distribution.

4. The corresponding standardised design point $\mathbf{u^*} = \{u_1^*, u_2^* \ldots u_n^*\}$ from the standardised random variable $\mathbf{U} = [U_1, U_2 \ldots U_n]$ can now be determined with equation 70. The standardised design point can be seen in E9 to E12 of Figure 75.

5. The next step is to evaluate the partial derivatives of the standardised variables $\mathbf{U} = [U_1, U_2 \ldots U_n]$ at the design point. Let the vector denote **D**. From equation 71 it can be seen that the expression for **D** is given by $\mathbf{D} = \frac{\partial G}{\partial X_i} \sigma_{X_i}^e$. A numerical change must be made to the performance function $G(\mathbf{X})$ to be able to determine $\frac{\partial G}{\partial X_i}$. This derivative describes the change in the performance for a change in the variable under consideration. It was decided that each of the initial design values applied to the chosen structural model would be changed separately with a positive 5%. The value of the performance function in B4 of Figure 75 was therefore determined as follows:

   The initial wind speed value of 38.5 m/s was increased by 5 % to 40.425 m/s. The new calculated wind loads together with the original dead and live loads were then modelled on the chosen structural model in a structural analysis program. By performing a linear analysis, the new element forces for each failure mode in a specific element could be found. Seeing that

Stellenbosch University http://scholar.sun.ac.za

the element resistance R(**X**) will stay constant but the load effect E(**X**) will change, the value of the performance function G(**X**) will change correspondingly from 0 to a higher or lower value. The calculation of $\frac{\partial G}{\partial X_i}$, as shown in K9 of Figure 75 will be done as follows:

$$\left[\frac{G\{1.05x^*_{WL},x^*_{DL},x^*_{LLR},x^*_{LLF}\}-G\{x^*_{WL},x^*_{DL},x^*_{LLR},x^*_{LLF}\}}{x^*_{WL}(1.05-1)}\right] \quad 85$$

The partial derivative D can be calculated by multiplying equation 85 with the standard deviation of the equivalent normal distribution σ^e_{WL} obtained from the wind load.

By performing the calculations described above for each variable **X** it is possible to determine the partial vector **D.** The vector **D** can be seen in B9 to B 12 of Figure 75.

6. It is now possible to estimate the reliability index β for the first iteration by applying equation 73. The value of β can be seen in E16 of Figure 75.

7. With β known, it is now possible to determine the sensitivity factor α for each of the variables **X.** Seeing that there are a total of 4 variables (DL, LLF, LLR and WL) each of them will have their own α value. The sensitivity factor can therefore be written as a vector in the form {α}. The vector {α} can be calculated with equation 74. The values of {α} can be found in C18 to C22 of Figure 75.

8. A new design point can now be determined for n – 1 standardised and original basic variables with equations 75 and 76. These values can be found in B23 to B26 and B30 to B32.

9. The design value of the remaining basic variable is determined by the limit state function G(**x***) = 0. The value for the last basic variable can be found in B29 of Figure 75.

10. Steps 3 to 9 can now be repeated until β and the design point {**x***} converge to the required level of accuracy.

For the second iteration done the design point values $\mathbf{x_2}^*$ will be applied as loads to the chosen structural model in the structural analysis program. These new loads will now be altered in the same way as discussed in point 5 above to obtain the different partial derivatives.

Stellenbosch University http://scholar.sun.ac.za

The final converged design point values are the most likely combination of loads that will lead to exceedence of the design resistance. The β associated to this point can be used to calculate the probability of such a realisation of loads, using equation 48.

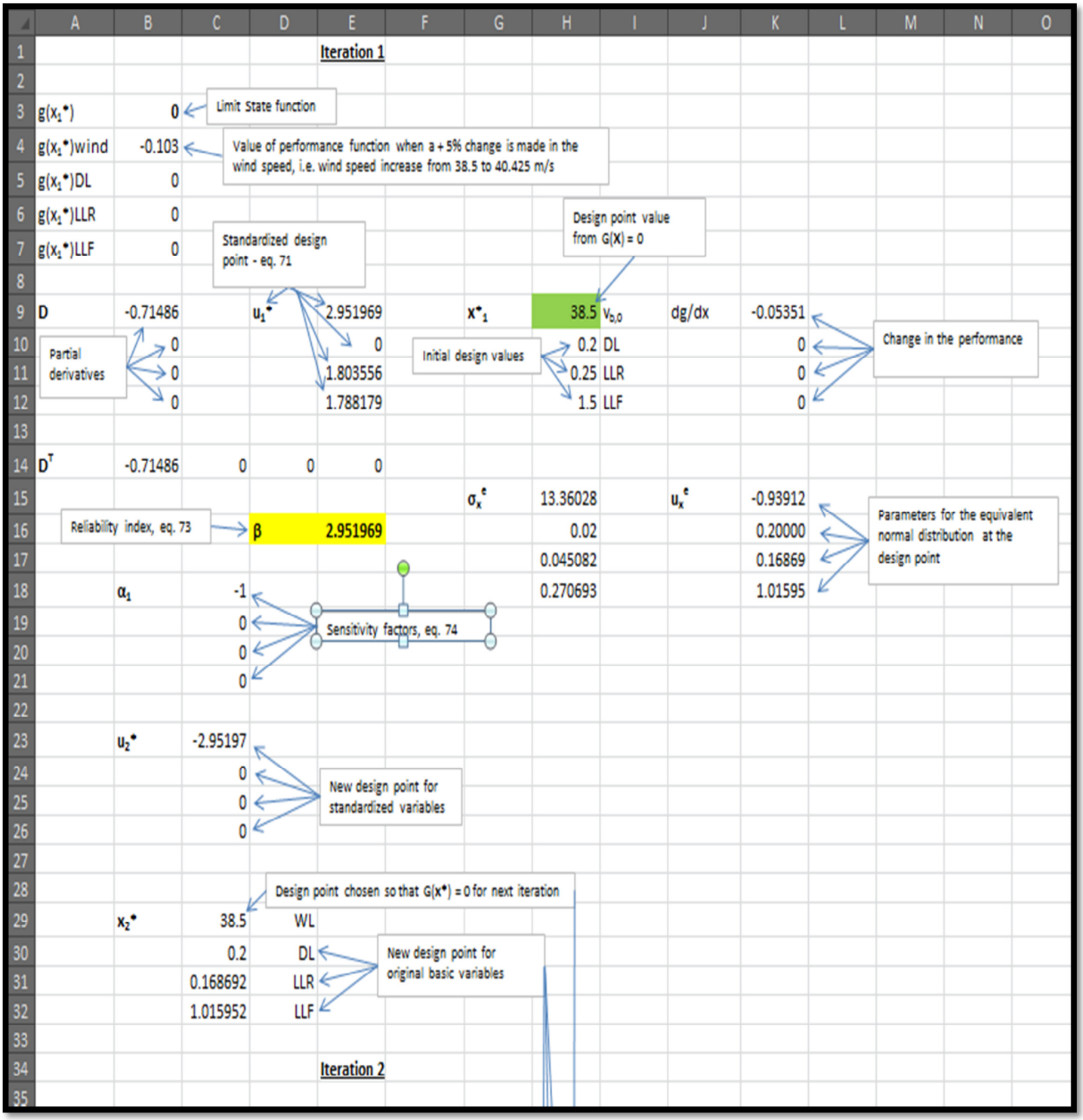

Figure 75: Iteration 1 of the FORM for axial load failure mode

Stellenbosch University http://scholar.sun.ac.za

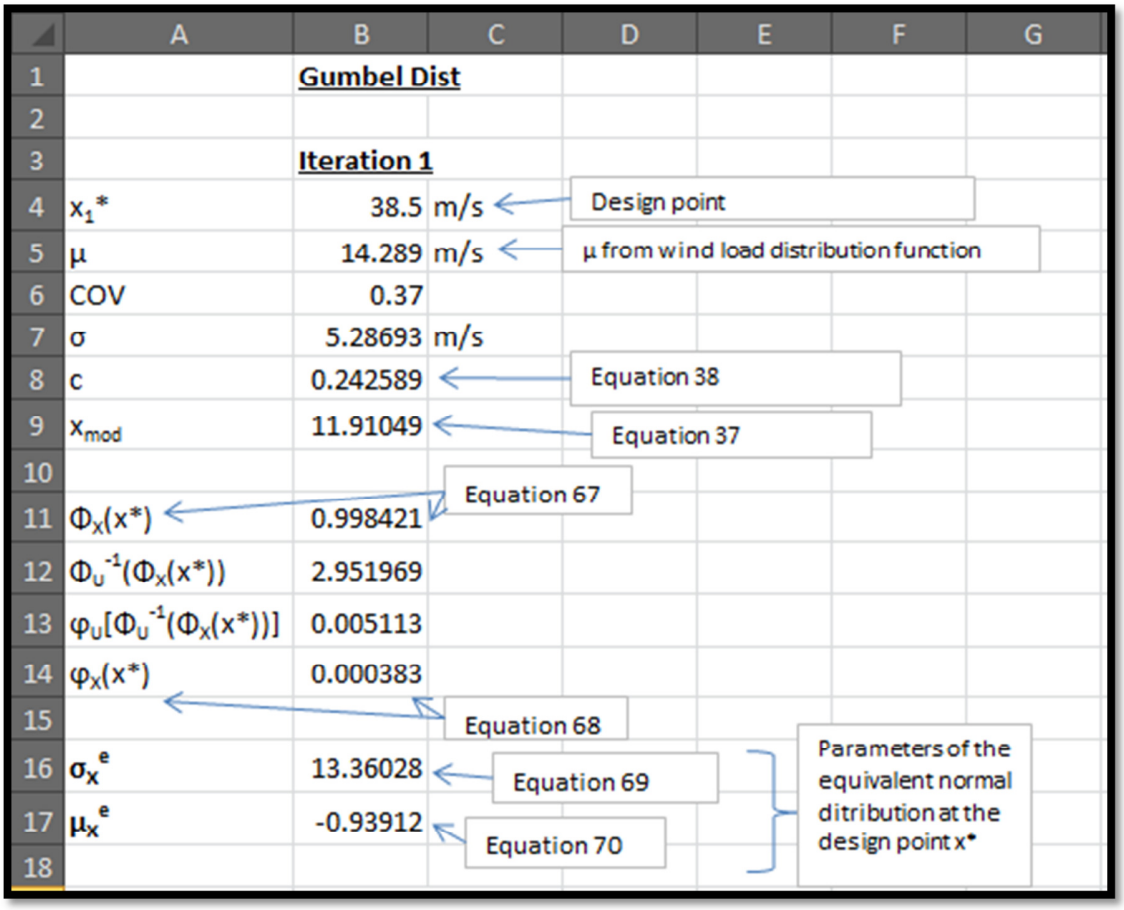

Figure 76: Transformation of original to standardised variables

Figure 76 shows the calculations to transform the original wind loads with a Gumbel distribution to equivalent standardised Normal distributions at the design point. The same must be done for both the dead and live loads induced on the chosen structural model. However, the method used to perform these transformations will be the same as shown in Figure 76 and explained in Chapter 5.6. It is therefore not necessary to give the same detailed discussion for the other types of loads on the structural model.

In the next sections the different β values obtained for each type of evaluation done on the different failure modes will be discussed.

Stellenbosch University http://scholar.sun.ac.za

10.2 Evaluation of failure modes - Case 1

As mentioned in Chapter 10.1, the evaluation of the element reliability β can be done by applying the FORM to three different cases.

In the first case the reliability margin implied by the design load was evaluated. It was assumed that only the loads the structure were probabilistic, i.e. that the loads follow their known distribution functions. This allows evaluating the probability that the load effect will exceed the deterministic design resistance.

According to South African standards, an overall β value of 3 must be obtained to ensure that the necessary level of reliability is achieved. The Eurocodes provide a factor by which β should be multiplied if only the loading side of the evaluation has probabilistic values. This value is said to be -0.7 (Holicky, 2009). The required level of reliability that must therefore be reached for case 1 is -0.7*(3). Therefore, the different failure modes will have a sufficient level of reliability if the obtained β's are larger than 2.1. The level of reliability that was obtained for this case 1 for each of the failure modes discussed in Chapter 6.7will be given below.

10.2.1 Reliability index with design values for the different failure modes

By performing evaluations similar to the one shown in Figure 75, it was possible to calculate the level of reliability for each failure mode. The detailed spread sheet calculations can be found in Appendix J: Spread sheet calculations for evaluation of β-Case 1. A summary of the results is given below.

Stellenbosch University http://scholar.sun.ac.za

- **Failure mode for axial loading**

$\beta = 2.952$

Table 4: Most probable loads that will lead to failure in axial loading

	Design point x*	
Basic wind speed	38.5	m/s
Dead load	0.2	kPa
Live load roof	0.178	kPa
Live load floor	1.07	kPa

- **Failure mode for shear about strong axis**

$\beta = 2.365$

Table 5 Most probable loads that will lead to failure in shear about the strong axis

	Design point x*	
Basic wind speed	31.17	m/s
Dead load	0.2	kPa
Live load roof	0.178	kPa
Live load floor	1.12	kPa

- **Failure mode for shear about the weak axis**

$\beta = 3.15$

Table 6: Most probable loads that will lead to failure in shear about the weak axis

	Design point x*	
Basic wind speed	41.23	m/s
Dead load	0.2	kPa
Live load roof	0.178	kPa
Live load floor	1.072	kPa

Stellenbosch University http://scholar.sun.ac.za

- **Failure mode for tension**

$\beta = 2.133$

Table 7: Most probable loads that will lead to failure in tension

	Design point x*	
Basic wind speed	28.8	m/s
Dead load	0.2	kPa
Live load roof	0.178	kPa
Live load floor	1.069	kPa

- **Failure mode for interaction between axial load and moments**

$\beta = 2.042$

Table 8: Most probable loads that will lead to failure of interaction between axial load and bending

	Design point x*	
Basic wind speed	27.875	m/s
Dead load	0.2	kPa
Live load roof	0.178	kPa
Live load floor	1.069	kPa

10.2.2 Summary of β value for the first case

All the β values that were calculated in Chapter 10.2.1 were based on the assumption that only the loads in the performance function G(**X**) were probabilistic. A summary of all the failure modes with their respective β values are shown in Table 9.

Stellenbosch University http://scholar.sun.ac.za

Table 9: Summary of β value for case 1

Failure mode	Reliability Index β	Reliability governed by variability of
Axial load	2.952	WL
Shear about the strong axis	2.365	WL
Shear about the weak axis	3.15	WL
Tension	2.133	WL
Axial load & bending moment interaction	2.042	WL

As mentioned in Chapter 10.2, a minimum value of β larger than 2.1 should be obtained by all failure modes to ensure that the necessary level of reliability is achieved. From the summarised values in Table 9 it can be seen that all failure modes do achieve the minimum level of reliability except the failure mode for interaction between axial load and bending. However, the obtained β value is still very close to the required reliability. From the results shown in Table 9 it is clear that the reliability is governed by the uncertainty in the wind load (WL) on the structure. This follows from the high values (close to 1) of the sensitivity factor α_{WL} associated to the wind load, compared to the α values of other variables (see Appendix J: Spread sheet calculations for evaluation of β-Case 1). Mr. Andries Kruger recently completed his PhD on updating the basic characteristic wind speed map of South Africa. This research will improve the description of wind loads for South Africa in the future. However, seeing that this updated and improved map is not yet used in the loading code SANS 517:2009, it is not used in the designing of structures in South Africa at the moment.

In Chapter 8.1.3 a Gumbel distribution was used to describe the annual wind speed with the following statistical parameters;

$\mu = 14.289$ m/s

$COV = 0.37$

$\sigma = 5.287$ m/s

Therefore the basic wind speed of 28 m/s used was the 98% fractile of the distribution function. The basic wind speed value is a characteristic value having an annual probability of exceedence of 0.02, which is equivalent to a mean return period of 50 years.

This distribution function was then used as basis to calculate the wind loads that were applied to the structural model.

Stellenbosch University http://scholar.sun.ac.za

Seeing that all the wind load calculations are based on a mean return period of 50 years, a basic wind speed model for the probability of exceedence in a life time of 50 years should have been used and not the annual probability of exceedence. The best model to describe the wind model for this research was therefore not used. Furthermore most of the available wind load models in literature describe the actual characteristic wind loads imposed on a structure and not the basic characteristic wind speed as was done for this research. A further possible margin of error was therefore introduced into the model used, because the COV of 0.37 is applicable to the model described in the JCSS for the characteristic wind loads and not the characteristic basic wind speeds.

From the sensitivity factors obtained in the reliability analysis shown in Chapter 10.2.1, it was clear that the load effect is dominated by the wind load and its variability. Thus, the reliability margin between the mean wind load and the codified design value for wind loading can be considered an approximate estimate of the total reliability implied by the conservative choice of design loads. Two other wind load models are used to evaluate this reliability margin between the mean wind load and the design wind load. These are the wind load model that was used in the calibration of SANS 10160 and the wind load model that was used in Eurocode respectively. The SANS model assumes a lower mean wind load than the Eurocode model and correspondingly a larger reliability margin is estimated for the SANS model. However, significant model uncertainty exists and it is not clear which model should be considered a better approximation of the true wind loading.

10.2.3 Reliability evaluation assuming other wind load models

Before the accuracy or validity of the results discussed in Chapter 10.2.2 can be defended, calculation must be performed with a more correct distribution model of the wind loads induced on the structural model. These calculations will be performed by using a wind model that will describe a load with the probability of exceedence in 50 and not a model that only describes the model for the annual probability of exceedence as was used until now. Seeing that the wind load on the structure was by far the most dominant load effect and that this will not change if the wind loads were described by a more accurate distribution function the calculations performed in this section will assume that the wind load on the structure is the only load, i.e. the influence of the dead- and live-load on the structural mode will be neglected. This will ensure that a simplified

Stellenbosch University http://scholar.sun.ac.za

performance function can be developed that will still predict the actual level of reliability accurately. According to Holicky, the conventional model of basic variables, to describe wind load on a structure, for time-invariant reliability analysis is as shown in Table 10 below.

Table 10: Conventional models of basic variables

Code under consideration	**Name of basic variables**	**Distribution.**	**Mean μ_{WL}**	**St. dev. σ_{WL}**
Eurocode 1990	Wind - 50 years	GU	$0.7q_p$	$0.35\mu_{WL}$
SANS 10160	Wind - 50 years	GU	$0.41q_p$	$0.35\mu_{WL}$

The basic characteristic wind pressure q_p on the chosen structural model was calculated as 0.8264 kPa. Detailed calculations of q_p can be seen in Appendix D: Detailed wind load calculations. It can be observed that the only difference in the model used to describe wind load for the Eurocode 1990 and for SANS 10160:2011 is the factors of 0.7 and 0.41 respectively. These factors are so called bias factors applied to obtain the mean values of the distribution function describing the wind loads. (Retief et al., 2011). The aim of these factors is to allow for statistical uncertainty found in the wind load models as well as in the parameters present in the calculation of q_p. According to Eurocode 1990 the following expression can be used to calculate q_p.

$$q_p = 0.5\rho v^2 c_r c_a c_g c_d = Q_{ref}\, c_r c_a c_g c_d \qquad 86$$

Table 11 shows indicative parameters of the variables used in equation 86. These parameters were adopted from the JCSS.

Stellenbosch University http://scholar.sun.ac.za

Table 11: Indicative parameters of the wind components (Holicky, 2009)

Symbol	Name of variable	Relative mean	COV
Q_{ref}	Annual pressure extreme	0.8	0.2
c_r	Roughness factor	0.8	0.15
c_a	Aerodynamic shape factor	1	0.2
c_g	Gust factor	1	0.15
c_d	Dynamic factor	1	0.15

In Table 11 it can be seen that Q_{ref} and c_r has relative means of 0.8. in equation 86 these relative mean must be brought into account. Therefore by multiplying all the relative means with each other a value of 0.64 is obtained. Because of the many statistical uncertainties in the wind model this value is then increased to 0.7, which is the bias factor found in Eurocode 1990. Due to different relative means for variables shown above in Table 11 the bias factor for SANS 10160:2011 has a value of 0.41.

It is now possible to calculate the reliability margin implied for both the mentioned codes by developing a very simple performance function $G(X) = \gamma_{WL}.\mathbf{Q}_{WL,k} - \mathbf{Q}_{WL}$

where:

γ_{WL} = partial wind load factor of 1.3

$\mathbf{Q}_{WL,k}$ = characteristic wind load calculated to be 0.8264 kPa

$\mathbf{Q}_{WL}$ = realisation of the wind load from its assumed statistical model

$\mathbf{Q}_{WL,d} = \gamma_{WL}.\mathbf{Q}_{WL,k}$

Therefore the value of $\mathbf{Q}_{WL,d}$ can be calculated as a deterministic value of 1.074 kPa

Furthermore the value of $\mathbf{Q}_{WL}$ will be described by the new probabilistic distribution function, based on the statistical parameters in Table 10.

An illustration of the performance function can be seen in Figure 77.

Stellenbosch University http://scholar.sun.ac.za

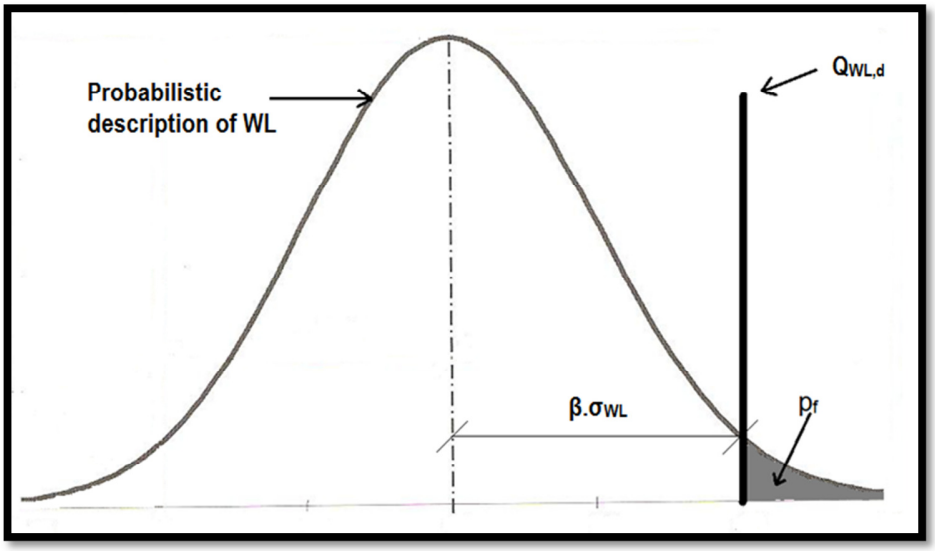

Figure 77: Illustration of the simplified performance function G(X) used

By using the software VAP an illustration of β can be seen in Figure 77. The β value obtained will therefore in essence describe the margin of safety that is built into the codes by the partial wind load factor of $\gamma_{WL} = 1.3$. Because different bias factors are applied to the respective wind models of Eurocode 1990 and SANS 10160:2011, two different β values will be obtained for the respective wind models.

If the β values that were obtained from the evaluation done for case 1 are somewhere between the two new calculated β values it is an indication that the obtained results (from case 1) still have credit and that it can be used as an indication towards the actual level of reliability that was achieved in the evaluation for case 1, but only with a very clear understanding of the implications of the shortcomings in the evaluation. Furthermore, a thorough explanation to why β falls in this margin although a wind load model was used that is not entirely accurate has to be done to eliminate incorrect interpretation of the results.

10.2.3.1 Reliability implied by the wind model of Eurocode 1990

By referring to Table 10 and by using the statistical parameters applicable to Eurocode 1990, the following could be calculated:

$\mu_{WL} = 0.7*0.8264$

Stellenbosch University http://scholar.sun.ac.za

$= 0.578$ kPa

$\sigma_{WL} = 0.35\ \mu_{WL}$

$= 0.202$

By using the mean and standard deviation to describe the probabilistic distribution function illustrated in Figure 77 and with the known deterministic design wind load of 1.074 kPa the calculated β value is 1.98.

10.2.3.2 Reliability implied by the wind model of SANS 10160:2011

By referring to Table 10 and by using the statistical parameters applicable to SANS 10160:2011, the following could be calculated:

$\mu_{WL} = 0.41*0.8264$

$= 0.339$ kPa

$\sigma_{WL} = 0.35\ \mu_{WL}$

$= 0.1187$

By using the mean and standard deviation to describe the probabilistic distribution function shown in Figure 77 and with the known deterministic design wind load of 1.074 the calculated β value is 3.54.

10.2.4 Comparison of the obtained β from case 1 with the β values for Eurocode 1990 and SANS 10160:2011

The Eurocode and SANS 10160:2011 wind load models can be seen as the upper and lower estimates of possible correct approximations of the actual wind load. The β values are 1.98 and 3.54 for Eurocode 1990 and SANS 10160:2011 respectively. Any obtained value of β from the evaluations done in Chapter 10.2.1 between these two values is a good indication of the reliability margin implied by the design load. It therefore entails that the summarised β values shown in Table 9 serve as a good indication of the level of reliability that was achieved for case 1 for the different failure modes.

Stellenbosch University http://scholar.sun.ac.za

Although the levels of reliability achieved for the failure modes investigated in case 1 falls within the upper and lower limits of acceptable β values, the question arises: How is it possible that the calculated reliability values shown in Table 9 can still be in the range discussed when the description of the wind load model had some shortcomings? By using the statistical model of the annual probability of exceedence in stead of the statistical model of the probability of exceedence in 50 years, a less conservative approach in calculating β was used. On the other hand by not multiplying the calculated wind load q_p with the corresponding bias factor for the 1 year wind load given in (Holicky, 2009) as 0.3 a more conservative or higher wind load was induced on the structure. Therefore these two separate shortcomings in the wind load calculations cancelled each other out to a large extend so that repetition of that analysis were not warranted.

10.2.5 Final conclusions for case 1

From the discussion in Chapter 10.2.4 it becomes clear that the original obtained results for case 1 are within the acceptable range of β values and still serve as a good indication to the actual level of reliability achieved. This therefore implies that if all the reliability evaluations that were performed for case 1 had to be repeated with the SANS 10160 wind model, higher levels of reliability would be estimated. SANS 10160:2011 forms the bases of SANS 517:2009 and therefore the improved estimates of the β values will lean more toward the reliability margin of $\beta = 3.54$ implied by the SANS 10160 wind model than to the reliability margin of $\beta = 1.98$ implied by Eurocode wind model.

The final conclusion can therefore be summarised as follows: The obtained result shown in Table 9 provide a good estimate of the level of reliability that can be achieved for the case where the reliability margin implied by the design load was evaluated. However, these values are underestimated due to an overestimation of the wind load compared to the model proposed for SANS 10160. It is believed that the actual levels of reliability for the different failure modes are in fact higher than the required β of 2.1 (discussed in Chapter 10.2).

10.3 Evaluation of failure modes-Case 2

As mentioned in Chapter 10.1, the evaluation of β can be done by applying the FORM to three different cases. For case 2 it was assumed that certain profile parameters, namely yield stress

Stellenbosch University http://scholar.sun.ac.za

(f_y), thickness (t) and the internal radius (r_i), have probabilistic values. For this case the loads applied to the chosen structural model were taken as deterministic values. No changes to these values were made throughout the calculation of β for the different failure modes investigated. The Eurocodes provide a factor by which β should be multiplied if only the resistance side of the evaluation has probabilistic values. This value is said to be 0.8 (Holicky, 2009). The required level of reliability that must therefore be reached for case 2, is 0.8*(3). Therefore, the different failure modes will have a sufficient level of reliability if the obtained β is larger than 2.4. The reliability index will now be based on the three chosen profile parameters. It must be noted that the two profile parameters t and r_i have Normal distributions. The mean, μ and standard deviation, σ, will therefore be equal to the mean, μ^e and standard deviation, σ^e, of the equivalent normal distribution. The level of reliability that was obtained for each of the failure modes discussed in Chapter 6.7, based on the FORM evaluation of the second case, will be given below.

10.3.1 Reliability index with calculated profile parameters for the different failure modes

By performing evaluations similar to the one shown in Figure 75, it was possible to calculate the level of reliability for each failure mode. The detailed spread sheet calculations can be found in Appendix K: Spread sheet calculations for evaluation of β-Case 2. A short discussion of the results will be given below.

- **Failure mode for axial loading**

$\beta = 6.852$

Table 12: Most probable realisations of profile parameters that will lead to failure in axial loading

	Design point x*	
Yield stress f_y	574.86	MPa
Thickness t	0.605	mm
Internal radius r_i	1.999	mm

Stellenbosch University http://scholar.sun.ac.za

- **Failure mode for shear about strong axis**

$\beta = 0.248$

Table 13: Most probable realisations of profile parameters that will lead to failure in shear about the strong axis

	Design point x*	
Yield stress f_y	578.28	MPa
Thickness t	0.9375	mm
Internal radius r_i	2	mm

- **Failure mode for shear about the weak axis**

$\beta = 3.992$

Table 14: Most probable realisations of profile parameters that will lead to failure in shear about the weak axis

	Design point x*	
Yield stress f_y	578.28	MPa
Thickness t	0.749	mm
Internal radius r_i	2	mm

- **Failure mode for tension**

For the evaluation of β for the failure mode of tension it must be noted that the ultimate yield stress, f_u, of the profile was used and not the yield stress, f_y, as in the case of the other failure modes.

$\beta = 2.16$

Table 15: Most probable realisations of profile parameters that will lead to failure in tension

	Design point x*	
Yield stress f_u	555.76	MPa
Thickness t	0.862	mm

Stellenbosch University http://scholar.sun.ac.za

Internal radius r_i	2	mm

- **Failure mode for interaction between axial load and moments**

$\beta = 0.409$

Table 16: Most probable realisations of profile parameters that will lead to failure in axial load and bending

	Design point x*	
Yield stress f_y	576.54	MPa
Thickness t	0.93	mm
Internal radius r_i	2	mm

10.3.2 Summary of β value for the second case

All the β values that were calculated in Chapter 10.3.1 were based on the assumption that only the three chosen profile parameters in the performance function G(**X**) were probabilistic. A summary of all the failure modes with their respective β values are shown in Table 17.

Table 17: Summary of β value for case 2

Failure mode	Reliability Index β	Reliability governed by variability of
Axial load	6.852	t
Shear about the strong axis	0.248	t
Shear about the weak axis	3.99	t
Tension	2.16	t, fu
Axial load & bending moment interaction	0.409	t, fy

Stellenbosch University http://scholar.sun.ac.za

From the results shown in Table 17, it is clear that only the failure mode for axial load and shear about the weak axis reaches the required level of reliability ($\beta = 2.4$). Two of the failure modes (shear about the strong axis and interaction) have a very low level of reliability. By referring back to Figure 29, it can be said that β can be expressed as the number of standard deviation that the load is away from the mean of the distribution function of the resistance.

The question now arises, are the reliability results obtained from the FORM calculations for case 2 correct? More so, are the capacity calculations given in Appendix F: Detailed calculation of shear capacity correct? It can be said with good faith that the resistance calculations as well as the FORM evaluation done for case 2 are correct. With this in mind the question still remains, how is it possible that such low levels of reliability can be achieved for certain failure modes. Figure 78 will aim to provide an explanation to why such low levels of reliability were obtained.

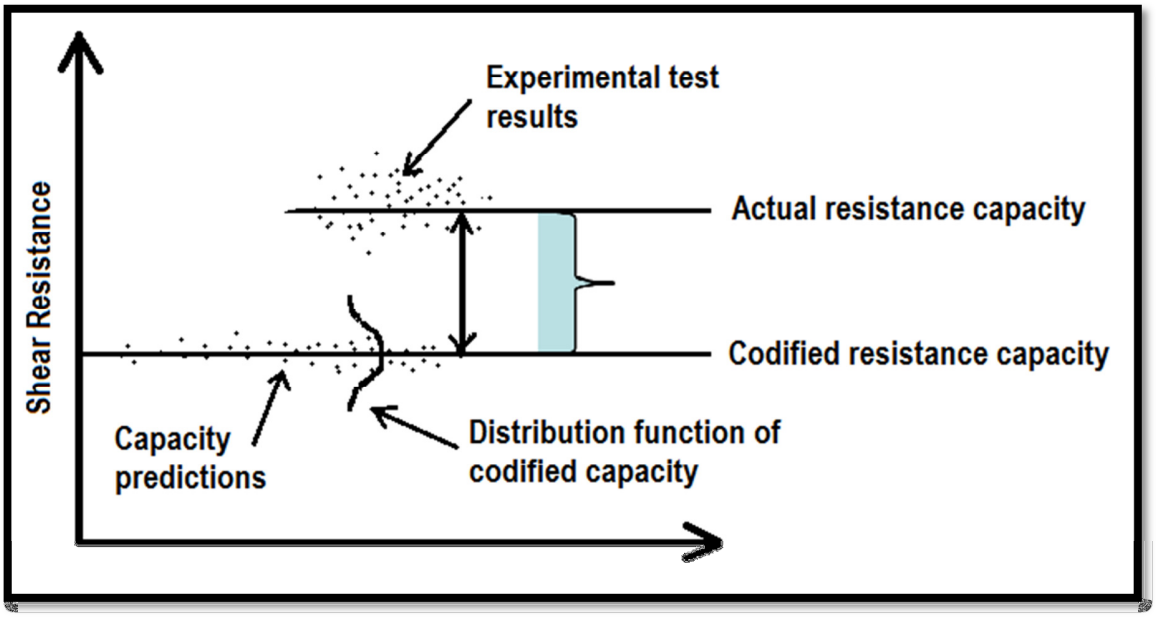

Figure 78: Illustration of codified versus experimental profile capacity

Figure 78 illustrates the resistance of a typical cold formed thin walled member for a given failure mode. Two different sets of data point can be found in this figure. Firstly, the actual resistance values that would be obtained when experimental tests were conducted and secondly the resistance capacity prediction provided by the expressions found in the design code, SANS

Stellenbosch University http://scholar.sun.ac.za

10162-2:2010. The difference between these two values can be expressed by introducing a certain model factor of the ratio between the predicted and actual capacity. Idealistically, a prediction model should strive to be accurate (i.e. have a small model factor), but at all times the prediction model should provide conservative estimates. To achieve this in practice, large model factors are often present in prediction models to ensure adequate conservatism. However, in the case of the failure mode of web crippling for cold formed steel members the difference between the codified resistance and the actual experimental resistance is in some cases more than 100 %. (Beshara & Schuster, 2000). The difference will introduce a very big model factor and the conservatism implied by this in not included in the β evaluation done in Chapter 10.3.1. If this were to be included the β values would be higher assuming that a conservative bias exists between the predicted and actual resistances. This difference entails that there are two different β values for the same failure mode. Firstly the true β and the secondly the calculated β, reflecting the model factor bias which influence the calculated β in a negative way. The β that was estimated for the codified resistance will therefore be much lower than the actual reliability of the profile with regards to its experimental test capacity. The results published in (Beshara & Schuster, 2000) were based on the investigation of the North American code AISI-1996. Originally the North American code for the design of cold formed steel section formed the basis for the Australian design code AS 4600:2005, which again formed the basis of the new SANS 10162-2:2010.

Furthermore, the β value for the failure mode of shear about the strong axis is only dependent on the thickness of the profile. Seeing that the profile has a mean thickness of 0.95 mm it is clear that the smallest deviation to this value can make a very big difference in the final level of reliability for this failure mode. By referring back to Chapter 9.1.3, it can be seen that the profile thickness has a COV of 0.053. It must also be noted that the load on the element (8.05 kN) is very close to the resistance capacity (8.34 kN) of the profile. If the model factor was therefore included correctly a reliability index of at least 2.4 should have been achieved. This is however not the case and this contributes to the believe that a possibly large model factor is not taken into account in the codified resistance calculations. It is believed that this small difference between the applied load and capacity of the profile is the only reason why the obtained β was larger than zero. The conclusion is therefore that the resistance side for this failure mode is governed by the thickness t and no partial factor is applied to t because the resistance side contributes nothing to the

Stellenbosch University http://scholar.sun.ac.za

element reliability. If it was governed by f_y, the partial factor on f_y would have ensured that some extra reliability is built into the design.

For the failure mode of shear capacity about the weak axis, a large β was obtained. This was due to the fact that a much bigger positive difference between the applied load (4.458 kN) and capacity (9.1 kN) is found. If these two values were closer to each other it is believed that it would show a similar lack of reliability as does shear about the strong axis.

For the failure mode of interaction between axial loads and bending moments, the β value will depend on the yield stress f_y and the profile thickness, t. The thickness will however have a much greater influence on the capacity than the yield stress as can be seen from the respective sensitivity factors from FORM ($\alpha_t = 0.968$ vs. $\alpha_{fy} = 0.25$). Therefore, a small change in the thickness will have a very significant influence on the capacity of the profile.

Although the current reliability margin implied by the resistance side is very close to zero, as indicated in the discussion above and in Table 17, it is believed that the actual levels of reliability for the failure modes investigated might be much higher than the values given in Table 17. This statement can be made on the assumption that a fairly big model factor may be present and that the codified resistance prediction models for some failure modes do not explicitly treat this model factor. However, the validity of this statement can only be proven if detailed experiments are conducted on all failure modes to be able to quantify the model factor present.

The final conclusion for case 2 can therefore be summarised as follows: Although the obtained β values are mathematically correct they cannot be used to quantify the reliability margin implied by the resistance of the profile was evaluated. This is due to the lack of information with regards to the model factor as discussed. Further research needs to be conducted in order to obtain β values that will represent the real reliability for this case.

10.4 Evaluation of failure modes – Case 3

The third case to evaluate β will serve as the most comprehensive and representative case of a real life situation. For this evaluation, both the loads and resistances of the profile will have probabilistic values with given distribution functions. According to South African standards a

Stellenbosch University http://scholar.sun.ac.za

reliability level of $\beta = 3$ must be achieved in evaluations where both the resistance and loading on a profile are probabilistic. The reliability index will now be based on the three chosen profile parameters, namely yield stress (f_y), thickness (t) and the internal radius (r_i) as well as all the loading variables such as wind load (WL), dead load (DL) and live load (LL). It must be noted that the variables for the parameters t and r_i as well as the dead load on the element have Normal distributions. The mean, μ and standard deviation, σ, will therefore be equal to the mean, μ^e and standard deviation, σ^e, of the equivalent normal distribution. The level of reliability that was obtained for each of the failure modes discussed in Chapter 6.7, based on the third case of FORM evaluation, are given below.

10.4.1 Reliability index with calculated profile parameters for the different failure modes

By performing FORM evaluations similar to the one shown in Figure 75, it was possible to calculate the level of reliability for each failure mode. The detailed spread sheet calculations can be found in Appendix L: Spread sheet calculations for evaluation of β-Case 3. The results are shortly discussed below.

Stellenbosch University http://scholar.sun.ac.za

- **Failure mode for axial loading**

$\beta = 2.95$

Table 18: Most probable realisation of load and profile parameter variables that will lead to axial failure

	Design point x*	
Basic wind speed	38.23	m/s
Dead load	0.2	kPa
Live load roof	0.178	kPa
Live load floor	1.069	kPa
Yield stress	577.78	MPa
Thickness	0.935	mm
Internal radius	2	mm

- **Failure mode for shear about strong axis**

$\beta = 2.24$

Table 19: Most probable realisation of load and profile parameter variables that will lead to failure in shear about the strong axis

	Design point x*	
Basic wind speed	28.276	m/s
Dead load	0.2	kPa
Live load roof	0.187	kPa
Live load floor	1.125	kPa
Yield stress	578.28	MPa
Thickness	0.923	mm
Internal radius	2	mm

Stellenbosch University http://scholar.sun.ac.za

- **Failure mode for shear about the weak axis**

$\beta = 3.06$

Table 20: Most probable realisation of load and profile parameter variables that will lead to failure in shear about the weak axis

	Design point x*	
Basic wind speed	38.96	m/s
Dead load	0.2	kPa
Live load roof	0.178	kPa
Live load floor	1.073	kPa
Yield stress	578.28	MPa
Thickness	0.915	mm
Internal radius	2	mm

- **Failure mode for tension**

For the evaluation of β for the failure mode of tension it must be noted that the ultimate yield stress, f_u, of the profile were used as one of the three chosen profile parameters instead of the yield stress, f_y.

$\beta = 2.2$

Stellenbosch University http://scholar.sun.ac.za

Table 21: Most probable realisation of load and profile parameter variables that will lead to failure in tension

	Design point x*	
Basic wind speed	29.41	m/s
Dead load	0.2	kPa
Live load roof	0.177	kPa
Live load floor	1.066	kPa
Yield stress	576.64	MPa
Thickness	0.944	mm
Internal radius	2	mm

- **Failure mode for interaction between axial load and moments**

$\beta = 2.09$

Table 22: Most probable realisation of load and profile parameter variables that will lead to failure under axial loading and bending moment

	Design point x*	
Basic wind speed	28.28	m/s
Dead load	0.2	kPa
Live load roof	0.178	kPa
Live load floor	1.069	kPa
Yield stress	579.33	MPa
Thickness	0.96	mm
Internal radius	2	mm

Stellenbosch University http://scholar.sun.ac.za

10.4.2 Summary of β value for the third case

The β values that were calculated in Chapter 10.4.1 were based on the fact that both the loading and resistance side of the performance function G(**X**) were probabilistic values. A presentation of such a performance function can be seen in Figure 30. A summary of the β values obtained from this evaluation are shown in Table 23.

Table 23: Summary of β value for case 3

Failure mode	Reliability Index β	Reliability governed by variability of
Axial load	2.948	WL, t
Shear about the strong axis	2.237	WL, t
Shear about the weak axis	3.062	WL, t
Tension	2.195	WL
Axial load & bending moment interaction	2.093	WL

As mentioned in Chapter 10.4, according to reliability standards in South Africa, a reliability index of $\beta = 3$ should be achieved in these designs. From the results shown in Table 23, it is clear that only the failure mode for axial load and shear about the weak axis reaches the required level of reliability ($\beta = 3$). However, as mentioned, it is believed that the reliability margin for shear about the weak axis will decrease drastically if the design load and design resistance of the profile had similar values. All the other failure modes fall short of the target reliability level.

When a comparison between the results obtained in case 1 is made with the results obtained in case 3 it can be seen that these values are very similar. Although the profile thickness contributes to the final level of reliability achieved for case 3 it is a very small contribution. This can be said because the results for case 1 and case 3 are very similar and case 1 was only dependent on the wind loads on the structure.

With the abovementioned fact taken into account it becomes quite clear that the same shortcoming in the description of the wind load model that occurred in the evaluations done for case 1 will also will be present in case 3. A detailed discussion of this shortcoming and its implications is done in Chapter 10.2.2 to Chapter 10.2.5.

Stellenbosch University http://scholar.sun.ac.za

Again the question arises. What is implication of the shortcoming, in case 1 and case 3, to the obtained levels of reliability for case 3? It is known that the wind load will have by far the greatest influence in the level of reliability achieved for case 3. Therefore by applying the same train of thought that was used to evaluate and rectify the shortcoming in case 1 it will also be possible to conclude on the actual levels of reliability that would have being achieved for case 3 if a more accurate prediction of the wind load model was used.

10.4.2.1 Final conclusion on calculated levels reliability achieved

As mentioned and shown in Table 23, the calculated β values for case 3 were lower than the required level of reliability that needs to be achieved ($\beta = 3$).

From the discussion in Chapter 10.2.4 it becomes clear that the original obtained results for case 3 will be between the upper and lower limits of acceptable β values if the same simplification to the performance function is used. This therefore entails that if all the reliability evaluations that were performed for case 3 had to be repeated with a more accurate prediction of the wind model, higher levels of reliability would be achieved. SANS 10160:2011 forms the bases of SANS 517:2009 and therefore the correct β values will lean more towards the reliability margin implied by SANS 10160:2011 (3.54) than to the reliability margin implied by Eurocode 1990 (1.98). This is discussed in more detail in Chapter 10.2.4 to 10.2.5.

The final conclusion can therefore be summarised as follows: Although case 3 is a combination of case 1 and case 2, the probabilistic profile parameters from case 2 plays a very small part in the final level of reliability achieved in case 3. The wind load in case 1 is by far the most dominant factor influencing the levels of reliability achieved for the different failure modes in case 3. Due to the shortcomings in the model used to predict the wind load the obtained result shown in Table 23 underestimates the actual level of reliability that can be achieved for the case where the reliability margin implied by both the resistance and loads was evaluated.

Without further calculations it is difficult to conclude if the actual level of reliability for the different failure modes will be higher than the required level of 3. However, it can be said with certainty that the actual reliability levels will be higher than the results given in Table 23.

Stellenbosch University http://scholar.sun.ac.za

In the design of LSFB the wall cladding and floor panels are not taken into consideration when the steel structure for such a building is designed. These cladding elements can add a great deal of extra stability and strength to the structure as a whole (SASFA, 2010).

The mentioned cladding elements provide up to 30 % extra stability to the structure as a whole (SASFA, 2010). With the extra stability provided and by revaluating the β calculations done for case 3 the necessary level of reliability of 3 could easily be achieved.

Stellenbosch University http://scholar.sun.ac.za

11. Final summary and conclusions

In Chapter 10 it was mentioned that the probabilistic based evaluation of codes can be performed in two different ways. For this research the focus was on the first category, specifically to assess the achieved element reliability of a typical structure designed according to SANS 517:2009 and SANS 10162-2:2010. The evaluation of β will therefore be performed on the most critical elements for each failure mode. The main focus was therefore on the evaluation of the reliability index β and not the calibration of partial factors in the respective codes that will influence the calculated β values.

This Chapter will focus on the main results obtained and the implications of these results.

11.1 Main results obtained

In Chapter 6.7 the main failure modes investigated were discussed. As shown in Table 24, a total of 5 different failure modes were investigated. The FORM analysis for each failure mode was performed in three different ways. One aspect of the analysis that influence the obtained reliability indices is the fact that a section profile was chosen that would be adequate to carry the deterministically determined design loads. The critical element for each failure mode was simply the element that was loaded to a level closest to the design capacity. However, in many cases this loaded level was still significantly lower than the profile's deterministic capacity, as can be seen in Table 24. The designer's choice of profile thus adds some conservatism to the codified capacity requirements and adds to the evaluated indices. The reliability indices thus reflect the reliability for this typical structure, but it should be noted that lower values can be expected to reflect the codified requirements. A short summary of all the results obtained in this research is presented in Table 24.

Stellenbosch University http://scholar.sun.ac.za

Table 24: Summarising table of results

Failure mode	Deterministic design load as obtained from Chap. 6.7	Deterministic capacity as calculated in Chap. 7	β-case 1	β-case 2	β-case 3
Axial load	15.76 kN	29.84 kN	2.952	6.852	2.948
Shear about the strong axis	8.05 kN	8.38 kN	2.365	0.248	2.237
Shear about the weak axis	4.458 kN	9.1 kN	3.15	3.99	3.062
Tension	16.93 kN	17.9 kN	2.133	2.16	2.195
Axial load & bending moment interaction	Axial: 12.54 kN M_x: 0.267 kNm M_y: 0.163 kNm Eq. 77,78	Axial: 29.84 kN M_x: 1.66 kNm M_y: 0.644 kNm Eq. 77,78	2.042	0.409	2.093

11.1.1 Case 1

Firstly, the reliability margin implied by the design load was evaluated. It was assumed that the resistance of the profile had a deterministic value while the loads (WL, LLF, LLR and DL) applied to the structure were taken as probabilistic, i.e. following their known distribution function with a certain variability that will influence the final level of reliability achieved for case 1. The assumption to take the profile parameters as deterministic entailed that none of the variability of the profile parameters was taken into consideration. The reliability level achieved for case 1 is therefore dependent on the loads applied to the structure as well as the extra conservatism due to the designer's choice of a profile. It must be noted that the wind loads have a much greater influence on LSFB compared to conventional hot rolled steel- or concrete-structures. Thus, by using such a conservative COV of 0.37, the wind load on the structure had by far the largest influence on the level of reliability achieved for this evaluation.

The basic wind speed values are characteristic values having an annual probability of exceedence of 0.02, which is equivalent to a mean return period of 50 years.

This distribution function was then used as basis to calculate the wind loads that were applied to the structural model.

Stellenbosch University http://scholar.sun.ac.za

Seeing that all the wind load calculations are based on a mean return period of 50 years, a basic wind speed model for the probability of exceedence in a life time of 50 years should have been used and not the annual probability of exceedence. Therefore the best model to describe wind load conditions was not used in this research.

The full implications and detailed discussion to the shortcoming in the wind model used is this research are given in Chapter 10.2, which let to the following final conclusions.

The obtained results shown in Table 9 provide a reasonable estimate and indication to the actual level of reliability that can be achieved for the case where the reliability margin implied by the design load was evaluated. However, these values have some shortcomings due to the reasons discussed in Chapter 10.2.2 . It is believed that the final and correct levels of reliability for the different failure modes are in fact higher than the required β of 2.1 (discussed in Chapter 10.2).

11.1.2 Case 2

Secondly, the reliability margin implied by the resistance of the profile was evaluated. The loading was assumed to have a single deterministic value. The resistance of the profile was taken as probabilistic with a certain distribution function. Furthermore, it was assumed that only the profile parameters f_y, t and r_i had probabilistic values with know distribution functions. The other profile parameters were taken as deterministic values. The assumption made therefore entailed that only the variability of the profile parameters (f_y, t and r_i) influenced the level of reliability achieved for case 2. With the simplification made that all the other profile parameters influencing the resistance capacity of the profile had deterministic values, an amount of variability found in the capacity of the profile is ignored. As discussed in Chapter 9.1, the resistance of the profile mostly depends on the variability of f_y, t and r_i. Therefore the assumption made to use a deterministic value for all other profile parameters is reasonable.

From this evaluation it could be seen that a very low level of reliability was achieved for the failure modes of shear working in on the strong axis of the profile as well as interaction between bending and axial load.

The results obtained for some of the failure modes in case 2 were not as expected(β values in the order of 2.4). The obtained results let to the question, are the reliability results obtained from

Stellenbosch University http://scholar.sun.ac.za

the FORM calculations for case 2 correct? More so, are the capacity calculations given in Appendix F: Detailed calculation of shear capacity correct? It can be said with good faith that the resistance calculations as well as the FORM evaluation done for case 2 are correct. Therefore some other factors, not taken into account, played a significant role in the levels of reliability achieved for case 2. A detailed discussion of possible factors and their implications are given in Chapter 10.3.2, with the main findings summarised as follows:

The results obtained may not be an indication of a deficiency in the shear resistance procedure, but it is certainly indicative of the need to re-evaluate the procedure in terms of reliability. The insufficient reliability obtained from the shear resistance is expected to arise from systematic estimates of the resistance by the codified procedure. A proper codified formulation should have provided a model factor to indicate such systematic adjustment. The absence of such a factor did not allow for illustrating this effect in the reliability analysis. Furthermore no information on the comparison between codified predictions and actual resistance is readily available. This is an illustration of the implication that codified procedures have to be accepted in good faith, without sufficient background information that could be used. Therefore, although the obtained β values are mathematically correct they cannot be used to quantify the reliability margin implied by the resistance of the profile was evaluated. Further research needs to be conducted in order to obtain β values that will represent the real life.

11.1.3 Case 3

Thirdly, the reliability margin implied by both the resistance and loads was evaluated. The resistance and loading values were taken as probabilistic with their known distribution functions. Again, on the resistance side, only f_y, t and r_i were taken as probabilistic values. In a real life situation both loads and resistances would have variability.

In case 1 and case 2 the variability in the loads and profile parameters respectively influenced the level of reliability achieved. Case 3 is a combination of case 1 and case 2 and therefore the variability influencing the reliability results in case 3 is also a combination of the variability that was found in case 1 and case 2. From the results obtained for the evaluation performed for case 3 it was found that the wind load on the structure as well as the thickness of the profile had the biggest influence on the level of reliability achieved for the failure modes in shear and the failure mode for axial loading. This is shown in Table 23. Therefore the variability for these three modes

Stellenbosch University http://scholar.sun.ac.za

will be a combination of the individual variabilities used in case 1 (wind load) and case 2 (profile thickness). It is very difficult to quantify the combination of variability. For the other failure modes the wind load was the only dominant influence on the level of reliability. It is therefore easier to quantify the variability.

However, the sensitivity factor of the wind load is still much larger than the sensitivity factor of the profile thickness. This is shown in Appendix L: Spread sheet calculations for evaluation of β-Case 3. Therefore the final level of reliability achieved for all failure modes were dominated by the level of reliability achieved in case 1 (loading on structure taken as probabilistic) and not by the level of reliability achieved in case 2 (resistance of profile taken as probabilistic). The wind load on the structure is therefore by far this most dominant factor or load influencing the final level of reliability achieved.

When a comparison between the results obtained in case 1 is made with the results obtained in case 3 it can be seen that these values are very similar. Although the profile thickness contributes to the final level of reliability achieved for case 3 it is a very small contribution. This can be said because the results for case 1 and case 3 are very similar and case 1 was only dependent on the wind loads on the structure.

From the discussion in Chapter 10.2.4 it becomes clear that the original obtained results for case 3 will be between the upper and lower limits of acceptable β values if the same simplification to the performance function is used.

The final conclusion can therefore be summarised as follows: Although case 3 is a combination of case 1 and case 2, the probabilistic profile parameters from case 2 plays a very small part in the final level of reliability achieved in case 3. The wind load in case 1 is by far the most dominant factor influencing the levels of reliability achieved for the different failure modes in case 3. Due to the shortcomings in the model used to predict the wind load the obtained result shown in Table 23 underestimates the actual level of reliability that can be achieved for the case where the reliability margin implied by both the resistance and loads was evaluated.

Without further calculations it is difficult to conclude if the actual level of reliability for the different failure modes will be higher than the required level of 3. However, it can be said with certainty that the actual reliability levels will be higher than the results given in Table 23.

Stellenbosch University http://scholar.sun.ac.za

In the design of LSFB the wall cladding and floor panels are not taken into consideration when the steel structure for such a building is designed. These cladding elements can add a great deal of extra stability and strength to the structure as a whole (SASFA, 2010).

The mentioned cladding elements provide up to 30 % extra stability to the structure as a whole (SASFA, 2010). With the extra stability provided and by revaluating the β calculations done for case 3 the necessary level of reliability of 3 could easily be achieved.

11.2 Implications of results

From the results obtained in Chapter 10 it is clear that the wind load WL (with a COV of 0.37) on the structural model and the profile section thickness t (with a COV of 0.053) are the predominant factors influencing the element reliability for the different failure modes. Furthermore it was seen that the necessary level of reliability was not achieved by all the failure modes investigated. However, it is believed that this is due to the fact that the best model to describe the wind model for this research was not used. To obtain the actual level of reliability further research will have to be conducted. If the actual reliability levels are still lower than the required level of reliability (which seems unlikely at this stage) ways must be found to improve the level of reliability for these failure modes to such an extend that they achieve the desired level of reliability of $\beta = 3$.

One option to improve the reliability of LSFB would be to increase the partial wind load factor γ_{WL} in the SANS 517:2009 code. This would ensure more reliable structures, but it would also entail higher building costs.

There are indications that the current map, in SANS 517:2009 and SANS 10160-3:2009, with the characteristic basic wind speed for South Africa is conservative (Retief et al., 2011). Because of this conservative map a conservative COV of 0.37 for WL was used in the reliability evaluations

Stellenbosch University http://scholar.sun.ac.za

performed. Mr. Andries Kruger just completed his PhD study on updating this map for South Africa. The updated map will improve the statistical description of basic wind speeds in South Africa. In the future it should therefore be justified to use a more realistic and less conservative probabilistic model for wind loads in South Africa. This could influence the estimated reliability of LSFB structures in a positive way. To update the current wind map in the loading codes will take some time.

On the resistance side of the reliability evaluations, the thickness t of the profile and the model factor or difference between the codified resistance and the actual profile resistance were the predominant factors to influence the level of reliability achieved. Currently the design codes do not incorporate or provide a partial factor for t in the resistance calculations for cold formed steel sections. Furthermore, Table 24 shows that very little or no reliability is found on the resistance side of the reliability evaluations performed. This is a great case for concern. It is recommended that a partial factor should be created to apply to the section thickness parameter and that the model factor should be investigated in detail so that it can be quantified. This factor should be calibrated to ensure that adequate resistance reliability is built into the predicted capacity of the SANS 10162 code. A partial factor is provided for the yield stress f_y and the influence of r_i to the resistance of the profile is so small that no partial factor is needed.

All designs of LSFB in South Africa are computer aided designs, where design packages (based on SANS 10162-2:2010 and SANS 517:2009) are used to develop drawings similar to the ones used to develop the structural model for this research. These drawings are then checked and sent to the manufacturer, where the sections are cut and drilled according to plan. It is therefore of utmost importance that a person with the necessary knowledge and understanding of the design package, is responsible for the plans. Furthermore, it must be ensured that all plans are checked by a professional engineer. Thus by incorporating more experience into the design of LSFB in South Africa a more robust structure can be designed that could make a positive contribution to the current level of reliability achieved by these structures until a further study into the material factors can be done.

Stellenbosch University http://scholar.sun.ac.za

11.3 Future work

The research performed for this MSc Eng. study was a first of its kind in South Africa. There are therefore still a lot of grey or untouched areas that need to be investigated in the near future to ensure that LSFB in South Africa are designed in the most optimum and cost efficient way possible. This section will therefore focus on identifying possible areas that still need to be investigated. Furthermore it will also look at subjects that were only touched on briefly in the study conducted for this research, i.e. the shortcoming of this research will be highlighted and possible solutions will be found to improve these shortcomings for future research.

11.3.1 Possible shortcomings in current research

By not using the best probabilistic model to predict the wind load on the structure influenced the obtained results in this research. The solution is addressed in detail in Chapter 11.1.1. Therefore the first improvement to this research would be to use the most accurate wind load model to perform the evaluation calculations to obtain the actual level of reliability for the different failure modes. Further possible shortcomings to the research conducted will follow.

11.3.1.1 Connection reliability and the influence of boundary conditions

Connections form a very important part of any structure. It is no different in the case of LSFB. With this in mind a thorough investigation into the connections found in LSFB must form a study that is conducted on its own. Therefore, for the research conducted in this study only one critical connection was designed and evaluated. It is therefore assumed that if all the other connections in the chosen structure were to be designed in the same way, the structure would be safe from a deterministic point of view. The chosen connection is very case specific and it does not represent the reliability of connections for LSFB in general.

The reliability evaluation of connections is influenced by two different factors. Firstly the profile parameters influence the resistance of a specific connection. Secondly the boundary conditions of a specific connection are very important in determining the resistance of the connection.

Stellenbosch University http://scholar.sun.ac.za

- **Profile parameters**

  The profile parameters (f_y, t, r_i, width, height, number of fasteners etc.) will influence the resistance of a connection. For this research these factors were taken into account for the reliability analysis performed on the chosen connection.

- **Boundary conditions**

  The way in which the boundary conditions of a connection are modelled will influence the reliability achieved by that connection. No specific attention was given to the modelling of these boundary conditions in this research. For the current study, connections were modelled as either pinned or fully fixed, whichever represented reality most adequately. Correspondingly, the effective lengths used in the resistance calculations corresponded to pinned or fixed element boundary conditions.

It is therefore suggested that a thorough investigation into the level of reliability achieved by connections in LSFB are investigated based on the work done by Mr. Andries Van Der Merwe in his final year project (Van der Merwe, 2010). By modelling all the different types of connections in a structural analysis program and by taking into account the boundary conditions of such connections, it will be possible to evaluate the level of reliability achieved, by both of the factors mentioned above, for the different connections very accurately. The effect of these factors can then be quantified on the overall structural reliability that was achieved.

11.3.1.2 Inclusion of probabilistic description for profile width and height in the reliability analysis

As mentioned, in this research only three profile parameters (f_y, t and r_i) were taken as probabilistic values with their given distribution functions. All the other profile parameters were taken as deterministic values. Although it is believed that the most critical or influential parameters (to the resistance of a profile) were taken as probabilistic, it is still possible that the simplification made will influence the obtained levels of reliability for the different failure modes, especially in case 2 where the reliability level implied by the resistance were evaluated.

Stellenbosch University http://scholar.sun.ac.za

It is therefore necessary to investigate the influence of this simplification in future studies. This can be done by performing the same reliability evaluation on specific elements where on the one hand only the three profile parameters f_y, t and r_i are taken as probabilistic and on the other hand all profile parameters are taken as probabilistic. By comparing the obtained results it will be possible to quantify the possible error due to the simplification made in this research.

Based on the preliminary sensitivity study referred to in Chapter 9.1, it is believed that the error would be less than 5%.

11.3.2 New research topics in LSFB

The aim of this section is to provide areas or topics in LSFB that were not covered by the research conducted in this study.

11.3.2.1 Specific element reliability evaluations

In the analysis done for this research a typical structure was considered where the critical elements were simply the ones loaded to a level closest to the theoretical (codified) capacity of the profile. However, in all cases, some reserve capacity was left due to a slightly conservative choice of profile. It cannot be ensured that this will be the case for all designs, thus less reliable designs can be obtained within the specifications provided by the current design codes.

Further research needs to be done where the element's theoretical capacity equals the design capacity, so that the reliability in worst case conditions is evaluated. By performing such a reliability evaluation it will be ensured that no extra margin of safety is built into a certain element because of the designer's conservative choice of a profile. The achieved level of reliability will therefore only be based on the safety margin implied by the different partial factors.

Stellenbosch University http://scholar.sun.ac.za

11.3.2.2 Reliability contribution of wall cladding panels

Only the reliability level achieved by the steel frame of LSFB was evaluated in this research. Therefore, the steel frame was designed in such a way that it complied with the buckling analysis discussed in Chapter 6.5. None of the cladding panels present in real life were modelled in the structural model. As mentioned, these panels can provide a significant amount of extra stability to a structure as a whole. Furthermore these panels will serve as a diaphragm transmitting forces to the vertical bracing walls (SASFA, 2010). Although the forces on these panels were calculated and transferred to the steel frame of the structural model used, it is still possible that the actual forces in the structural members would differ if the wall cladding was added to the structural model, specifically in the case of bracing members. Furthermore these panels would ad to the overall robustness of the structure and form alternative paths for loads to be distributed by.

It is therefore necessary to conduct a further investigation into the influence of the cladding panels to the overall structural stability that was evaluated in this research. The most important aspect of such an investigation will be to ensure that the connection between the steel frame and the actual cladding panels represent a real life situation. Without such an investigation it will not be possible to quantify the additional level of reliability that a structure can achieve if the cladding panels are taken into account.

From the above mentioned points it is clear that a lot of additional research still needs to be conducted on LSFB in South Africa.

Stellenbosch University http://scholar.sun.ac.za

Bibliography

Alfredo H - S. Ang, Wilson H. Tang, n.d. *Probability Concepts in Engineering Planning and Design*.

Anon., 2005. SANS 10162 - 1: 2005. *Part 1: Limit - stat design of hot rolled steelwork*.

Anon., 2008. SAISC. p.5.75.

Anon., 2009. Draft SANS 10160:Part 3, wind actions. *Part 3: Wind actions*, pp.11 - 78.

Beshara, B. & Schuster, R.M., 2000. *Web Crippling Data and calibrations of cold formed steel members*. Ontario: University of Waterloo, Canada.

Cao Hung Pham, Gregory J Hancock, March 2009. Direct Strength Desing of Cold - Formed Purlins. *Journal of Structural Engineering*, pp.229 - 238.

Cardoso, J.B., Almeida, J.R.d., Dias, J.M. & Coelho, P.G., 2008. Structural reliability analysis using Monte Carlo simulation and neural networks. *Advances in Engineering Software*, 39, pp.505-13.

Chen, J. & Young, B., 2006. Corner properties of cold - formed steel sections at elebated temperatures. *This - Walled Structures 44*, pp.216-23.

Coetzee, L., 2009. *clotansteel*. [Online] Available at: http//www.clotansteel/co.za [Accessed 16 September 2009].

Faber, P.M.H., 2009. Risk and Safety in Engineering., 2009.

Holicky, M., 2009. *Reliability analysis for structural design*. Stellenbosch: SUN MeDIA Stellenbosch.

Lau, S.C.W. & Hancock, G.J., 1986. Buckling of Thin Flat-Walled Structures by a Spline Finite Strip Method. *Thin-Walled Structures 4*, pp.269 - 294.

Metal Forming Technologies, 2006. [Online] Available at: www.steelframecad.com [Accessed 15 February 2011].

Pham, C.H. & Hancock, G., March 2009. Direct Strength Design of Cold - Formed Purlins. *Journal of Structural Engineering*, pp.229-38.

Retief, J.V., Barnardo, C. & Dinthe, M., 2011. Reliability basis for adopting Eurocodes as South African standards. *ICASP 2011*.

SANS, 2009. *SANS 517*. SANS.

SASFA, 2010. *Light Steel Frame Building*. SASFA.

Stellenbosch University http://scholar.sun.ac.za

Schafer, B.W., 2006. REVIEW: THE DIRECT STRENGTH METHOD OF. *STABILITY AND DUCTILITY OF STEEL STRUCTURES*.

Schafer, B.W., Grigoriu, M. & Pekoz, T., 1998. A probabilistic examination of the ultimate strength of cold - formed steel elements. *Thin - Walled Structures 31*, pp.271 - 288.

Schafer, B.W., October 2006. Designing Cold-Formed Steel Using the Direct Strength Method. In *18th International Specialty Conference on Cold-Formed Steel Structures*. Florida, October 2006.

Schafer, B.W., September 2006. REVIEW: THE DIRECT STRENGTH METHOD OF COLD-FORMED STEEL MEMBER DESIGN. *STABILITY AND DUCTILITY OF STEEL STRUCTURES*.

Van der Merwe, A.J., 2010. *S14 Kapasiteit van verbindings in ligte staal strukture*. Stellenbosch: University of Stellenbosch.

Varpasuo, P., August 2001. STOCHASTIC ANALYSIS OF WIND AND SNOW LOADS IN LOAD. In *Paper 1863*. Washington DC, August 2001.

Stellenbosch University http://scholar.sun.ac.za

Appendix A: User manual for the use of CSFUM

Tutorial 1

- Default Cee section in bending
- Objective

  To introduce the conventional finite strip method and gain a rudimentary understanding of how to perform an analysis and interpret the results.
- A the end of the tutorial you should be able to
  - enter simple geometry
  - enter loads (stresses)
  - perform a finite strip analysis
  - manipulate the post-processor

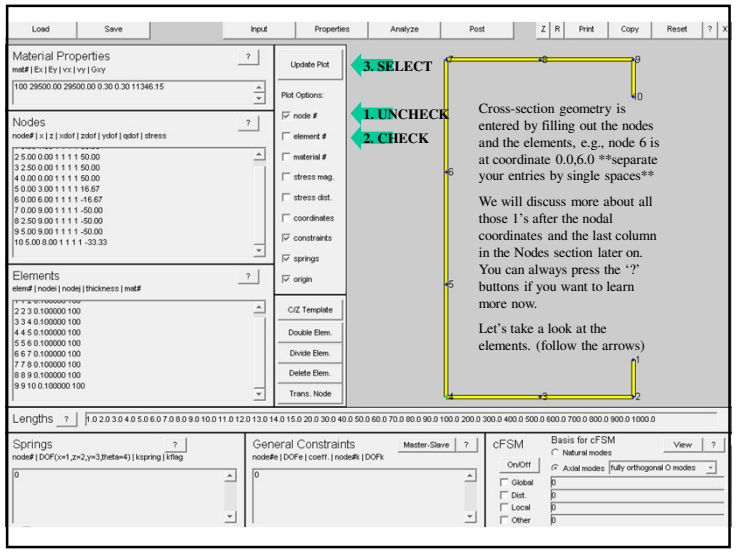

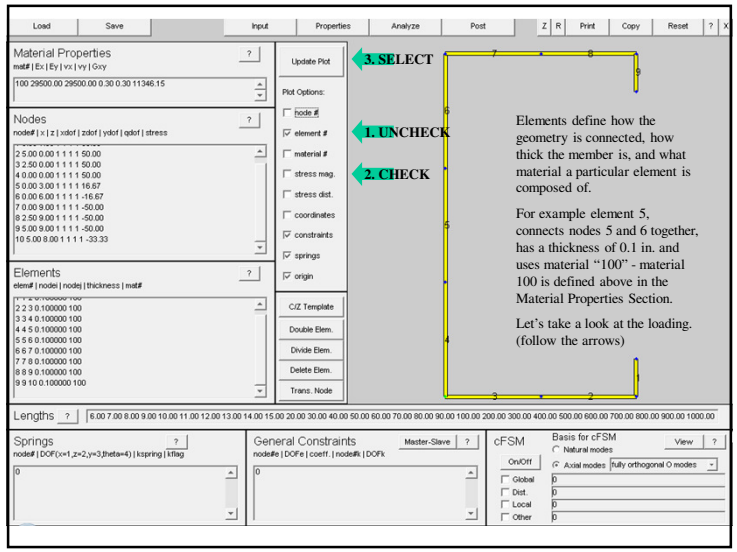

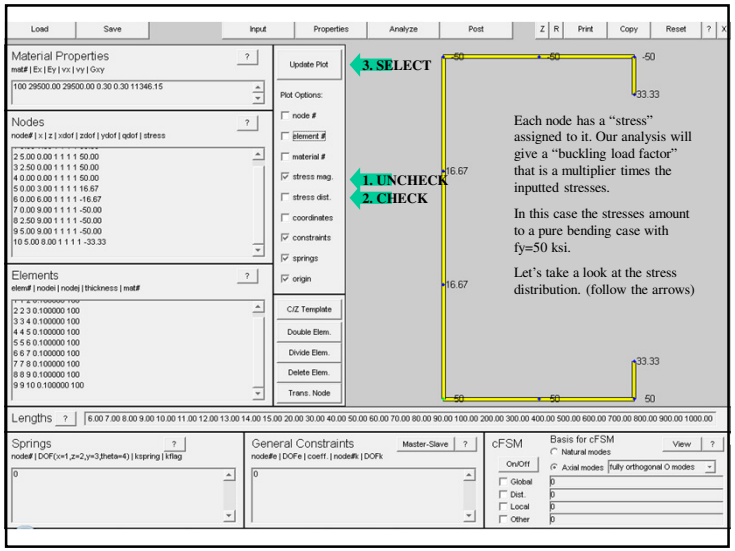
3. SELECT
1. UNCHECK
2. CHECK
Each node has a "stress" assigned to it. Our analysis will give a "buckling load factor" that is a multiplier times the inputted stresses.
In this case the stresses amount to a pure bending case with fy=50 ksi.
Let's take a look at the stress distribution. (follow the arrows)

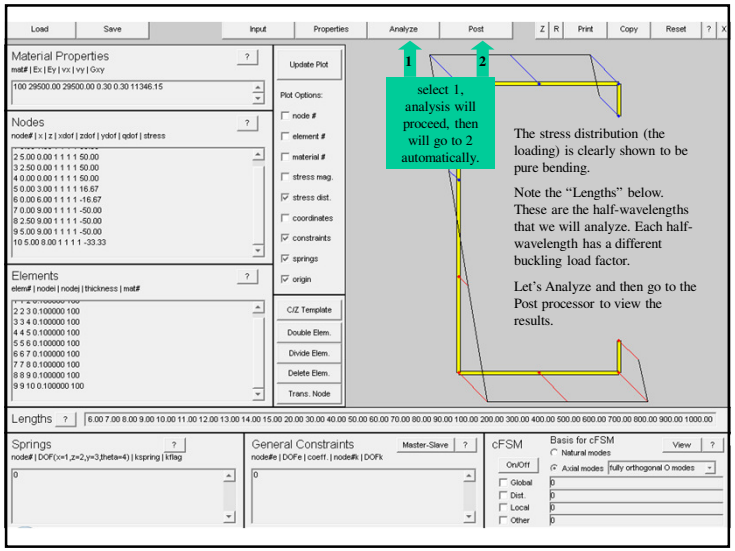
select 1, analysis will proceed, then will go to 2 automatically.
The stress distribution (the loading) is clearly shown to be pure bending.
Note the "Lengths" below. These are the half-wavelengths that we will analyze. Each half-wavelength has a different buckling load factor.
Let's Analyze and then go to the Post processor to view the results.

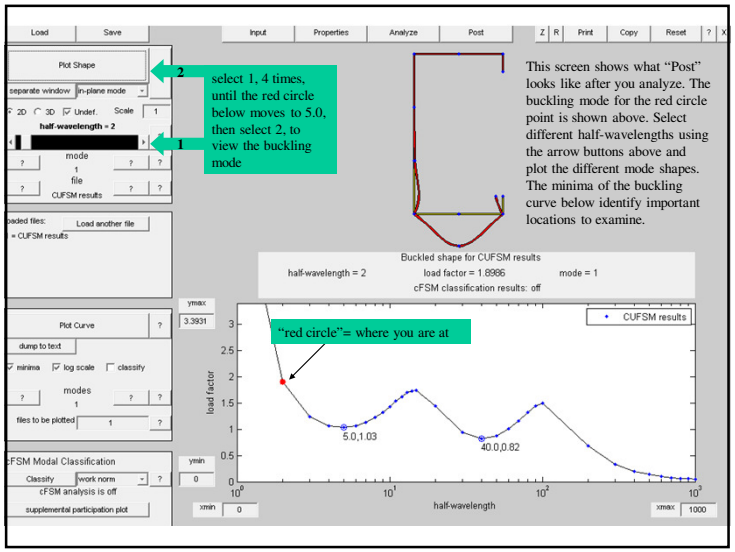
select 1, 4 times, until the red circle below moves to 5.0, then select 2, to view the buckling mode
This screen shows what "Post" looks like after you analyze. The buckling mode for the red circle point is shown above. Select different half-wavelengths using the arrow buttons above and plot the different mode shapes. The minima of the buckling curve below identify important locations to examine.
"red circle"= where you are at
Buckled shape for CUFSM results
half-wavelength = 2
load factor = 1.8986
mode = 1
cFSM classification results: off
5.0,1.03
40.0,0.82
load factor
half-wavelength

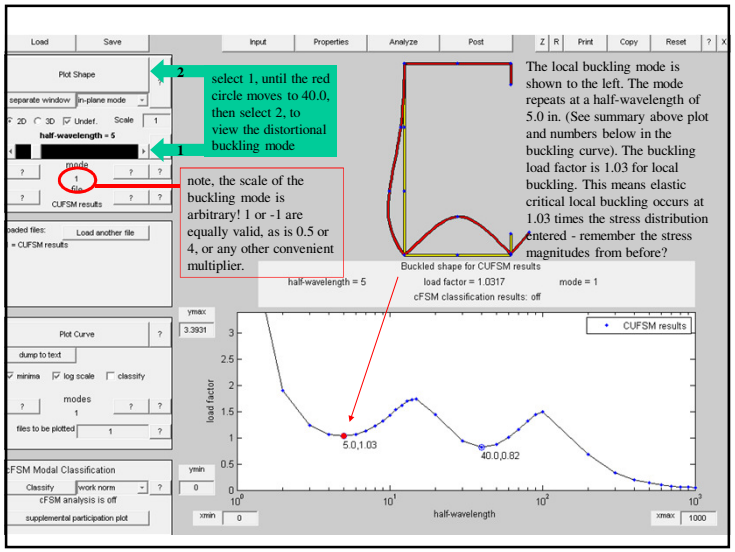
select 1, until the red circle moves to 40.0, then select 2, to view the distortional buckling mode
note, the scale of the buckling mode is arbitrary! 1 or -1 are equally valid, as is 0.5 or 4, or any other convenient multiplier.
The local buckling mode is shown to the left. The mode repeats at a half-wavelength of 5.0 in. (See summary above plot and numbers below in the buckling curve). The buckling load factor is 1.03 for local buckling. This means elastic critical local buckling occurs at 1.03 times the stress distribution entered - remember the stress magnitudes from before?
Buckled shape for CUFSM results
half-wavelength = 5
load factor = 1.0317
mode = 1
cFSM classification results: off
5.0,1.03
40.0,0.82
load factor
half-wavelength

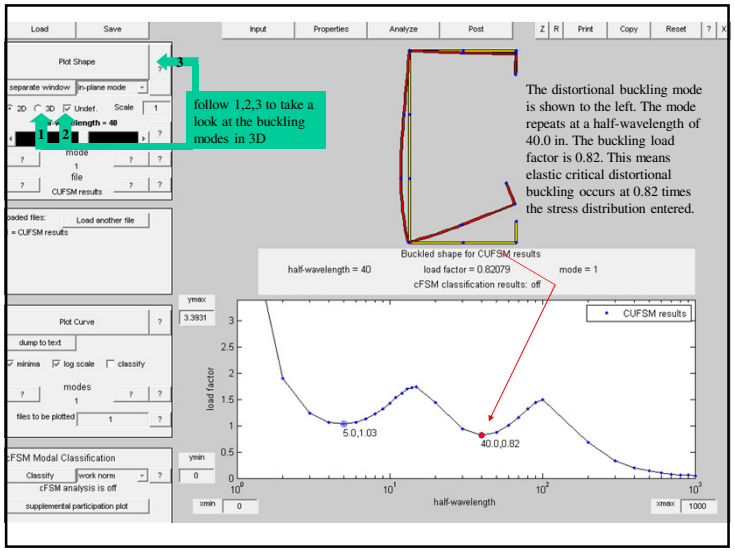
follow 1,2,3 to take a look at the buckling modes in 3D
The distortional buckling mode is shown to the left. The mode repeats at a half-wavelength of 40.0 in. The buckling load factor is 0.82. This means elastic critical distortional buckling occurs at 0.82 times the stress distribution entered.
Buckled shape for CUFSM results
half-wavelength = 40
load factor = 0.82079
mode = 1
cFSM classification results: off
CUFSM results
5.0,1.03
40.0,0.82
load factor
half-wavelength

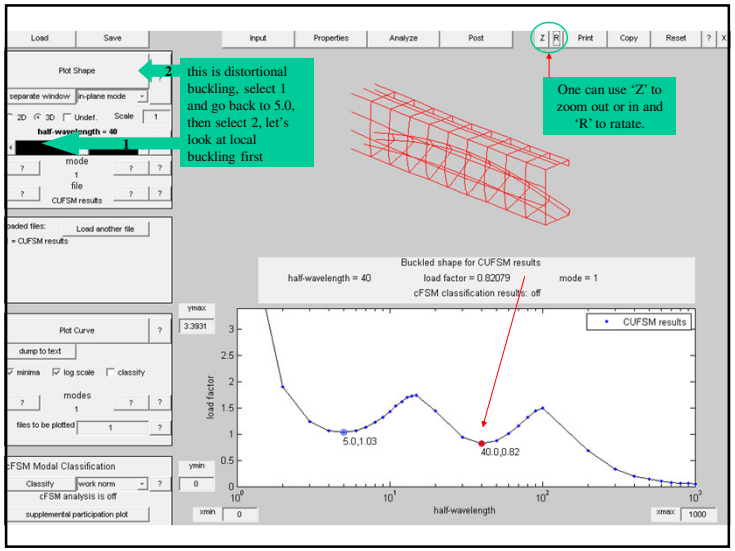
this is distortional buckling, select 1 and go back to 5.0, then select 2, let's look at local buckling first
One can use 'Z' to zoom out or in and 'R' to ratate.
Buckled shape for CUFSM results
half-wavelength = 40
load factor = 0.82079
mode = 1
cFSM classification results: off
CUFSM results
5.0,1.03
40.0,0.82
load factor
half-wavelength

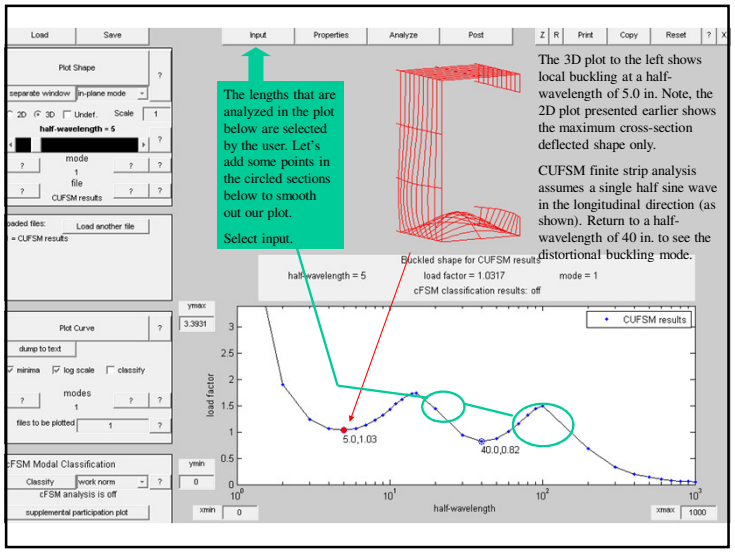
The lengths that are analyzed in the plot below are selected by the user. Let's add some points in the circled sections below to smooth out our plot.
Select input.
The 3D plot to the left shows local buckling at a half-wavelength of 5.0 in. Note, the 2D plot presented earlier shows the maximum cross-section deflected shape only.
CUFSM finite strip analysis assumes a single half sine wave in the longitudinal direction (as shown). Return to a half-wavelength of 40 in. to see the distortional buckling mode.
Buckled shape for CUFSM results
half-wavelength = 5
load factor = 1.0317
mode = 1
cFSM classification results: off
CUFSM results
5.0,1.03
40.0,0.82
load factor
half-wavelength

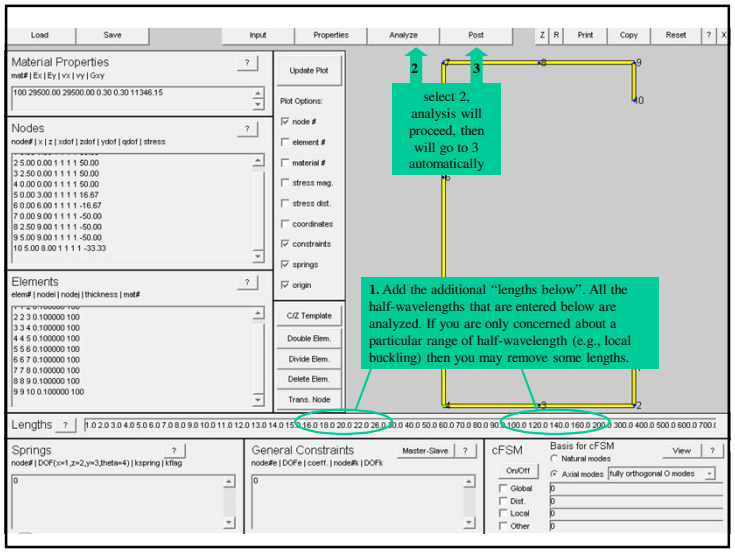
select 2, analysis will proceed, then will go to 3 automatically
1. Add the additional "lengths below". All the half-wavelengths that are entered below are analyzed. If you are only concerned about a particular range of half-wavelength (e.g., local buckling) then you may remove some lengths.
Material Properties
Nodes
Elements
Lengths
Springs
General Constraints
cFSM

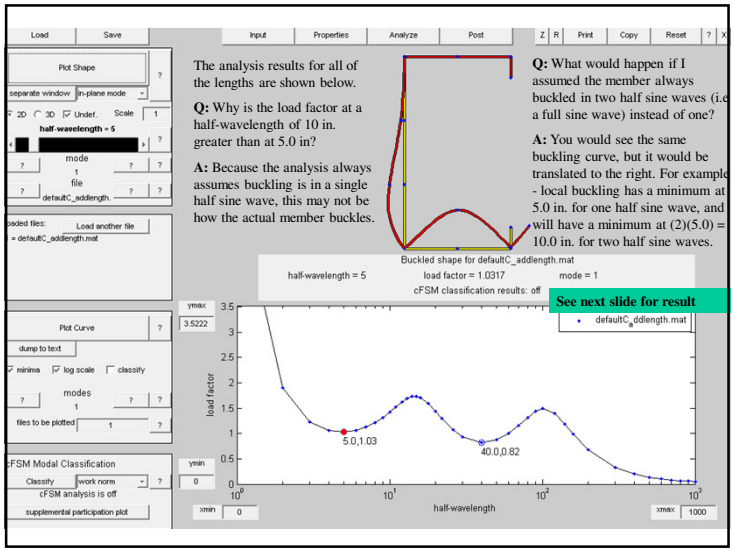

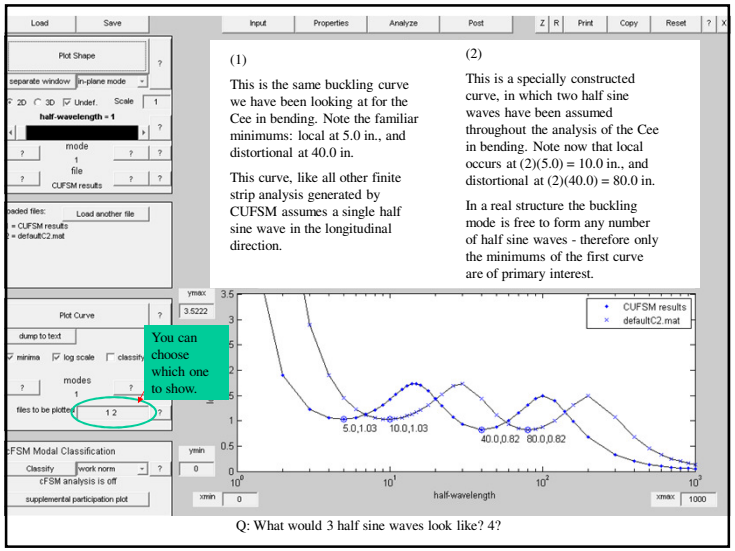

CUFSM3.12

Tutorial 1: Conclusions

- Default Cee section in bending
- Objective

  To introduce the conventional finite strip method and gain a rudimentary understanding of how to perform an analysis and interpret the results.
- A the end of the tutorial you should be able to
  - enter simple geometry
  - enter loads (stresses)
  - perform a finite strip analysis
  - manipulate the post-processor

Tutorial 2

- SSMA Cee in Compression: 600S200-33 F_y = 50ksi
- Objective

  To model a typical Cee stud in compression and determine the elastic critical local buckling load ($P_{cr\ell}$)and elastic critical distortional buckling load (P_{crd}).
- A the end of the tutorial you should be able to
  - enter material, nodes, elements, and lengths from scratch
  - apply a reference load P, or M as desired
  - interpret a simple buckling curve
  - identify local and distortional buckling in a simple member
  - determine $P_{cr\ell}$ and P_{crd}

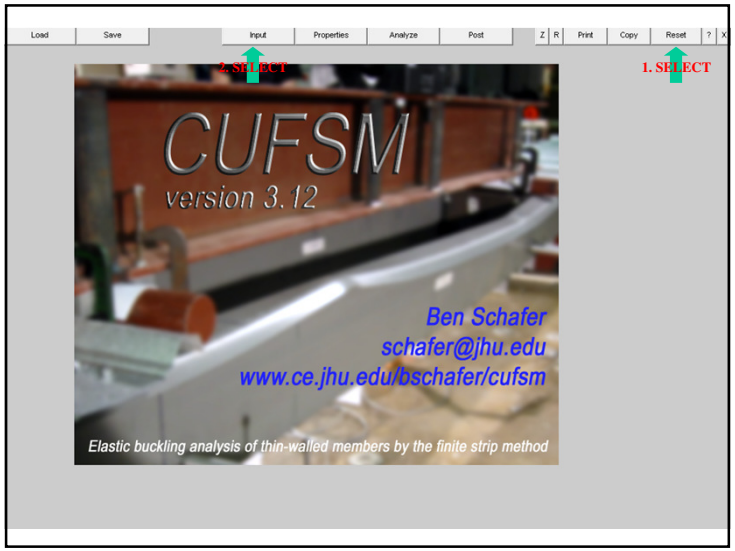

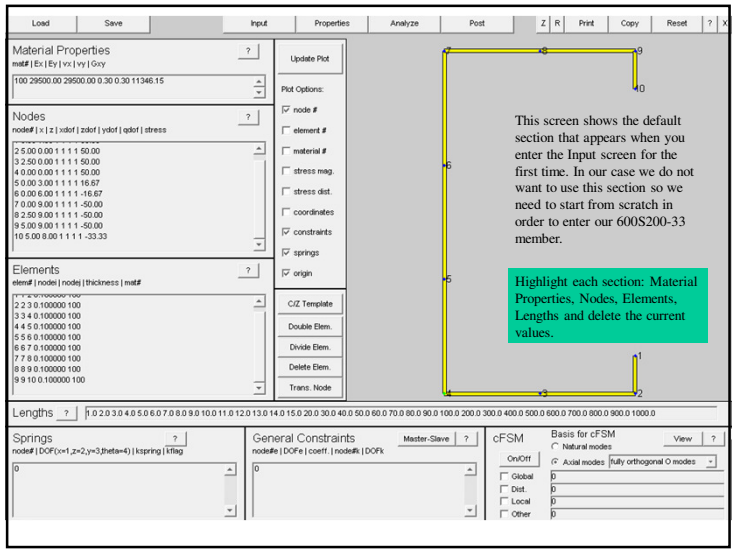

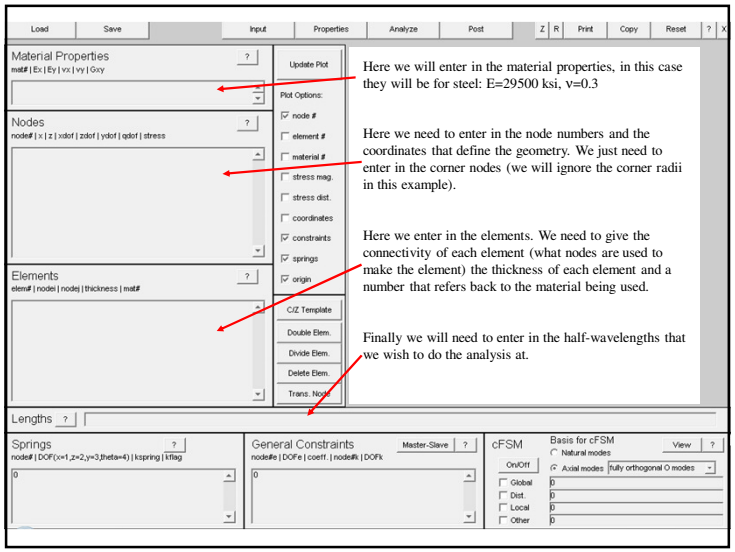

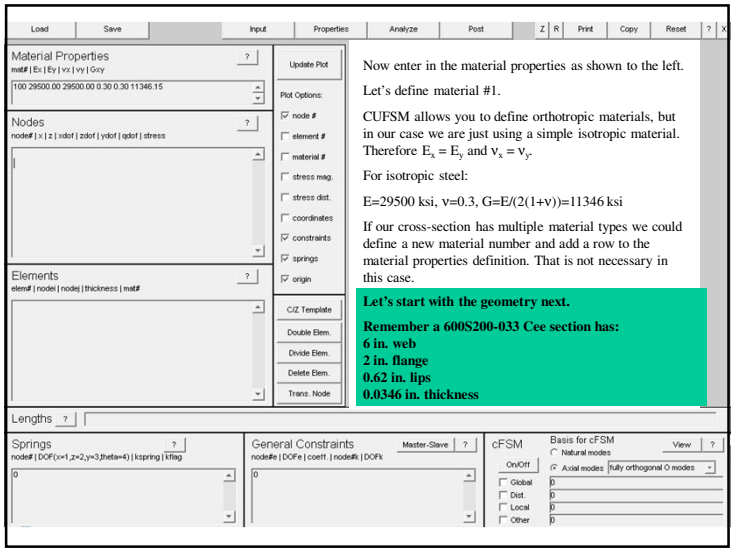

Now enter in the material properties as shown to the left.

Let's define material #1.

CUFSM allows you to define orthotropic materials, but in our case we are just using a simple isotropic material. Therefore $E_x = E_y$ and $\nu_x = \nu_y$.

For isotropic steel:

E=29500 ksi, ν=0.3, G=E/(2(1+ν))=11346 ksi

If our cross-section has multiple material types we could define a new material number and add a row to the material properties definition. That is not necessary in this case.

Let's start with the geometry next.

Remember a 600S200-033 Cee section has:
6 in. web
2 in. flange
0.62 in. lips
0.0346 in. thickness

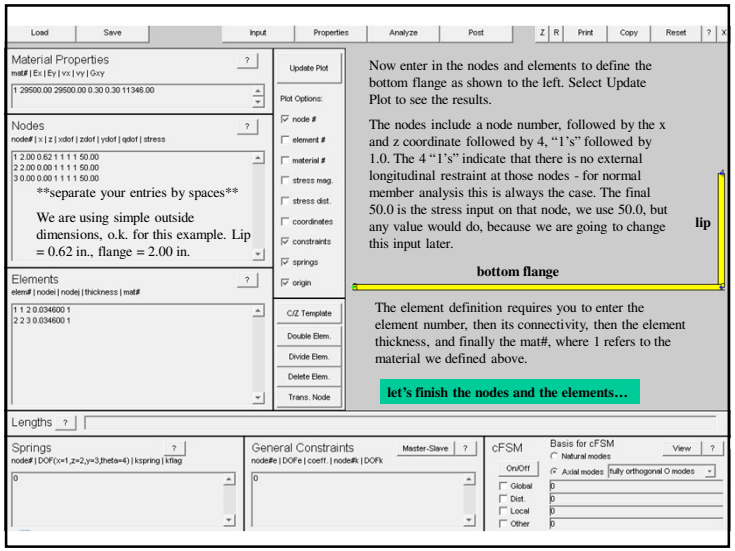

Now enter in the nodes and elements to define the bottom flange as shown to the left. Select Update Plot to see the results.

The nodes include a node number, followed by the x and z coordinate followed by 4, "1's" followed by 1.0. The 4 "1's" indicate that there is no external longitudinal restraint at those nodes - for normal member analysis this is always the case. The final 50.0 is the stress input on that node, we use 50.0, but any value would do, because we are going to change this input later.

lip

bottom flange

The element definition requires you to enter the element number, then its connectivity, then the element thickness, and finally the mat#, where 1 refers to the material we defined above.

let's finish the nodes and the elements…

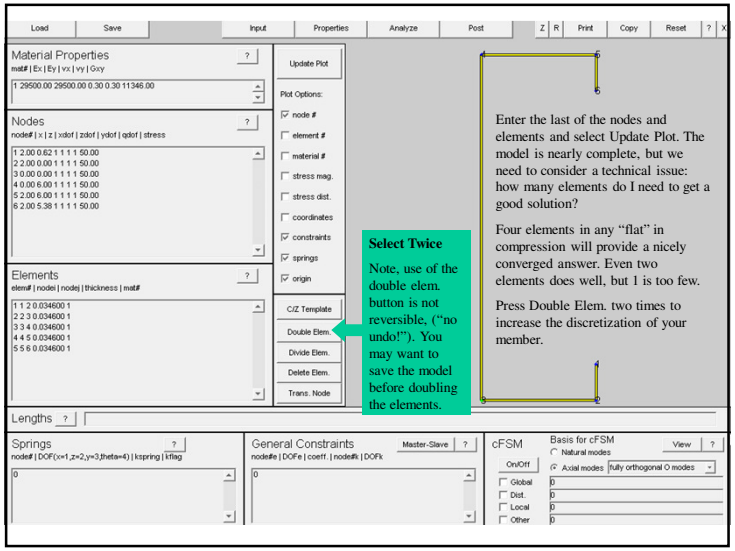

Select Twice

Note, use of the double elem. button is not reversible, ("no undo!"). You may want to save the model before doubling the elements.

Enter the last of the nodes and elements and select Update Plot. The model is nearly complete, but we need to consider a technical issue: how many elements do I need to get a good solution?

Four elements in any "flat" in compression will provide a nicely converged answer. Even two elements does well, but 1 is too few.

Press Double Elem. two times to increase the discretization of your member.

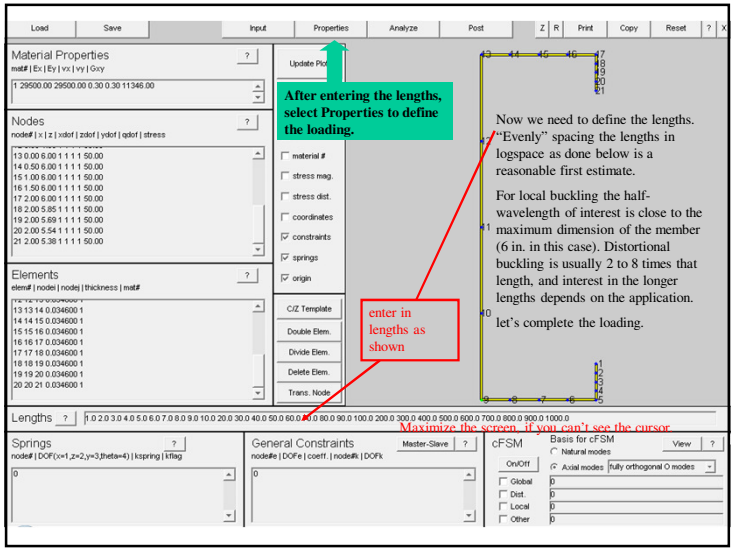

After entering the lengths, select Properties to define the loading.

enter in lengths as shown

Maximize the screen, if you can't see the cursor

Now we need to define the lengths. "Evenly" spacing the lengths in logspace as done below is a reasonable first estimate.

For local buckling the half-wavelength of interest is close to the maximum dimension of the member (6 in. in this case). Distortional buckling is usually 2 to 8 times that length, and interest in the longer lengths depends on the application.

let's complete the loading.

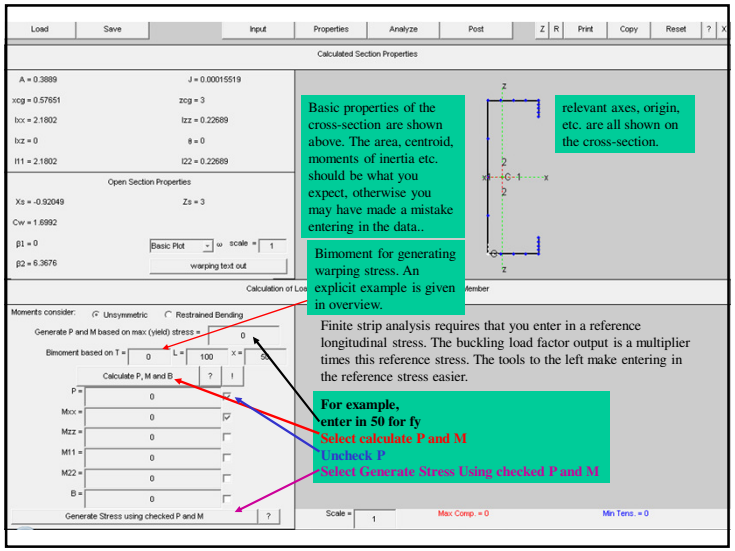
Basic properties of the cross-section are shown above. The area, centroid, moments of inertia etc. should be what you expect, otherwise you may have made a mistake entering in the data..
relevant axes, origin, etc. are all shown on the cross-section.
Bimoment for generating warping stress. An explicit example is given in overview.
Finite strip analysis requires that you enter in a reference longitudinal stress. The buckling load factor output is a multiplier times this reference stress. The tools to the left make entering in the reference stress easier.
For example,
enter in 50 for fy
Select calculate P and M
Uncheck P
Select Generate Stress Using checked P and M

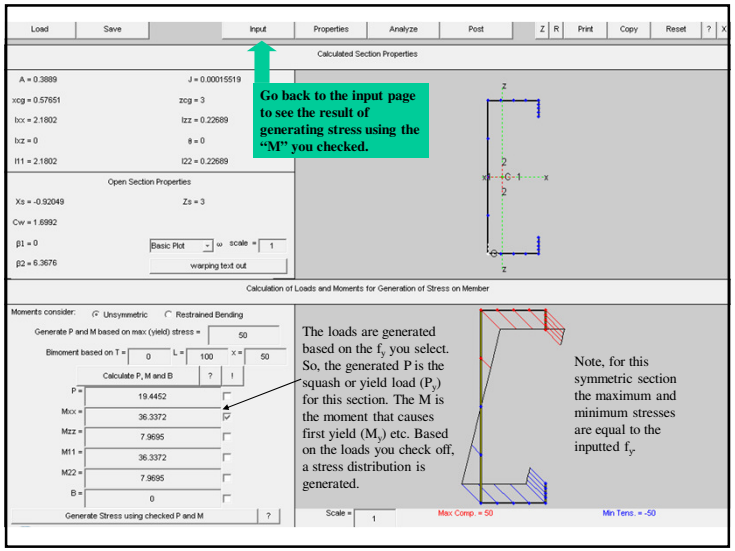
Go back to the input page to see the result of generating stress using the "M" you checked.
The loads are generated based on the fy you select. So, the generated P is the squash or yield load (Py) for this section. The M is the moment that causes first yield (My) etc. Based on the loads you check off, a stress distribution is generated.
Note, for this symmetric section the maximum and minimum stresses are equal to the inputted fy.

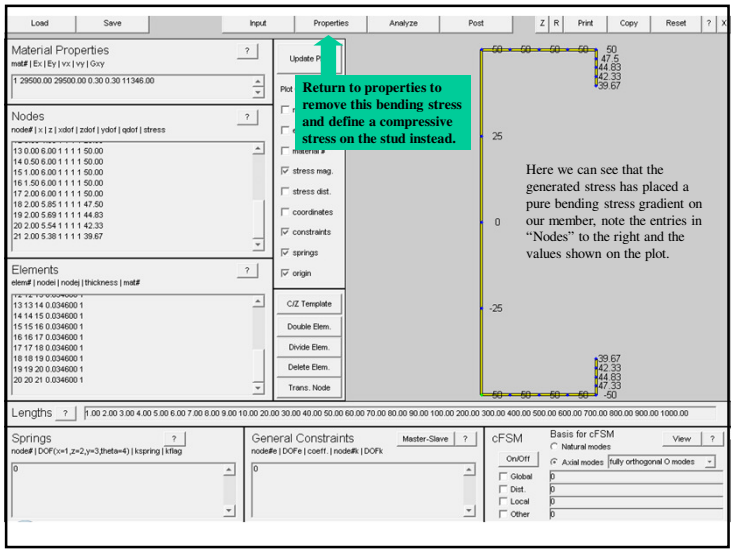
Return to properties to remove this bending stress and define a compressive stress on the stud instead.
Here we can see that the generated stress has placed a pure bending stress gradient on our member, note the entries in "Nodes" to the right and the values shown on the plot.

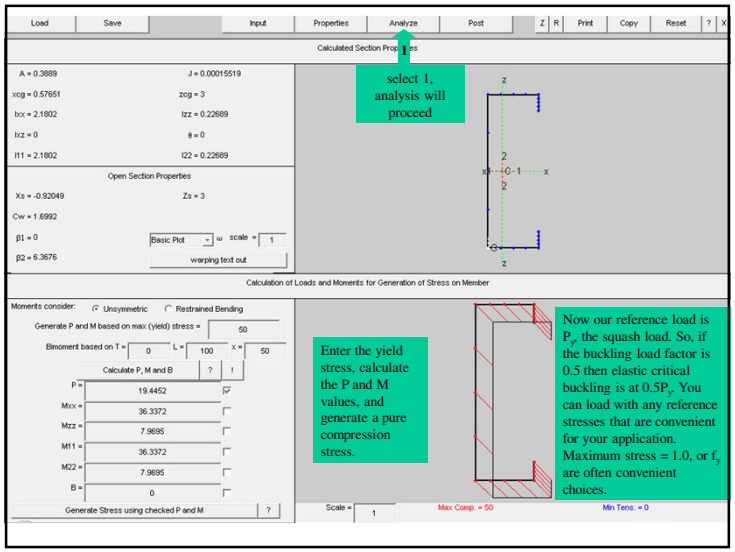
select 1, analysis will proceed
Enter the yield stress, calculate the P and M values, and generate a pure compression stress.
Now our reference load is Py, the squash load. So, if the buckling load factor is 0.5 then elastic critical buckling is at 0.5Py. You can load with any reference stresses that are convenient for your application. Maximum stress = 1.0, or fy are often convenient choices.

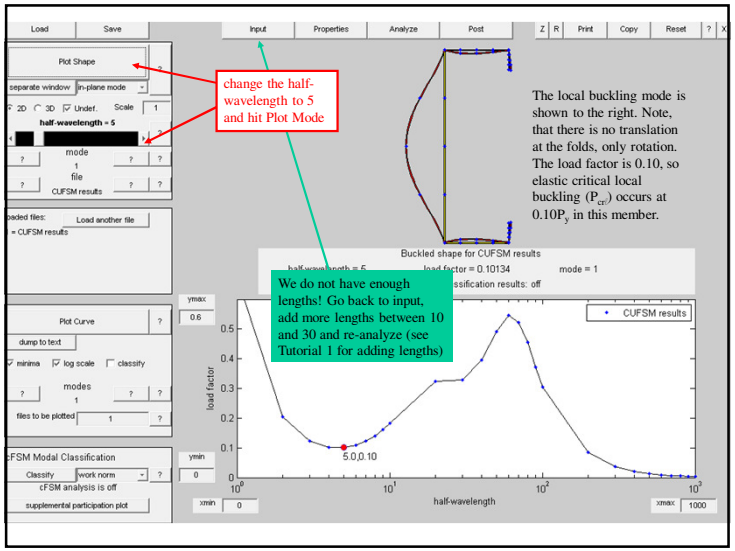
change the half-wavelength to 5 and hit Plot Mode
The local buckling mode is shown to the right. Note, that there is no translation at the folds, only rotation. The load factor is 0.10, so elastic critical local buckling (P_{cr}) occurs at $0.10P_y$ in this member.
We do not have enough lengths! Go back to input, add more lengths between 10 and 30 and re-analyze (see Tutorial 1 for adding lengths)
Buckled shape for CUFSM results
half-wavelength = 5
load factor = 0.10134
mode = 1
cFSM classification results: off
CUFSM results
5.0,0.10
load factor
half-wavelength

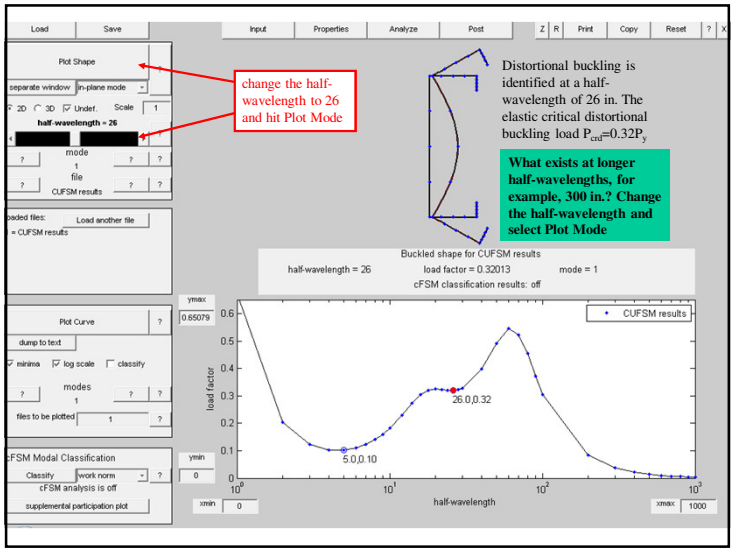
change the half-wavelength to 26 and hit Plot Mode
Distortional buckling is identified at a half-wavelength of 26 in. The elastic critical distortional buckling load P_{crd}=0.32P_y
What exists at longer half-wavelengths, for example, 300 in.? Change the half-wavelength and select Plot Mode
Buckled shape for CUFSM results
half-wavelength = 26
load factor = 0.32013
mode = 1
cFSM classification results: off
CUFSM results
26.0,0.32
5.0,0.10
load factor
half-wavelength

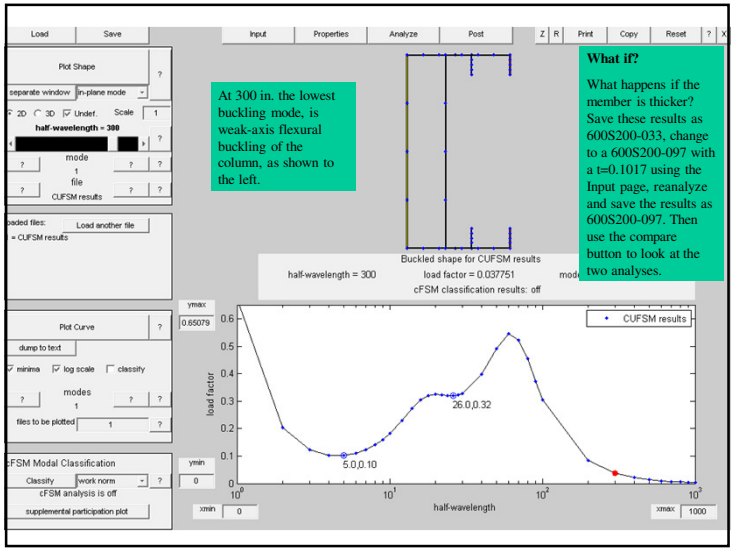
At 300 in. the lowest buckling mode, is weak-axis flexural buckling of the column, as shown to the left.
What if?
What happens if the member is thicker? Save these results as 600S200-033, change to a 600S200-097 with a t=0.1017 using the Input page, reanalyze and save the results as 600S200-097. Then use the compare button to look at the two analyses.
Buckled shape for CUFSM results
half-wavelength = 300
load factor = 0.037751
cFSM classification results: off
CUFSM results
26.0,0.32
5.0,0.10
load factor
half-wavelength

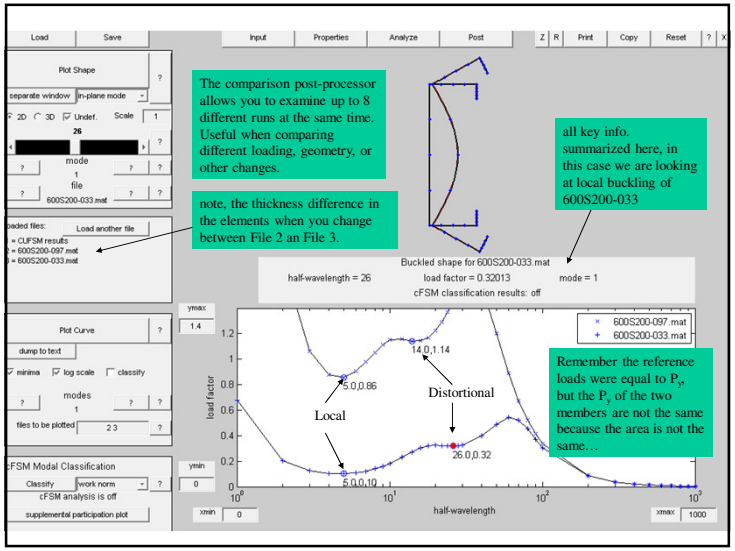
The comparison post-processor allows you to examine up to 8 different runs at the same time. Useful when comparing different loading, geometry, or other changes.
note, the thickness difference in the elements when you change between File 2 an File 3.
all key info. summarized here, in this case we are looking at local buckling of 600S200-033
Buckled shape for 600S200-033.mat
half-wavelength = 26
load factor = 0.32013
mode = 1
cFSM classification results: off
600S200-097.mat
600S200-033.mat
14.0,1.14
5.0,0.86
Distortional
Local
26.0,0.32
5.0,0.10
Remember the reference loads were equal to P_y, but the P_y of the two members are not the same because the area is not the same…
load factor
half-wavelength

CUFSM3.12

Tutorial 2: Conclusion

- SSMA Cee in Compression: 600S200-33 F_y = 50ksi
- Objective

  To model a typical Cee stud in compression and determine the elastic critical local buckling load ($P_{cr\ell}$)and elastic critical distortional buckling load (P_{crd}).
- A the end of the tutorial you should be able to
  - enter material, nodes, elements, and lengths from scratch
  - apply a reference load P, or M as desired
  - interpret a simple buckling curve
  - identify local and distortional buckling in a simple member
  - determine $P_{cr\ell}$ and P_{crd}

Tutorial 3

- LGSI Zee in Bending: Z 12 x 2.5 14g, F_y = 50ksi
- Objective

  To model a typical Zee purlin or girt in bending and determine the elastic critical local buckling moment ($M_{cr\ell}$)and elastic critical distortional buckling moment (M_{crd}).
- A the end of the tutorial you should be able to
  - enter material, nodes, elements, and lengths from scratch
  - OR use the C and Z template to enter a geometry
  - apply a reference load P, or M as desired
  - interpret a simple buckling curve
  - identify local and distortional buckling in a simple member
  - determine $M_{cr\ell}$ and M_{crd}

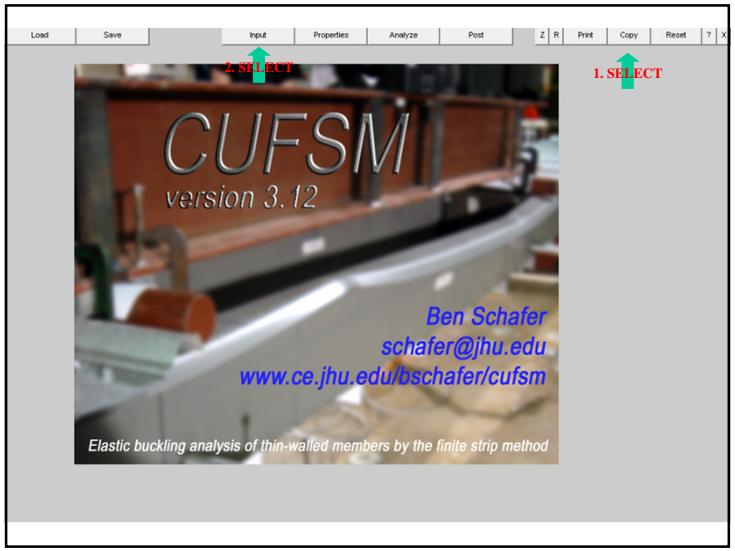

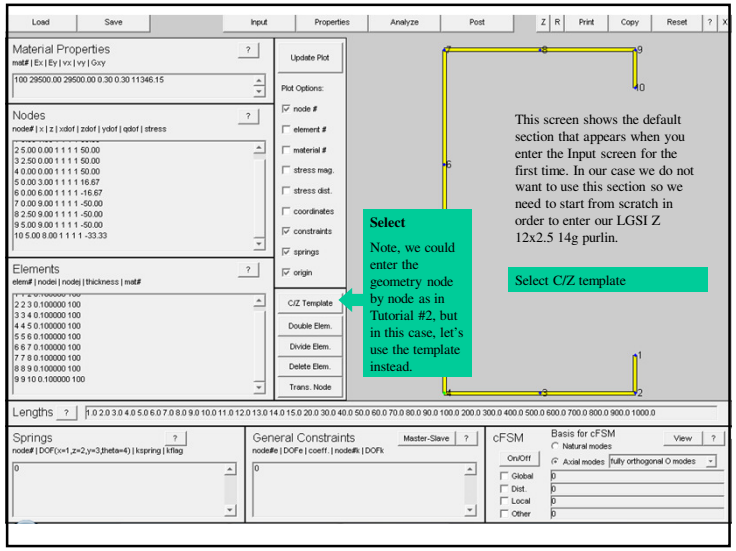

This is the default template that comes up when you select the template button. Note that all dimensions are centerline dimensions - e.g., h is the flat distance, not the out-to-out distance as is typically listed in product catalogs, etc.

Enter in all the appropriate dimensions and select Submit to input.

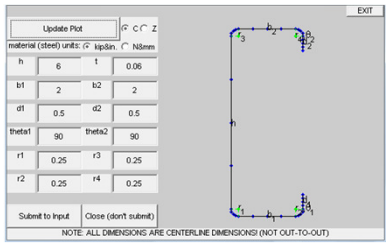

The centerline dimensions for an LGSI Z 12 x 2.5 14g member are shown to the right. Enter in these dimensions and then press Update Plot. When complete select Submit to Input.

Note, the material is assumed to be steel, but two units systems are supported. Geometry other than the typical Cee or Zee can be entered.

The template automatically selects an adequate number of elements.

The template automatically selects lengths to be analyzed as well.

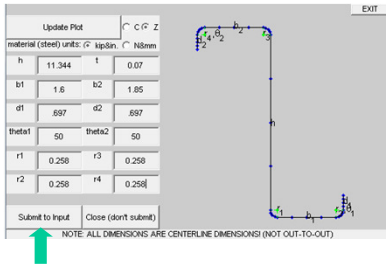

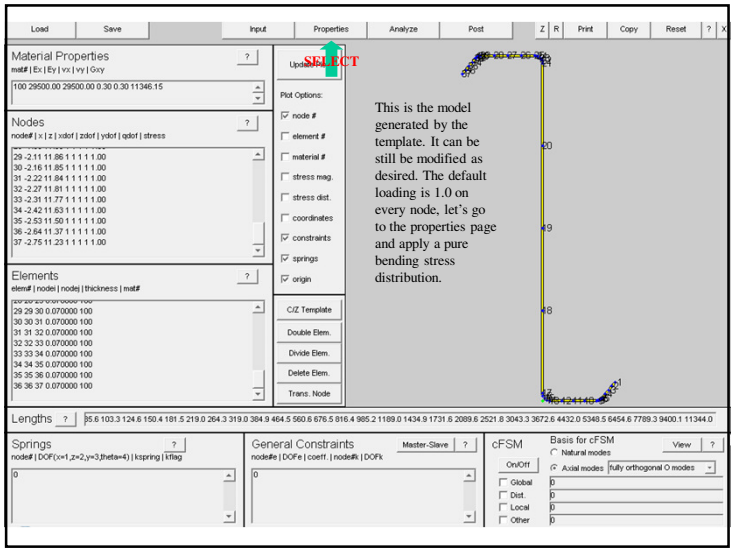
SELECT
This is the model generated by the template. It can be still be modified as desired. The default loading is 1.0 on every node, let's go to the properties page and apply a pure bending stress distribution.

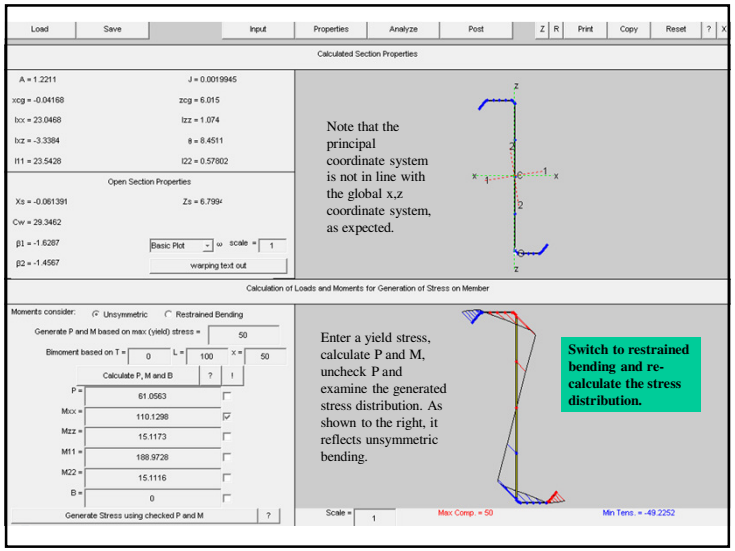
Note that the principal coordinate system is not in line with the global x,z coordinate system, as expected.
Enter a yield stress, calculate P and M, uncheck P and examine the generated stress distribution. As shown to the right, it reflects unsymmetric bending.
Switch to restrained bending and re-calculate the stress distribution.

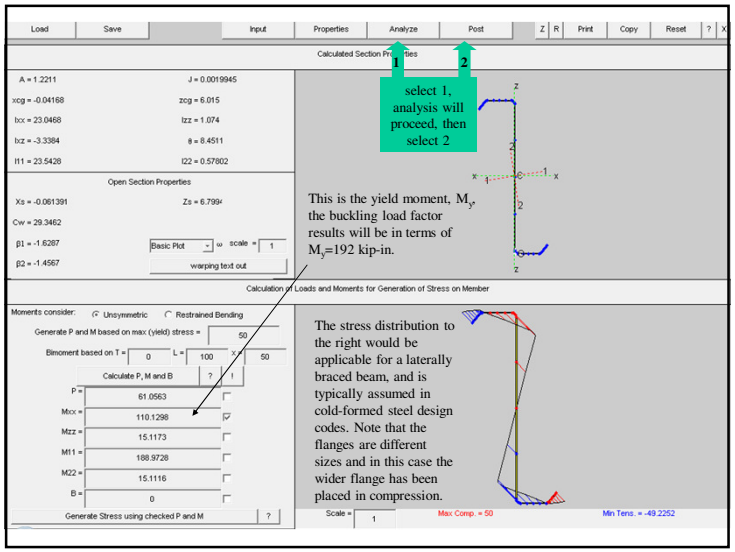
1
2
select 1, analysis will proceed, then select 2
This is the yield moment, My, the buckling load factor results will be in terms of My=192 kip-in.
The stress distribution to the right would be applicable for a laterally braced beam, and is typically assumed in cold-formed steel design codes. Note that the flanges are different sizes and in this case the wider flange has been placed in compression.

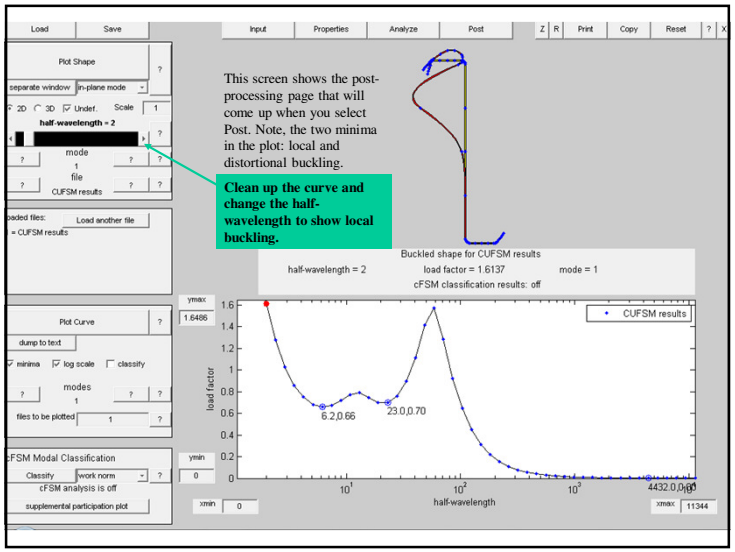
This screen shows the post-processing page that will come up when you select Post. Note, the two minima in the plot: local and distortional buckling.
Clean up the curve and change the half-wavelength to show local buckling.
Buckled shape for CUFSM results
half-wavelength = 2
load factor = 1.6137
mode = 1
cFSM classification results: off
CUFSM results
load factor
half-wavelength
6.2,0.66
23.0,0.70

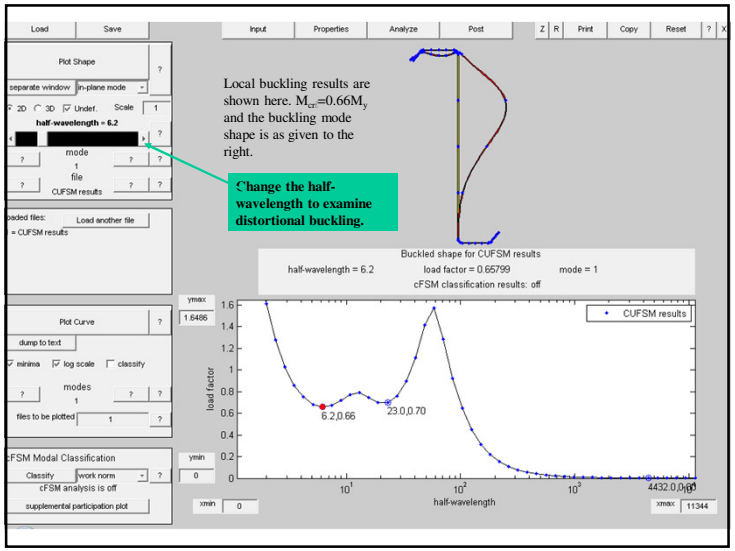

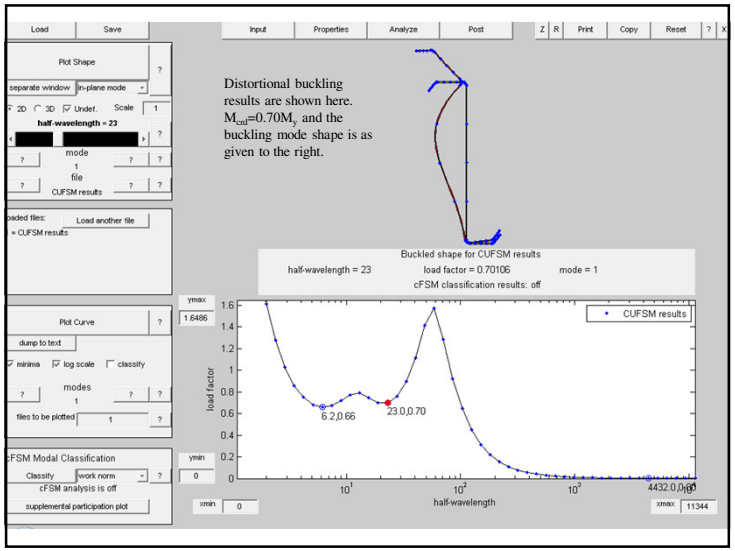

CUFSM3.12

Tutorial 3

- LGSI Zee in Bending: Z 12 x 2.5 14g F_y = 50ksi
- Objective

  To model a typical Zee purlin or girt in bending and determine the elastic critical local buckling moment ($M_{cr\ell}$)and elastic critical distortional buckling moment (M_{crd}).
- A the end of the tutorial you should be able to
  - enter material, nodes, elements, and lengths from scratch
  - OR use the C and Z template to enter a geometry
  - apply a reference load P, or M as desired
  - interpret a simple buckling curve
  - identify local and distortional buckling in a simple member
  - determine $M_{cr\ell}$ and M_{crd}

Stellenbosch University http://scholar.sun.ac.za

APPENDIX B: Profile parameters for the S8995 profile

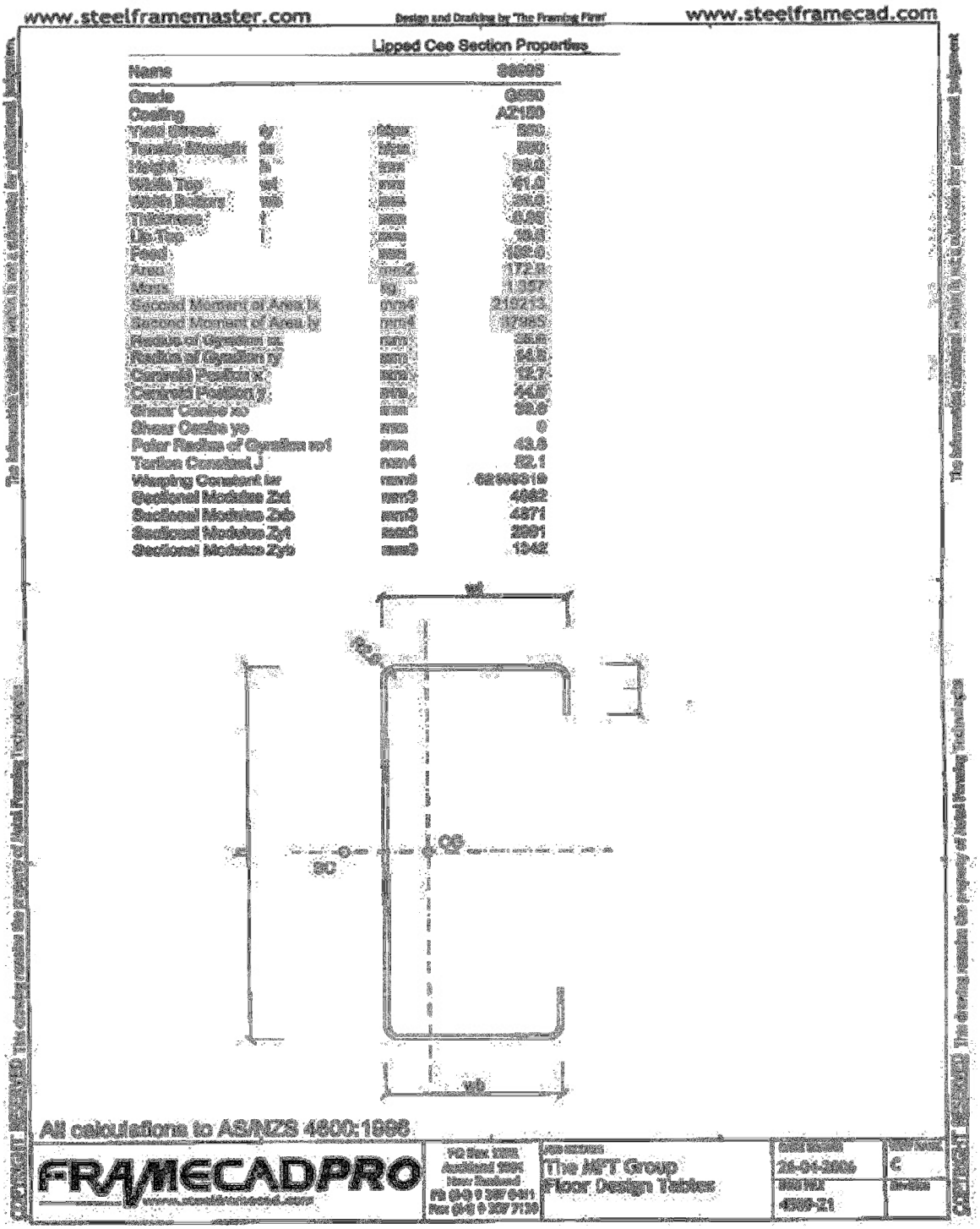

(Metal Forming Technologies, 2006)

Stellenbosch University http://scholar.sun.ac.za

APPENDIX C: Detailed drawings and layouts for structural model

Stellenbosch University http://scholar.sun.ac.za

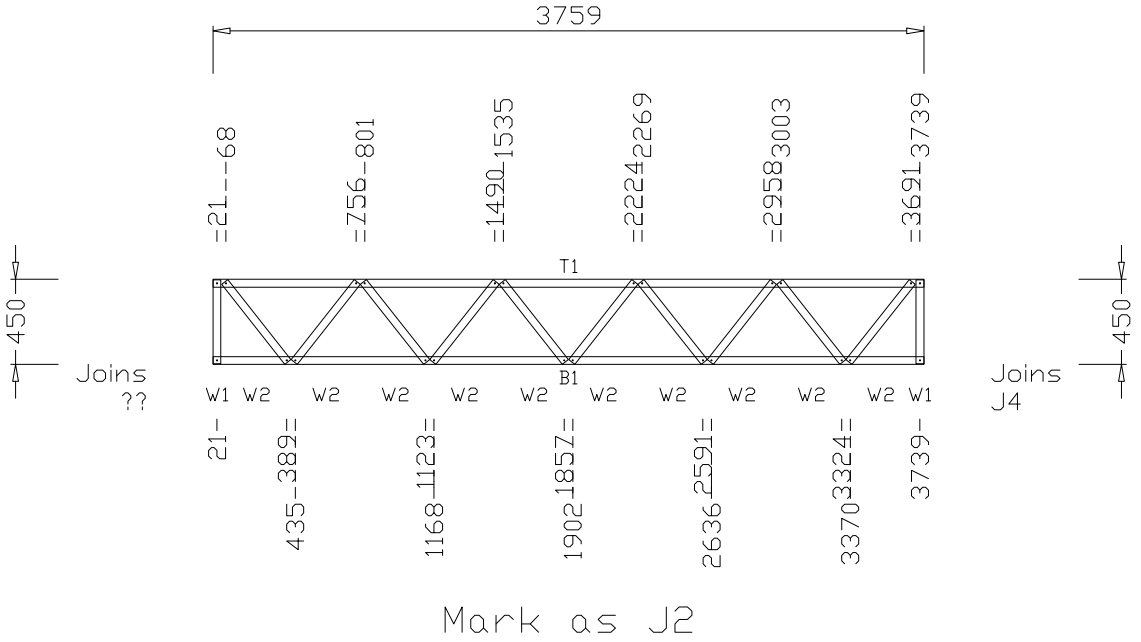

Mark as J2

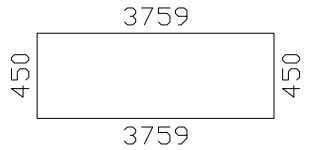

UNIVERSITY OF STELLENBOSCH			SCALE 1:40 MEASURED IN mm	TITLE FLOOR JOIST J2	
STUDENT No. 14859890	DRAWN BY FDT OOSTHUIZEN		DATE 22/09/2011	SHEET . OF .	No. 00

Stellenbosch University http://scholar.sun.ac.za

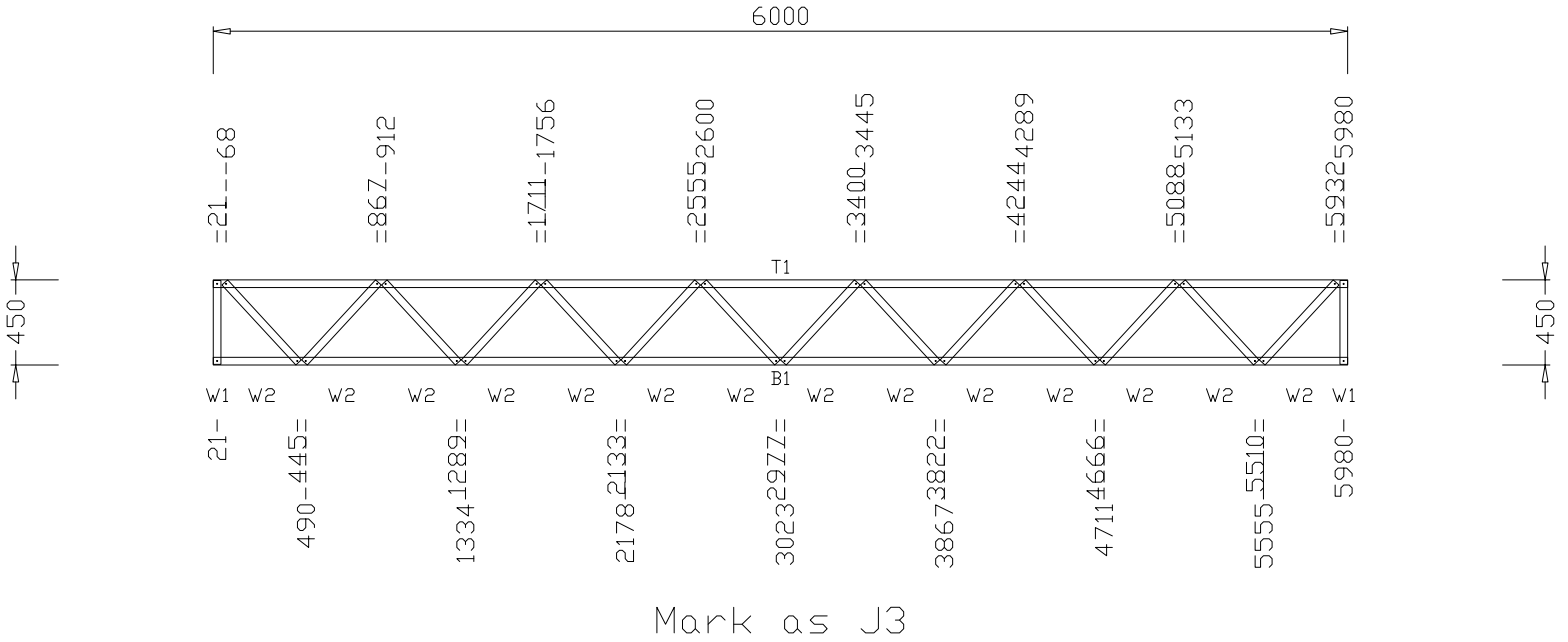

Mark as J3

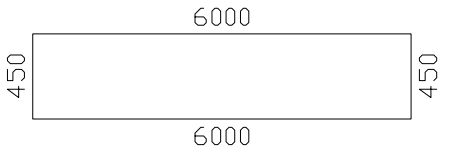

UNIVERSITY OF STELLENBOSCH			SCALE 1:40 MEASURED IN mm	TITLE FLOOR JOIST J3	
STUDENT No. 14859890	DRAWN BY FDT OOSTHUIZEN		DATE 22/09/2011	SHEET . OF .	No. 00

Stellenbosch University http://scholar.sun.ac.za

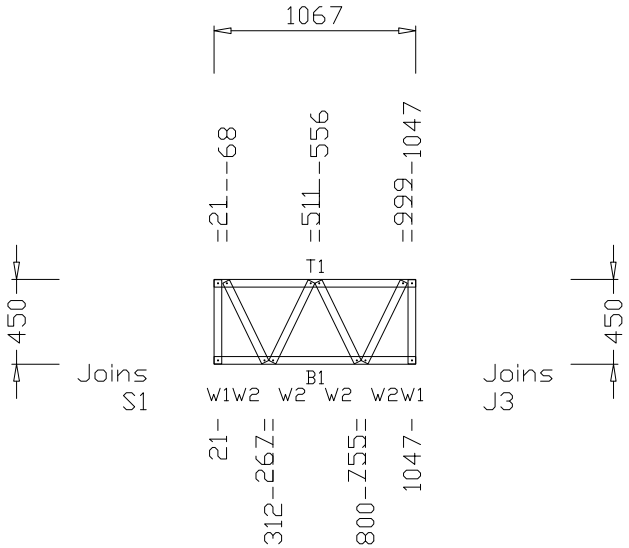

Mark as J4

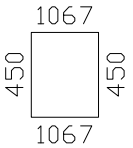

UNIVERSITY OF STELLENBOSCH			SCALE 1:40 MEASURED IN mm	TITLE FLOOR JOIST J4	
STUDENT No. 14859890	DRAWN BY FDT OOSTHUIZEN		DATE 22/09/2011	SHEET . OF .	No. 00

Stellenbosch University http://scholar.sun.ac.za

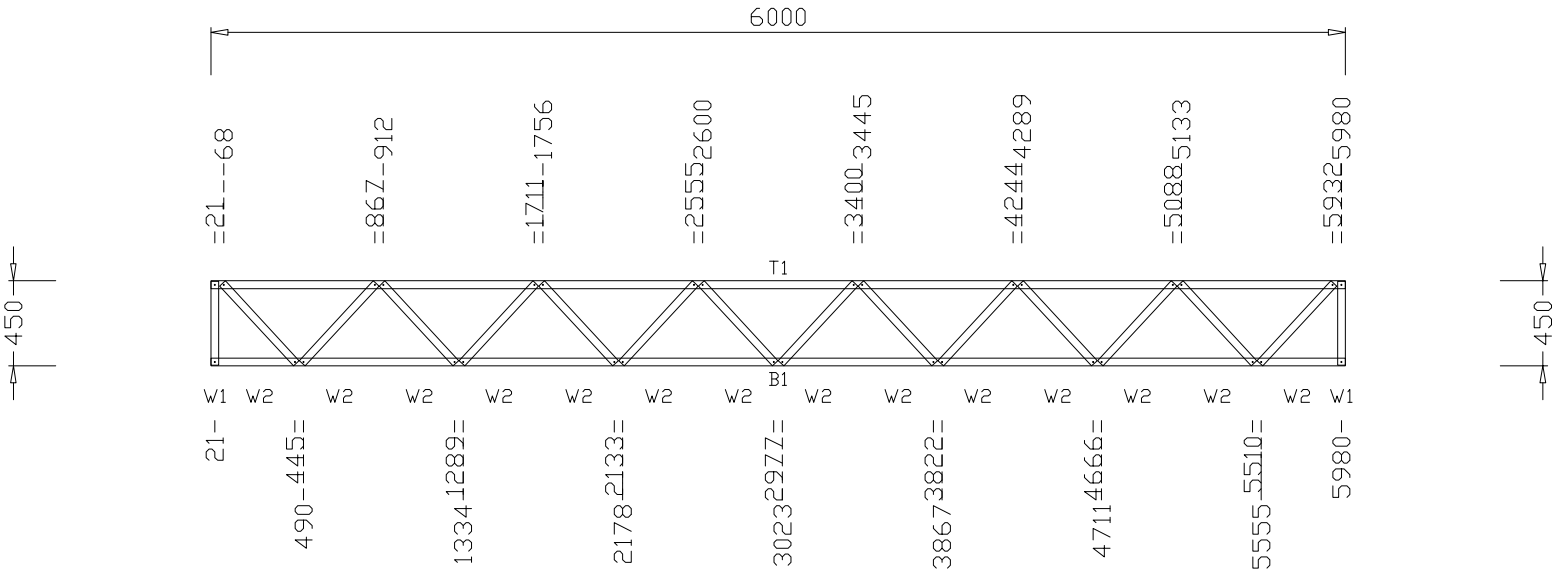

Mark as S1

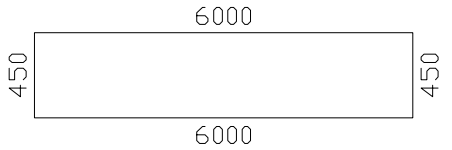

UNIVERSITY OF STELLENBOSCH			SCALE 1:40 MEASURED IN mm	TITLE FLOOR JOIST S1	
STUDENT No. 14859890	DRAWN BY FDT OOSTHUIZEN		DATE 22/09/2011	SHEET . OF .	No. 00

Stellenbosch University http://scholar.sun.ac.za

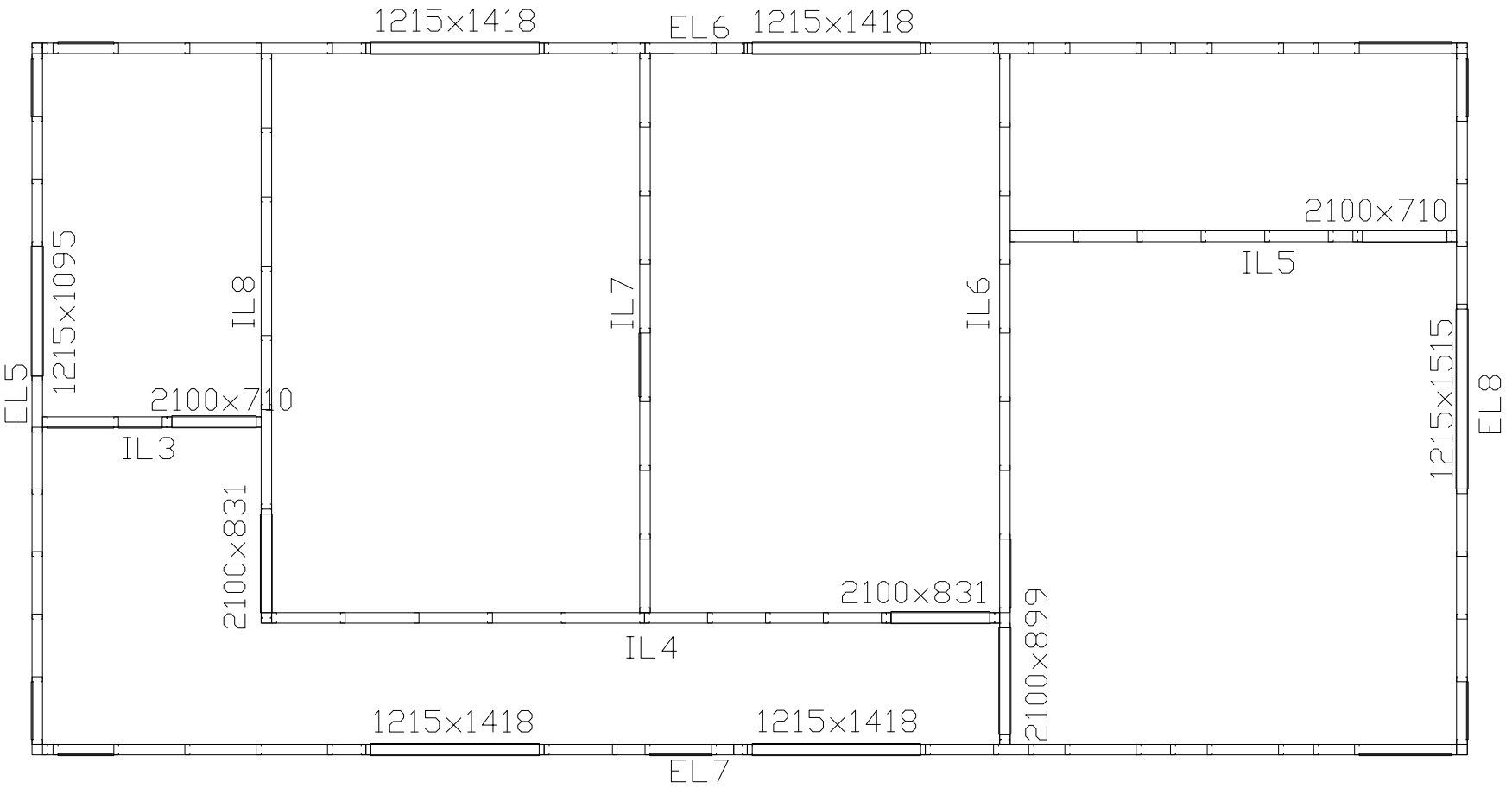

UNIVERSITY OF STELLENBOSCH			SCALE 1:55 MEASURED IN mm	TITLE FIRST FLOOR	
STUDENT No. 14859890	DRAWN BY FDT 00STHUIZEN		DATE 22/09/2011	SHEET . OF .	No. 00

Stellenbosch University http://scholar.sun.ac.za

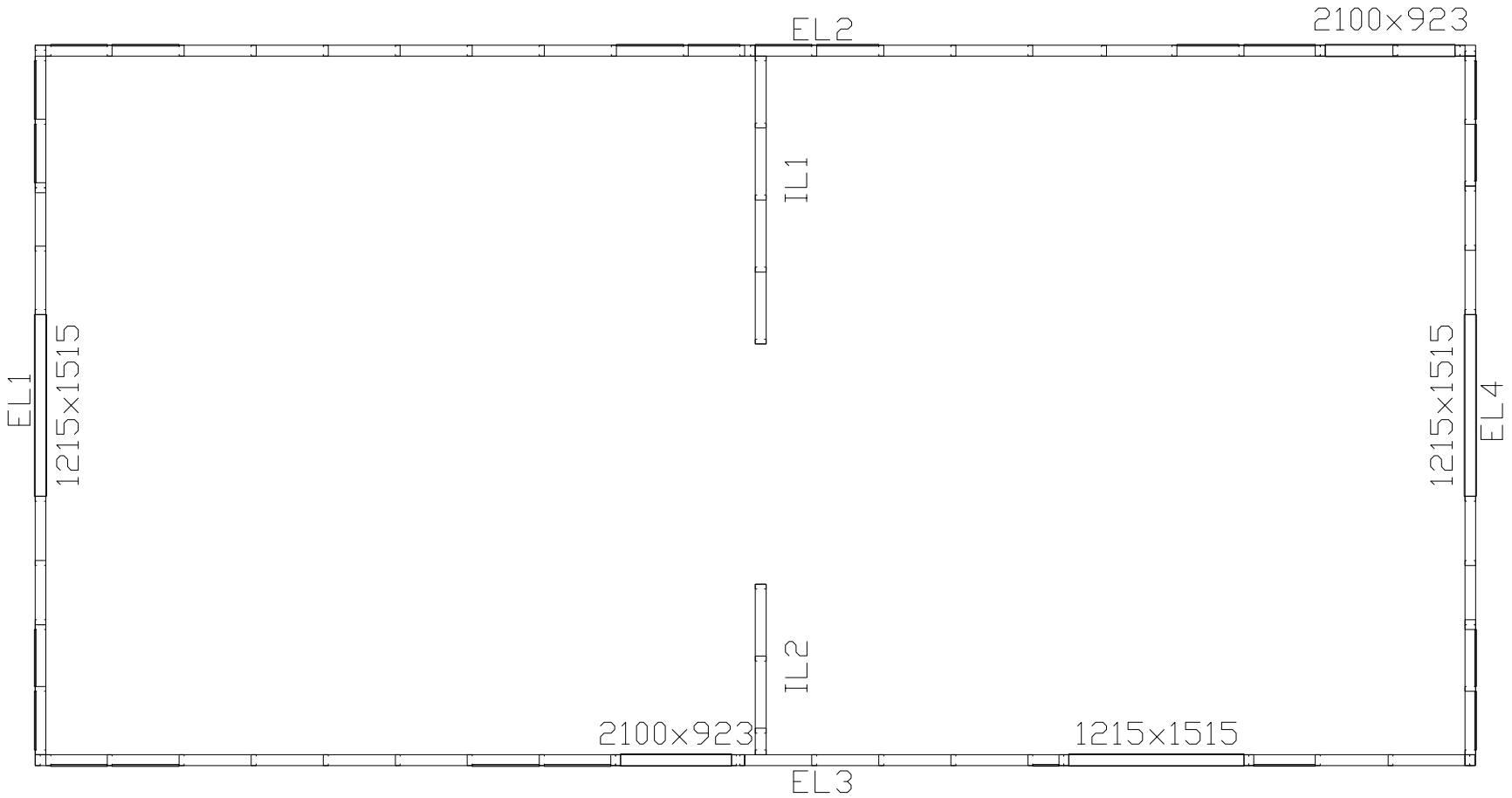

UNIVERSITY OF STELLENBOSCH			SCALE 1:55 MEASURED IN mm	TITLE LAYOUT - GROUND FLOOR	
STUDENT No. 14859890	DRAWN BY FDT OOSTHUIZEN		DATE 22/09/2011	SHEET . OF .	No. 00

Stellenbosch University http://scholar.sun.ac.za

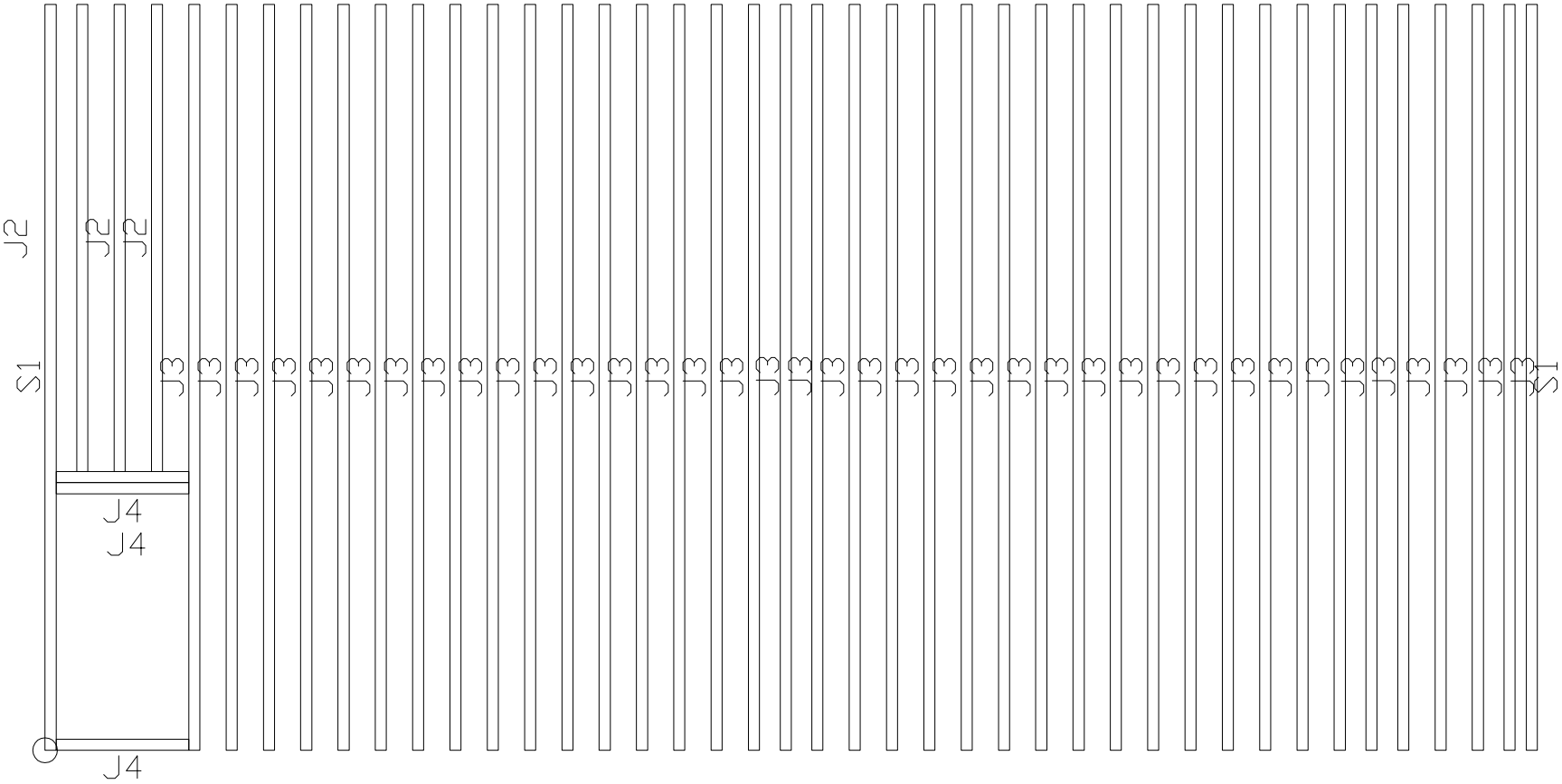

UNIVERSITY OF STELLENBOSCH			SCALE 1:55 MEASURED IN mm	TITLE LAYOUT - FLOOR JOISTS	
STUDENT No. 14859890	DRAWN BY FDT 00STHUIZEN		DATE 22/09/2011	SHEET . OF .	No. 00

Stellenbosch University http://scholar.sun.ac.za

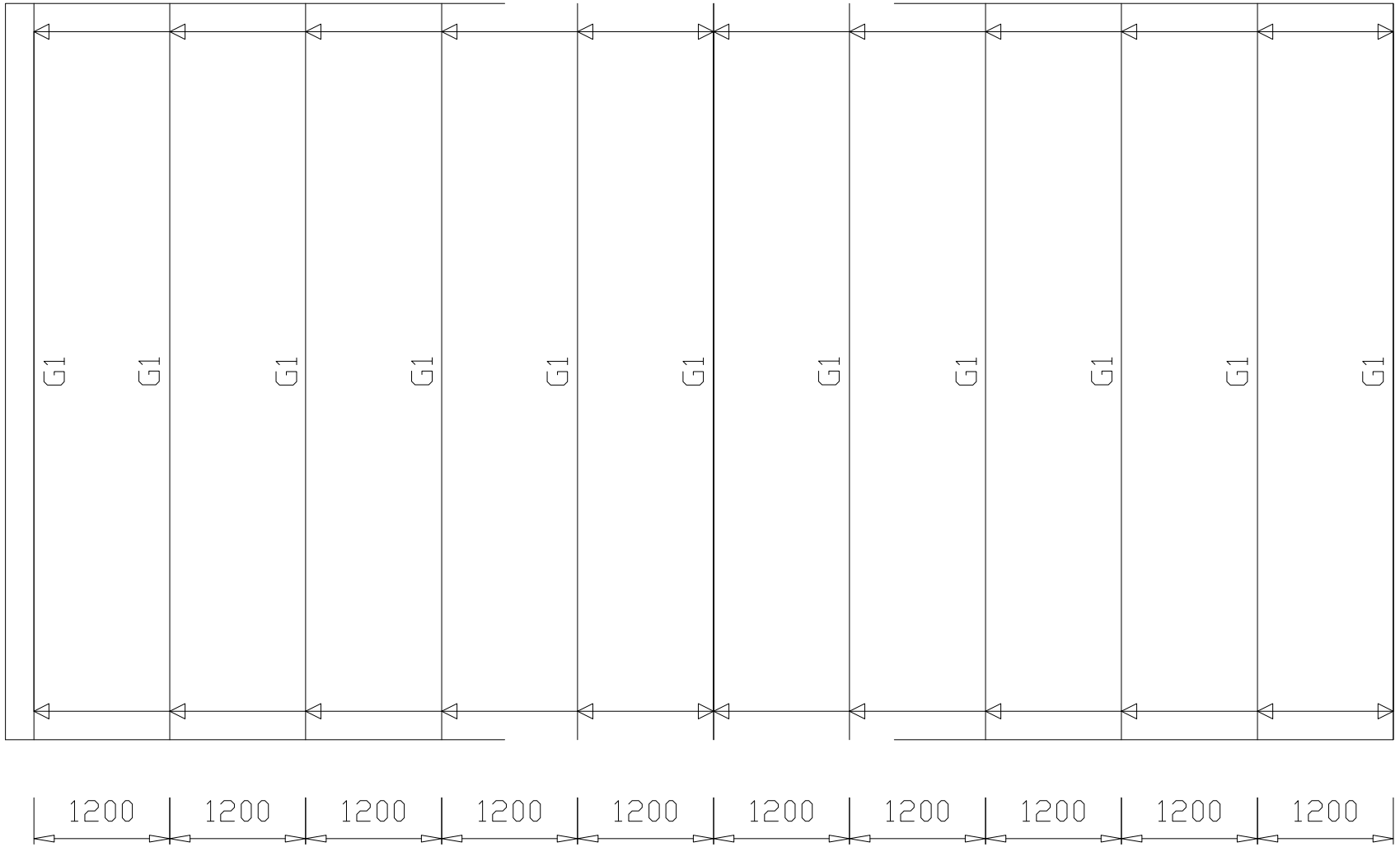

UNIVERSITY OF STELLENBOSCH			SCALE 1:55 MEASURED IN mm	TITLE LAYOUT - ROOF TRUSSES	
STUDENT No. 14859890	DRAWN BY FDT 00STHUIZEN		DATE 22/09/2011	SHEET . OF .	No. 00

Stellenbosch University http://scholar.sun.ac.za

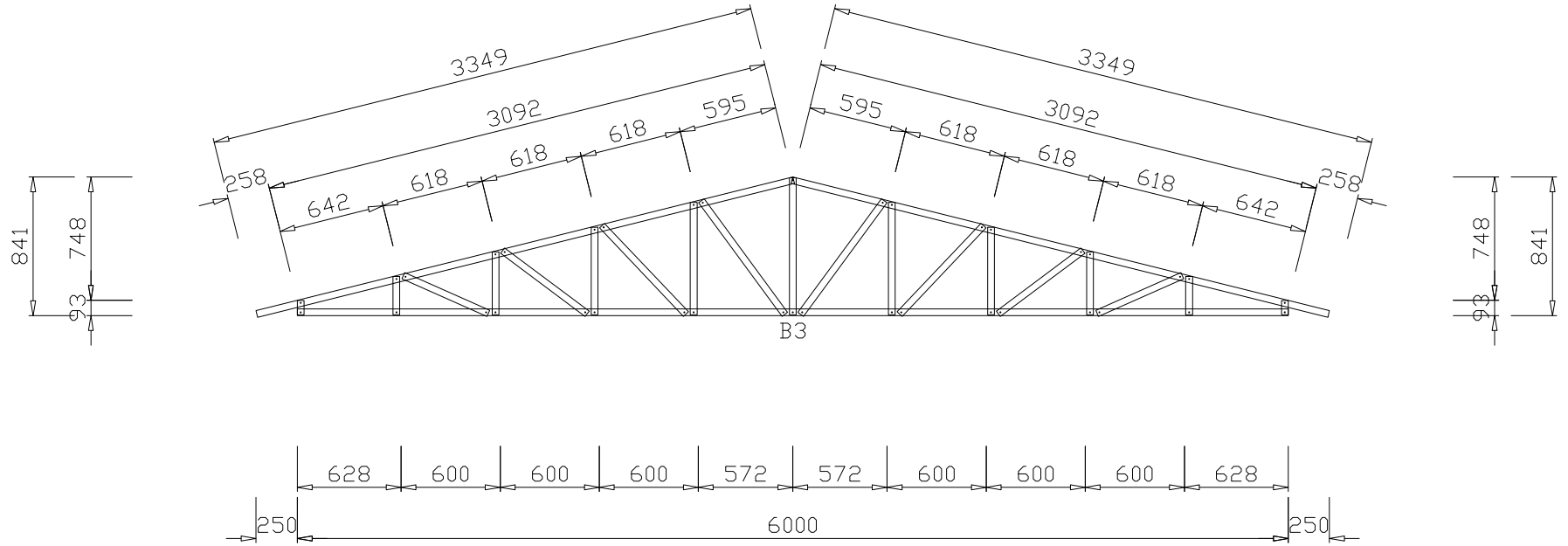

UNIVERSITY OF STELLENBOSCH			SCALE 1:40 MEASURED IN mm	TITLE ROOF TRUSS	
STUDENT No. 14859890	DRAWN BY FDT OOSTHUIZEN		DATE 22/09/2011	SHEET . OF .	No. 00

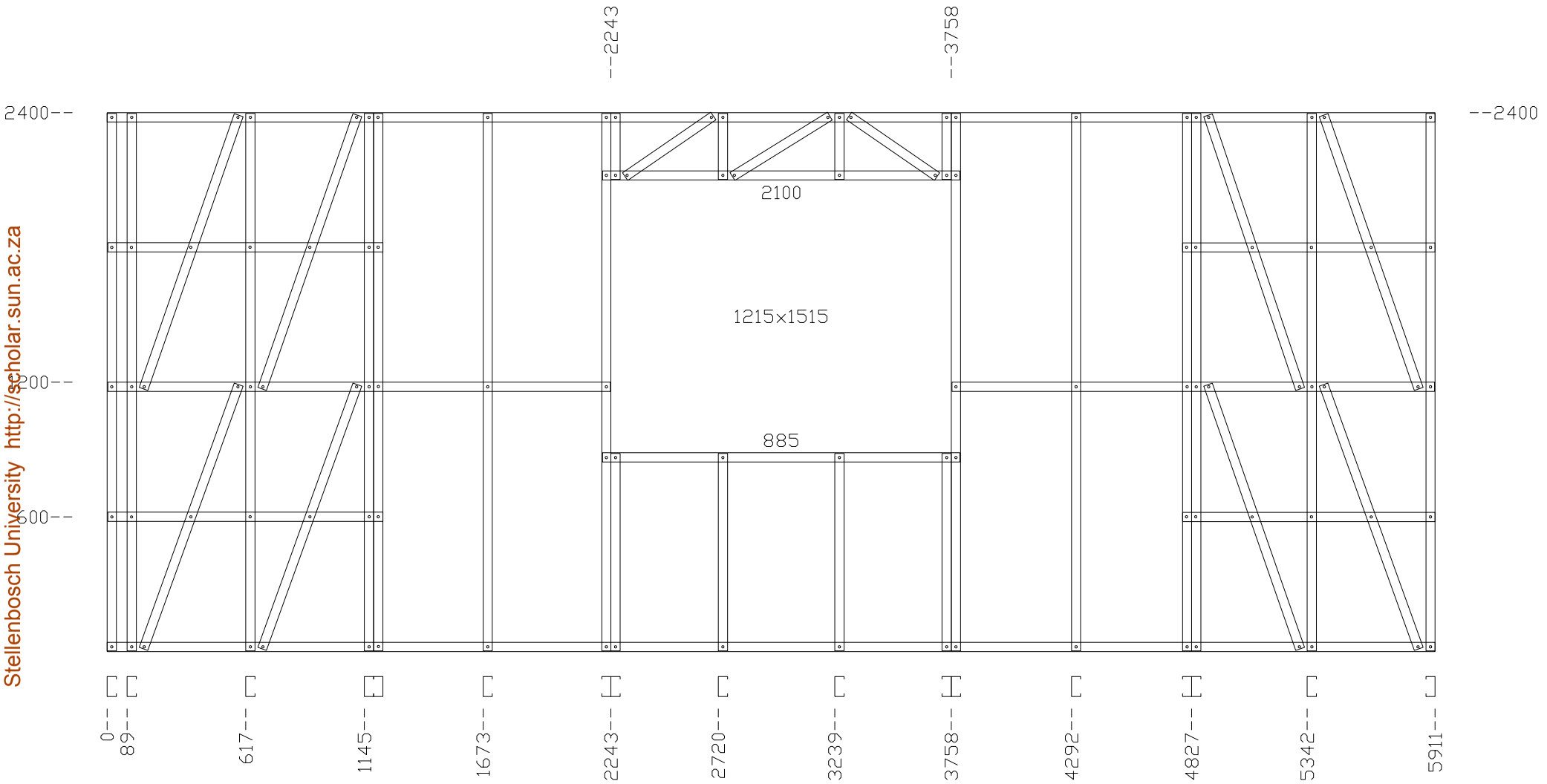

Stellenbosch University http://scholar.sun.ac.za

UNIVERSITY OF STELLENBOSCH			SCALE 1:25 MEASURED IN mm	TITLE EL1	
STUDENT No. 14859890	DRAWN BY FDT OOSTHUIZEN		DATE 22/09/2011	SHEET . OF .	No. 00

Stellenbosch University http://scholar.sun.ac.za

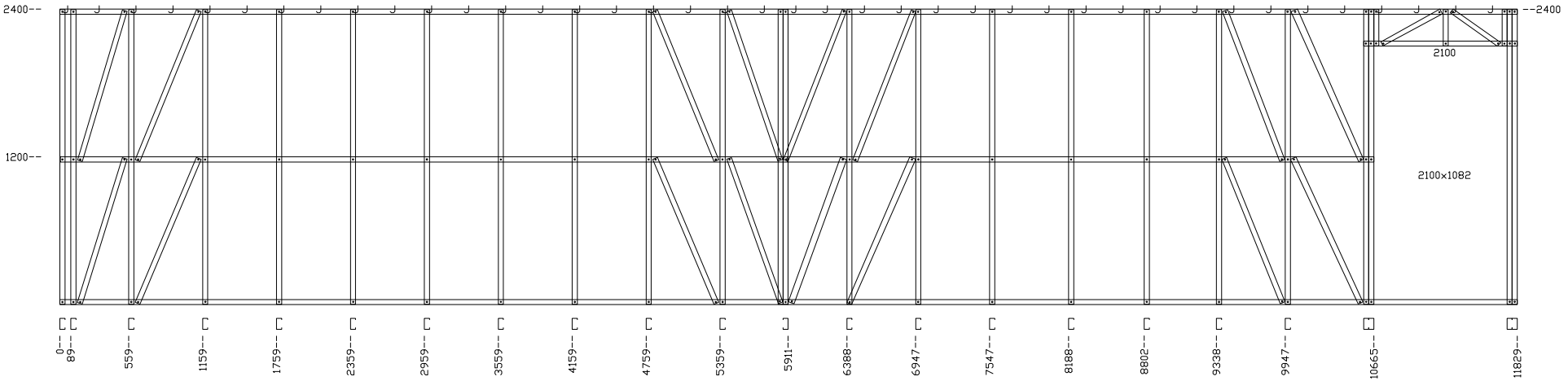

UNIVERSITY OF STELLENBOSCH

STUDENT No. 14859890	DRAWN BY FDT OOSTHUIZEN		DATE 22/09/2011	SHEET . OF .	No. 00

SCALE 1:50
MEASURED IN mm

TITLE EL2

Stellenbosch University http://scholar.sun.ac.za

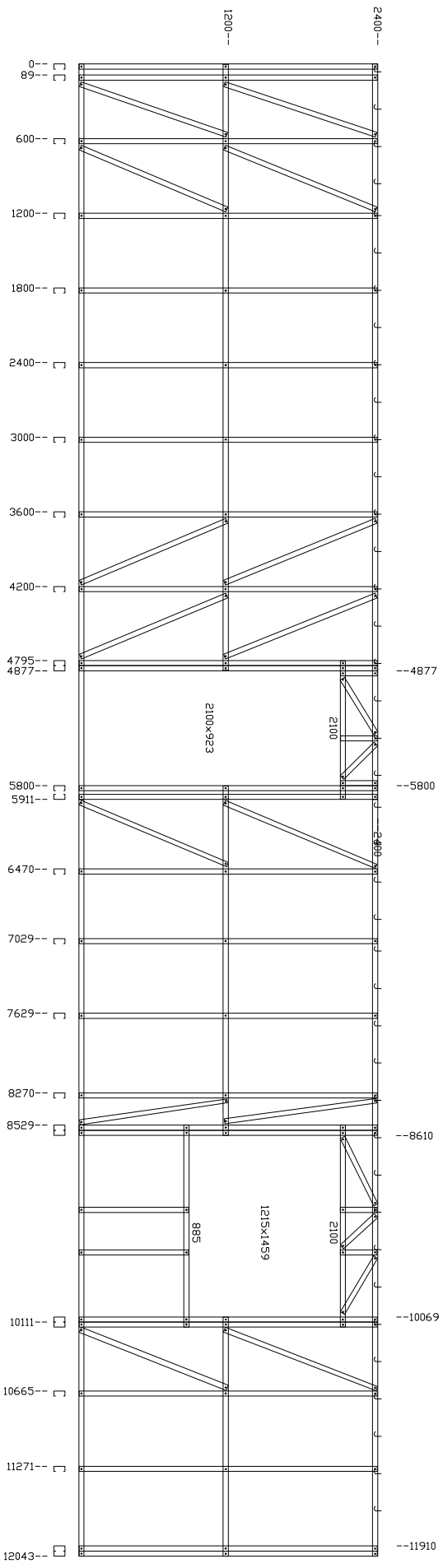

UNIVERSITY OF STELLENBOSCH

STUDENT No. 14859890		SCALE 1:50	TITLE EL3
DRAWN BY FDT OOSTHUIZEN		MEASURED IN mm	
		DATE 22/09/2011	SHEET . OF .
			No. 00

Stellenbosch University http://scholar.sun.ac.za

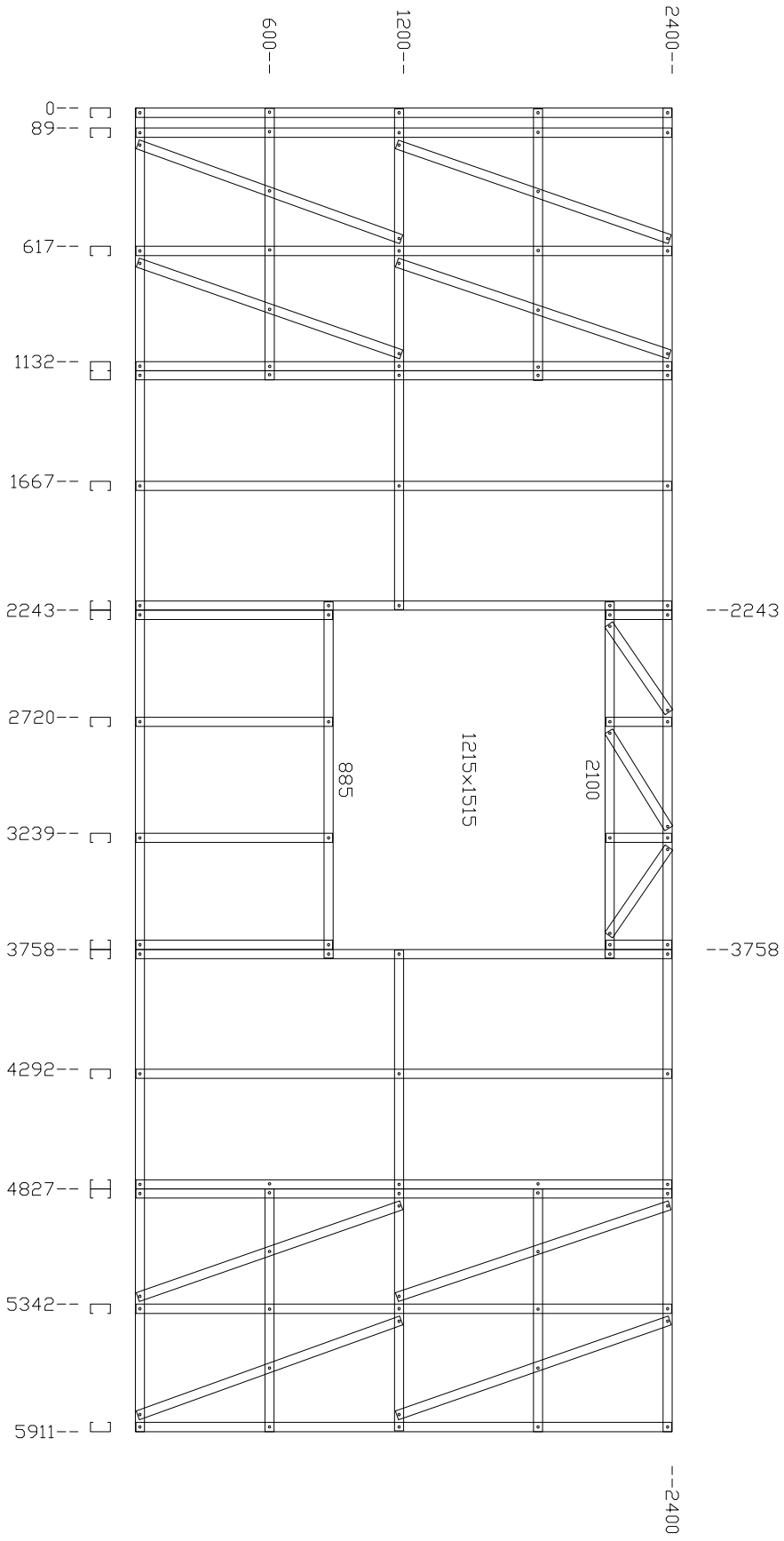

UNIVERSITY OF STELLENBOSCH

STUDENT No. 14859890		SCALE 1:30 MEASURED IN mm	TITLE EL4
DRAWN BY FDT OOSTHUIZEN		DATE 22/09/2011	SHEET . OF .
			No. 00

Stellenbosch University http://scholar.sun.ac.za

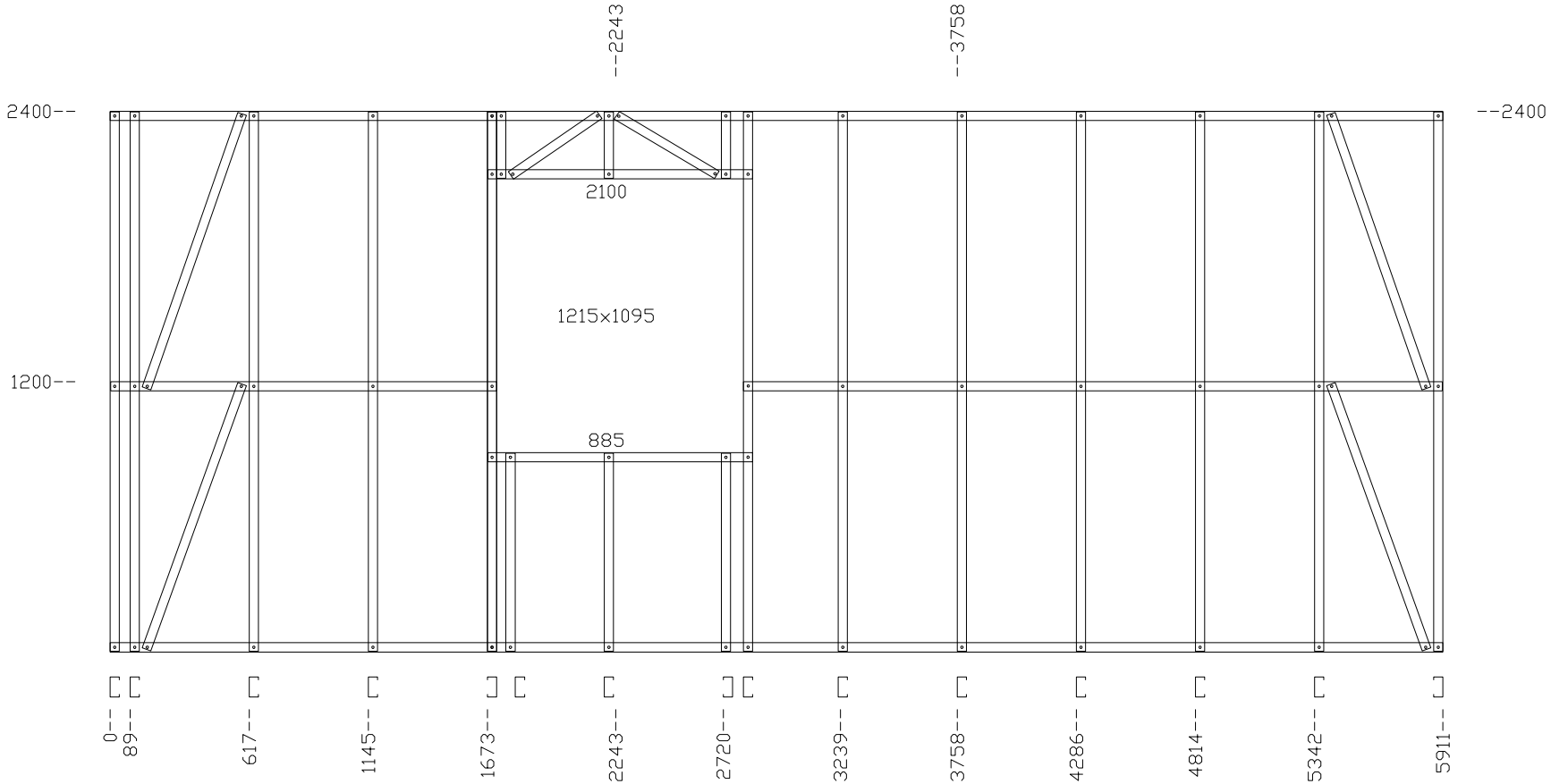

UNIVERSITY OF STELLENBOSCH			SCALE 1:30 MEASURED IN mm	TITLE EL5	
STUDENT No. 14859890	DRAWN BY FDT OOSTHUIZEN		DATE 22/09/2011	SHEET . OF .	No. 00

Stellenbosch University http://scholar.sun.ac.za

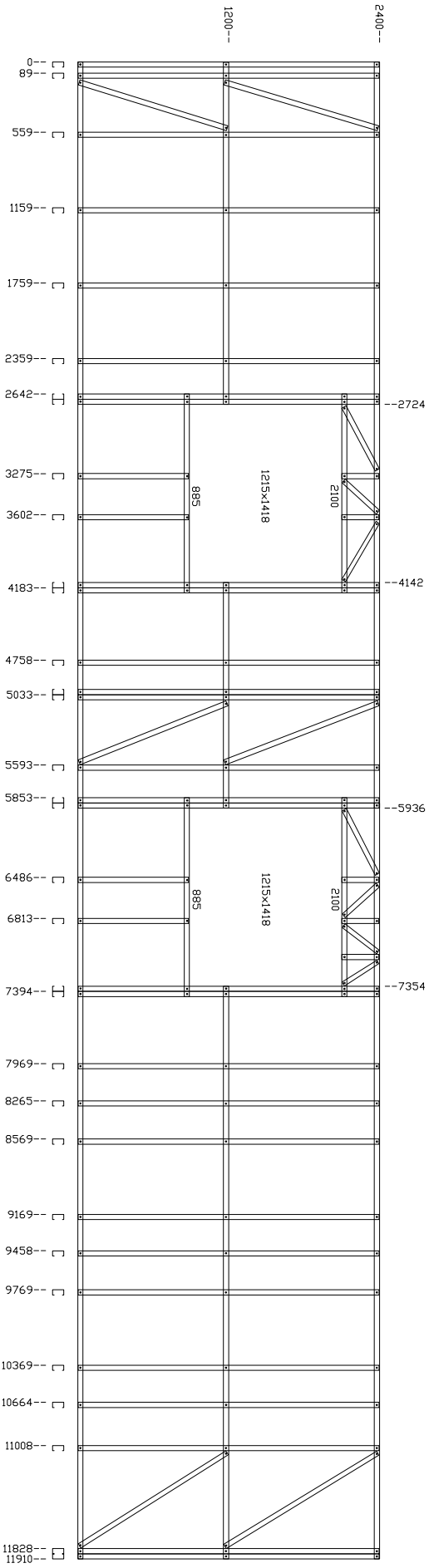

UNIVERSITY OF STELLENBOSCH

STUDENT No. 14859890	SCALE 1:50 MEASURED IN mm	TITLE EL6
DRAWN BY FDT OOSTHUIZEN	DATE 22/09/2011	SHEET . OF .
		No. 00

Stellenbosch University http://scholar.sun.ac.za

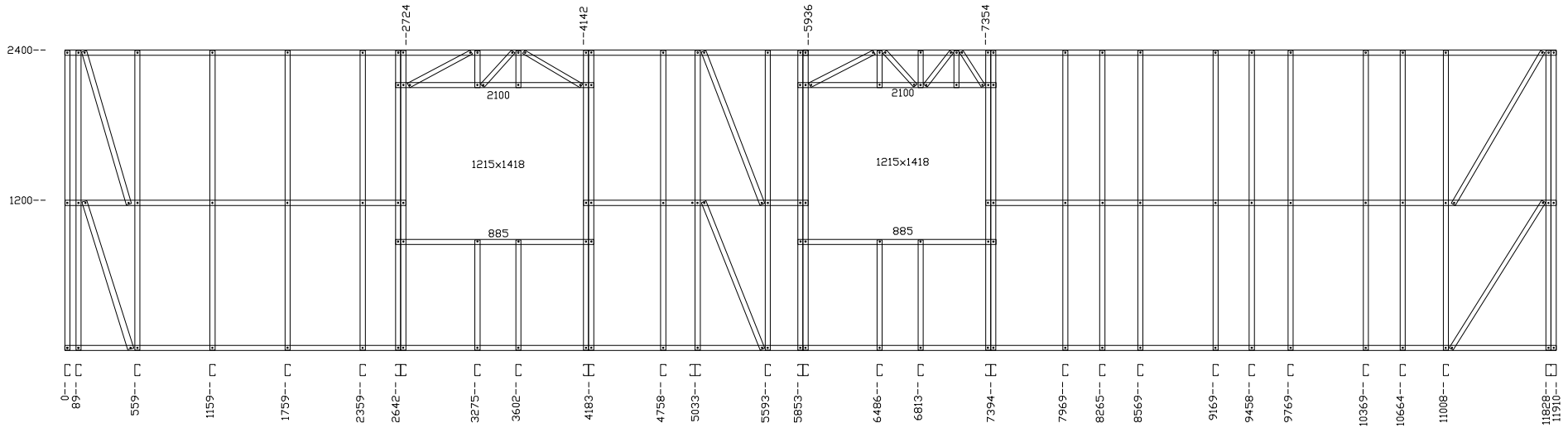

UNIVERSITY OF STELLENBOSCH			SCALE 1:50 MEASURED IN mm	TITLE EL7	
STUDENT No. 14859890	DRAWN BY FDT OOSTHUIZEN		DATE 22/09/2011	SHEET . OF .	No. 00

Stellenbosch University http://scholar.sun.ac.za

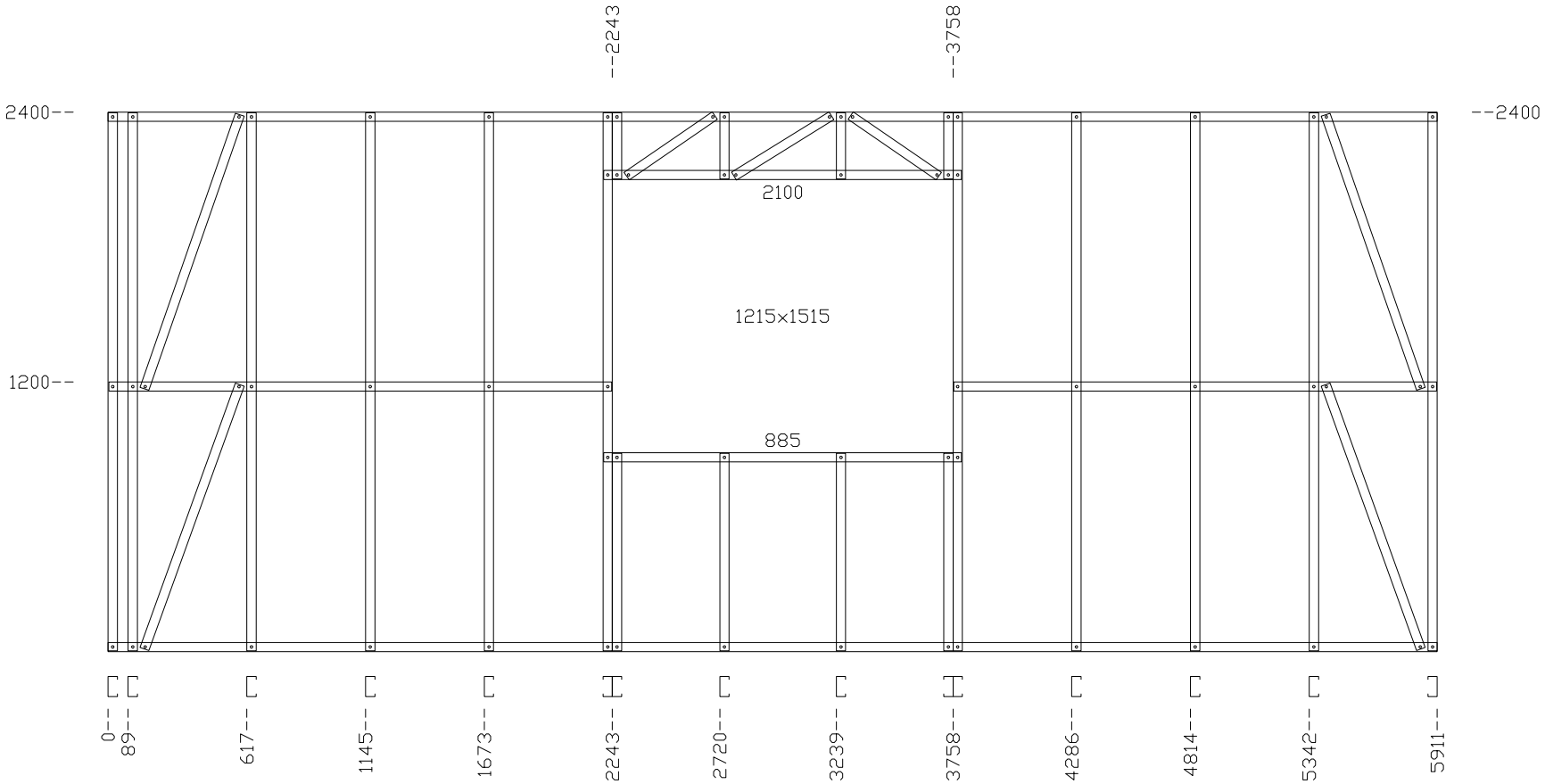

UNIVERSITY OF STELLENBOSCH			SCALE 1:30 MEASURED IN mm	TITLE EL8	
STUDENT No. 14859890	DRAWN BY FDT OOSTHUIZEN		DATE 22/09/2011	SHEET . OF .	No. 00

Stellenbosch University http://scholar.sun.ac.za

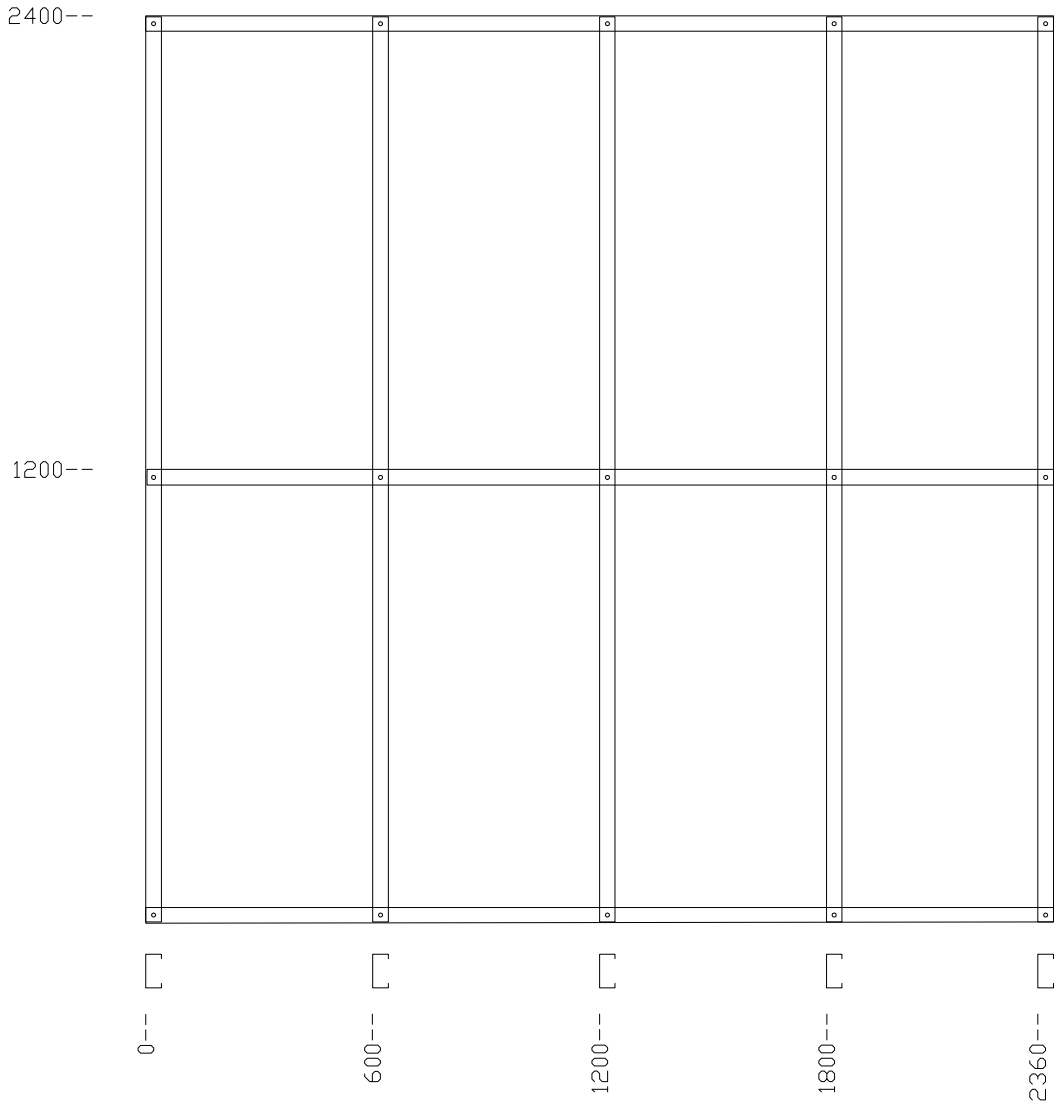

UNIVERSITY OF STELLENBOSCH			SCALE 1:20 MEASURED IN mm	TITLE IL1	
STUDENT No. 14859890	DRAWN BY FDT OOSTHUIZEN		DATE 22/09/2011	SHEET . OF .	No. 00

Stellenbosch University http://scholar.sun.ac.za

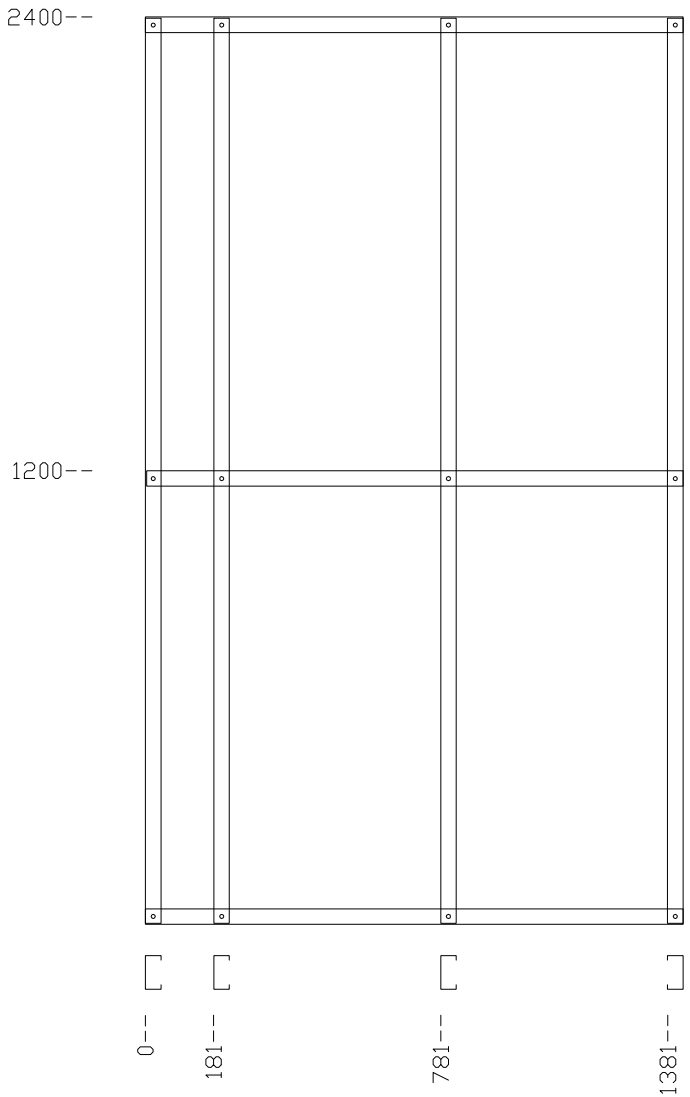

UNIVERSITY OF STELLENBOSCH			SCALE 1:20 MEASURED IN mm	TITLE IL2	
STUDENT No. 14859890	DRAWN BY FDT OOSTHUIZEN		DATE 22/09/2011	SHEET . OF .	No. 00

Stellenbosch University http://scholar.sun.ac.za

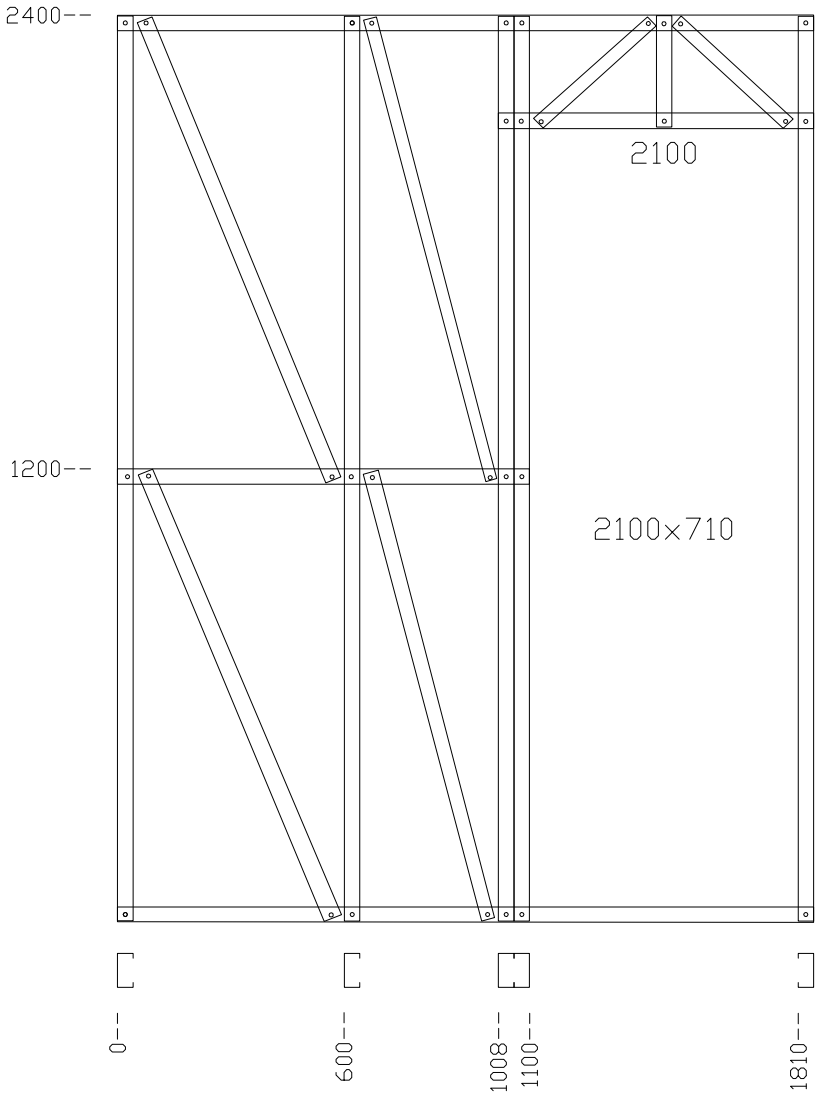

UNIVERSITY OF STELLENBOSCH			SCALE 1:20 MEASURED IN mm	TITLE IL3	
STUDENT No. 14859890	DRAWN BY FDT OOSTHUIZEN		DATE 22/09/2011	SHEET . OF .	No. 00

Stellenbosch University http://scholar.sun.ac.za

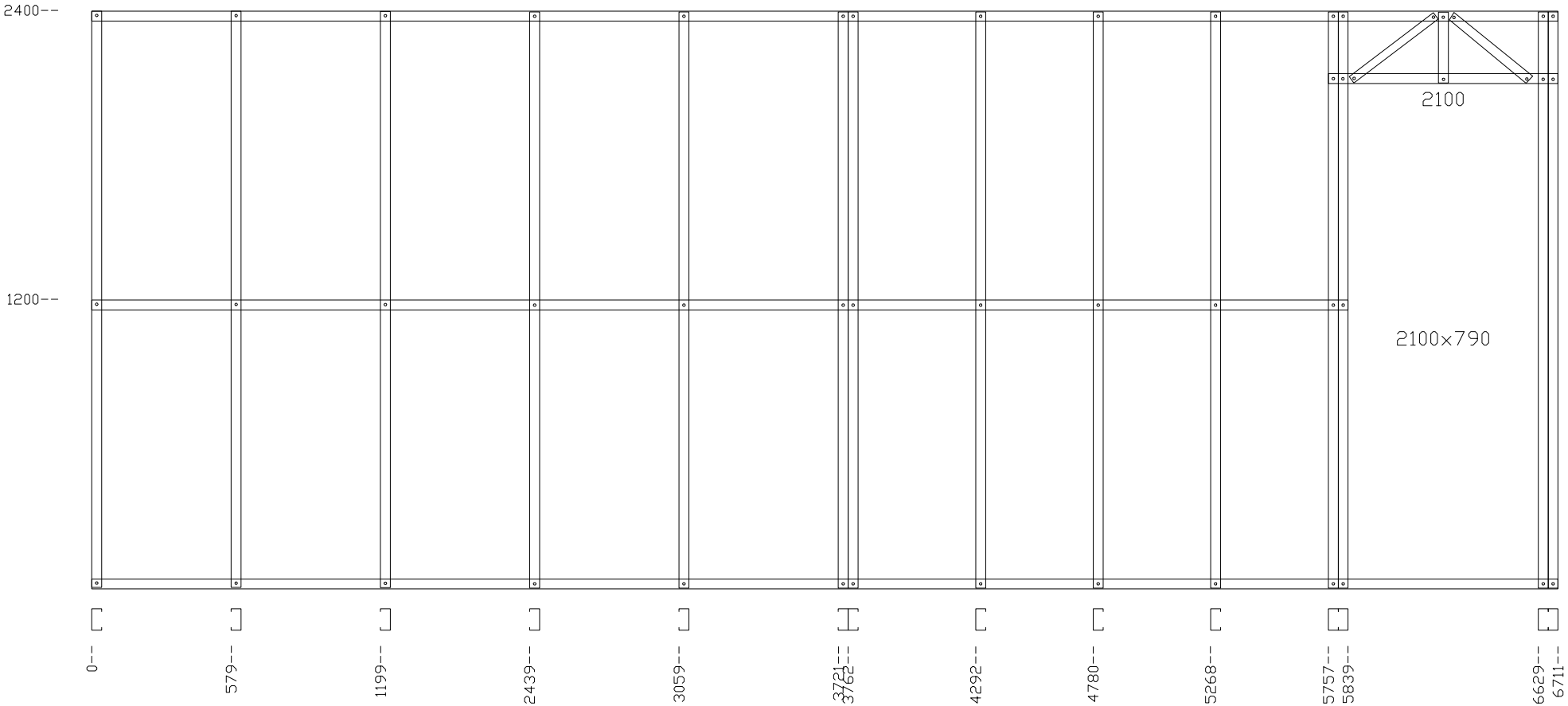

UNIVERSITY OF STELLENBOSCH			SCALE 1:25 MEASURED IN mm	TITLE IL4	
STUDENT No. 14859890	DRAWN BY FDT OOSTHUIZEN		DATE 22/09/2011	SHEET . OF .	No. 00

Stellenbosch University http://scholar.sun.ac.za

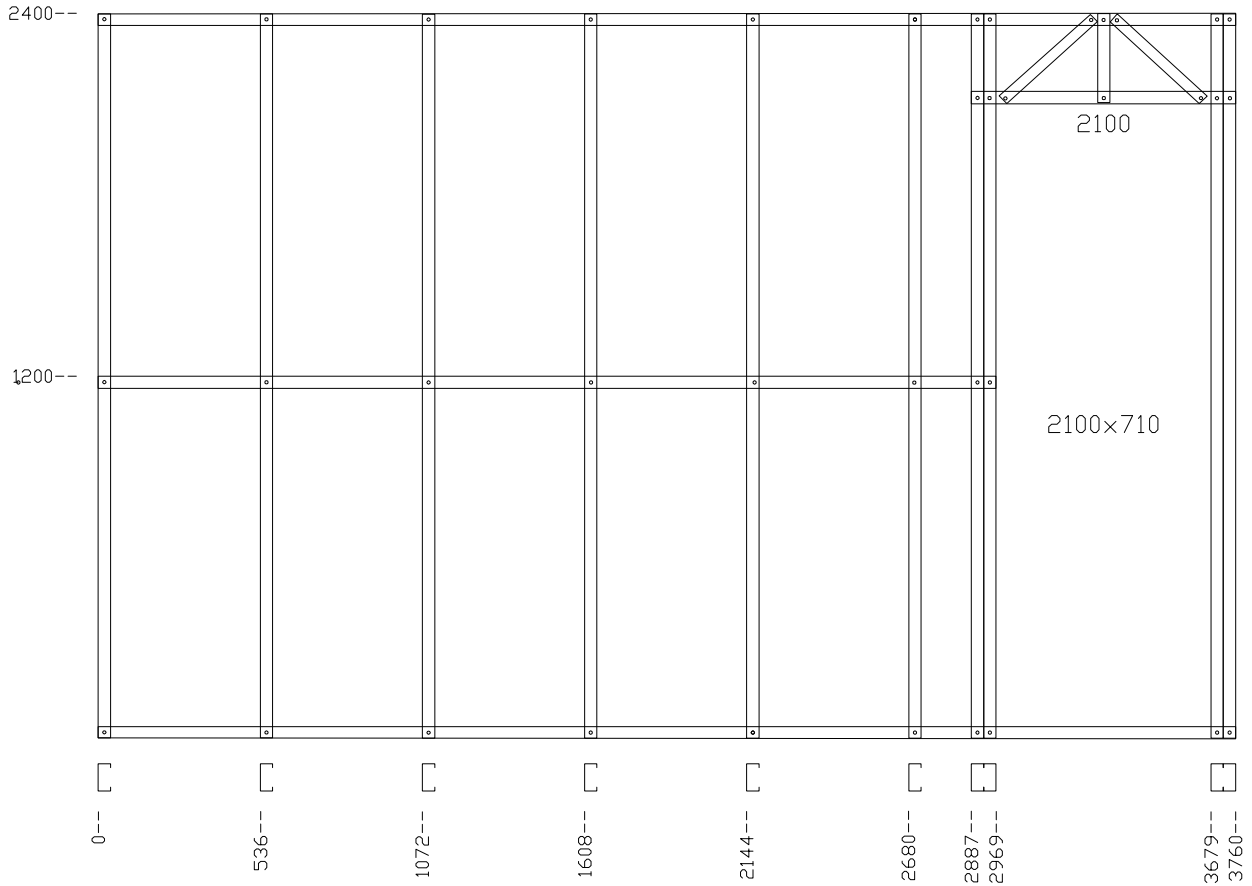

UNIVERSITY OF STELLENBOSCH			SCALE 1:25 MEASURED IN mm	TITLE IL5	
STUDENT No. 14859890	DRAWN BY FDT OOSTHUIZEN		DATE 22/09/2011	SHEET . OF .	No. 00

Stellenbosch University http://scholar.sun.ac.za

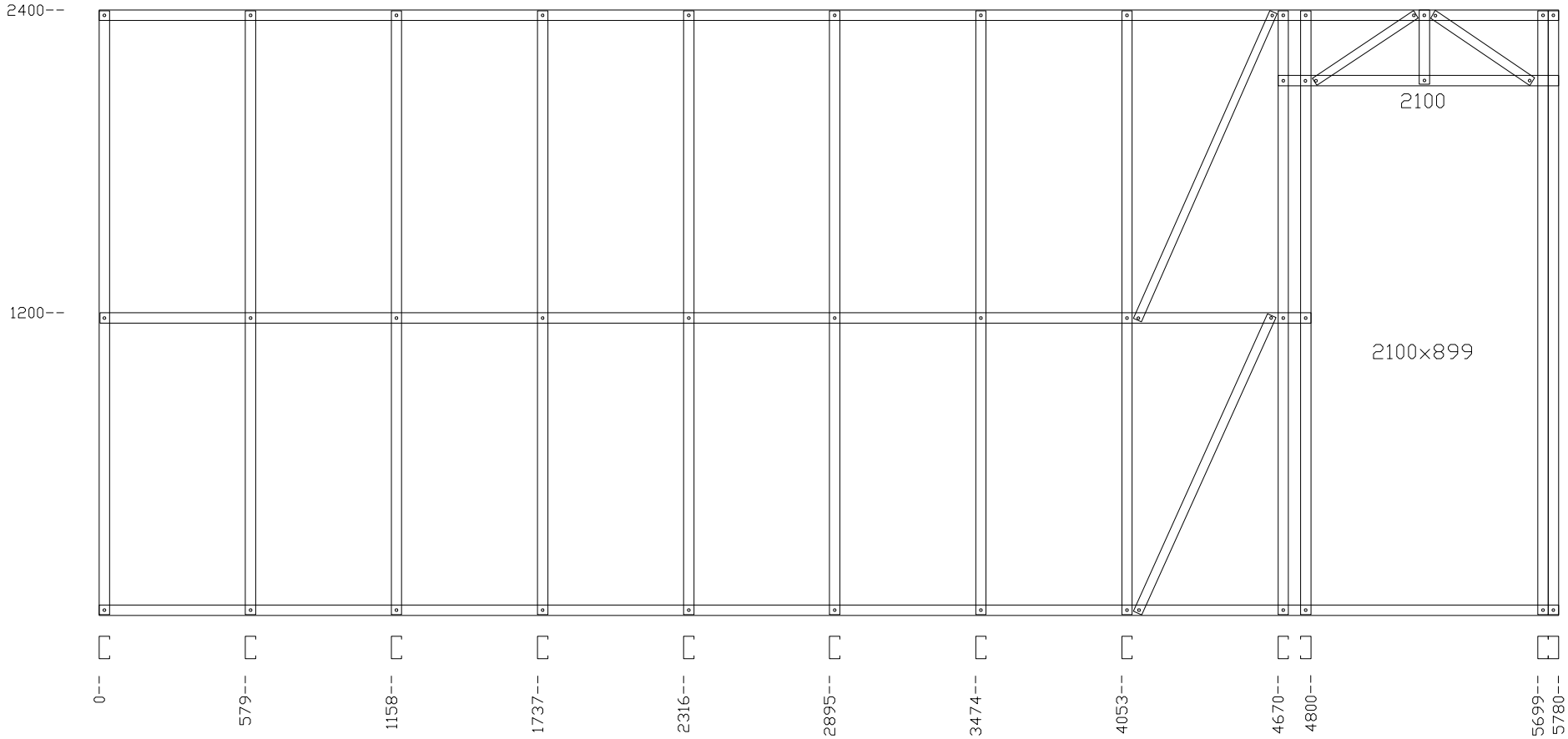

UNIVERSITY OF STELLENBOSCH

STUDENT No. 14859890	DRAWN BY FDT OOSTHUIZEN		DATE 22/09/2011	SHEET . OF .	No. 00

SCALE 1:25
MEASURED IN mm

TITLE IL6

Stellenbosch University http://scholar.sun.ac.za

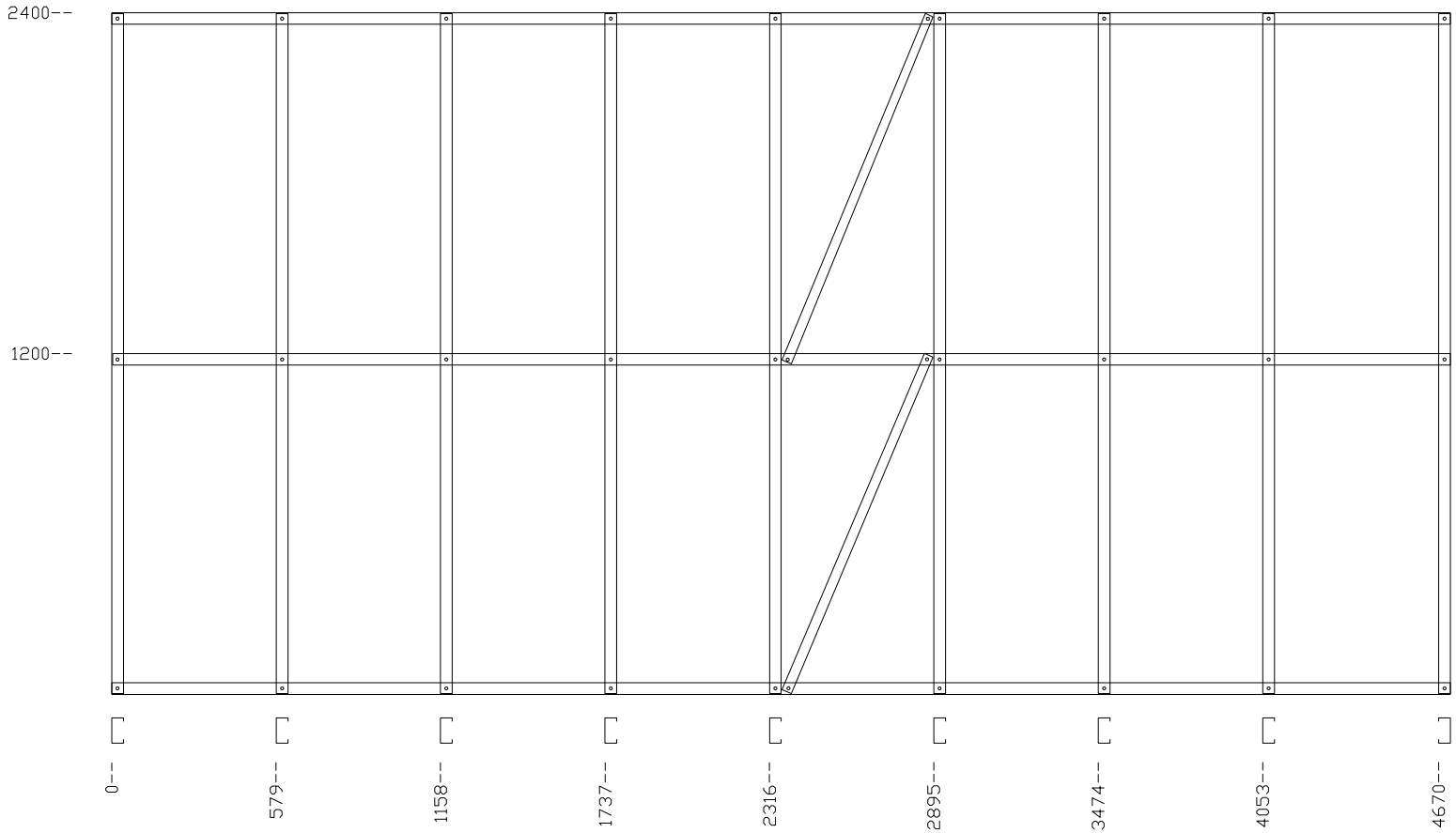

UNIVERSITY OF STELLENBOSCH			SCALE 1:25 MEASURED IN mm	TITLE IL7	
STUDENT No. 14859890	DRAWN BY FDT OOSTHUIZEN		DATE 22/09/2011	SHEET . OF .	No. 00

Stellenbosch University http://scholar.sun.ac.za

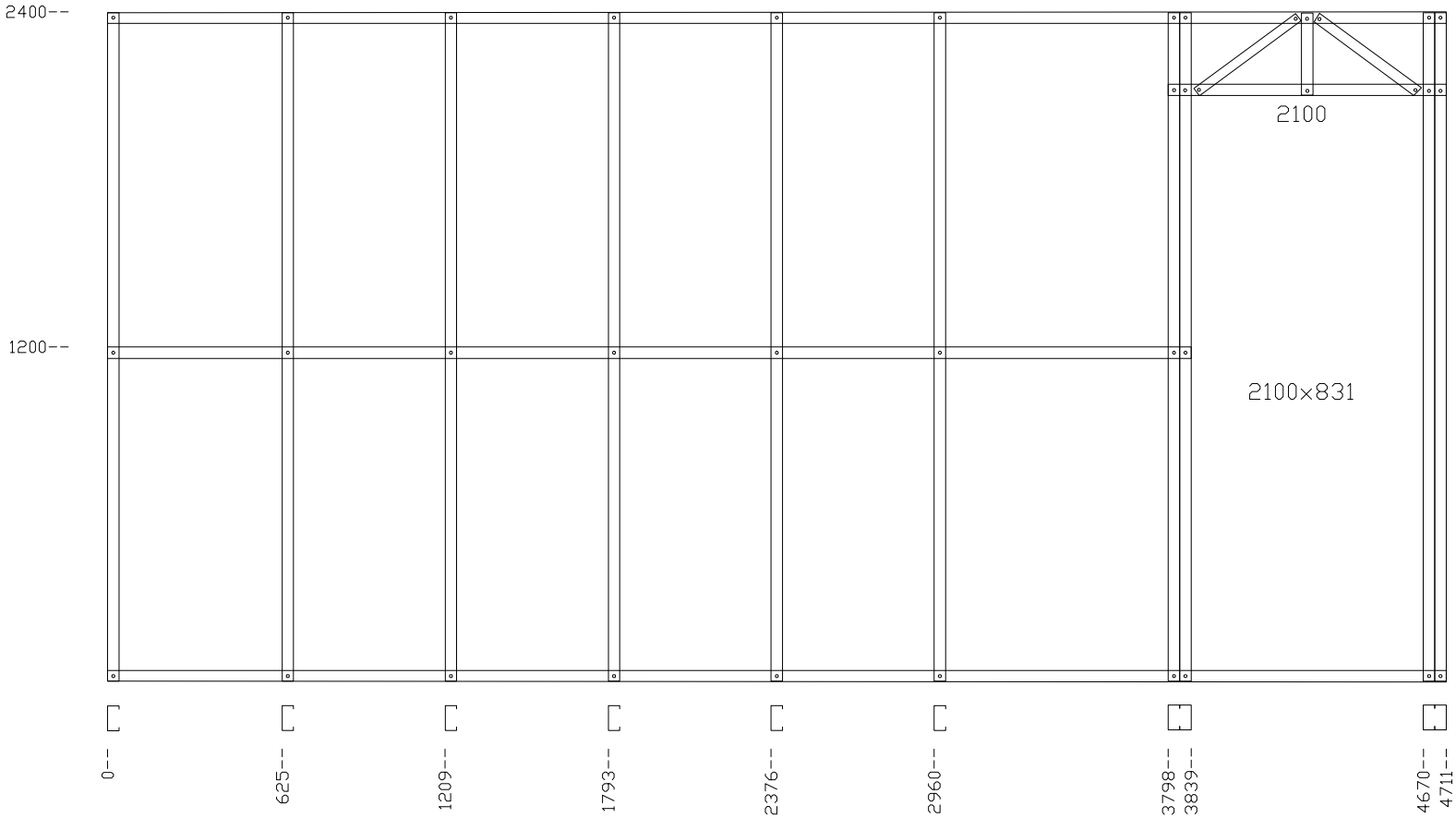

UNIVERSITY OF STELLENBOSCH			SCALE 1:25 MEASURED IN mm	TITLE IL8	
STUDENT No. 14859890	DRAWN BY FDT OOSTHUIZEN		DATE 22/09/2011	SHEET . OF .	No. 00

Stellenbosch University http://scholar.sun.ac.za

Appendix D: Detailed wind load calculations

		Windforces on the proposed structural model							1
SANS 517			Only enter values in the			Blocks			
5.3.3.2			$v_{b,0}$	28	m/s				
		$V_{b,peak}$ =	1.4*V_b						
			39.2	m/s				$V_{b,peak}$ =	39.2
		Dimensions of building							
		length	12	m					
		width	6	m					
		wall height	5.3	m					
		roof height	0.8	m					
SANS 517		Z	6.1	m	Height of building inc. roof				
P25		roof pitch	14.9267	°	0.2605204	rad			
SANS 517		C_r	0.98						
P25		ρ	1.12	kg/m^3					
		$q_p = \frac{1}{2000}\rho(1.4c_r v_{b,0})^2$							
			0.82644	kN/m^2					
		WIND CONDITION 1							
		CASE 1:	Structure has no dominant openings						
			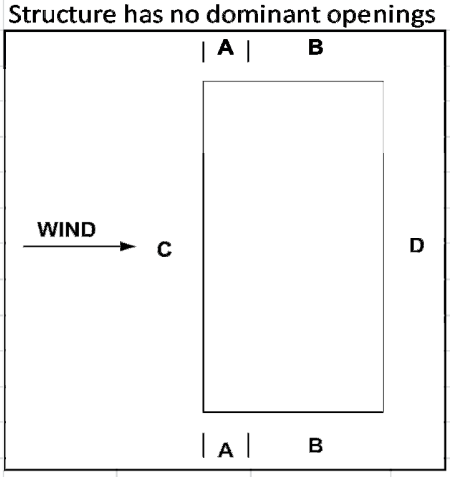						
		h	6.1	m					
		b	12	m					
		d	6	m					
		e	2.4	m					

Stellenbosch University http://scholar.sun.ac.za

Pressure coeff on walls

SANS 517 P.28

Zone	Coeff
A	-1.2
B	-0.8
C	0.8
D	-0.5

Wind pressure on roof overhangs

SANS 517 5.3.3.3.5

C_{pe} 0.8

or

C_{pe} -0.5

Pressure on underside of roof overhang is equal to pressure on the wall to which its connected

Truss spacing 1.2 m

Force:

	Vertical		Horisontal	
For zone C	0.7666123	kN/m	0.2044	kN/m
For zone D	-0.479133	kN/m	-0.128	kN/m

Wind pressure on roof

SANS 517 Tab3

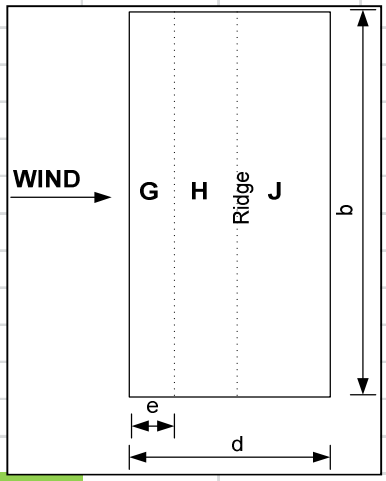

b	12.0	m
d	6.0	m
h	6.1	m
e	1.2	m
pitch angle	14.9267	

Stellenbosch University http://scholar.sun.ac.za

SANS 517
Tab 3

Zone	coeff
G	-0.8
H	-0.3
J	-0.4

Internal pressure coefficient

Choose Cpi in such a way that it acts with the external pressure coeff

C_{pi} 0.2

Summary for condition 1

Walls

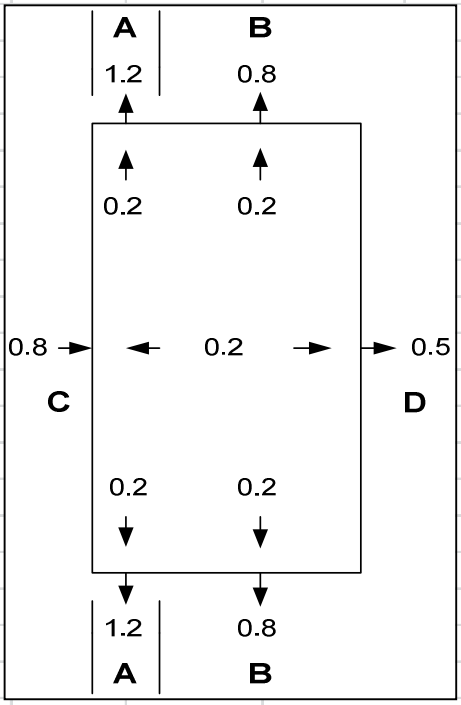

Zone	Coeff	Direction
A	1.4	Outwards
B	1	Outwards
C	-0.6	Inwards
D	0.7	Outwards

Stellenbosch University http://scholar.sun.ac.za

Windforces on the proposed structural model

Roof

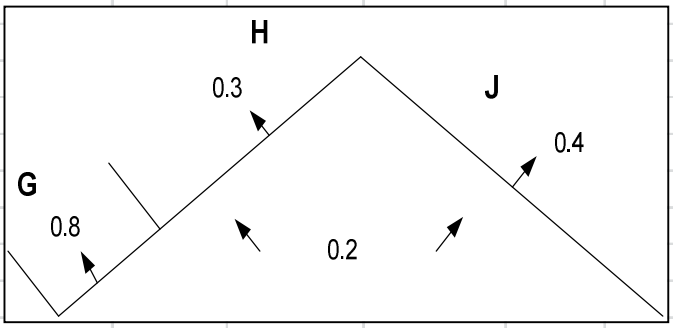

Zone	Coeff	Direction
G	1	Outward
H	0.5	Outward
J	0.6	Outward

Calculation of forces for Condition 1

Wall stud spacing	0.6	m
Truss spacing	1.2	m

Zone	Cpe	Vertical Force kn/m	Horisontal Force kN/m	Direction
A	1.4	0.69		**Outward**
B	1.0	0.50		**Outward**
C	-0.6	-0.30		**Inward**
D	0.7	0.35		**Outward**
G	1.0	0.96	0.255	**Outward**
H	0.5	0.48	0.128	**Outward**
J	0.6	0.57	0.153	**Outward**

Stellenbosch University http://scholar.sun.ac.za

WIND CONDITION 2

CASE 2: Building still has no dominant openings

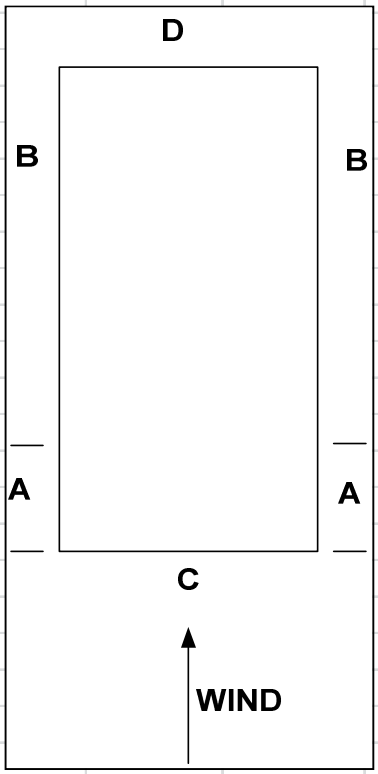

b =	6	m	e =	1.2	m
d =	12	m			
h =	6.1	m			

Pressure coeff on walls

Zone	Coeff
A	-1.2
B	-0.8
C	0.8
D	-0.5

Stellenbosch University http://scholar.sun.ac.za

Wind pressure on roof overhangs

C_{pe} -1.2 for piece in zone A

or

C_{pe} -0.8 for piece in zone B

Pressure on underside of roof overhang is equal to pressure on the wall to which its connected

Truss spacing 1.2 m

Force:

	Vertical		Horisontal	
For zone A	-1.15	kN/m	-0.31	kN/m
For zone B	-0.77	kN/m	-0.20	kN/m

Wind pressure on roof

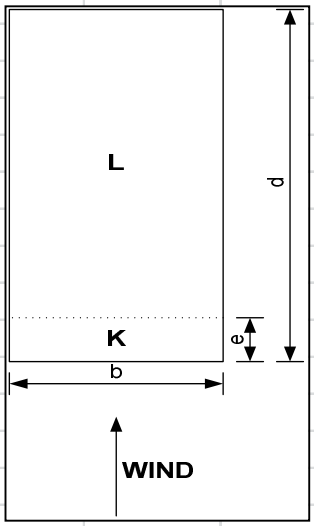

b	12.0	m
d	6.0	m
h	6.1	m
e	1.2	m
pitch angle	14.9267	

Zone	coeff
K	-1.3
L	-0.6

Stellenbosch University http://scholar.sun.ac.za

Internal pressure coefficient

Choose Cpi in such a way that it acts with the external pressure coeff

C_{pi} 0.2

Summary for condition 2

Walls

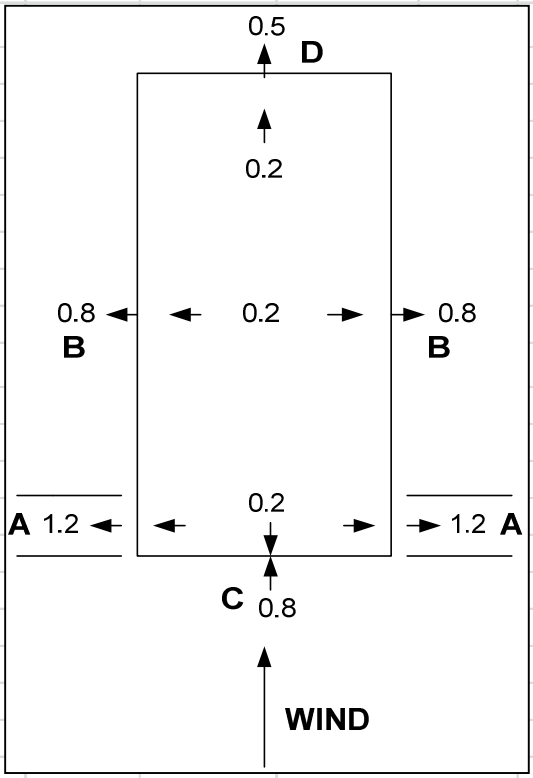

Zone	Coeff	Direction
A	1.4	Outwards
B	1	Outwards
C	-0.6	Inwards
D	0.7	Outwards

Check C_{pe} values as shown in Tab 6 of SANS 10160:3

Check C_{pe} values as shown in Tab 11 of SANS 10160:3

Stellenbosch University http://scholar.sun.ac.za

Roof

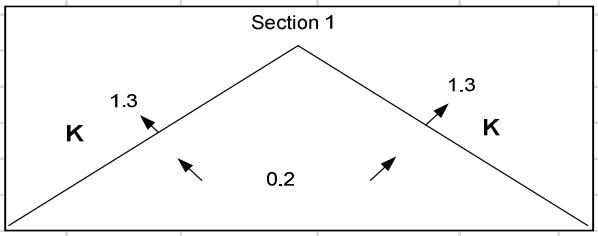

Zone	Coeff	Direction
K	1.5	Outward

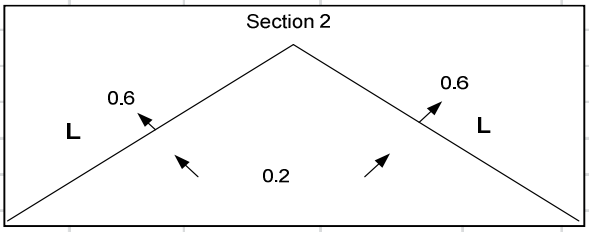

Zone	Coeff	Direction
L	0.8	Outward

Calculation of forces for Condition 2

Wall stud spacing	0.6	m
Truss spacing	1.2	m

Zone	Cpe	Vertical Force kn/m	Horisontal Force kN/m	Direction
A	1.4	0.694		**Outward**
B	1.0	0.496		**Outward**
C	-0.6	-0.298		**Inward**
D	0.7	0.347		**Outward**
K	1.5	1.437	0.383	**Outward**
L	0.8	0.767	0.204	**Outward**

Stellenbosch University http://scholar.sun.ac.za

WIND CONDITION 3

CASE 1: Structure has no dominant openings

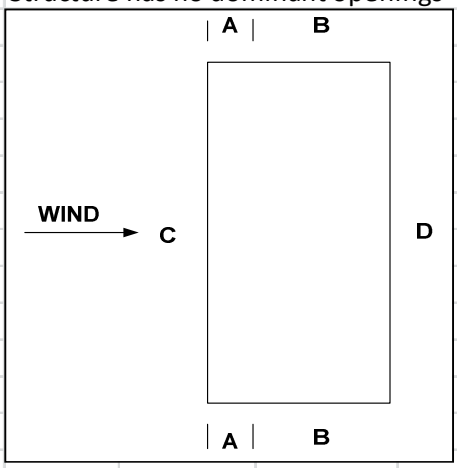

	h	6.1	m
	b	12	m
	d	6	m
	e	2.4	m

Pressure coeff on walls

SANS 517 P.28

Zone	Coeff
A	-1.2
B	-0.8
C	0.8
D	-0.5

Wind pressure on roof overhangs

SANS 517 5.3.3.3.5

C_{pe} 0.8 For zone C

or

C_{pe} -0.5 For zone A

Pressure on underside of roof overhang is equal to pressure on the wall to which its connected

Truss spacing 1.2 m

Stellenbosch University http://scholar.sun.ac.za

Force:

	Vertical	Horisontal
For zone C	0.767 kN/m	0.204 kN/m
For zone D	-0.479 kN/m	-0.128 kN/m

Wind pressure on roof

SANS 517 Tab3

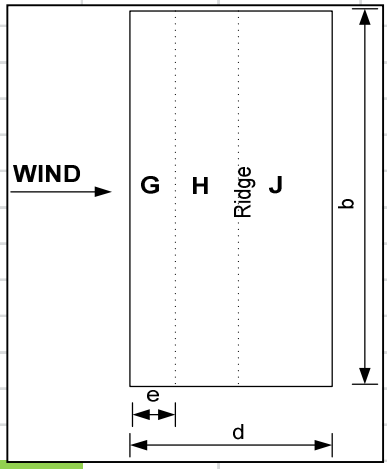

b	12.0	m
d	6.0	m
h	6.1	m
e	1.2	m
pitch angle	14.9267	

SANS 517 Tab 3

Zone	coeff
G	0.2
H	0.2
J	0

Internal pressure coefficient

Choose Cpi in such a way that it acts with the external pressure coeff

C_{pi} -0.3

Stellenbosch University http://scholar.sun.ac.za

Summary for condition 3

Walls

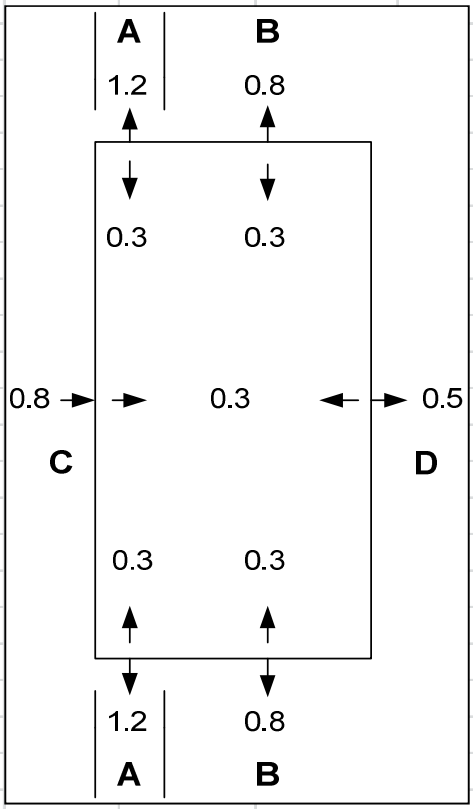

Zone	Coeff	Direction
A	0.9	Outwards
B	0.5	Outwards
C	-1.1	Inwards
D	0.2	Outwards

Roof

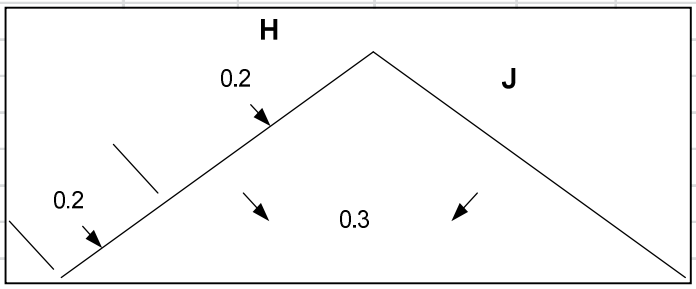

Zone	Coeff	Direction
G	-0.5	Inward
H	-0.5	Inward
J	-0.3	Inward

Stellenbosch University http://scholar.sun.ac.za

Calculation of forces for Condition 3

Wall stud spacing	0.6	m
Truss spacing	1.2	m

Zone	Cpe	Vertical Force kn/m	Horisontal Force kN/m	Direction
A	0.9	0.446		**Outward**
B	0.5	0.248		**Outward**
C	-1.1	-0.545		**Inward**
D	0.2	0.099		**Outward**
G	-0.5	-0.479	-0.128	**Inward**
H	-0.5	-0.479	-0.128	**Inward**
J	-0.3	-0.287	-0.077	**Inward**

Stellenbosch University http://scholar.sun.ac.za

Appendix E: Detailed axial load calculations

Note: All clauses refer to SANS 10162-2:2010

LIPPED CHANNEL IN COMPRESSION CLAUSE 3.4

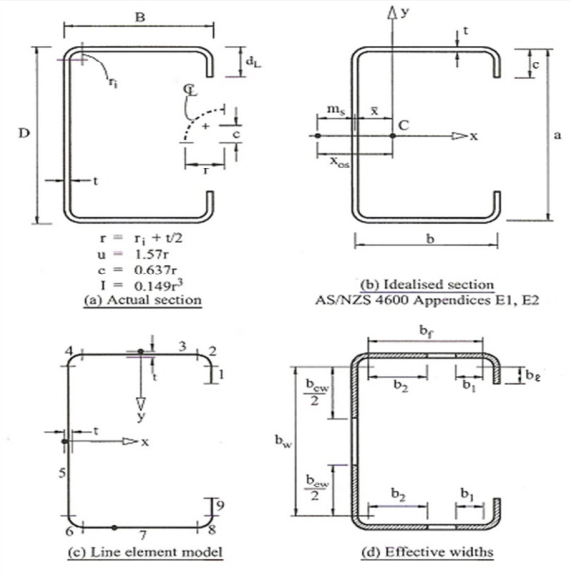

lex	2400	mm
ley	600	mm
lez	600	mm
fy	550	Mpa
B	41	mm
D	89	mm
dl	10.6	mm
ri	2	mm
t	0.95	mm
r	2.475	mm
u	3.88575	mm
c	1.577	mm
bf	35.1	mm
bw	83.1	mm
bl	7.65	mm
A	174.9359	mm2

$$I_x = 2t\left[2u\left(\frac{b_w}{2}+c\right)^2 + b_f\left(\frac{D}{2}-\frac{t}{2}\right)^2 + b_l\left[\frac{D}{2}-(r_i-t)-\frac{b_l}{2}\right]^2\right] + t\frac{b_w{}^3}{12}$$

224973.9 mm4

$$x_c = \left[\frac{t}{2}b_w + 2u(t+r_i-c) + 2u(B-r_i-t+c) + 2b_f\left(\frac{B}{2}\right) + 2b_l\left(B-\frac{t}{2}\right)\right]\frac{t}{A}$$

13.13 mm

$$I_y = \left[\left(\frac{t}{2}\right)^2 b_w + 2u(t-r_i-c)^2 + 2u(B-r_i-t+c)^2 + 2b_f\left(\frac{B}{2}\right)^2 + 2b_l\left(B-\frac{t}{2}\right)^2\right]t + 2t\frac{b_f^3}{12} - Ax_c^2$$

40261.34 mm4

$$J = \frac{At^2}{3}$$

52.63 mm4

SHEAR AND WARPING CONSTANTS

Use APP E1 of SANS 10162:2

a	88.05	mm
b	40.05	mm
c	10.125	mm

$$I_{xs} = 2t\left[b\left(\frac{a}{2}\right)^2 + c\left(\frac{a}{2}-\frac{c}{2}\right)^2\right] + t\frac{a^3}{12} + 2t\frac{c^3}{12}$$

230898 mm4

$$m_s = \frac{a^2b^2t}{I_{xs}}\left(\frac{1}{4}+\frac{c}{2b}-\frac{2}{3}\frac{c^3}{3a^2b}\right)$$

19.221 mm

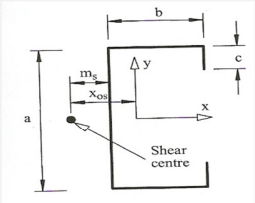

Stellenbosch University http://scholar.sun.ac.za

$$\bar{x} = \frac{b(b+2c)}{a+2b+2c}$$

12.819 mm

$$x_{os} = m_s + \bar{x}$$

32.039 mm

$$I_w = \frac{b^2 t}{6}(4c^3 + 6ac^2 + 3a^2 c + a^2 b) - m_s{}^2 I_{xs}$$

68172812 mm6

$$r_x = \sqrt{\frac{I_x}{A}}$$

35.861 mm

$$r_y = \sqrt{\frac{I_y}{A}}$$

15.17 mm

$$r_{o1} = \sqrt{\frac{I_x + I_y}{A} + x_{os}^2}$$

50.425 mm

Monosymmetry parameter

$$I_{ys} = \frac{2b^3 t}{12} + 2bt\left(\frac{b}{2} - \bar{x}\right)^2 + at\bar{x}^2 + 2ct(b-\bar{x})^2$$

42133.378 mm4

Refer to App E2

$\bar{x}$ -12.819 mm x_{os} -32.039 mm

$$\beta_w = \frac{t\bar{x}a^3}{12} + t\bar{x}^3 a$$ -868924 mm5

$$\beta_f = \frac{1}{2}t[(b+\bar{x})^4 - \bar{x}^4] + \frac{1}{4}a^2 t[(b+\bar{x})^2 - \bar{x}^2]$$ 1311238 mm5

$$\beta_l = 2ct(\bar{x}+b)^3 + \frac{2}{3}t(\bar{x}+b)\left[\left(\frac{a}{2}\right)^3 - \left(\frac{a}{2}-c\right)^3\right]$$ 1188216 mm5

$$\beta_y = \frac{\beta_w + \beta_f + \beta_l}{I_{ys}} - 2x_{os}$$ 102.7773 mm

Centroid of effective section under axial force alone

$$b_{ef1} = \left(\frac{I_s}{I_a}\right)\left(\frac{b_{ef}}{2}\right)$$ 5.109741 mm

$$b_{ef2} = b_{ef} - b_{ef1}$$ 25.35896 mm

$$x_1 = \left[\frac{t}{2}b_{ew} + 2u(t + r_i - c) + 2u(B - r_i - t + c)\right]$$ 338.559 mm2

$$x_2 = \left[2b_{ef2}\left(t + r_i + \frac{b_{ef2}}{2}\right) + 2b_{ef1}\left(t + r_i + b_f - \frac{b_{ef1}}{2}\right) + 2d_s\left(B - \frac{t}{2}\right)\right]$$ 1775.469 mm2

$$x_{cea} = (x_1 + x_2)\frac{t}{A_e}$$ 17.10867 mm2

CRITICAL STRESS FN CLAUSE 3.4

3.3.3.2.1 Open section members
For singly, doubly and point symmetric sections as in clause a

f_{ox}	440.717	MPa	E	2.00E+05	MPa
f_{oy}	1262.95	MPa	G	7.70E+04	MPa
f_{oz}	850.149	MPa	v	0.3	
			fy	550	MPa

f_{oc} = f_{oy} 1536.602 MPa **Clause 3.4.2**

f_{oxz} 345.341 MPa β 0.59629276

f_{oc} will be the lesser of f_{oc} and f_{oxz} 345.341 MPa

EFECTIVE AREA AT CRITICAL STRESS f_n AS SHOWN FIGURE D UNDER SECTION PROPERTIES
WHERE f_n WILL BE THE CRITICAL STRESS FOR AXIAL LOAD (COLOMN LOADS)

$\tau_c = \sqrt{\frac{f_y}{f_{oc}}}$ 1.261993248

f_n 282.3997757 MPa

FOR AXIAL LOADS (COLUMN LOADS)

Choose the value of f* to be fn for the first iteration and calculate effective width of web and flange. For second iteration use f* = fy and calculate effective width of web and flange. These values can then be used to calculate N_c and N_s

VALUE OF f* 282.3998 **MPa**

FOR COLOMN LOADS

Clause 2.2 applied to web

1. Calculate effective width with f* = fn and use to calculate Nc
2. Calculate effective width with f* = fy to calculate Ns

f* 282.3997757 MPa k 4

$f_{cr} = \left(\frac{k\pi^2 E}{12(1-v^2)}\right)\left(\frac{t}{b}\right)^2$ 94.50 MPa

$\tau = \sqrt{\frac{f^*}{f_{cr}}}$ 1.728727

b_{ew} 41.9526 mm

Stellenbosch University http://scholar.sun.ac.za

Element 2 Clause 2.3.1 applied to lips of channel

COLUMN LOADS

For axial load (column loads) f* = fn or f* = fy

f*	282.399776	MPa
k	0.43	
d	7.65	mm

$$f_{cr} = \left(\frac{k\pi^2 E}{12(1-v^2)}\right)\left(\frac{t}{d}\right)^2$$ 1198.669 MPa

$$\tau = \sqrt{\frac{f^*}{f_{cr}}}$$ 0.485

d se 7.65 mm

$$I_s = \frac{d^3 t}{12}$$ 35.44269 mm4

MEMBER COMPRESSION CAPACITY CLAUSE 3.4

$$A_e = t(b_{ew} + 2b_{ef} + 4u + 2d_s)$$

117.387 mm2

b ew	41.953	mm
b ef	30.469	mm
u	3.886	mm
ds	2.566	mm
t	0.95	mm

$N_c = A_e f_n$ 33.150 kN

$N_s = A_e f_y$ kN

Stellenbosch University http://scholar.sun.ac.za

Appendix F: Detailed calculation of shear capacity

Note: All clauses refer to SANS 10162:2 – 2010

SHEAR CAPACITY AS IN CLAUSE 3.3.4

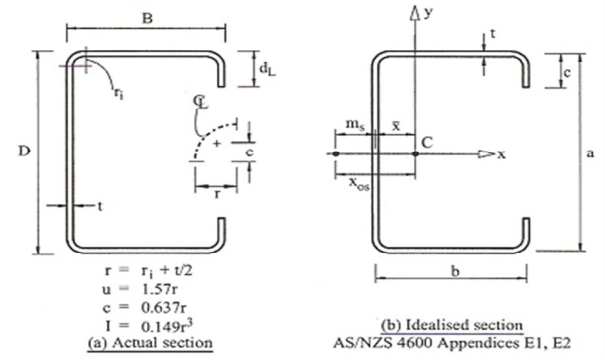

lex	600	mm
ley	600	mm
lez	600	mm
fy	550	Mpa
B	41	mm
D	89	mm
dl	10.6	mm
ri	2	mm
t	0.95	mm
Φ_v	0.9	
k_v	5.34	
E	200.000	Gpa

Web

dl/t	93.68421
$\sqrt{Ek_v/f_y}$	44.06607
V_v	9.311 kN

Flanges

2B/t	86.31579
$\sqrt{Ek_v/f_y}$	44.06607
V_v	10.10594 kN

Stellenbosch University http://scholar.sun.ac.za

Appendix G: Detailed Tensile capacity calculations

All Clauses and formulas refer to SANS 10162:2 – 2010

Material properties - Two Sheet Connections

f_y =	583.54	**MPa**
f_u =	583.54	**MPa**

Section properties

width of sheet (b) =	55	**mm**
thickness of sheet (t_1)=	2	**mm**
thickness of plate (t_2) =	0.8625	**mm**

(click on link for pictures defining the parameters)

t1, t2, b picture

Choose preferred calculation :

nr of Bolts
Bearing Capacity
Tearout Capacity

A: plate strength for Net plate

washers under both head and nut :	N		("Y" for yes and "N" for no)
bolts perpendicular or paralel to force:	L		("L" for perpendicular and "P" for paralel)
Double or single shear	S		("D" for double shear,"S" for single shear)
d_f =	10	**mm**	df picture
s_f =		**mm**	sf picture
nr of bolts perpendicular to force	2		
d_h =	11	**mm**	
ø =	0.65		

Lesser of :

1	$N_t = A_g f_y$	27681.68	**N**	27.68168 **KN**
	$=(bt)f_y$			
2	$N_t = 0.85 k_t A_n f_u$	14117.66	**N**	14.12 **KN**

Plate strength = 14.12 **KN**

$N_d = øNt$

12.71 **KN**

N_f =	51351.52	**N**	51.35152 **KN**
øN_f =	33.38	**KN**	

Design capacity of connection: 12.71 **KN**

B Number of bolts required

nr of bolts	2	
f_{uf} =	400	**MPa**
n_n =	1	(number of shear planes with threads intercepting the shear plane)
n_x =	1	(number of shear planes without threads intercepting the shear plane)
ø =	0.8	
A_o =	78.54	**mm²**
A_c =		**mm²**

$V_{fv} = 0.62 f_{uf}(n_n A_c + n_x A_o)$ **5.3.5.1(2)**

V_{fv} =	19477.87	**N**	19.48 **KN**

Shear capacity : 31.16 **KN**

Stellenbosch University http://scholar.sun.ac.za

C Check Bearing Capacity

nr of bolts	2			
d_f =	10	**mm**	df picture	
α =	0.75		alpha description	
ø =	0.6			
C =	2.84058			
t =	0.8625	**mm**		
$V_b = \alpha C d_f t f_u$				**5.3.4.2**
V_b =	10722.55	**N**	10.72255	**KN**
Total bearing capacity :			12.86706	**KN**

D Tearout

nr of bolts	2			
e =	25	**mm**	e picture	
ø =	0.6			
t=	0.8625	**mm**		
$V_f = tef_u$				**5.3.2(2)**
V_f =	12582.58	**N**	12.58258	**KN**
Total tearout capacity:			15.0991	**KN**

Stellenbosch University http://scholar.sun.ac.za

Screwed connection

A Section Capacity

Multiple screws in the line parallel to the force		N		("Y" for yes and "N" for no)
	d_f =	5	mm	(nominal screw diameter)
	s_f =	1	mm	sf picture
nr of screws perpendicular to force		2		
	ø=	0.65		
	A_g =	159.1901	mm^2	
	t_2 =	0.95	mm	
	A_n =	149.6901	mm^2	

Lesser of :

1	$N_t = A_g f_y$	92893.8	N	92.8938	KN
	$=(bt)f_y$				
2	$N_t = 0.85 k_t A_n f_u$	74247.64	N	74.24764	KN

Section strength = 74.24764 KN

$N_d = øNt$

66.82288 KN

N_t =	87350.17 N	87.35017	KN
øN_t =	56.77761 KN		
Design capacity of connection:		56.77761	KN

B Tilting and hole bearing

d_f=	5	mm	nominal screw diameter
f_{u1} =	583.54	MPa	tensile strength of sheet not in contact with screw head
f_{u2}=	583.54	MPa	tensile strength of sheet in contact with screw head
nr of screws	2		
C =	2.7		
C_1 =	2.7		
C_2 =	2.7		
ø=	0.5		
t_2/t_1=	1.000		
t_1=	0.95	mm	
t_2 =	0.95	mm	
d_f/t_1 =	5.26		
d_f/t_2 =	5.263158		

$V_b = 4.2\sqrt{(t_2^3 d_f)} f_{u2}$	5.07	KN	**5.4.2.3(2)**
$V_b = C_1 t_1 d_f f_{u1}$	7.483901	KN	**5.4.2.3(3)**
$V_b = C_2 t_2 d_f f_{u2}$	7.483901	KN	**5.4.2.3(4)**
Minimum (5.4.2.3(2)-(4))	5.07	KN	
$V_b = 2.7 t_1 d_f f_{u1}$	7.483901	KN	**5.4.2.3(5)**
$V_b = 2.7 t_2 d_f f_{u2}$	7.483901	KN	**5.4.2.3(6)**
Minimum (5.4.2.3(5)-(6) =	7.483901	KN	
	5.07	KN	

Stellenbosch University http://scholar.sun.ac.za

C Connection shear as limited by edge distance

nr of screws	2				
e_1 =	19	mm	e1, e2 picture		
e_2 =	21	mm			
t_1 =	0.95	mm			
t_2 =	0.95	mm			
f_u/f_y =	1.000				
ø =	0.6				

$V_{fv} = tef_u$ **5.4.2.4(2)**

V_{fv1} = 10.5329 **KN** V_{fv2} = 11.641623 **KN**

Tearout capacity 12.63948 **KN**

Block shear Rupture

d_f =	5	mm	(nominal screw diameter)
b_1 =	19	mm	b1,b2,sf picture
b_2 =	21	mm	
s_f =	1	mm	
nr of screws in line with force	0		
nr of screws perpendicular to force	2		
t_1 =	0.95	mm	
t_2 =	0.95	mm	
A_{nt1} =	-7.6	mm²	
A_{nt2} =	-7.6	mm²	
A_{nv1} =	81.7	mm²	
A_{nv2} =	89.3	mm²	
A_{gv1} =	72.2	mm²	
A_{gv2} =	79.8	mm²	
A_{gt1} =	1.9	mm²	
A_{gt2} =	1.9	mm²	
ø =	0.65		

f_uA_{nt1} =	-4434.9	<	$0.6f_uA_{nv1}$ =	28605.1308	R_{n1} =	29.71386 **KN**
f_uA_{nt2} =	-4434.9	<	$0.6f_uA_{nv2}$ =	31266.0732	R_{n2} =	32.3748 **KN**

Block shear capacity (section 1) = 19.3140069 **KN**

Block shear capacity (section 2) = 21.0436195 **KN**

E Tensile capacity of bolt

d_f =	5	mm
nr of bolts	1	
f_{uf} =	400	MPa
ø =	0.8	
A_s =	14.72622	mm²

$N_{ft} = A_s f_{uf}$ **5.3.5.2(2)**

Bolt Capacity: 4.712389 **KN**

Appendix H: Detailed calculation of moments about the strong axis

All clauses refer to SANS 10162:2 – 2010

LIPPED CHANNEL IN COMPRESSION CLAUSE 3.4

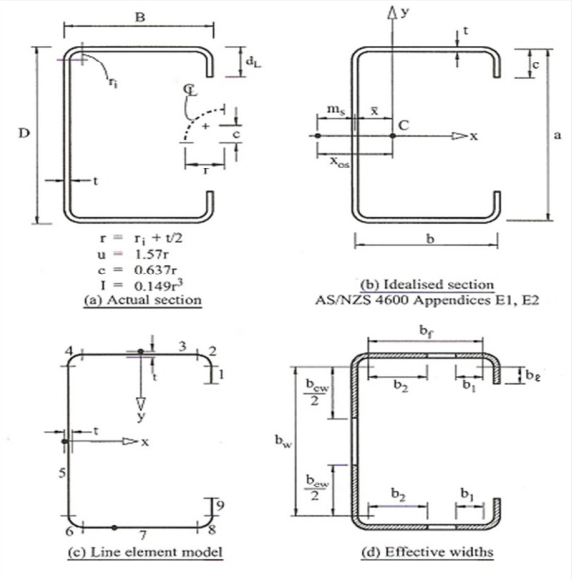

lex	2400	mm
ley	600	mm
lez	600	mm
fy	550	Mpa
B	41	mm
D	89	mm
dl	10.6	mm
ri	2	mm
t	0.95	mm
r	2.475	mm
u	3.88575	mm
c	1.577	mm
bf	35.1	mm
bw	83.1	mm
bl	7.65	mm
A	174.9359	mm2

$$I_x = 2t\left[2u\left(\frac{b_w}{2}+c\right)^2 + b_f\left(\frac{D}{2}-\frac{t}{2}\right)^2 + b_l\left[\frac{D}{2}-(r_i-t)-\frac{b_l}{2}\right]^2\right] + t\frac{b_w^3}{12}$$

224973.9 mm4

$$x_c = \left[\frac{t}{2}b_w + 2u(t+r_i-c) + 2u(B-r_i-t+c) + 2b_f\left(\frac{B}{2}\right) + 2b_l\left(B-\frac{t}{2}\right)\right]\frac{t}{A}$$

13.13 mm

$$I_y = \left[\left(\frac{t}{2}\right)^2 b_w + 2u(t-r_i-c)^2 + 2u(B-r_i-t+c)^2 + 2b_f\left(\frac{B}{2}\right)^2 + 2b_l\left(B-\frac{t}{2}\right)^2\right]t + 2t\frac{b_f^3}{12} - Ax_c^2$$

40261.34 mm4

$$J = \frac{At^2}{3}$$

52.63 mm4

SHEAR AND WARPING CONSTANTS

Use APP E1 of SANS 10162:2

a	88.05	mm
b	40.05	mm
c	10.125	mm

$$I_{xs} = 2t\left[b\left(\frac{a}{2}\right)^2 + c\left(\frac{a}{2}-\frac{c}{2}\right)^2\right] + t\frac{a^3}{12} + 2t\frac{c^3}{12}$$

230898 mm4

$$m_s = \frac{a^2b^2t}{I_{xs}}\left(\frac{1}{4}+\frac{c}{2b}-\frac{2}{3}\frac{c^3}{3a^2b}\right)$$

19.221 mm

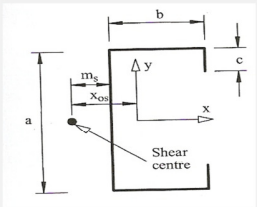

Stellenbosch University http://scholar.sun.ac.za

$$\bar{x} = \frac{b(b+2c)}{a+2b+2c}$$

12.819 mm

$$x_{os} = m_s + \bar{x}$$

32.039 mm

$$I_w = \frac{b^2 t}{6}(4c^3 + 6ac^2 + 3a^2 c + a^2 b) - m_s{}^2 I_{xs}$$

68172812 mm6

$$r_x = \sqrt{\frac{I_x}{A}}$$

35.861 mm

$$r_y = \sqrt{\frac{I_y}{A}}$$

15.17 mm

$$r_{o1} = \sqrt{\frac{I_x + I_y}{A} + x_{os}^2}$$

50.425 mm

Monosymmetry parameter

$$I_{ys} = \frac{2b^3 t}{12} + 2bt\left(\frac{b}{2} - \bar{x}\right)^2 + at\bar{x}^2 + 2ct(b-\bar{x})^2$$

42133.378 mm4

<u>Refer to App E2</u>

$\bar{x}$ -12.819 mm x_{os} -32.039 mm

$$\beta_w = \frac{t\bar{x}a^3}{12} + t\bar{x}^3 a$$

-868924 mm5

$$\beta_f = \frac{1}{2}t[(b+\bar{x})^4 - \bar{x}^4] + \frac{1}{4}a^2 t[(b+\bar{x})^2 - \bar{x}^2]$$

1311238 mm5

$$\beta_l = 2ct(\bar{x}+b)^3 + \frac{2}{3}t(\bar{x}+b)\left[\left(\frac{a}{2}\right)^3 - \left(\frac{a}{2}-c\right)^3\right]$$

1188216 mm5

$$\beta_y = \frac{\beta_w + \beta_f + \beta_l}{I_{ys}} - 2x_{os}$$

102.7773 mm

<u>Centroid of effective section under axial force alone</u>

$$b_{ef1} = \left(\frac{I_s}{I_a}\right)\left(\frac{b_{ef}}{2}\right)$$

5.109741 mm

$$b_{ef2} = b_{ef} - b_{ef1}$$

25.35896 mm

$$x_1 = \left[\frac{t}{2}b_{ew} + 2u(t + r_i - c) + 2u(B - r_i - t + c)\right]$$

338.559 mm2

$$x_2 = \left[2b_{ef2}\left(t + r_i + \frac{b_{ef2}}{2}\right) + 2b_{ef1}\left(t + r_i + b_f - \frac{b_{ef1}}{2}\right) + 2d_s\left(B - \frac{t}{2}\right)\right]$$

1775.469 mm2

$$x_{cea} = (x_1 + x_2)\frac{t}{A_e}$$

17.10867 mm2

Stellenbosch University http://scholar.sun.ac.za

CRITICAL STRESS FN CLAUSE 3.4

3.3.3.2.1 Open section members
For singly, doubly and point symmetric sections as in clause a

f_{ox}	440.717	MPa	E	2.00E+05	MPa
f_{oy}	1262.95	MPa	G	7.70E+04	MPa
f_{oz}	850.149	MPa	v	0.3	
			fy	550	MPa

f_{oc} = f_{oy} 1536.602 MPa **Clause 3.4.2**

f_{oxz} 345.341 MPa β 0.59629276

f_{oc} will be the lesser of f_{oc} and f_{oxz} 345.341 MPa

EFECTIVE AREA AT CRITICAL STRESS f_n AS SHOWN FIGURE D UNDER SECTION PROPERTIES WHERE f_n WILL BE THE CRITICAL STRESS FOR AXIAL LOAD (COLOMN LOADS)

$\tau_c = \sqrt{\frac{f_y}{f_{oc}}}$ 1.261993248

f_n 282.3997757 MPa

FOR BEAM LOADS

To get the effective width of the web that can be used for calculations use f* = fy
But to get the the Ix value of the whole section choose a value for f* in such a way that bew > bcw. The Ix value can then be used to calculate the different moments

VALUE OF f* **550** **MPa**

Stellenbosch University http://scholar.sun.ac.za

FOR BEAM LOADS

Element1 Clause 2.2.3.2 applied to web of channel

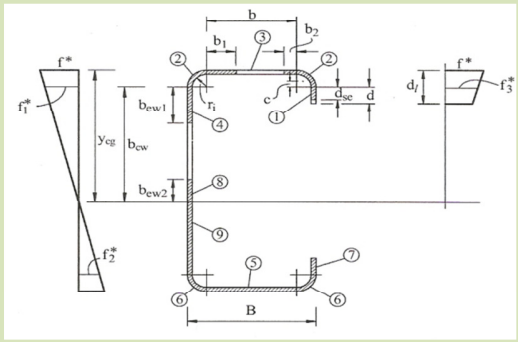

L1	1.853	mm	y1	3.876489	mm	I_1'	0.530 mm^3
L2	7.7715	mm	y2	1.373425	mm	I_2'	4.52 mm^3
L3	23.136	mm	y3	0.475	mm	I_3'	0.00 mm^3
L4	83.1	mm	y4	44.5	mm	I_4'	47821.35 mm^3
L5	35.1	mm	y5	88.525	mm	I_5'	0.00 mm^3
L6	7.7715	mm	y6	87.62658	mm	I_6'	4.52 mm^3
L7	7.65	mm	y7	82.225	mm	I_7'	37.31 mm^3
L_{tot}	166.382	mm	y_{tot}	308.6015	mm	I_{tot}	47868.223 mm^3

Ly_{tot} 8144.034925 mm^2

Ly^2_{tot} 551067.9011 mm^3

$y_{eg1} = \frac{\sum_{i=1}^{7} L_i y_i}{\sum_{i=1}^{7} L_i}$ 48.94780159 mm

$I_{Ly2} = \sum_{i=1}^{7} L_i y_{eg}^2$ 398632.606 mm^3

I_x' 200303.519 mm^3

I_x 190288.3 mm^4

Z_{ex} 3887.576903 mm^3

Stellenbosch University http://scholar.sun.ac.za

Calculate k value of web as in Clause 2.2.3.2

For first iteration use y_{cg1} as calculated
Use guessed y_{cg} for 2nd itteration

ycg 48.9478016 mm

$$f_1^* = [y_{cg} - (r_i + t)]\frac{f_1^*}{y_{cg}}$$ 516.8524 MPa

$$f_2^* = -[d_1 + (r_i + t) - y_{cg}]\frac{f_1^*}{y_{cg}}$$ -416.897 MPa

$$\psi = \frac{f_2^*}{f_1^*}$$ -0.80661

$$k = 4 + 2(1 - \psi)^3 + 2(1 - \psi)$$ 19.40615

k 19.4061494

$$f_{cr} = \left(\frac{k\pi^2 E}{12(1 - v^2)}\right)\left(\frac{t}{b}\right)^2$$ 458.45 MPa

Recalculate τ_c

$$\tau = \sqrt{\frac{f^*}{f_{cr}}}$$ 1.095

2.2.1.2 Effective width for capacity calculations

b_{ew} 60.630 mm

$$b_{ew1} = \frac{b_{ew}}{3 - \psi}$$ 15.92764294 mm

b_{ew2} 30.31514715 mm

$$b_{cw} = y_{cg} - (r_i + t)$$ 45.9978 mm

b_{ew} 46.24279009 mm

Web is fully effective since bew>bcw, no need for second iteration, use ycg1 as calculated

Stellenbosch University http://scholar.sun.ac.za

BEAM LOADS

For beam loads use f* = fy

f*	550	MPa
k	0.43	
d	7.65	mm

$$f_{cr} = \left(\frac{k\pi^2 E}{12(1-v^2)}\right)\left(\frac{t}{d}\right)^2$$ 1198.669 MPa

$$\tau = \sqrt{\frac{f^*}{f_{cr}}}$$ 0.677

$$I_s = \frac{d^3 t}{12}$$ 35.4426891 mm^4

dse 7.625603 mm

Stellenbosch University http://scholar.sun.ac.za

ELEMENT 3 - FLAT FLANGE

BEAM LOAD

		bf	35.1 mm
See clause 2.1.3.1 fore thickness ratios		t	0.95 mm

$\frac{b_f}{t}$ 36.95 Value O.K

Clause 2.4 Uniformly compressed elements with an edge stiffener

$S = 1.28\sqrt{\frac{E}{f'}}$ 24.41 Flange not fully effective without stiffeners

I_{a2} 541.7414594 mm4

I_{a3} 145.86 mm4

I_a 145.86 mm4

n 0.150 0.333333 n must be 1/3 at least

Calculate buckling cooefficient (k) and stiffener reduced effective wind ds

$\frac{d_L}{b_f}$ 0.301994302

See Table 2.4.2 for determination of k factor

k 2.658

ds 1.853 mm

Clause 2.2.1.2 Effective width of flange Element 3 for strength

$f_{cr} = \left(\frac{k\pi^2 E}{12(1-v^2)}\right)\left(\frac{t}{b}\right)^2$ 351.928 MPa

$\tau = \sqrt{\frac{f'}{f_{cr}}}$ 1.250

b ef 23.136 mm

Stellenbosch University http://scholar.sun.ac.za

ELASTIC CRITICAL MOMENT FOR FLEXURAL TORSOINAL BUCKLING DUE TO BENDING ABOUT THE SYMMETRY AXIS

Clause 3.3.3.2.1 a

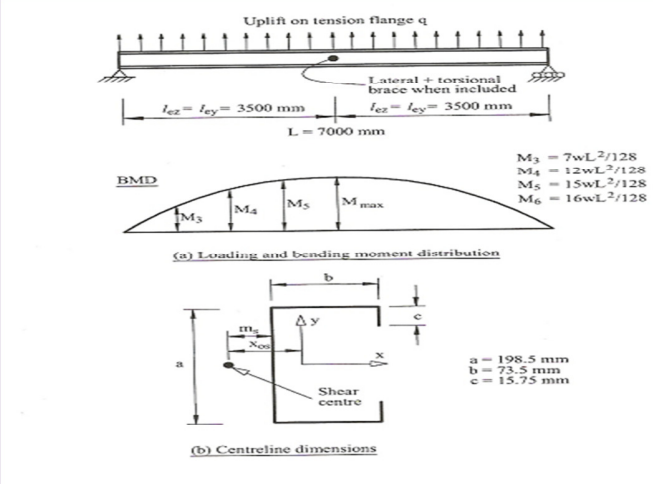

β_y	102.78	mm
f_{oz}	850.15	Mpa
f_{oy}	1262.95	Mpa
Mmax	0.125	kNm
M3	0.054688	kNm
M4	0.09375	kNm
M5	0.117188	kNm
A	174.9359	mm2
r_{o1}	50.43	mm

$$C_b = \frac{12.5M_{max}}{2.5M_{max} + 3M_3 + 4M_4 + 3M_5}$$ 1.299

$$M_o = C_b A r_{o1} \sqrt{f_{oy} f_{oz}}$$ 11.871 kNm

$$Z_{xf} = \frac{I_x}{\left(\frac{D}{2}\right)}$$ 5055.593 mm3

$$M_y = Z_{fx} f_y$$ 2.780576 kNm

$$\tau_b = \sqrt{\frac{M_y}{M_o}}$$ 0.483983

LATERAL BUCKLING AS IN CLAUSE 3.3.3.2

Critical moment Mc as in section 3.3.3.2

Mc	2.780576	kNm
fc = Mc/Zfx	550	Mpa

Nominal member moment capacity Mb

			Z_{ex}	3.89E+03 mm^3
$M_b = Z_{ex} * f_c$	2.138	kNm	f_c	550 Mpa

DISTORTIONAL BUCKLING AS IN CLAUSE 3.3.3.3 A

			f_{od}	355.8694 Mpa
$M_{od} = f_{od} * Z_{ex}$	1.799131	kNm		

$$\tau_b = \sqrt{\frac{M_y}{M}}$$ 1.243186

Appendix I: Detailed calculation of moments about the weak axis

All clause refer to SANS 10162:2

LIPPED CHANNEL IN COMPRESSION CLAUSE 3.4

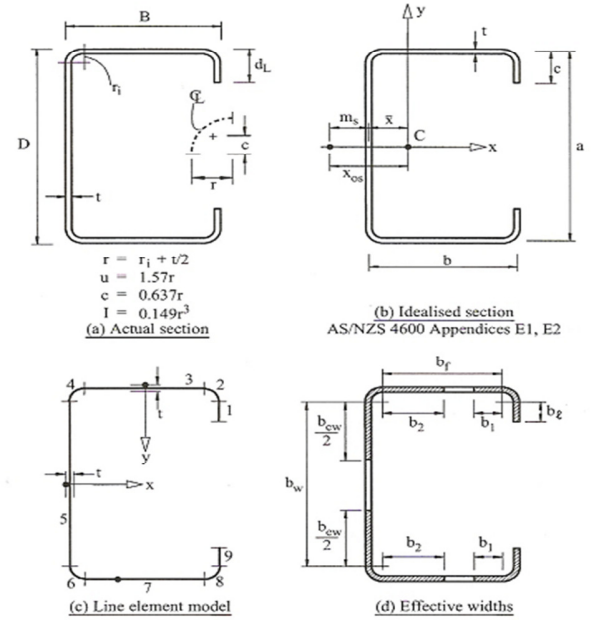

lex	2400	mm
ley	600	mm
lez	600	mm
fy	550	Mpa
B	41	mm
D	89	mm
dl	10.6	mm
ri	2	mm
t	0.95	mm
r	2.475	mm
u	3.88575	mm
c	1.577	mm
bf	35.1	mm
bw	83.1	mm
bl	7.65	mm
A	174.9359	mm2

$$I_x = 2t\left[2u\left(\frac{b_w}{2}+c\right)^2 + b_f\left(\frac{D}{2}-\frac{t}{2}\right)^2 + b_l\left[\frac{D}{2}-(r_i-t)-\frac{b_l}{2}\right]^2\right] + t\frac{b_w^3}{12}$$

224973.9 mm4

$$x_c = \left[\frac{t}{2}b_w + 2u(t+r_i-c) + 2u(B-r_i-t+c) + 2b_f\left(\frac{B}{2}\right) + 2b_l\left(B-\frac{t}{2}\right)\right]\frac{t}{A}$$

13.13 mm

$$I_y = \left[\left(\frac{t}{2}\right)^2 b_w + 2u(t-r_i-c)^2 + 2u(B-r_i-t+c)^2 + 2b_f\left(\frac{B}{2}\right)^2 + 2b_l\left(B-\frac{t}{2}\right)^2\right]t + 2t\frac{b_f^3}{12} - Ax_c^2$$

40261.34 mm4

$$J = \frac{At^2}{3}$$

52.63 mm4

SHEAR AND WARPING CONSTANTS

Use APP E1 of SANS 10162:2

a	88.05	mm
b	40.05	mm
c	10.125	mm

$$I_{xs} = 2t\left[b\left(\frac{a}{2}\right)^2 + c\left(\frac{a}{2}-\frac{c}{2}\right)^2\right] + t\frac{a^3}{12} + 2t\frac{c^3}{12}$$

230898 mm4

$$m_s = \frac{a^2b^2t}{I_{xs}}\left(\frac{1}{4}+\frac{c}{2b}-\frac{2}{3}\frac{c^3}{3a^2b}\right)$$

19.221 mm

$$\bar{x} = \frac{b(b+2c)}{a+2b+2c}$$

12.819 mm

$$x_{os} = m_s + \bar{x}$$

32.039 mm

$$I_w = \frac{b^2 t}{6}(4c^3 + 6ac^2 + 3a^2 c + a^2 b) - m_s{}^2 I_{xs}$$

68172812 mm6

$$r_x = \sqrt{\frac{I_x}{A}}$$

35.861 mm

$$r_y = \sqrt{\frac{I_y}{A}}$$

15.17 mm

$$r_{o1} = \sqrt{\frac{I_x + I_y}{A} + x_{os}^2}$$

50.425 mm

Monosymmetry parameter

$$I_{ys} = \frac{2b^3 t}{12} + 2bt\left(\frac{b}{2} - \bar{x}\right)^2 + at\bar{x}^2 + 2ct(b-\bar{x})^2$$

42133.378 mm4

Refer to App E2

$\bar{x}$ -12.819 mm x_{os} -32.039 mm

$$\beta_w = \frac{t\bar{x}a^3}{12} + t\bar{x}^3 a$$

-868924 mm5

$$\beta_f = \frac{1}{2}t[(b+\bar{x})^4 - \bar{x}^4] + \frac{1}{4}a^2 t[(b+\bar{x})^2 - \bar{x}^2]$$

1311238 mm5

$$\beta_l = 2ct(\bar{x}+b)^3 + \frac{2}{3}t(\bar{x}+b)\left[\left(\frac{a}{2}\right)^3 - \left(\frac{a}{2}-c\right)^3\right]$$

1188216 mm5

$$\beta_y = \frac{\beta_w + \beta_f + \beta_l}{I_{ys}} - 2x_{os}$$

102.7773 mm

Centroid of effective section under axial force alone

$$b_{ef1} = \left(\frac{I_s}{I_a}\right)\left(\frac{b_{ef}}{2}\right)$$

3.730734 mm

$$b_{ef2} = b_{ef} - b_{ef1}$$

22.7089 mm

$$x_1 = \left[\frac{t}{2}b_{ew} + 2u(t + r_i - c) + 2u(B - r_i - t + c)\right]$$

335.6905 mm2

$$x_2 = \left[2b_{ef2}\left(t + r_i + \frac{b_{ef2}}{2}\right) + 2b_{ef1}\left(t + r_i + b_f - \frac{b_{ef1}}{2}\right) + 2d_s\left(B - \frac{t}{2}\right)\right]$$

1094.645 mm2

$$x_{cea} = (x_1 + x_2)\frac{t}{A_e}$$

13.16417 mm2

Stellenbosch University http://scholar.sun.ac.za

CRITICAL STRESS FN CLAUSE 3.4

3.3.3.2.1 Open section members
For singly, doubly and point symmetric sections as in clause a

f_{ox} 440.717 Mpa

f_{oy} 1262.95 Mpa

f_{oz} 850.504 Mpa

E 2.00E+05 Mpa
G 8.00E+04 MPa
v 0.3

f_{oc} = f_{oy} 391.0113 Mpa **Clause 3.4.2**

f_{oxz} 345.380 Mpa β 0.596293

f_{oc} will be the lesser of f_{oc} and f_{oxz} 345.380 Mpa

$$\tau_c = \sqrt{\frac{f_y}{f_{oc}}}$$ 1.262

f_n 282.421 Mpa Where yield occur

EFECTIVE AREA AT CRITICAL STRESS f_n AS SHOWN FIGURE D UNDER SECTION PROPERTIES

Element1 Clause 2.2 applied to web of channel

k 4

Assume $f^* = f_n$ 404.000 Mpa

Use only the first 2 values for Comp
Use last 2 values for bending and comp

$$f_{cr} = \left(\frac{k\pi^2 E}{12(1-v^2)}\right)\left(\frac{t}{b}\right)^2$$ 94.50 Mpa

Recalculate τ_c

$$\tau = \sqrt{\frac{f^*}{f_{cr}}}$$ 2.068

2.2.1.2 Effective width for capacity calculations

b ew 35.914 mm

Stellenbosch University http://scholar.sun.ac.za

Element2 Clause 2.3 applied to lips of channel

k 0.43

d 7.65 mm

$f_{cr} = \left(\frac{k\pi^2 E}{12(1-v^2)}\right)\left(\frac{t}{d}\right)^2$ 1199.432 Mpa

$\tau = \sqrt{\frac{f^*}{f_{cr}}}$ 0.580

d se 7.65 mm $I_s = \frac{d^3 t}{12}$ 35.44269 mm4

Element 3 Flat Flange

bf 35.1 mm

See clause 2.1.3.1 fore thickness ratios t 0.95 mm

$\frac{b_f}{t}$ 36.94737 Value O.K

Clause 2.4 Uniformly compressed elements with an edge stiffener

$S = 1.28\sqrt{\frac{E}{f^*}}$ 28.48 Flange not fully effective without stiffeners

I_{a2} 295.9902 mm4

I_{a3} 125.59 mm4

I_a 125.591 mm4

n 0.212 0.333333 n must be 1/3 at least

Calculate buckling cooefficient (k) and stiffener reduced effective wind ds

$\frac{d_L}{b_f}$ 0.301994

See Table 2.4.2 for determination of k factor

k 2.772

ds 2.159 mm

Clause 2.2.1.2 Effective width of flange Element 3 for strength

$f_{cr} = \left(\frac{k\pi^2 E}{12(1-v^2)}\right)\left(\frac{t}{b}\right)^2$ 367.012 Mpa

$\tau = \sqrt{\frac{f^*}{f_{cr}}}$ 1.049

b ef 26.440 mm

Stellenbosch University http://scholar.sun.ac.za

ELASTIC CRITICAL MOMENT FOR FLEXURAL TORSOINAL BUCKLING DUE TO BENDING IN PLANE OF SYMMETRY

Clause 3.3.3.2.1

β_y	102.78	mm
f_{oz}	850.50	Mpa
f_{ox}	440.72	Mpa
M_1	2	kNm
M_2	2	kNm
A	174.9359	mm2
r_{o1}	50.43	mm

M_1 is the smaller and M_2 the larger bending moment at the ends of the unbraced length. The sign of ratio will be possitive if moments have same sign. See 3.3.3.2.1(ii)

$$C_{TF} = 0..6 - 0.4\left(\frac{M_1}{M_2}\right)$$

1 Uniform moment

Compression condition as in Figure E1: Moment causing compression on shear centre

C_s 1

$$M_o = \frac{C_s A f_{ox}\left[\left(\frac{\beta_y}{2}\right) + C_s\sqrt{\left(\beta_y/2\right)^2 + r_{o1}^2\left(f_{oz}/f_{ox}\right)}\right]}{C_{TF}}$$

10.660 kNm

$$Z_{fy} = \frac{I_y}{x_c}$$ 3067.07429 mm3

$$M_y = Z_{fy} f_y$$ 1.68689086 kNm

$$\tau_b = \sqrt{\frac{M_y}{M_o}}$$ 0.39780112

LATERAL BUCKLING AS IN CLAUSE 3.3.3.2

Critical moment M_c as in section 3.3.3.2

M_c 1.68689086 kNm

$f_c = M_{cy}/Z_{fy}$ 550 MPa

Nominal member moment capacity M_b

$M_b = Z_{cy} * f_c$ 0.962 kNm

Z_{cy} 1.75E+03 mm^3

f_c 550 Mpa

DISTORTIONAL BUCKLING AS IN CLAUSE 3.3.3.3 A

M_c 1.68689086 kNm

$f_c = M_{cy}/Z_{fy}$ 550 MPa

Nominal member moment capacity M_b

$M_b = Z_{cy} * f_c$ 1.68689086 kNm

Z_c 3067.074 mm^3

Design moment 0.962 kNm

Stellenbosch University http://scholar.sun.ac.za

EFFECTIVE SECTION MODULES Z_{cy} AND NOMINAL MEMBER MOMENT CAPACITY AT A STRESS ($f_c=M_{cy}/Z_{fy}$)

t	0.95	mm
b_{ef}	35.1	mm
u	3.88575	mm
b_l	7.65	mm
r_i	2	mm
c	1.576575	mm
B	41	mm
f_y	550	Mpa

Clause 2.2 applied to web of channel

Calculate b ew from "Critical stress fn", applied to web

Use $f^* = f_c$ for the first interation to calculate b_{ew}

Where f_c is calculated in "Elastic critical moment"

f^* for the second iteration where yield occur

b_{ew} 35.91366 mm

$A_e = t(b_{ew} + 2b_{ef} + 4u + 2b_l)$ 130.1088 mm2

$$x_{ce} = \left[\frac{t}{2}b_{ew} + 2b_f\left(\frac{B}{2}\right) + 2u(t + r_i - c) + 2u(B - r_i - t + c) + 2b_l\left(B - \frac{t}{2}\right)\right]\frac{t}{A_e}$$

17.49 mm ft 551.341 MPa

$$I_{ye} = \left[\left(\frac{t}{2}\right)^2 b_{ew} + 2b_f\left(\frac{B}{2}\right)^2 + 2u(t + r_i - c)^2 + 2u(B - r_i - t + c)^2 + 2b_l\left(B - \frac{t}{2}\right)^2\right]t + 2t\frac{b_f^3}{12} - A_e x_{ce}^2$$

30576.56 mm4

$Z_{cy} = \frac{I_{ye}}{x_{ce}}$ 1748.632 mm3 $Z_{ey} = \frac{I_{ye}}{(B - x_{ce})}$ 1300.355 mm3

$M_{by} = Z_{cy}\left(\frac{M_{cy}}{Z_{fy}}\right)$ 0.000 kNm FALSE

$M_{sy} = Z_{ey}f_y$ 0.715195 kNm Tension flange at yield

Use smallest of Mb and Msy as design moment

Stellenbosch University http://scholar.sun.ac.za

Appendix J: Spread sheet calculations for evaluation of β-Case 1

FORM-Axial load

				Iteration 1						
$g(x_2^*)$	**0**									
$g(x_2^*)$wind	-0.103									
$g(x_2^*)$DL	0									
$g(x_2^*)$LLR	0									
$g(x_2^*)$LLF	0									
D	-0.71486		u_1^*	2.951969		x^*_1	38.5	$v_{b,0}$	dg/dx	-0.05351
	0			0			0.2	DL		0
	0			1.803556			0.25	LLR		0
	0			1.788179			1.5	LLF		0
$\mathbf{D}^T$	-0.71486	0	0	0						
						σ_x^e	13.36028		u_x^e	-0.93912
			β	**2.951969**			0.02			0.20000
							0.045082			0.16869
	α_1	-1					0.270693			1.01595
		0								
		0								
		0								
	u_2^*	-2.95197								
		0								
		0								
		0								
	x_2^*	38.5	WL							
		0.2	DL							
		0.168692	LLR							
		1.015952	LLF							

Stellenbosch University http://scholar.sun.ac.za

				Iteration 2					
$g(x_2^*)$	**0.001**								
$g(x_2^*)$wind	-0.103								
$g(x_2^*)$DL	0.001								
$g(x_2^*)$LLR	0.001								
$g(x_2^*)$LLF	0.001								
D	-0.7218		u_2^*	2.951969		x^*_2	38.5	$v_{b,0}$	dg/dx	-0.05403
	0			0			0.2	DL		0
	0			-0.25624			0.168692	LLR		0
	0			-0.25147			1.015952	LLF		0
D^T	-0.7218	0	0	0						
						σ_x^e	13.36028		u_x^e	-0.93912
			β	**2.951969**			0.02			0.20000
							0.034351			0.17749
	α_2	-1					0.206808			1.06796
		0								
		0								
		0								
	u_3^*	-2.95197								
		0								
		0								
		0								
	x_3^*	38.5	WL							
		0.2	DL							
		0.177494	LLR							
		1.067958	LLF							

Stellenbosch University http://scholar.sun.ac.za

				Iteration 3						
$g(x_3^*)$	**0.001**									
$g(x_3^*)$wind	-0.103									
$g(x_3^*)$DL	0.001									
$g(x_3^*)$LLR	0.001									
$g(x_3^*)$LLF	0.001									
D	-0.7218		u_3^*	2.951969		x^*_3	38.5	$v_{b,0}$	dg/dx	-0.05403
	0			0			0.2	DL		0
	0			-0.00424			0.177494	LLR		0
	0			-0.00408			1.067958	LLF		0
D^T	-0.7218	0	0	0						
						σ_x^e	13.36028		u_x^e	-0.93912
			β	**2.951969**			0.02			0.20000
							0.035513			0.17764
	α_3	-1					0.213672			1.06883
		0								
		0								
		0								
	u_4^*	-2.95197								
		0								
		0								
		0								
	x_4^*	38.5	WL							
		0.2	DL							
		0.177645	LLR							
		1.06883	LLF							

Stellenbosch University http://scholar.sun.ac.za

				Iteration 4						
$g(x_4^*)$	**0.001**									
$g(x_4^*)$wind	-0.103									
$g(x_4^*)$DL	0.001									
$g(x_4^*)$LLR	0.001									
$g(x_4^*)$LLF	0.001									
D	-0.7218		$\mathbf{u_4^*}$	2.951969		$\mathbf{x^*_4}$	38.5	$v_{b,0}$	dg/dx	-0.05403
	0			0			0.2	DL		0
	0			-1.2E-06			0.177645	LLR		0
	0			-1.1E-06			1.06883	LLF		0
$\mathbf{D^T}$	-0.7218	0	0	0						
						$\boldsymbol{\sigma_x^e}$	13.36028		$\mathbf{u_x^e}$	-0.93912
			β	**2.951969**			0.02			0.20000
							0.035533			0.17764
	$\boldsymbol{\alpha_4}$	-1					0.213787			1.06883
		0								
		0								
		0								
	$\mathbf{u_5^*}$	-2.95197								
		0								
		0								
		0								
	$\mathbf{x_5^*}$	38.5	WL							
		0.2	DL							
		0.177645	LLR							
		1.068831	LLF							

Stellenbosch University http://scholar.sun.ac.za

Live load distribution

	Gamma Dist - applied as Log Normal with lower skewness					
			Iteration 1			
	Roof				**Floor**	
x_1*	0.25	kPa		x_1*	1.5	kPa
μ	0.18	kPa		u	1.083	kPa
COV	0.2			COV	0.2	
σ	0.036	kPa		σ	0.2166	kPa
skew	0.4			skew	0.4	
c	0.132557			c	0.132557	
u	1.944444			u	1.925208	
$\Phi_X(x^*)$	0.964349			$\Phi_X(x^*)$	0.963126	
$\Phi_U^{-1}(\Phi_X(x^*))$	1.803556			$\Phi_U^{-1}(\Phi_X(x^*))$	1.788179	
$\varphi_U[\Phi_U^{-1}(\Phi_X(x^*))]$	0.078446			$\varphi_U[\Phi_U^{-1}(\Phi_X(x^*))]$	0.080642	
$\varphi_X(x^*)$	1.740075			$\varphi_X(x^*)$	0.297911	
σ_X^e	0.045082			σ_X^e	0.270693	
μ_X^e	0.17			μ_X^e	1.02	
			Iteration 2			
	Roof				**Floor**	
x_2*	0.168692	kPa		x_2*	1.015952	kPa
μ	0.18	kPa		u	1.083	kPa
COV	0.2			COV	0.2	
σ	0.036	kPa		σ	0.2166	kPa
skew	0.4			skew	0.4	
c	0.132557			c	0.132557	
u	-0.314106			u	-0.30955	
$\Phi_X(x^*)$	0.398881			$\Phi_X(x^*)$	0.400726	
$\Phi_U^{-1}(\Phi_X(x^*))$	-0.256244			$\Phi_U^{-1}(\Phi_X(x^*))$	-0.25147	
$\varphi_U[\Phi_U^{-1}(\Phi_X(x^*))]$	0.386057			$\varphi_U[\Phi_U^{-1}(\Phi_X(x^*))]$	0.386526	
$\varphi_X(x^*)$	11.23863			$\varphi_X(x^*)$	1.869004	
σ_X^e	0.034351			σ_X^e	0.206808	
μ_X^e	0.18			μ_X^e	1.07	

Stellenbosch University http://scholar.sun.ac.za

			Iteration 3			
	Roof				**Floor**	
x_3*	0.177494	kPa		x_3*	1.067958	kPa
μ	0.18	kPa		u	1.083	kPa
COV	0.2			COV	0.2	
σ	0.036	kPa		σ	0.2166	kPa
skew	0.4			skew	0.4	
c	0.132557			c	0.132557	
u	-0.069599			u	-0.06945	
$\Phi_X(x^*)$	0.498309			$\Phi_X(x^*)$	0.498371	
$\Phi_U^{-1}(\Phi_X(x^*))$	-0.004238			$\Phi_U^{-1}(\Phi_X(x^*))$	-0.00408	
$\varphi_U[\Phi_U^{-1}(\Phi_X(x^*))]$	0.398939			$\varphi_U[\Phi_U^{-1}(\Phi_X(x^*))]$	0.398939	
$\varphi_X(x^*)$	11.2337			$\varphi_X(x^*)$	1.867061	
$\boldsymbol{\sigma_X^e}$	0.035513			$\boldsymbol{\sigma_X^e}$	0.213672	
$\boldsymbol{\mu_X^e}$	0.18			$\boldsymbol{\mu_X^e}$	1.07	
			Iteration 4			
	Roof				**Floor**	
x_4*	0.177645	kPa		x_4*	1.06883	kPa
μ	0.18	kPa		u	1.083	kPa
COV	0.2			COV	0.2	
σ	0.036	kPa		σ	0.2166	kPa
skew	0.4			skew	0.4	
c	0.132557			c	0.132557	
u	-0.065419			u	-0.06542	
$\Phi_X(x^*)$	0.5			$\Phi_X(x^*)$	0.5	
$\Phi_U^{-1}(\Phi_X(x^*))$	-1.18E-06			$\Phi_U^{-1}(\Phi_X(x^*))$	-1.1E-06	
$\varphi_U[\Phi_U^{-1}(\Phi_X(x^*))]$	0.398942			$\varphi_U[\Phi_U^{-1}(\Phi_X(x^*))]$	0.398942	
$\varphi_X(x^*)$	11.22752			$\varphi_X(x^*)$	1.866071	
$\boldsymbol{\sigma_X^e}$	0.035533			$\boldsymbol{\sigma_X^e}$	0.213787	
$\boldsymbol{\mu_X^e}$	0.18			$\boldsymbol{\mu_X^e}$	1.07	

Stellenbosch University http://scholar.sun.ac.za

Wind load distribution

	Gumbel Dist	
	Iteration 1	
x_1*	38.5	m/s
μ	14.289	m/s
COV	0.37	
σ	5.28693	m/s
c	0.242589	
x_{mod}	11.91049	
$\Phi_X(x^*)$	0.998421	
$\Phi_U^{-1}(\Phi_X(x^*))$	2.951969	
$\varphi_U[\Phi_U^{-1}(\Phi_X(x^*))]$	0.005113	
$\varphi_X(x^*)$	0.000383	
σ_X^e	13.36028	
μ_X^e	-0.93912	
	Iteration 2	
x_2*	38.5	m/s
μ	14.289	m/s
COV	0.37	
σ	5.28693	m/s
c	0.242589	
x_{mod}	11.91049	
$\Phi_X(x^*)$	0.998421	
$\Phi_U^{-1}(\Phi_X(x^*))$	2.951969	
$\varphi_U[\Phi_U^{-1}(\Phi_X(x^*))]$	0.005113	
$\varphi_X(x^*)$	0.000383	
σ_X^e	13.36028	
μ_X^e	-0.93912	

	Iteration 3	
x_3*	38.5	m/s
μ	14.289	m/s
COV	0.37	
σ	5.28693	m/s
c	0.242589	
x_{mod}	11.91049	
$\Phi_X(x^*)$	0.998421	
$\Phi_U^{-1}(\Phi_X(x^*))$	2.951969	
$\varphi_U[\Phi_U^{-1}(\Phi_X(x^*))]$	0.005113	
$\varphi_X(x^*)$	0.000383	
σ_X^e	13.36028	
μ_X^e	-0.93912	
	Iteration 4	
x_4*	38.5	m/s
μ	14.289	m/s
COV	0.37	
σ	5.28693	m/s
c	0.242589	
x_{mod}	11.91049	
$\Phi_X(x^*)$	0.998421	
$\Phi_U^{-1}(\Phi_X(x^*))$	2.951969	
$\varphi_U[\Phi_U^{-1}(\Phi_X(x^*))]$	0.005113	
$\varphi_X(x^*)$	0.000383	
σ_X^e	13.36028	
μ_X^e	-0.93912	

Stellenbosch University http://scholar.sun.ac.za

FORM – Shear about strong axis

				Iteration 1: strong axis shear						
$g(x_2^*)$	**0.002**									
$g(x_2^*)$wind	-0.0558									
$g(x_2^*)$DL	0									
$g(x_2^*)$LLR	0.001									
$g(x_2^*)$LLF	-0.014									
D	-0.41544		u_1^*	2.151781		x^*_1	29	$v_{b,0}$	dg/dx	-0.03986
	-0.004			0			0.2	DL		-0.2
	-0.00361			1.803556			0.25	LLR		-0.08
	-0.05775			1.788179			1.5	LLF		-0.21333
D^T	-0.41544	-0.004	-0.00361	-0.05775						
						σ_x^e	10.42205		u_x^e	6.574024
			β	**2.392794**			0.02			0.20000
							0.045082			0.16869
	α_1	-0.9904					0.270693			1.01595
		-0.00954								
		-0.0086								
		-0.13767								
	u_2^*	-2.36981								
		-0.02282								
		-0.02057								
		-0.32941								
	x_2^*	31.27233	WL							
		0.200456	DL							
		0.16962	LLR							
		1.105121	LLF							

Stellenbosch University http://scholar.sun.ac.za

				Iteration 2: strong axis shear						
$g(x_2^*)$	**0.000**									
$g(x_2^*)$wind	-0.068									
$g(x_2^*)$DL	-0.002									
$g(x_2^*)$LLR	-0.001									
$g(x_2^*)$LLF	-0.013									
D	-0.48583		u_2^*	2.362072		x^*_2	31.27	$v_{b,0}$	dg/dx	-0.04349
	-0.00399			0.022817			0.200456	DL		-0.19954
	-0.00406			-0.22929			0.16962	LLR		-0.11791
	-0.05142			0.167878			1.105121	LLF		-0.23527
$\mathbf{D}^T$	-0.48583	-0.00399	-0.00406	-0.05142						
						σ_x^e	11.17058		u_x^e	4.88427
			β	**2.364739**			0.02			0.20000
							0.034473			0.17752
	α_2	-0.99438					0.218577			1.06843
		-0.00817								
		-0.00832								
		-0.10525								
	u_3^*	-2.35144								
		-0.01932								
		-0.01967								
		-0.24889								
	x_3^*	31.15126	WL							
		0.200386	DL							
		0.178202	LLR							
		1.12283	LLF							

Stellenbosch University http://scholar.sun.ac.za

				Iteration 3: strong axis shear						
$g(x_3^*)$	**0**									
$g(x_3^*)$wind	-0.066									
$g(x_3^*)$DL	-0.001									
$g(x_3^*)$LLR	0									
$g(x_3^*)$LLF	-0.012									
D	-0.47171		u_3^*	2.351424		x^*_3	31.15126	$v_{b,0}$	dg/dx	-0.04237
	-0.002			0.019316			0.200386	DL		-0.09981
	0			0.015671			0.178202	LLR		0
	-0.04722			0.248464			1.12283	LLF		-0.21375
$\mathbf{D}^T$	-0.47171	-0.002	0	-0.04722						
						σ_x^e	11.13218		u_x^e	4.97477
			β	**2.36454**			0.02			0.20000
							0.035606			0.17764
	α_3	-0.99502					0.220914			1.06794
		-0.00421								
		0								
		-0.0996								
	u_4^*	-2.35276								
		-0.00996								
		0								
		-0.23552								
	x_4^*	31.16613	WL							
		0.200199	DL							
		0.177644	LLR							
		1.119969	LLF							

Stellenbosch University http://scholar.sun.ac.za

				Iteration 4: strong axis shear						
$g(x_4^*)$	**0**									
$g(x_4^*)$wind	-0.066									
$g(x_4^*)$DL	-0.001									
$g(x_4^*)$LLR	0									
$g(x_4^*)$LLF	-0.012									
D	-0.47169		u_4^*	2.35276		x^*_4	31.16613	$v_{b,0}$	dg/dx	-0.04235
	-0.002			0.009956			0.200199	DL		-0.0999
	0			-1.6E-05			0.177644	LLR		0
	-0.04726			0.235505			1.119969	LLF		-0.21429
$\mathbf{D}^T$	-0.47169	-0.002	0	-0.04726						
						σ_x^e	11.137		u_x^e	4.963448
			β	**2.364538**			0.02			0.20000
							0.035532			0.17764
	α_4	-0.99501					0.220537			1.06803
		-0.00421								
		0								
		-0.09969								
	u_5^*	-2.35274								
		-0.00997								
		0								
		-0.23572								
	x_5^*	31.16589	WL							
		0.200199	DL							
		0.177645	LLR							
		1.120017	LLF							

Stellenbosch University http://scholar.sun.ac.za

Live load distribution

	Gamma Dist - applied as Log Normal with lower skewness					
			Iteration 1			
	Roof				**Floor**	
x_1*	0.25	kPa		x_1*	1.5	kPa
μ	0.18	kPa		u	1.083	kPa
COV	0.2			COV	0.2	
σ	0.036	kPa		σ	0.2166	kPa
skew	0.4		E17	skew	0.4	
c	0.132557		F17	c	0.132557	
u	1.944444		I17	u	1.925208	
$\Phi_X(x^*)$	0.964349		L17	$\Phi_X(x^*)$	0.963126	
$\Phi_U^{-1}(\Phi_X(x^*))$	1.803556		J17	$\Phi_U^{-1}(\Phi_X(x^*))$	1.788179	
$\varphi_U[\Phi_U^{-1}(\Phi_X(x^*))]$	0.078446			$\varphi_U[\Phi_U^{-1}(\Phi_X(x^*))]$	0.080642	
$\varphi_X(x^*)$	1.740075		K17	$\varphi_X(x^*)$	0.297911	
σ_X^e	0.045082			σ_X^e	0.270693	
μ_X^e	0.17			μ_X^e	1.02	
			Iteration 2			
	Roof				**Floor**	
x_2*	0.16962	kPa		x_2*	1.105121	kPa
μ	0.18	kPa		u	1.083	kPa
COV	0.2			COV	0.2	
σ	0.036	kPa		σ	0.2166	kPa
skew	0.4		E17	skew	0.4	
c	0.132557		F17	c	0.132557	
u	-0.288343		I17	u	0.10213	
$\Phi_X(x^*)$	0.409321		L17	$\Phi_X(x^*)$	0.56666	
$\Phi_U^{-1}(\Phi_X(x^*))$	-0.229293		J17	$\Phi_U^{-1}(\Phi_X(x^*))$	0.167878	
$\varphi_U[\Phi_U^{-1}(\Phi_X(x^*))]$	0.388592			$\varphi_U[\Phi_U^{-1}(\Phi_X(x^*))]$	0.39336	
$\varphi_X(x^*)$	11.27224		K17	$\varphi_X(x^*)$	1.79964	
σ_X^e	0.034473			σ_X^e	0.218577	
μ_X^e	0.18			μ_X^e	1.07	

L

Stellenbosch University http://scholar.sun.ac.za

			Iteration 3				
	Roof					**Floor**	
x_3*	0.178202	kPa			x_3*	1.12283	kPa
μ	0.18	kPa			u	1.083	kPa
COV	0.2				COV	0.2	
σ	0.036	kPa			σ	0.2166	kPa
skew	0.4		E17		skew	0.4	
c	0.132557		F17		c	0.132557	
u	-0.049934		I17		u	0.183886	
$\Phi_X(x^*)$	0.506251		L17		$\Phi_X(x^*)$	0.598112	
$\Phi_U^{-1}(\Phi_X(x^*))$	0.015671		J17		$\Phi_U^{-1}(\Phi_X(x^*))$	0.248464	
$\varphi_U[\Phi_U^{-1}(\Phi_X(x^*))]$	0.398893				$\varphi_U[\Phi_U^{-1}(\Phi_X(x^*))]$	0.386816	
$\varphi_X(x^*)$	11.20295		K17		$\varphi_X(x^*)$	1.750979	
$\boldsymbol{\sigma_X^e}$	0.035606				$\boldsymbol{\sigma_X^e}$	0.220914	
$\boldsymbol{\mu_X^e}$	0.18				$\boldsymbol{\mu_X^e}$	1.07	
			Iteration 4				
	Roof					**Floor**	
x_4*	0.177644	kPa			x_4*	1.119969	kPa
μ	0.18	kPa			u	1.083	kPa
COV	0.2				COV	0.2	
σ	0.036	kPa			σ	0.2166	kPa
skew	0.4		E17		skew	0.4	
c	0.132557		F17		c	0.132557	
u	-0.065434		I17		u	0.170679	
$\Phi_X(x^*)$	0.499994		L17		$\Phi_X(x^*)$	0.593091	
$\Phi_U^{-1}(\Phi_X(x^*))$	-1.62E-05		J17		$\Phi_U^{-1}(\Phi_X(x^*))$	0.235505	
$\varphi_U[\Phi_U^{-1}(\Phi_X(x^*))]$	0.398942				$\varphi_U[\Phi_U^{-1}(\Phi_X(x^*))]$	0.388031	
$\varphi_X(x^*)$	11.22755		K17		$\varphi_X(x^*)$	1.759486	
$\boldsymbol{\sigma_X^e}$	0.035532				$\boldsymbol{\sigma_X^e}$	0.220537	
$\boldsymbol{\mu_X^e}$	0.18				$\boldsymbol{\mu_X^e}$	1.07	

Stellenbosch University http://scholar.sun.ac.za

Wind load distribution

	Gumbel Dist	
	Iteration 1	
x_1*	29	m/s
μ	14.289	m/s
COV	0.37	
σ	5.28693	m/s
c	0.242589	
x_{mod}	11.91049	
$\Phi_X(x^*)$	0.984293	
$\Phi_U^{-1}(\Phi_X(x^*))$	2.151781	
$\varphi_U[\Phi_U^{-1}(\Phi_X(x^*))]$	0.039399	
$\varphi_X(x^*)$	0.00378	
$\boldsymbol{\sigma_X^e}$	10.42205	
$\boldsymbol{\mu_X^e}$	6.574024	
	Iteration 2	
x_1*	31.27	m/s
μ	14.289	m/s
COV	0.37	
σ	5.28693	m/s
c	0.242589	
x_{mod}	11.91049	
$\Phi_X(x^*)$	0.990913	
$\Phi_U^{-1}(\Phi_X(x^*))$	2.362072	
$\varphi_U[\Phi_U^{-1}(\Phi_X(x^*))]$	0.024511	
$\varphi_X(x^*)$	0.002194	
$\boldsymbol{\sigma_X^e}$	11.17058	
$\boldsymbol{\mu_X^e}$	4.88427	

	Iteration 3	
x_3*	31.15126	m/s
μ	14.289	m/s
COV	0.37	
σ	5.28693	m/s
c	0.242589	
x_{mod}	11.91049	
$\Phi_X(x^*)$	0.990649	
$\Phi_U^{-1}(\Phi_X(x^*))$	2.351424	
$\varphi_U[\Phi_U^{-1}(\Phi_X(x^*))]$	0.025134	
$\varphi_X(x^*)$	0.002258	
$\boldsymbol{\sigma_X^e}$	11.13218	
$\boldsymbol{\mu_X^e}$	4.97477	
	Iteration 4	
x_4*	31.16613	m/s
μ	14.289	m/s
COV	0.37	
σ	5.28693	m/s
c	0.242589	
x_{mod}	11.91049	
$\Phi_X(x^*)$	0.990683	
$\Phi_U^{-1}(\Phi_X(x^*))$	2.35276	
$\varphi_U[\Phi_U^{-1}(\Phi_X(x^*))]$	0.025055	
$\varphi_X(x^*)$	0.00225	
$\boldsymbol{\sigma_X^e}$	11.137	
$\boldsymbol{\mu_X^e}$	4.963448	

Stellenbosch University http://scholar.sun.ac.za

FORM – shear about the weak axis

				Iteration 1: weak axis shear						
$g(x_2^*)$	**0**									
$g(x_2^*)$wind	-0.098									
$g(x_2^*)$DL	0									
$g(x_2^*)$LLR	-0.001									
$g(x_2^*)$LLF	-0.001									
D	-0.67192		u_1^*	3.134352		x^*_1	41	$v_{b,0}$	dg/dx	-0.0478
	0			0			0.2	DL		0
	-0.00361			1.803556			0.25	LLR		-0.08
	-0.00361			1.788179			1.5	LLF		-0.01333
$\mathbf{D}^T$	-0.67192	0	-0.00361	-0.00361						
						σ_x^e	14.05554		u_x^e	-3.05502
			β	**3.153547**			0.02			0.20000
							0.045082			0.16869
	α_1	-0.99997					0.270693			1.01595
		0								
		-0.00537								
		-0.00537								
	u_2^*	-3.15346								
		0								
		-0.01693								
		-0.01694								
	x_2^*	41.26852	WL							
		0.2	DL							
		0.169455	LLR							
		1.020537	LLF							

Stellenbosch University http://scholar.sun.ac.za

				Iteration 2: weak axis shear						
$g(x_2^*)$	**0.000**									
$g(x_2^*)$wind	-0.099									
$g(x_2^*)$DL	0.000									
$g(x_2^*)$LLR	-0.001									
$g(x_2^*)$LLF	-0.001									
D	-0.67786		u_2^*	3.153441		x^*_2	41.269	$v_{b,0}$	dg/dx	-0.04798
	0			0			0.2	DL		0
	-0.00407			-0.23406			0.169455	LLR		-0.11803
	-0.00406			-0.22933			1.020537	LLF		-0.0196
D^T	-0.67786	0	-0.00407	-0.00406						
						σ_x^e	14.12867		u_x^e	-3.28491
			β	**3.150549**			0.02			0.20000
							0.034452			0.17752
	α_2	-0.99996					0.207414			1.06810
		0								
		-0.006								
		-0.006								
	u_3^*	-3.15044								
		0								
		-0.0189								
		-0.01889								
	x_3^*	41.22653	WL							
		0.2	DL							
		0.17817	LLR							
		1.072022	LLF							

Stellenbosch University http://scholar.sun.ac.za

				Iteration 3: weak axis shear						
$g(x_3^*)$	**0**									
$g(x_3^*)$wind	-0.099									
$g(x_3^*)$DL	0									
$g(x_3^*)$LLR	-0.001									
$g(x_3^*)$LLF	-0.001									
D	-0.67801		u_3^*	3.150434		x^*_3	41.22653	$v_{b,0}$	dg/dx	-0.04803
	0			0			0.2	DL		0
	-0.004			0.014767			0.17817	LLR		-0.11225
	-0.004			0.014912			1.072022	LLF		-0.01866
$\mathbf{D}^T$	-0.67801	0	-0.004	-0.004						
						σ_x^e	14.11714		u_x^e	-3.24859
			β	**3.1505**			0.02			0.20000
							0.035602			0.17764
	α_3	-0.99997					0.214209			1.06883
		0								
		-0.00589								
		-0.00589								
	u_4^*	-3.15039								
		0								
		-0.01857								
		-0.01857								
	x_4^*	41.22591	WL							
		0.2	DL							
		0.178306	LLR							
		1.072805	LLF							

Stellenbosch University http://scholar.sun.ac.za

				Iteration 4: weak axis shear						
$g(x_4^*)$	**0**									
$g(x_4^*)$wind	-0.099									
$g(x_4^*)$DL	0									
$g(x_4^*)$LLR	-0.001									
$g(x_4^*)$LLF	-0.001									
D	-0.67801		u_4^*	3.15039		x^*_4	41.22591	$v_{b,0}$	dg/dx	-0.04803
	0			0			0.2	DL		0
	-0.004			0.018568			0.178306	LLR		-0.11217
	-0.004			0.018568			1.072805	LLF		-0.01864
$\mathbf{D}^T$	-0.67801	0	-0.004	-0.004						
						σ_x^e	14.11697		u_x^e	-3.24806
			β	**3.1505**			0.02			0.20000
							0.03562			0.17764
	α_4	-0.99997					0.214312			1.06883
		0								
		-0.00589								
		-0.00589								
	u_5^*	-3.15039								
		0								
		-0.01856								
		-0.01856								
	x_5^*	41.22591	WL							
		0.2	DL							
		0.178305	LLR							
		1.072804	LLF							

Stellenbosch University http://scholar.sun.ac.za

Live load distribution

	Gamma Dist - applied as Log Normal with lower skewness						
			Iteration 1				
	Roof					**Floor**	
x_1*	0.25	kPa			x_1*	1.5	kPa
μ	0.18	kPa			u	1.083	kPa
COV	0.2				COV	0.2	
σ	0.036	kPa			σ	0.2166	kPa
skew	0.4		E17		skew	0.4	
c	0.132557		F17		c	0.132557	
u	1.944444		I17		u	1.925208	
$\Phi_X(x^*)$	0.964349		L17		$\Phi_X(x^*)$	0.963126	
$\Phi_U^{-1}(\Phi_X(x^*))$	1.803556		J17		$\Phi_U^{-1}(\Phi_X(x^*))$	1.788179	
$\varphi_U[\Phi_U^{-1}(\Phi_X(x^*))]$	0.078446				$\varphi_U[\Phi_U^{-1}(\Phi_X(x^*))]$	0.080642	
$\varphi_X(x^*)$	1.740075		K17		$\varphi_X(x^*)$	0.297911	
σ_X^e	0.045082				σ_X^e	0.270693	
μ_X^e	0.17				μ_X^e	1.02	
			Iteration 2				
	Roof					**Floor**	
x_2*	0.169455	kPa			x_2*	1.020537	kPa
μ	0.18	kPa			u	1.083	kPa
COV	0.2				COV	0.2	
σ	0.036	kPa			σ	0.2166	kPa
skew	0.4		E17		skew	0.4	
c	0.132557		F17		c	0.132557	
u	-0.292909		I17		u	-0.28838	
$\Phi_X(x^*)$	0.407468		L17		$\Phi_X(x^*)$	0.409307	
$\Phi_U^{-1}(\Phi_X(x^*))$	-0.234063		J17		$\Phi_U^{-1}(\Phi_X(x^*))$	-0.22933	
$\varphi_U[\Phi_U^{-1}(\Phi_X(x^*))]$	0.388162				$\varphi_U[\Phi_U^{-1}(\Phi_X(x^*))]$	0.388588	
$\varphi_X(x^*)$	11.26688		K17		$\varphi_X(x^*)$	1.873495	
σ_X^e	0.034452				σ_X^e	0.207414	
μ_X^e	0.18				μ_X^e	1.07	

Stellenbosch University http://scholar.sun.ac.za

			Iteration 3				
	Roof					**Floor**	
x_3*	0.17817	kPa			x_3*	1.072022	kPa
μ	0.18	kPa			u	1.083	kPa
COV	0.2				COV	0.2	
σ	0.036	kPa			σ	0.2166	kPa
skew	0.4		E17		skew	0.4	
c	0.132557		F17		c	0.132557	
u	-0.050828		I17		u	-0.05068	
$\Phi_X(x^*)$	0.505891		L17		$\Phi_X(x^*)$	0.505949	
$\Phi_U^{-1}(\Phi_X(x^*))$	0.014767		J17		$\Phi_U^{-1}(\Phi_X(x^*))$	0.014912	
$\varphi_U[\Phi_U^{-1}(\Phi_X(x^*))]$	0.398899				$\varphi_U[\Phi_U^{-1}(\Phi_X(x^*))]$	0.398898	
$\varphi_X(x^*)$	11.20444		K17		$\varphi_X(x^*)$	1.862194	
$\boldsymbol{\sigma_X^e}$	0.035602				$\boldsymbol{\sigma_X^e}$	0.214209	
$\boldsymbol{\mu_X^e}$	0.18				$\boldsymbol{\mu_X^e}$	1.07	
			Iteration 4				
	Roof					**Floor**	
x_4*	0.178306	kPa			x_4*	1.072805	kPa
μ	0.18	kPa			u	1.083	kPa
COV	0.2				COV	0.2	
σ	0.036	kPa			σ	0.2166	kPa
skew	0.4		E17		skew	0.4	
c	0.132557		F17		c	0.132557	
u	-0.047068		I17		u	-0.04707	
$\Phi_X(x^*)$	0.507407		L17		$\Phi_X(x^*)$	0.507407	
$\Phi_U^{-1}(\Phi_X(x^*))$	0.018568		J17		$\Phi_U^{-1}(\Phi_X(x^*))$	0.018568	
$\varphi_U[\Phi_U^{-1}(\Phi_X(x^*))]$	0.398874				$\varphi_U[\Phi_U^{-1}(\Phi_X(x^*))]$	0.398874	
$\varphi_X(x^*)$	11.19811		K17		$\varphi_X(x^*)$	1.861182	
$\boldsymbol{\sigma_X^e}$	0.03562				$\boldsymbol{\sigma_X^e}$	0.214312	
$\boldsymbol{\mu_X^e}$	0.18				$\boldsymbol{\mu_X^e}$	1.07	

Stellenbosch University http://scholar.sun.ac.za

Wind load distribution

	Gumbel Dist	
	Iteration 1	
x_1*	41	m/s
μ	14.289	m/s
COV	0.37	
σ	5.28693	m/s
c	0.242589	
x_{mod}	11.91049	
$\Phi_X(x^*)$	0.999139	
$\Phi_U^{-1}(\Phi_X(x^*))$	3.134352	
$\varphi_U[\Phi_U^{-1}(\Phi_X(x^*))]$	0.002935	
$\varphi_X(x^*)$	0.000209	
σ_X^e	14.05554	
μ_X^e	-3.05502	
	Iteration 2	
x_1*	41.269	m/s
μ	14.289	m/s
COV	0.37	
σ	5.28693	m/s
c	0.242589	
x_{mod}	11.91049	
$\Phi_X(x^*)$	0.999193	
$\Phi_U^{-1}(\Phi_X(x^*))$	3.153441	
$\varphi_U[\Phi_U^{-1}(\Phi_X(x^*))]$	0.002764	
$\varphi_X(x^*)$	0.000196	
σ_X^e	14.12867	
μ_X^e	-3.28491	

	Iteration 3	
x_3*	41.22653	m/s
μ	14.289	m/s
COV	0.37	
σ	5.28693	m/s
c	0.242589	
x_{mod}	11.91049	
$\Phi_X(x^*)$	0.999185	
$\Phi_U^{-1}(\Phi_X(x^*))$	3.150434	
$\varphi_U[\Phi_U^{-1}(\Phi_X(x^*))]$	0.00279	
$\varphi_X(x^*)$	0.000198	
σ_X^e	14.11714	
μ_X^e	-3.24859	
	Iteration 4	
x_4*	41.22591	m/s
μ	14.289	m/s
COV	0.37	
σ	5.28693	m/s
c	0.242589	
x_{mod}	11.91049	
$\Phi_X(x^*)$	0.999185	
$\Phi_U^{-1}(\Phi_X(x^*))$	3.15039	
$\varphi_U[\Phi_U^{-1}(\Phi_X(x^*))]$	0.002791	
$\varphi_X(x^*)$	0.000198	
σ_X^e	14.11697	
μ_X^e	-3.24806	

Stellenbosch University http://scholar.sun.ac.za

FORM – Tension

				Iteration 1: Tension						
$g(x_2^*)$	**0**									
$g(x_2^*)$wind	-0.104									
$g(x_2^*)$DL	0									
$g(x_2^*)$LLR	0.001									
$g(x_2^*)$LLF	0.001									
D	-0.74784		u_1^*	2.132528		x^*_1	28.8	$v_{b,0}$	dg/dx	-0.07222
	0			0			0.2	DL		0
	0.003607			1.803556			0.25	LLR		0.08
	0.003609			1.788179			1.5	LLF		0.013333
D^T	-0.74784	0	0.003607	0.003609						
						σ_x^e	10.35464		u_x^e	6.71843
			β	**2.115151**			0.02			0.20000
							0.045082			0.16869
	α_1	-0.99998					0.270693			1.01595
		0								
		0.004823								
		0.004826								
	u_2^*	-2.1151								
		0								
		0.0102								
		0.010208								
	x_2^*	28.61955	WL							
		0.2	DL							
		0.168232	LLR							
		1.013189	LLF							

Stellenbosch University http://scholar.sun.ac.za

				Iteration 2: Tension						
$g(x_2^*)$	**0.000**									
$g(x_2^*)$wind	-0.104									
$g(x_2^*)$DL	0.000									
$g(x_2^*)$LLR	0.000									
$g(x_2^*)$LLF	0.000									
D	-0.74779		u_2^*	2.135424		x^*_2	28.83	$v_{b,0}$	dg/dx	-0.07215
	0			0			0.2	DL		0
	0			-0.26964			0.168232	LLR		0
	0			-0.26484			1.013189	LLF		0
D^T	-0.74779	0	0	0						
						σ_x^e	10.36477		u_x^e	6.69682
			β	**2.135424**			0.02			0.20000
							0.03429			0.17748
	α_2	-1					0.206444			1.06786
		0								
		0								
		0								
	u_3^*	-2.13542								
		0								
		0								
		0								
	x_3^*	28.83	WL							
		0.2	DL							
		0.177478	LLR							
		1.067864	LLF							

Stellenbosch University http://scholar.sun.ac.za

				Iteration 3: Tension					
$g(x_3^*)$	**0**								
$g(x_3^*)$wind	-0.104								
$g(x_3^*)$DL	0								
$g(x_3^*)$LLR	0								
$g(x_3^*)$LLF	0								
D	-0.74784		u_3^*	2.132528		x^*_3	28.8	$v_{b,0}$	dg/dx	-0.07222
	0			0			0.2	DL		0
	0			-0.00469			0.177478	LLR		0
	0			-0.00452			1.067864	LLF		0
$\mathbf{D}^T$	-0.74784	0	0	0						
						σ_x^e	10.35464		u_x^e	6.71843
			β	**2.132528**			0.02			0.20000
							0.035511			0.17764
	α_3	-1					0.21366			1.06883
		0								
		0								
		0								
	u_4^*	-2.13253								
		0								
		0								
		0								
	x_4^*	28.8	WL							
		0.2	DL							
		0.177645	LLR							
		1.06883	LLF							

Stellenbosch University http://scholar.sun.ac.za

				Iteration 4: Tension						
$g(x_4^*)$	**0**									
$g(x_4^*)$wind	-0.104									
$g(x_4^*)$DL	0									
$g(x_4^*)$LLR	0									
$g(x_4^*)$LLF	0									
D	-0.74784		u_4^*	2.132528		x^*_4	28.8	$v_{b,0}$	dg/dx	-0.07222
	0			0			0.2	DL		0
	0			-1.4E-06			0.177645	LLR		0
	0			-1.3E-06			1.06883	LLF		0
$\mathbf{D}^T$	-0.74784	0	0	0						
						σ_x^e	10.35464		u_x^e	6.71843
			β	**2.132528**			0.02			0.20000
							0.035533			0.17764
	α_4	-1					0.213787			1.06883
		0								
		0								
		0								
	u_5^*	-2.13253								
		0								
		0								
		0								
	x_5^*	28.8	WL							
		0.2	DL							
		0.177645	LLR							
		1.068831	LLF							

Stellenbosch University http://scholar.sun.ac.za

Live load distribution

	Gamma Dist - applied as Log Normal with lower skewness						
			Iteration 1				
	Roof					**Floor**	
x_1*	0.25	kPa			x_1*	1.5	kPa
μ	0.18	kPa			u	1.083	kPa
COV	0.2				COV	0.2	
σ	0.036	kPa			σ	0.2166	kPa
skew	0.4		E17		skew	0.4	
c	0.132557		F17		c	0.132557	
u	1.944444		I17		u	1.925208	
$\Phi_X(x^*)$	0.964349		L17		$\Phi_X(x^*)$	0.963126	
$\Phi_U^{-1}(\Phi_X(x^*))$	1.803556		J17		$\Phi_U^{-1}(\Phi_X(x^*))$	1.788179	
$\varphi_U[\Phi_U^{-1}(\Phi_X(x^*))]$	0.078446				$\varphi_U[\Phi_U^{-1}(\Phi_X(x^*))]$	0.080642	
$\varphi_X(x^*)$	1.740075		K17		$\varphi_X(x^*)$	0.297911	
σ_X^e	0.045082				σ_X^e	0.270693	
μ_X^e	0.17				μ_X^e	1.02	
			Iteration 2				
	Roof					**Floor**	
x_2*	0.168232	kPa			x_2*	1.013189	kPa
μ	0.18	kPa			u	1.083	kPa
COV	0.2				COV	0.2	
σ	0.036	kPa			σ	0.2166	kPa
skew	0.4		E17		skew	0.4	
c	0.132557		F17		c	0.132557	
u	-0.32688		I17		u	-0.3223	
$\Phi_X(x^*)$	0.393717		L17		$\Phi_X(x^*)$	0.395566	
$\Phi_U^{-1}(\Phi_X(x^*))$	-0.269643		J17		$\Phi_U^{-1}(\Phi_X(x^*))$	-0.26484	
$\varphi_U[\Phi_U^{-1}(\Phi_X(x^*))]$	0.3847				$\varphi_U[\Phi_U^{-1}(\Phi_X(x^*))]$	0.385194	
$\varphi_X(x^*)$	11.21892		K17		$\varphi_X(x^*)$	1.865853	
σ_X^e	0.03429				σ_X^e	0.206444	
μ_X^e	0.18				μ_X^e	1.07	

Stellenbosch University http://scholar.sun.ac.za

			Iteration 3				
	Roof					**Floor**	
x_3*	0.177478	kPa			x_3*	1.067864	kPa
μ	0.18	kPa			u	1.083	kPa
COV	0.2				COV	0.2	
σ	0.036	kPa			σ	0.2166	kPa
skew	0.4		E17		skew	0.4	
c	0.132557		F17		c	0.132557	
u	-0.070042		I17		u	-0.06988	
$\Phi_X(x^*)$	0.49813		L17		$\Phi_X(x^*)$	0.498195	
$\Phi_U^{-1}(\Phi_X(x^*))$	-0.004687		J17		$\Phi_U^{-1}(\Phi_X(x^*))$	-0.00452	
$\varphi_U[\Phi_U^{-1}(\Phi_X(x^*))]$	0.398938				$\varphi_U[\Phi_U^{-1}(\Phi_X(x^*))]$	0.398938	
$\varphi_X(x^*)$	11.23435		K17		$\varphi_X(x^*)$	1.867166	
$\boldsymbol{\sigma_X^e}$	0.035511				$\boldsymbol{\sigma_X^e}$	0.21366	
$\boldsymbol{\mu_X^e}$	0.18				$\boldsymbol{\mu_X^e}$	1.07	
			Iteration 4				
	Roof					**Floor**	
x_4*	0.177645	kPa			x_4*	1.06883	kPa
μ	0.18	kPa			u	1.083	kPa
COV	0.2				COV	0.2	
σ	0.036	kPa			σ	0.2166	kPa
skew	0.4		E17		skew	0.4	
c	0.132557		F17		c	0.132557	
u	-0.065419		I17		u	-0.06542	
$\Phi_X(x^*)$	0.499999		L17		$\Phi_X(x^*)$	0.499999	
$\Phi_U^{-1}(\Phi_X(x^*))$	-1.45E-06		J17		$\Phi_U^{-1}(\Phi_X(x^*))$	-1.3E-06	
$\varphi_U[\Phi_U^{-1}(\Phi_X(x^*))]$	0.398942				$\varphi_U[\Phi_U^{-1}(\Phi_X(x^*))]$	0.398942	
$\varphi_X(x^*)$	11.22753		K17		$\varphi_X(x^*)$	1.866071	
$\boldsymbol{\sigma_X^e}$	0.035533				$\boldsymbol{\sigma_X^e}$	0.213787	
$\boldsymbol{\mu_X^e}$	0.18				$\boldsymbol{\mu_X^e}$	1.07	

Stellenbosch University http://scholar.sun.ac.za

Wind load distribution

	Gumbel Dist	
	Iteration 1	
x_1*	28.8	m/s
μ	14.289	m/s
COV	0.37	
σ	5.28693	m/s
c	0.242589	
x_{mod}	11.91049	
$\Phi_X(x^*)$	0.983518	
$\Phi_U^{-1}(\Phi_X(x^*))$	2.132528	
$\varphi_U[\Phi_U^{-1}(\Phi_X(x^*))]$	0.041058	
$\varphi_X(x^*)$	0.003965	
σ_X^e	10.35464	
μ_X^e	6.71843	
	Iteration 2	
x_1*	28.83	m/s
μ	14.289	m/s
COV	0.37	
σ	5.28693	m/s
c	0.242589	
x_{mod}	11.91049	
$\Phi_X(x^*)$	0.983637	
$\Phi_U^{-1}(\Phi_X(x^*))$	2.135424	
$\varphi_U[\Phi_U^{-1}(\Phi_X(x^*))]$	0.040805	
$\varphi_X(x^*)$	0.003937	
σ_X^e	10.36477	
μ_X^e	6.69682	

	Iteration 3	
x_3*	28.8	m/s
μ	14.289	m/s
COV	0.37	
σ	5.28693	m/s
c	0.242589	
x_{mod}	11.91049	
$\Phi_X(x^*)$	0.983518	
$\Phi_U^{-1}(\Phi_X(x^*))$	2.132528	
$\varphi_U[\Phi_U^{-1}(\Phi_X(x^*))]$	0.041058	
$\varphi_X(x^*)$	0.003965	
σ_X^e	10.35464	
μ_X^e	6.71843	
	Iteration 4	
x_4*	28.8	m/s
μ	14.289	m/s
COV	0.37	
σ	5.28693	m/s
c	0.242589	
x_{mod}	11.91049	
$\Phi_X(x^*)$	0.983518	
$\Phi_U^{-1}(\Phi_X(x^*))$	2.132528	
$\varphi_U[\Phi_U^{-1}(\Phi_X(x^*))]$	0.041058	
$\varphi_X(x^*)$	0.003965	
σ_X^e	10.35464	
μ_X^e	6.71843	

Stellenbosch University http://scholar.sun.ac.za

FORM – Interaction between axial and bending moments

				Iteration 1: Interaction						
$g(x_2^*)$	**0**									
$g(x_2^*)$wind	-0.1207									
$g(x_2^*)$DL	0									
$g(x_2^*)$LLR	-0.001									
$g(x_2^*)$LLF	-0.001									
D	-0.86927		u_1^*	2.054238		x^*_1	28	$v_{b,0}$	dg/dx	-0.08621
	0			0			0.2	DL		0
	-0.00361			1.803556			0.25	LLR		-0.08
	-0.00361			1.788179			1.5	LLF		-0.01333
$\mathbf{D}^T$	-0.86927	0	-0.00361	-0.00361						
						σ_x^e	10.08264		u_x^e	7.287851
			β	**2.06911**			0.02			0.20000
							0.045082			0.16869
	α_1	-0.99998					0.270693			1.01595
		0								
		-0.00415								
		-0.00415								
	u_2^*	-2.06907								
		0								
		-0.00858								
		-0.00859								
	x_2^*	28.14959	WL							
		0.2	DL							
		0.169079	LLR							
		1.018278	LLF							

Stellenbosch University http://scholar.sun.ac.za

				Iteration 2: Interaction						
$g(x_2^*)$	**0.000**									
$g(x_2^*)$wind	-0.098									
$g(x_2^*)$DL	0.000									
$g(x_2^*)$LLR	0.000									
$g(x_2^*)$LLF	0.000									
D	-0.70594		$\mathbf{u_2^*}$	2.041814		$\mathbf{x^*_2}$	27.875	$v_{b,0}$	dg/dx	-0.07031
	0			0			0.2	DL		0
	0			-0.24499			0.169079	LLR		0
	0			-0.24023			1.018278	LLF		0
$\mathbf{D^T}$	-0.70594	0	0	0						
						$\boldsymbol{\sigma_x^e}$	10.03981		$\mathbf{u_x^e}$	7.375585
			β	**2.041814**			0.02			0.20000
							0.034402			0.17751
	$\boldsymbol{\alpha_2}$	-1					0.207115			1.06803
		0								
		0								
		0								
	$\mathbf{u_3^*}$	-2.04181								
		0								
		0								
		0								
	$\mathbf{x_3^*}$	27.875								
		0.2								
		0.177507								
		1.068033								

				Iteration 3: Interaction						
$g(x_3^*)$	**0**									
$g(x_3^*)$wind	-0.098									
$g(x_3^*)$DL	0									
$g(x_3^*)$LLR	0									
$g(x_3^*)$LLF	0									
D	-0.70594		u_3^*	2.041814		x^*_3	27.875	$v_{b,0}$	dg/dx	-0.07031
	0			0			0.2	DL		0
	0			-0.00388			0.177507	LLR		0
	0			-0.00373			1.068033	LLF		0
D^T	-0.70594	0	0	0						
						σ_x^e	10.03981		u_x^e	7.375585
			β	**2.041814**			0.02			0.20000
							0.035514			0.17764
	α_3	-1					0.213682			1.06883
		0								
		0								
		0								
	u_4^*	-2.04181								
		0								
		0								
		0								
	x_4^*	27.875								
		0.2								
		0.177645								
		1.06883								

Stellenbosch University http://scholar.sun.ac.za

				Iteration 4: Interaction						
$g(x_4^*)$	**0**									
$g(x_4^*)$wind	-0.098									
$g(x_4^*)$DL	0									
$g(x_4^*)$LLR	0									
$g(x_4^*)$LLF	0									
D	-0.70594		u_4^*	2.041814		x^*_4	27.875	$v_{b,0}$	dg/dx	-0.07031
	0			0			0.2	DL		0
	0			-9.9E-07			0.177645	LLR		0
	0			-9.2E-07			1.06883	LLF		0
$\mathbf{D}^T$	-0.70594	0	0	0						
						σ_x^e	10.03981		u_x^e	7.375585
			β	**2.041814**			0.02			0.20000
							0.035533			0.17764
	α_4	-1					0.213787			1.06883
		0								
		0								
		0								
	u_5^*	-2.04181								
		0								
		0								
		0								
	x_5^*	27.875								
		0.2								
		0.177645								
		1.068831								

Stellenbosch University http://scholar.sun.ac.za

Live load distribution

	Gamma Dist - applied as Log Normal with lower skewness						
			Iteration 1				
	Roof					**Floor**	
x_1*	0.25	kPa			x_1*	1.5	kPa
μ	0.18	kPa			u	1.083	kPa
COV	0.2				COV	0.2	
σ	0.036	kPa			σ	0.2166	kPa
skew	0.4		E17		skew	0.4	
c	0.132557		F17		c	0.132557	
u	1.944444		I17		u	1.925208	
$\Phi_X(x^*)$	0.964349		L17		$\Phi_X(x^*)$	0.963126	
$\Phi_U^{-1}(\Phi_X(x^*))$	1.803556		J17		$\Phi_U^{-1}(\Phi_X(x^*))$	1.788179	
$\varphi_U[\Phi_U^{-1}(\Phi_X(x^*))]$	0.078446				$\varphi_U[\Phi_U^{-1}(\Phi_X(x^*))]$	0.080642	
$\varphi_X(x^*)$	1.740075		K17		$\varphi_X(x^*)$	0.297911	
σ_X^e	0.045082				σ_X^e	0.270693	
μ_X^e	0.17				μ_X^e	1.02	
			Iteration 2				
	Roof					**Floor**	
x_2*	0.169079	kPa			x_2*	1.018278	kPa
μ	0.18	kPa			u	1.083	kPa
COV	0.2				COV	0.2	
σ	0.036	kPa			σ	0.2166	kPa
skew	0.4		E17		skew	0.4	
c	0.132557		F17		c	0.132557	
u	-0.303356		I17		u	-0.29881	
$\Phi_X(x^*)$	0.403233		L17		$\Phi_X(x^*)$	0.405075	
$\Phi_U^{-1}(\Phi_X(x^*))$	-0.244987		J17		$\Phi_U^{-1}(\Phi_X(x^*))$	-0.24023	
$\varphi_U[\Phi_U^{-1}(\Phi_X(x^*))]$	0.387148				$\varphi_U[\Phi_U^{-1}(\Phi_X(x^*))]$	0.387595	
$\varphi_X(x^*)$	11.25365		K17		$\varphi_X(x^*)$	1.871397	
σ_X^e	0.034402				σ_X^e	0.207115	
μ_X^e	0.18				μ_X^e	1.07	

Stellenbosch University http://scholar.sun.ac.za

			Iteration 3				
	Roof					**Floor**	
x_3*	0.177507	kPa			x_3*	1.068033	kPa
μ	0.18	kPa			u	1.083	kPa
COV	0.2				COV	0.2	
σ	0.036	kPa			σ	0.2166	kPa
skew	0.4		E17		skew	0.4	
c	0.132557		F17		c	0.132557	
u	-0.069244		I17		u	-0.0691	
$\Phi_X(x^*)$	0.498453		L17		$\Phi_X(x^*)$	0.498512	
$\Phi_U^{-1}(\Phi_X(x^*))$	-0.003877		J17		$\Phi_U^{-1}(\Phi_X(x^*))$	-0.00373	
$\varphi_U[\Phi_U^{-1}(\Phi_X(x^*))]$	0.398939				$\varphi_U[\Phi_U^{-1}(\Phi_X(x^*))]$	0.39894	
$\varphi_X(x^*)$	11.23319		K17		$\varphi_X(x^*)$	1.866976	
$\boldsymbol{\sigma_X^e}$	0.035514				$\boldsymbol{\sigma_X^e}$	0.213682	
$\boldsymbol{\mu_X^e}$	0.18				$\boldsymbol{\mu_X^e}$	1.07	
			Iteration 4				
	Roof					**Floor**	
x_4*	0.177645	kPa			x_4*	1.06883	kPa
μ	0.18	kPa			u	1.083	kPa
COV	0.2				COV	0.2	
σ	0.036	kPa			σ	0.2166	kPa
skew	0.4		E17		skew	0.4	
c	0.132557		F17		c	0.132557	
u	-0.065419		I17		u	-0.06542	
$\Phi_X(x^*)$	0.5		L17		$\Phi_X(x^*)$	0.5	
$\Phi_U^{-1}(\Phi_X(x^*))$	-9.92E-07		J17		$\Phi_U^{-1}(\Phi_X(x^*))$	-9.2E-07	
$\varphi_U[\Phi_U^{-1}(\Phi_X(x^*))]$	0.398942				$\varphi_U[\Phi_U^{-1}(\Phi_X(x^*))]$	0.398942	
$\varphi_X(x^*)$	11.22752		K17		$\varphi_X(x^*)$	1.866071	
$\boldsymbol{\sigma_X^e}$	0.035533				$\boldsymbol{\sigma_X^e}$	0.213787	
$\boldsymbol{\mu_X^e}$	0.18				$\boldsymbol{\mu_X^e}$	1.07	

Stellenbosch University http://scholar.sun.ac.za

Wind load distribution

	Gumbel Dist	
	Iteration 1	
x_1*	28	m/s
μ	14.289	m/s
COV	0.37	
σ	5.28693	m/s
c	0.242589	
x_{mod}	11.91049	
$\Phi_X(x^*)$	0.980024	
$\Phi_U^{-1}(\Phi_X(x^*))$	2.054238	
$\varphi_U[\Phi_U^{-1}(\Phi_X(x^*))]$	0.04837	
$\varphi_X(x^*)$	0.004797	
$\boldsymbol{\sigma_X^e}$	10.08264	
$\boldsymbol{\mu_X^e}$	7.287851	
	Iteration 2	
x_1*	27.875	m/s
μ	14.289	m/s
COV	0.37	
σ	5.28693	m/s
c	0.242589	
x_{mod}	11.91049	
$\Phi_X(x^*)$	0.979415	
$\Phi_U^{-1}(\Phi_X(x^*))$	2.041814	
$\varphi_U[\Phi_U^{-1}(\Phi_X(x^*))]$	0.049616	
$\varphi_X(x^*)$	0.004942	
$\boldsymbol{\sigma_X^e}$	10.03981	
$\boldsymbol{\mu_X^e}$	7.375585	

	Iteration 3	
x_3*	27.875	m/s
μ	14.289	m/s
COV	0.37	
σ	5.28693	m/s
c	0.242589	
x_{mod}	11.91049	
$\Phi_X(x^*)$	0.979415	
$\Phi_U^{-1}(\Phi_X(x^*))$	2.041814	
$\varphi_U[\Phi_U^{-1}(\Phi_X(x^*))]$	0.049616	
$\varphi_X(x^*)$	0.004942	
$\boldsymbol{\sigma_X^e}$	10.03981	
$\boldsymbol{\mu_X^e}$	7.375585	
	Iteration 4	
x_4*	27.875	m/s
μ	14.289	m/s
COV	0.37	
σ	5.28693	m/s
c	0.242589	
x_{mod}	11.91049	
$\Phi_X(x^*)$	0.979415	
$\Phi_U^{-1}(\Phi_X(x^*))$	2.041814	
$\varphi_U[\Phi_U^{-1}(\Phi_X(x^*))]$	0.049616	
$\varphi_X(x^*)$	0.004942	
$\boldsymbol{\sigma_X^e}$	10.03981	
$\boldsymbol{\mu_X^e}$	7.375585	

Stellenbosch University http://scholar.sun.ac.za

Appendix K: Spread sheet calculations for evaluation of β-Case 2

Form – Axial load

				Iteration 1: Axial load						
$g(x_1^*)$	**0**									
$g(x_1^*)f_y$	0.007			1.007						
$g(x_1^*)t$	0.08			1.08						
$g(x_1^*)r_i$	0.001			1.001						
D	0.004339		u_1^*	-1.61793		x^*_1	550	f_y	dg/dx	0.000255
	0.132609			-6.80238			0.6075	t		2.633745
	0.00028			0			2	r_i		0.01
D^T	0.004339	0.132609	0.00028							
						σ_x^e	17.04591		u_x^e	577.579
			β	**6.85164**			0.05035			0.95000
					6.85164		0.028			2.00000
	α_1	0.032702								
		0.999463								
		0.00211								
	u_2^*	0.224065								
		6.84796								
		0.014459								
	x_2^*	573.7597	f_y							
		0.605205	t							
		1.999595	r_i							

Stellenbosch University http://scholar.sun.ac.za

				Iteration 2: Axial load					
$g(x_2^*)$	**0.000**								
$g(x_2^*)f_y$	0.007								
$g(x_2^*)t$	0.080								
$g(x_2^*)r_i$	0.003								
D	0.004339		u_2^*	-0.25333		x^*_2	573.7597	f_y	dg/dx	0.000244
	0.133112			-6.84796			0.605205	t		2.643731
	0.00084			-0.01446			1.999595	r_i		0.030006
D^T	0.004339	0.133112	0.00084							
						σ_x^e	17.78228		u_x^e	578.2645
			β	**6.852533**			0.05035			0.95000
							0.028			2.00000
	α_2	0.032578								
		0.999449								
		0.006308								
	u_3^*	0.223244								
		6.848759								
		0.043228								
	x_3^*	574.2947								
		0.605165								
		1.99879								

Stellenbosch University http://scholar.sun.ac.za

				Iteration 3: Axial load						
$g(\mathbf{x_3}^*)$	**0**									
$g(\mathbf{x_3}^*)f_y$	0.006									
$g(\mathbf{x_3}^*)t$	0.08									
$g(\mathbf{x_3}^*)r_i$	0.002									
D	0.003719		$\mathbf{u_3}^*$	-0.22326		$\mathbf{x}^*_3$	574.2947	f_y	dg/dx	0.000209
	0.133121			-6.84876			0.605165	t		2.643907
	0.00056			-0.04323			1.99879	r_i		0.020012
$\mathbf{D}^T$	0.003719	0.133121	0.00056							
						$\boldsymbol{\sigma}_x^e$	17.79886		$\mathbf{u}_x^e$	578.2684
			β	**6.852444**			0.05035			0.95000
							0.028			2.00000
	$\boldsymbol{\alpha}_3$	0.027927								
		0.999601								
		0.004208								
	$\mathbf{u_4}^*$	0.191366								
		6.849711								
		0.028832								
	$\mathbf{x_4}^*$	574.8623								
		0.605117								
		1.999193								

Stellenbosch University http://scholar.sun.ac.za

				Iteration 4: Axial load						
$g(x_4^*)$	**0**									
$g(x_4^*)f_y$	0.006									
$g(x_4^*)t$	0.08									
$g(x_4^*)r_i$	0.003									
D	0.003719		u_4^*	-0.19138		x^*_4	574.8623	f_y	dg/dx	0.000209
	0.133131			-6.84971			0.605117	t		2.644116
	0.00084			-0.02883			1.999193	r_i		0.030012
D^T	0.003719	0.133131	0.00084							
						σ_x^e	17.81645		u_x^e	578.2721
			β	**6.852429**			0.05035			0.95000
							0.028			2.00000
	α_4	0.027924								
		0.99959								
		0.00631								
	u_5^*	0.191349								
		6.849621								
		0.043236								
	x_5^*	574.8629								
		0.605122								
		1.998789								

Stellenbosch University http://scholar.sun.ac.za

Yield stress distribution

Log - Normal distribution	
	Iteration 1
x_1^*	550
μ	578.56
COV	0.031
σ	17.93536
skew	0.09303
c	0.031
u	-1.59239
$\Phi_X(x^*)$	0.052839
$\Phi_U^{-1}(\Phi_X(x^*))$	-1.61793
$\varphi_U[\Phi_U^{-1}(\Phi_X(x^*))]$	0.107767
$\varphi_X(x^*)$	0.006322
σ_X^e	17.04591
μ_X^e	577.579
	Iteration 2
x_2^*	573.7597
μ	578.56
COV	0.031
σ	17.93536
skew	0.09303
c	0.031
u	-0.26765
$\Phi_X(x^*)$	0.400006
$\Phi_U^{-1}(\Phi_X(x^*))$	-0.25333
$\varphi_U[\Phi_U^{-1}(\Phi_X(x^*))]$	0.386344
$\varphi_X(x^*)$	0.021726
σ_X^e	17.78228
μ_X^e	578.2645

	Iteration 3
x_3^*	574.2747
μ	578.56
COV	0.031
σ	17.93536
skew	0.09303
c	0.031
u	-0.23893
$\Phi_X(x^*)$	0.411232
$\Phi_U^{-1}(\Phi_X(x^*))$	-0.22438
$\varphi_U[\Phi_U^{-1}(\Phi_X(x^*))]$	0.389025
$\varphi_X(x^*)$	0.021858
σ_X^e	17.79824
μ_X^e	578.2683
	Iteration 4
x_4^*	574.8623
μ	578.56
COV	0.031
σ	17.93536
skew	0.09303
c	0.031
u	-0.20617
$\Phi_X(x^*)$	0.424113
$\Phi_U^{-1}(\Phi_X(x^*))$	-0.19138
$\varphi_U[\Phi_U^{-1}(\Phi_X(x^*))]$	0.391703
$\varphi_X(x^*)$	0.021985
σ_X^e	17.81645
μ_X^e	578.2721

Stellenbosch University http://scholar.sun.ac.za

FORM – shear about the strong axis

				Iteration 1: Shear about strong axis						
$g(\mathbf{x_1}^*)$	**0**									
$g(\mathbf{x_1}^*)f_y$	0									
$g(\mathbf{x_1}^*)t$	0.164									
$g(\mathbf{x_1}^*)r_i$	0									
D	0		$\mathbf{u_1}^*$	-1.61793		$\mathbf{x}^*_1$	550	f_y	dg/dx	0
	0.176158			-0.24826			0.9375	t		3.498667
	0			0			2	r_i		0
$\mathbf{D}^T$	0	0.176158	0							
						σ_x^e	17.04591		u_x^e	577.579
			β	**0.248262**			0.05035			0.95000
							0.028			2.00000
	α_1	0								
		1								
		0								
	$\mathbf{u_2}^*$	0								
		0.248262								
		0								
	$\mathbf{x_2}^*$	577.579	f_y							
		0.9375	t							
		2	r_i							

Stellenbosch University http://scholar.sun.ac.za

				Iteration 2: Shear about strong axis						
$g(\mathbf{x_2}^*)$	**0.000**									
$g(\mathbf{x_2}^*)f_y$	0.000									
$g(\mathbf{x_2}^*)t$	0.164									
$g(\mathbf{x_2}^*)r_i$	0.000									
D	0		$\mathbf{u_2}^*$	-0.03926		$\mathbf{x}^*_2$	577.579		dg/dx	0
	0.176158			-0.24826			0.9375			3.498667
	0			0			2			0
$\mathbf{D}^T$	0	0.176158	0							
						σ_x^e	17.90065		u_x^e	578.2818
			β	**0.248262**			0.05035			0.95000
							0.028			2.00000
	α_2	0								
		1								
		0								
	$\mathbf{u_3}^*$	0								
		0.248262								
		0								
	$\mathbf{x_3}^*$	578.2818								
		0.9375								
		2								

Stellenbosch University http://scholar.sun.ac.za

				Iteration 3: Shear about strong axis						
$g(\mathbf{x_3}^*)$	**0**									
$g(\mathbf{x_3}^*)f_y$	0									
$g(\mathbf{x_3}^*)t$	0.164									
$g(\mathbf{x_3}^*)r_i$	0									
D	0		$\mathbf{u_3}^*$	-2.4E-05		$\mathbf{x}^*_3$	578.2818		dg/dx	0
	0.176158			-0.24826			0.9375			3.498667
	0			0			2			0
$\mathbf{D}^T$	0	0.176158	0							
						σ_x^e	17.92243		u_x^e	578.2822
			β	**0.248262**			0.05035			0.95000
							0.028			2.00000
	α_3	0								
		1								
		0								
	$\mathbf{u_4}^*$	0								
		0.248262								
		0								
	$\mathbf{x_4}^*$	578.2822								
		0.9375								
		2								

Stellenbosch University http://scholar.sun.ac.za

				Iteration 4: Shear about strong axis						
$g(\mathbf{x_4}^*)$	**0**									
$g(\mathbf{x_4}^*)f_y$	0									
$g(\mathbf{x_4}^*)t$	0.164									
$g(\mathbf{x_4}^*)r_i$	0									
D	0		$\mathbf{u_4}^*$	-8.8E-12		$\mathbf{x}^*_4$	578.2822		dg/dx	0
	0.176158			-0.24826			0.9375			3.498667
	0			0			2			0
$\mathbf{D}^T$	0	0.176158	0							
						σ_x^e	17.92244		u_x^e	578.2822
			β	**0.248262**			0.05035			0.95000
							0.028			2.00000
	α_4	0								
		1								
		0								
	$\mathbf{u_5}^*$	0								
		0.248262								
		0								
	$\mathbf{x_5}^*$	578.2822								
		0.9375								
		2								

Stellenbosch University http://scholar.sun.ac.za

Yield stress distribution

Log - Normal distribution	
	Iteration 1
x_1*	550
μ	578.56
COV	0.031
σ	17.93536
skew	0.09303
c	0.031
u	-1.59239
$\Phi_X(x^*)$	0.052839
$\Phi_U^{-1}(\Phi_X(x^*))$	-1.61793
$\varphi_U[\Phi_U^{-1}(\Phi_X(x^*))]$	0.107767
$\varphi_X(x^*)$	0.006322
σ_X^e	17.04591
μ_X^e	577.579
	Iteration 2
x_2*	577.579
μ	578.56
COV	0.031
σ	17.93536
skew	0.09303
c	0.031
u	-0.05469
$\Phi_X(x^*)$	0.484343
$\Phi_U^{-1}(\Phi_X(x^*))$	-0.03926
$\varphi_U[\Phi_U^{-1}(\Phi_X(x^*))]$	0.398635
$\varphi_X(x^*)$	0.022269
σ_X^e	17.90065
μ_X^e	578.2818

	Iteration 3
x_3*	578.2818
μ	578.56
COV	0.031
σ	17.93536
skew	0.09303
c	0.031
u	-0.01551
$\Phi_X(x^*)$	0.49999
$\Phi_U^{-1}(\Phi_X(x^*))$	-2.4E-05
$\varphi_U[\Phi_U^{-1}(\Phi_X(x^*))]$	0.398942
$\varphi_X(x^*)$	0.022259
σ_X^e	17.92243
μ_X^e	578.2822
	Iteration 4
x_4*	578.2822
μ	578.56
COV	0.031
σ	17.93536
skew	0.09303
c	0.031
u	-0.01549
$\Phi_X(x^*)$	0.5
$\Phi_U^{-1}(\Phi_X(x^*))$	-8.8E-12
$\varphi_U[\Phi_U^{-1}(\Phi_X(x^*))]$	0.398942
$\varphi_X(x^*)$	0.022259
σ_X^e	17.92244
μ_X^e	578.2822

Stellenbosch University http://scholar.sun.ac.za

FORM – Shear about the weak axis

				Iteration 1: Shear about weak axis						
$g(x_1^*)$	**0**									
$g(x_1^*)f_y$	0									
$g(x_1^*)t$	0.155									
$g(x_1^*)r_i$	0									
D	0		u_1^*	-1.61793		x^*_1	550	f_y	dg/dx	0
	0.208391			-3.99206			0.749	t		4.138852
	0			0			2	r_i		0
D^T	0	0.208391	0							
						σ_x^e	17.04591		u_x^e	577.579
			β	**3.992056**			0.05035			0.95000
							0.028			2.00000
	α_1	0								
		1								
		0								
	u_2^*	0								
		3.992056								
		0								
	x_2^*	577.579	f_y							
		0.749	t							
		2	r_i							

Stellenbosch University http://scholar.sun.ac.za

				Iteration 2: Shear about weak axis						
$g(x_2^*)$	**0.000**									
$g(x_2^*)f_y$	0.000									
$g(x_2^*)t$	0.155									
$g(x_2^*)r_i$	0.000									
D	0		u_2^*	-0.0392		x^*_2	577.58	f_y	dg/dx	0
	0.208391			-3.99206			0.749	t		4.138852
	0			0			2	r_i		0
D^T	0	0.208391	0							
						σ_x^e	17.90068		u_x^e	578.2818
			β	**3.992056**			0.05035			0.95000
							0.028			2.00000
	α_2	0								
		1								
		0								
	u_3^*	0								
		3.992056								
		0								
	x_3^*	578.2818								
		0.749								
		2								

Stellenbosch University http://scholar.sun.ac.za

				Iteration 3: Shear about weak axis						
$g(\mathbf{x_3}^*)$	**0**									
$g(\mathbf{x_3}^*)f_y$	0									
$g(\mathbf{x_3}^*)t$	0.155									
$g(\mathbf{x_3}^*)r_i$	0									
D	0		$\mathbf{u_3}^*$	-2.4E-05		$\mathbf{x}^*_3$	578.2818	f_y	dg/dx	0
	0.208391			-3.99206			0.749	t		4.138852
	0			0			2	r_i		0
$\mathbf{D}^T$	0	0.208391	0							
						σ_x^e	17.92243		u_x^e	578.2822
			β	**3.992056**			0.05035			0.95000
							0.028			2.00000
	α_3	0								
		1								
		0								
	$\mathbf{u_4}^*$	0								
		3.992056								
		0								
	$\mathbf{x_4}^*$	578.2822								
		0.749								
		2								

Stellenbosch University http://scholar.sun.ac.za

Iteration 4: Shear about weak axis

$g(x_4^*)$	**0**									
$g(x_4^*)f_y$	0									
$g(x_4^*)t$	0.155									
$g(x_4^*)r_i$	0									
D	0		u_4^*	-8.8E-12		x^*_4	578.2822	f_y	dg/dx	0
	0.208391			-3.99206			0.749	t		4.138852
	0			0			2	r_i		0
D^T	0	0.208391	0							
						σ_x^e	17.92244		u_x^e	578.2822
			β	**3.992056**			0.05035			0.95000
							0.028			2.00000
	α_4	0								
		1								
		0								
	u_5^*	0								
		3.992056								
		0								
	x_5^*	578.2822								
		0.749								
		2								

Stellenbosch University http://scholar.sun.ac.za

Yield stress distribution

Log - Normal distribution		
	Iteration 1	
x_1*	550	
μ	578.56	
COV	0.031	
σ	17.93536	
skew	0.09303	
c	0.031	
u	-1.59239	
$\Phi_X(x^*)$	0.052839	
$\Phi_U^{-1}(\Phi_X(x^*))$	-1.61793	
$\varphi_U[\Phi_U^{-1}(\Phi_X(x^*))]$	0.107767	
$\varphi_X(x^*)$	0.006322	
σ_X^e	17.04591	
μ_X^e	577.579	
	Iteration 2	
x_2*	577.58	
μ	578.56	
COV	0.031	
σ	17.93536	
skew	0.09303	
c	0.031	
u	-0.05464	
$\Phi_X(x^*)$	0.484364	
$\Phi_U^{-1}(\Phi_X(x^*))$	-0.0392	
$\varphi_U[\Phi_U^{-1}(\Phi_X(x^*))]$	0.398636	
$\varphi_X(x^*)$	0.022269	
σ_X^e	17.90068	
μ_X^e	578.2818	

	Iteration 3	
x_3*	578.2818	
μ	578.56	
COV	0.031	
σ	17.93536	
skew	0.09303	
c	0.031	
u	-0.01551	
$\Phi_X(x^*)$	0.499991	
$\Phi_U^{-1}(\Phi_X(x^*))$	-2.4E-05	
$\varphi_U[\Phi_U^{-1}(\Phi_X(x^*))]$	0.398942	
$\varphi_X(x^*)$	0.022259	
σ_X^e	17.92243	
μ_X^e	578.2822	
	Iteration 4	
x_4*	578.2822	
μ	578.56	
COV	0.031	
σ	17.93536	
skew	0.09303	
c	0.031	
u	-0.01549	
$\Phi_X(x^*)$	0.5	
$\Phi_U^{-1}(\Phi_X(x^*))$	-8.8E-12	
$\varphi_U[\Phi_U^{-1}(\Phi_X(x^*))]$	0.398942	
$\varphi_X(x^*)$	0.022259	
σ_X^e	17.92244	
μ_X^e	578.2822	

Stellenbosch University http://scholar.sun.ac.za

FORM – Tension

				Iteration 1: Tension						
$g(x_1^*)$	**0**									
$g(x_1^*)f_u$	0.05									
$g(x_1^*)t$	0.036									
$g(x_1^*)r_i$	0									
D	0.030993		u_1^*	-1.61793		x^*_1	550	f_u	dg/dx	0.001818
	0.041431			-1.48957			0.875	t		0.822857
	0			0			2	r_i		0
D^T	0.030993	0.041431	0							
						σ_x^e	17.04591		u_x^e	577.579
			β	**2.161914**			0.05035			0.95000
							0.028			2.00000
	α_1	0.599003								
		0.800747								
		0								
	u_2^*	1.294992								
		1.731146								
		0								
	x_2^*	555.5047	f_y							
		0.862837	t							
		2	r_i							

Stellenbosch University http://scholar.sun.ac.za

				Iteration 2: Tension						
$g(x_2^*)$	**0.000**									
$g(x_2^*)f_u$	0.049									
$g(x_2^*)t$	0.035									
$g(x_2^*)r_i$	0.000									
D	0.030373		u_2^*	-1.2966		x^*_2	555.5047	f_u	dg/dx	0.001764
	0.04084			-1.7279			0.863	t		0.811124
	0			0			2	r_i		0
D^T	0.030373	0.04084	0							
						σ_x^e	17.21651		u_x^e	577.8276
			β	**2.160263**			0.05035			0.95000
							0.028			2.00000
	α_2	0.596759								
		0.802421								
		0								
	u_3^*	1.289156								
		1.733439								
		0								
	x_3^*	555.6328								
		0.862721								
		2								

Stellenbosch University http://scholar.sun.ac.za

				Iteration 3: Tension						
$g(\mathbf{x_3}^*)$	**0**									
$g(\mathbf{x_3}^*)f_u$	0.05									
$g(\mathbf{x_3}^*)t$	0.036									
$g(\mathbf{x_3}^*)r_i$	0									
D	0.030993		$\mathbf{u_3}^*$	-1.28916		$\mathbf{x}^*_3$	555.6328	f_u	dg/dx	0.0018
	0.042022			-1.73386			0.8627	t		0.834589
	0			0			2	r_i		0
$\mathbf{D}^T$	0.030993	0.042022	0							
						σ_x^e	17.22048		u_x^e	577.8327
			β	**2.160587**			0.05035			0.95000
							0.028			2.00000
	α_3	0.593563								
		0.804788								
		0								
	$\mathbf{u_4}^*$	1.282444								
		1.738814								
		0								
	$\mathbf{x_4}^*$	555.7484								
		0.862451								
		2								

Stellenbosch University http://scholar.sun.ac.za

				Iteration 4: Tension						
$g(\mathbf{x_4}^*)$	**0**									
$g(\mathbf{x_4}^*)f_u$	0.05									
$g(\mathbf{x_4}^*)t$	0.036									
$g(\mathbf{x_4}^*)r_i$	0									
D	0.030993		$\mathbf{u_4}^*$	-1.28244		$\mathbf{x}^*_4$	555.7484	f_u	dg/dx	0.001799
	0.042031			-1.73784			0.8625	t		0.834783
	0			0			2	r_i		0
$\mathbf{D}^T$	0.030993	0.042031	0							
						σ_x^e	17.22406		u_x^e	577.8374
			β	**2.1598**			0.05035			0.95000
							0.028			2.00000
	α_4	0.593474								
		0.804853								
		0								
	$\mathbf{u_5}^*$	1.281784								
		1.738322								
		0								
	$\mathbf{x_5}^*$	555.7598								
		0.862475								
		2								

Stellenbosch University http://scholar.sun.ac.za

				Iteration 5: Tension						
$g(x_5^*)$	**0**									
$g(x_5^*)f_u$	0.05									
$g(x_5^*)t$	0.036									
$g(x_5^*)r_i$	0									
D	0.030993		u_4^*	-1.28178		x^*_4	555.7598	f_u	dg/dx	0.001799
	0.042031			-1.73784			0.8625	t		0.834783
	0			0			2	r_i		0
D^T	0.030993	0.042031	0							
						σ_x^e	17.22442		u_x^e	577.8378
			β	**2.159408**			0.05035			0.95000
							0.028			2.00000
	α_4	0.593474								
		0.804853								
		0								
	u_5^*	1.281784								
		1.738322								
		0								
	x_5^*	555.7598								
		0.862475								
		2								

Stellenbosch University http://scholar.sun.ac.za

Yield stress distribution

Log - Normal distribution	
Iteration 1	
x_1*	550
μ	578.56
COV	0.031
σ	17.93536
skew	0.09303
c	0.031
u	-1.59239
$\Phi_X(x^*)$	0.052839
$\Phi_U^{-1}(\Phi_X(x^*))$	-1.61793
$\varphi_U[\Phi_U^{-1}(\Phi_X(x^*))]$	0.107767
$\varphi_X(x^*)$	0.006322
σ_X^e	17.04591
μ_X^e	577.579
Iteration 2	
x_2*	555.5047
μ	578.56
COV	0.031
σ	17.93536
skew	0.09303
c	0.031
u	-1.28547
$\Phi_X(x^*)$	0.097385
$\Phi_U^{-1}(\Phi_X(x^*))$	-1.2966
$\varphi_U[\Phi_U^{-1}(\Phi_X(x^*))]$	0.172127
$\varphi_X(x^*)$	0.009998
σ_X^e	17.21651
μ_X^e	577.8276

	Iteration 3
x_3*	555.6328
μ	578.56
COV	0.031
σ	17.93536
skew	0.09303
c	0.031
u	-1.27832
$\Phi_X(x^*)$	0.098672
$\Phi_U^{-1}(\Phi_X(x^*))$	-1.28916
$\varphi_U[\Phi_U^{-1}(\Phi_X(x^*))]$	0.173791
$\varphi_X(x^*)$	0.010092
σ_X^e	17.22048
μ_X^e	577.8327
	Iteration 4
x_4*	555.7484
μ	578.56
COV	0.031
σ	17.93536
skew	0.09303
c	0.031
u	-1.27188
$\Phi_X(x^*)$	0.099843
$\Phi_U^{-1}(\Phi_X(x^*))$	-1.28244
$\varphi_U[\Phi_U^{-1}(\Phi_X(x^*))]$	0.175298
$\varphi_X(x^*)$	0.010177
σ_X^e	17.22406
μ_X^e	577.8374
	Iteration 5
x_5*	555.7598
μ	578.56
COV	0.031
σ	17.93536
skew	0.09303
c	0.031
u	-1.27124
$\Phi_X(x^*)$	0.099959
$\Phi_U^{-1}(\Phi_X(x^*))$	-1.28178
$\varphi_U[\Phi_U^{-1}(\Phi_X(x^*))]$	0.175446
$\varphi_X(x^*)$	0.010186
σ_X^e	17.22442
μ_X^e	577.8378

Stellenbosch University http://scholar.sun.ac.za

FORM – Axial load and bending interaction

				Iteration 1: Interaction						
$g(x_1^*)$	**0**									
$g(x_1^*)f_y$	0.028									
$g(x_1^*)t$	0.063									
$g(x_1^*)r_i$	-0.001									
D	0.017356		u_1^*	-1.61793		x^*_1	550	f_y	dg/dx	0.001018
	0.06678			0			0.95	t		1.326316
	-0.00028			0			2	r_i		-0.01
D^T	0.017356	0.06678	-0.00028							
						σ_x^e	17.04591		u_x^e	577.579
			β	**0.406969**			0.05035			0.95000
							0.028			2.00000
	α_1	0.251537								
		0.967839								
		-0.00406								
	u_2^*	0.102368								
		0.39388								
		-0.00165								
	x_2^*	575.8341	f_y							
		0.930168	t							
		2.000046	r_i							

				Iteration 2: Interaction						
$g(x_2^*)$	**0**									
$g(x_2^*)f_u$	0.027									
$g(x_2^*)t$	0.063									
$g(x_2^*)r_i$	-0.001									
D	0.016736		u_2^*	-0.13688		x^*_2	575.8341	f_y	dg/dx	0.000938
	0.068216			-0.39722			0.93	t		1.354839
	-0.00028			0.001651			2.000046	r_i		-0.01
D^T	0.016736	0.068216	-0.00028							
						σ_x^e	17.84657		u_x^e	578.277
			β	**0.418398**			0.05035			0.95000
							0.028			2.00000
	α_2	0.23827								
		0.971191								
		-0.00399								
	u_3^*	0.099692								
		0.406344								
		-0.00167								
	x_3^*	576.4979								
		0.929541								
		2.000047								

				Iteration 3: Interaction						
$g(\mathbf{x_3}^*)$	**0**									
$g(\mathbf{x_3}^*)f_u$	0.027									
$g(\mathbf{x_3}^*)t$	0.063									
$g(\mathbf{x_3}^*)r_i$	-0.001									
D	0.016736		$\mathbf{u_3}^*$	-0.09971		$\mathbf{x}^*_3$	576.4979	f_y	dg/dx	0.000937
	0.068216			-0.39722			0.93	t		1.354839
	-0.00028			0.001668			2.000047	r_i		-0.01
$\mathbf{D}^T$	0.016736	0.068216	-0.00028							
						σ_x^e	17.86714		u_x^e	578.2794
			β	**0.409541**			0.05035			0.95000
							0.028			2.00000
	α_3	0.23827								
		0.971191								
		-0.00399								
	$\mathbf{u_4}^*$	0.097581								
		0.397743								
		-0.00163								
	$\mathbf{x_4}^*$	576.5359								
		0.929974								
		2.000046								

				Iteration 4: Interaction						
$g(x_4^*)$	**0**									
$g(x_4^*)f_u$	0.027									
$g(x_4^*)t$	0.063									
$g(x_4^*)r_i$	-0.001									
D	0.016736		u_4^*	-0.09758		x^*_4	576.5359	f_y	dg/dx	0.000937
	0.068216			-0.39722			0.93	t		1.354839
	-0.00028			0.001633			2.000046	r_i		-0.01
D^T	0.016736	0.068216	-0.00028							
						σ_x^e	17.86832		u_x^e	578.2796
			β	**0.409033**			0.05035			0.95000
							0.028			2.00000
	α_4	0.23827								
		0.971191								
		-0.00399								
	u_5^*	0.09746								
		0.397249								
		-0.00163								
	x_5^*	576.5381								
		0.929999								
		2.000046								

Stellenbosch University http://scholar.sun.ac.za

				Iteration 5: Interaction						
$g(x_5^*)$	**0**									
$g(x_5^*)f_u$	0.027									
$g(x_5^*)t$	0.063									
$g(x_5^*)r_i$	-0.001									
D	0.016736		u_4^*	-0.09746		x^*_4	576.5381	f_y	dg/dx	0.000937
	0.068216			-0.39722			0.93	t		1.354839
	-0.00028			0.001631			2.000046	r_i		-0.01
D^T	0.016736	0.068216	-0.00028							
						σ_x^e	17.86839		u_x^e	578.2796
			β	**0.409004**			0.05035			0.95000
							0.028			2.00000
	α_4	0.23827								
		0.971191								
		-0.00399								
	u_5^*	0.09746								
		0.397249								
		-0.00163								
	x_5^*	576.5381								
		0.929999								
		2.000046								

Stellenbosch University http://scholar.sun.ac.za

Yield stress distribution

Log - Normal distribution	
	Iteration 1
x_1*	550
μ	578.56
COV	0.031
σ	17.93536
skew	0.09303
c	0.031
u	-1.59239
$\Phi_X(x^*)$	0.052839
$\Phi_U^{-1}(\Phi_X(x^*))$	-1.61793
$\varphi_U[\Phi_U^{-1}(\Phi_X(x^*))]$	0.107767
$\varphi_X(x^*)$	0.006322
σ_X^e	17.04591
μ_X^e	577.579
	Iteration 2
x_2*	575.8341
μ	578.56
COV	0.031
σ	17.93536
skew	0.09303
c	0.031
u	-0.15199
$\Phi_X(x^*)$	0.445561
$\Phi_U^{-1}(\Phi_X(x^*))$	-0.13688
$\varphi_U[\Phi_U^{-1}(\Phi_X(x^*))]$	0.395222
$\varphi_X(x^*)$	0.022146
σ_X^e	17.84657
μ_X^e	578.277

	Iteration 3
x_3*	576.4979
μ	578.56
COV	0.031
σ	17.93536
skew	0.09303
c	0.031
u	-0.11498
$\Phi_X(x^*)$	0.460286
$\Phi_U^{-1}(\Phi_X(x^*))$	-0.09971
$\varphi_U[\Phi_U^{-1}(\Phi_X(x^*))]$	0.396964
$\varphi_X(x^*)$	0.022218
σ_X^e	17.86714
μ_X^e	578.2794
	Iteration 4
x_4*	576.5359
μ	578.56
COV	0.031
σ	17.93536
skew	0.09303
c	0.031
u	-0.11285
$\Phi_X(x^*)$	0.461132
$\Phi_U^{-1}(\Phi_X(x^*))$	-0.09758
$\varphi_U[\Phi_U^{-1}(\Phi_X(x^*))]$	0.397047
$\varphi_X(x^*)$	0.022221
σ_X^e	17.86832
μ_X^e	578.2796
	Iteration 5
x_5*	576.5381
μ	578.56
COV	0.031
σ	17.93536
skew	0.09303
c	0.031
u	-0.11273
$\Phi_X(x^*)$	0.46118
$\Phi_U^{-1}(\Phi_X(x^*))$	-0.09746
$\varphi_U[\Phi_U^{-1}(\Phi_X(x^*))]$	0.397052
$\varphi_X(x^*)$	0.022221
σ_X^e	17.86839
μ_X^e	578.2796

Stellenbosch University http://scholar.sun.ac.za

Appendix L: Spread sheet calculations for evaluation of β-Case 3

FORM – Axial load

				Iteration 1: Axial load						
$g(x_2^*)$	**0**									
$g(x_2^*)$wind	-0.103									
$g(x_2^*)$DL	0									
$g(x_2^*)$LLR	0.001									
$g(x_2^*)$LLF	0.001									
$g(x_2^*)$fy	9.00E-03									
$g(x_2^*)$t	0.079									
$g(x_2^* r_i$	0.032									
D	-0.74179		u_1^*	2.054238		x^*_1	28	$v_{b,0}$	dg/dx	-0.073571
	0			0			0.2	DL		0
	0.003607			1.803556			0.25	LLR		0.08
	0.003609			1.788179			1.5	LLF		0.013333
	0.005579			-1.61793			550	f_y		0.000327
	0.130951			-6.80238			0.6075	t		2.600823
	0.00896			0			2	r_i		0.32
D^T	-0.74179	0	0.003607	0.003609	0.0055787	0.130951	0.00896			
						σ_x^e	10.08264		u_x^e	7.287851
			β	**3.199911**			0.02			0.20000
							0.045082			0.16869
							0.270693			1.01595
							17.04591			577.57904
							0.05035			0.95000
	α_1	-0.98465					0.028			2
		0								
		0.004787								
		0.004791								
		0.007405								
		0.173824								
		0.011893								
	u_2^*	-3.1508								
		0								
		0.015319								
		0.01533								
		0.023696								
		0.556222								
		0.038058								
	x_2^*	39.05629	WL							
		0.2	DL							
		0.168002	LLR							
		1.011802	LLF							
		577.1751	fy							
		0.921994	t							
		1.998934	ri							

Stellenbosch University http://scholar.sun.ac.za

Iteration 2: Axial load

$g(x_2^*)$	**0**									
$g(x_2^*)$wind	-0.103									
$g(x_2^*)$DL	0									
$g(x_2^*)$LLR	0									
$g(x_2^*)$LLF	0									
$g(x_2^*)$fy	0.041									
$g(x_2^*)$t	0.07									
$g(x_2^*r_i$	0									
D	-0.71297		u_2^*	2.993363		x^*_2	39.05629	$v_{b,0}$	dg/dx	-0.052744
	0			0			0.2	DL		0
	0			-0.27638			0.168002	LLR		0
	0			-0.27156			1.011802	LLF		0
	0.025414			-0.06183			577.1751	f_y		0.001421
	0.073122			0.278054			0.964	t		1.452282
	0			-0.03806			1.998934	r_i		0
$\mathbf{D}^T$	-0.71297	0	0	0	0.0254139	0.073122	0			
						σ_x^e	13.5175		u_x^e	-1.406496
			β	**2.949714**			0.02			0.20000
							0.03426			0.17747
							0.206261			1.06781
							17.88813			578.28114
							0.05035			0.95000
	α_2	-0.99416					0.028			2
		0								
		0								
		0								
		0.035437								
		0.101961								
		0								
	u_3^*	-2.93248								
		0								
		0								
		0								
		0.104528								
		0.300755								
		0								
	x_3^*	38.23329	WL							
		0.2	DL							
		0.17747	LLR							
		1.067815	LLF							
		576.4113	fy							
		0.934857	t							
		2	ri							

				Iteration 3: Axial load						
$g(x_2^*)$	**0**									
$g(x_2^*)$wind	-0.103									
$g(x_2^*)$DL	0									
$g(x_2^*)$LLR	0									
$g(x_2^*)$LLF	0									
$g(x_2^*)$fy	0.011									
$g(x_2^*)$t	0.07									
$g(x_2^*r_i$	0									
D	-0.71576		$\mathbf{u_3^*}$	2.931949		$\mathbf{x^*_3}$	38.23329	$v_{b,0}$	dg/dx	-0.05388
	0			0			0.2	DL		0
	0			-0.00492			0.17747	LLR		0
	0			-0.00475			1.067815	LLF		0
	0.006818			-0.10456			576.4113	f_y		0.000382
	0.07539			-0.29791			0.935	t		1.497326
	0			0			2	r_i		0
$\mathbf{D^T}$	-0.71576	0	0	0	0.0068184	0.07539	0			
						σ_x^e	13.28437		u_x^e	-0.715797
			β	**2.947884**			0.02			0.20000
							0.035509			0.17764
							0.213653			1.06883
							17.86446			578.27917
							0.05035			0.95000
	α_3	-0.99445					0.028			2
		0								
		0								
		0								
		0.009473								
		0.104745								
		0								
	$\mathbf{u_4^*}$	-2.93153								
		0								
		0								
		0								
		0.027926								
		0.308777								
		0								
	$\mathbf{x_4^*}$	38.22779	WL							
		0.2	DL							
		0.177645	LLR							
		1.06883	LLF							
		577.7803	fy							
		0.934453	t							
		2	ri							

Stellenbosch University http://scholar.sun.ac.za

				Iteration 4: Axial load						
$g(x_2^*)$	**0**									
$g(x_2^*)$wind	-0.103									
$g(x_2^*)$DL	0									
$g(x_2^*)$LLR	0									
$g(x_2^*)$LLF	0									
$g(x_2^*)$fy	0.011									
$g(x_2^*)$t	0.069									
$g(x_2^* r_i$	0.001									
D	-0.71578		$\mathbf{u_4^*}$	2.931535		$\mathbf{x^*_4}$	38.22779	$v_{b,0}$	dg/dx	-0.053888
	0			0			0.2	DL		0
	0			-1.6E-06			0.177645	LLR		0
	0			-1.5E-06			1.06883	LLF		0
	0.006818			-0.02802			577.7803	f_y		0.000381
	0.074353			-0.30785			0.9345	t		1.476726
	0.00028			0			2	r_i		0.01
$\mathbf{D^T}$	-0.71578	0	0	0	0.0068184	0.074353	0.00028			
						σ_x^e	13.2828		u_x^e	-0.711196
			β	**2.947785**			0.02			0.20000
							0.035533			0.17764
							0.213787			1.06883
							17.90689			578.28198
							0.05035			0.95000
	α_4	-0.9946					0.028			2
		0								
		0								
		0								
		0.009474								
		0.103317								
		0.000389								
	$\mathbf{u_5^*}$	-2.93188								
		0								
		0								
		0								
		0.027929								
		0.304556								
		0.001147								
	$\mathbf{x_5^*}$	38.23233	WL							
		0.2	DL							
		0.177645	LLR							
		1.068831	LLF							
		577.7819	fy							
		0.934666	t							
		1.999968	ri							

Stellenbosch University http://scholar.sun.ac.za

Live load distribution

	Gamma Dist - applied as Log Normal with lower skewness						
				Iteration 1			
	Roof					**Floor**	
x_1*	0.25	kPa			x_1*	1.5	kPa
μ	0.18	kPa			u	1.083	kPa
COV	0.2				COV	0.2	
σ	0.036	kPa			σ	0.2166	kPa
skew	0.4		E17		skew	0.4	
c	0.132557		F17		c	0.132557	
u	1.944444		I17		u	1.925208	
$\Phi_X(x^*)$	0.964349		L17		$\Phi_X(x^*)$	0.963126	
$\Phi_U^{-1}(\Phi_X(x^*))$	1.803556		J17		$\Phi_U^{-1}(\Phi_X(x^*))$	1.788179	
$\varphi_U[\Phi_U^{-1}(\Phi_X(x^*))]$	0.078446				$\varphi_U[\Phi_U^{-1}(\Phi_X(x^*))]$	0.080642	
$\varphi_X(x^*)$	1.740075		K17		$\varphi_X(x^*)$	0.297911	
σ_X^e	0.045082				σ_X^e	0.270693	
μ_X^e	0.17				μ_X^e	1.02	
				Iteration 2			
	Roof					**Floor**	
x_2*	0.168002	kPa			x_2*	1.011802	kPa
μ	0.18	kPa			u	1.083	kPa
COV	0.2				COV	0.2	
σ	0.036	kPa			σ	0.2166	kPa
skew	0.4		E17		skew	0.4	
c	0.132557		F17		c	0.132557	
u	-0.333289		I17		u	-0.32871	
$\Phi_X(x^*)$	0.39113		L17		$\Phi_X(x^*)$	0.39298	
$\Phi_U^{-1}(\Phi_X(x^*))$	-0.276376		J17		$\Phi_U^{-1}(\Phi_X(x^*))$	-0.27156	
$\varphi_U[\Phi_U^{-1}(\Phi_X(x^*))]$	0.383993				$\varphi_U[\Phi_U^{-1}(\Phi_X(x^*))]$	0.3845	
$\varphi_X(x^*)$	11.20828		K17		$\varphi_X(x^*)$	1.864146	
σ_X^e	0.03426				σ_X^e	0.206261	
μ_X^e	0.18				μ_X^e	1.07	

CV

Stellenbosch University http://scholar.sun.ac.za

			Iteration 3				
	Roof					**Floor**	
x_3*	0.17747	kPa			x_3*	1.067815	kPa
μ	0.18	kPa			u	1.083	kPa
COV	0.2				COV	0.2	
σ	0.036	kPa			σ	0.2166	kPa
skew	0.4		E17		skew	0.4	
c	0.132557		F17		c	0.132557	
u	-0.070273		I17		u	-0.07011	
$\Phi_X(x^*)$	0.498037		L17		$\Phi_X(x^*)$	0.498104	
$\Phi_U^{-1}(\Phi_X(x^*))$	-0.004921		J17		$\Phi_U^{-1}(\Phi_X(x^*))$	-0.00475	
$\varphi_U[\Phi_U^{-1}(\Phi_X(x^*))]$	0.398937				$\varphi_U[\Phi_U^{-1}(\Phi_X(x^*))]$	0.398938	
$\varphi_X(x^*)$	11.23468		K17		$\varphi_X(x^*)$	1.86722	
$\boldsymbol{\sigma_X^e}$	0.035509				$\boldsymbol{\sigma_X^e}$	0.213653	
$\boldsymbol{\mu_X^e}$	0.18				$\boldsymbol{\mu_X^e}$	1.07	
			Iteration 4				
	Roof					**Floor**	
x_4*	0.177645	kPa			x_4*	1.06883	kPa
μ	0.18	kPa			u	1.083	kPa
COV	0.2				COV	0.2	
σ	0.036	kPa			σ	0.2166	kPa
skew	0.4		E17		skew	0.4	
c	0.132557		F17		c	0.132557	
u	-0.065419		I17		u	-0.06542	
$\Phi_X(x^*)$	0.499999		L17		$\Phi_X(x^*)$	0.499999	
$\Phi_U^{-1}(\Phi_X(x^*))$	-1.6E-06		J17		$\Phi_U^{-1}(\Phi_X(x^*))$	-1.5E-06	
$\varphi_U[\Phi_U^{-1}(\Phi_X(x^*))]$	0.398942				$\varphi_U[\Phi_U^{-1}(\Phi_X(x^*))]$	0.398942	
$\varphi_X(x^*)$	11.22753		K17		$\varphi_X(x^*)$	1.866071	
$\boldsymbol{\sigma_X^e}$	0.035533				$\boldsymbol{\sigma_X^e}$	0.213787	
$\boldsymbol{\mu_X^e}$	0.18				$\boldsymbol{\mu_X^e}$	1.07	

Stellenbosch University http://scholar.sun.ac.za

Wind load distribution

	Gumbel Dist	
	Iteration 1	
x_1*	28	m/s
μ	14.289	m/s
COV	0.37	
σ	5.28693	m/s
c	0.242589	
x_{mod}	11.91049	
$\Phi_X(x^*)$	0.980024	
$\Phi_U^{-1}(\Phi_X(x^*))$	2.054238	
$\varphi_U[\Phi_U^{-1}(\Phi_X(x^*))]$	0.04837	
$\varphi_X(x^*)$	0.004797	
$\boldsymbol{\sigma_X^e}$	10.08264	
$\boldsymbol{\mu_X^e}$	7.287851	
	Iteration 2	
x_1*	39.05629	m/s
μ	14.289	m/s
COV	0.37	
σ	5.28693	m/s
c	0.242589	
x_{mod}	11.91049	
$\Phi_X(x^*)$	0.99862	
$\Phi_U^{-1}(\Phi_X(x^*))$	2.993363	
$\varphi_U[\Phi_U^{-1}(\Phi_X(x^*))]$	0.004521	
$\varphi_X(x^*)$	0.000334	
$\boldsymbol{\sigma_X^e}$	13.5175	
$\boldsymbol{\mu_X^e}$	-1.4065	

	Iteration 3	
x_3*	38.23329	m/s
μ	14.289	m/s
COV	0.37	
σ	5.28693	m/s
c	0.242589	
x_{mod}	11.91049	
$\Phi_X(x^*)$	0.998316	
$\Phi_U^{-1}(\Phi_X(x^*))$	2.931949	
$\varphi_U[\Phi_U^{-1}(\Phi_X(x^*))]$	0.005423	
$\varphi_X(x^*)$	0.000408	
$\boldsymbol{\sigma_X^e}$	13.28437	
$\boldsymbol{\mu_X^e}$	-0.7158	
	Iteration 4	
x_4*	38.22779	m/s
μ	14.289	m/s
COV	0.37	
σ	5.28693	m/s
c	0.242589	
x_{mod}	11.91049	
$\Phi_X(x^*)$	0.998314	
$\Phi_U^{-1}(\Phi_X(x^*))$	2.931535	
$\varphi_U[\Phi_U^{-1}(\Phi_X(x^*))]$	0.00543	
$\varphi_X(x^*)$	0.000409	
$\boldsymbol{\sigma_X^e}$	13.2828	
$\boldsymbol{\mu_X^e}$	-0.7112	

Stellenbosch University http://scholar.sun.ac.za

Yield stress distribution

Log - Normal distribution					
	Iteration 1			**Iteration 3**	
x_1^*	550		x_3^*	576.4113	
μ	578.56		μ	578.56	
COV	0.031		COV	0.031	
σ	17.93536		σ	17.93536	
skew	0.09303		skew	0.09303	
c	0.031		c	0.031	
u	-1.59239		u	-0.1198	
$\Phi_X(x^*)$	0.052839		$\Phi_X(x^*)$	0.458364	
$\Phi_U^{-1}(\Phi_X(x^*))$	-1.61793		$\Phi_U^{-1}(\Phi_X(x^*))$	-0.10456	
$\varphi_U[\Phi_U^{-1}(\Phi_X(x^*))]$	0.107767		$\varphi_U[\Phi_U^{-1}(\Phi_X(x^*))]$	0.396768	
$\varphi_X(x^*)$	0.006322		$\varphi_X(x^*)$	0.02221	
$\boldsymbol{\sigma_X^e}$	17.04591		$\boldsymbol{\sigma_X^e}$	17.86446	
$\boldsymbol{\mu_X^e}$	577.579		$\boldsymbol{\mu_X^e}$	578.2792	
	Iteration 2			**Iteration 4**	
x_2^*	577.1751		x_4^*	577.7803	
μ	578.56		μ	578.56	
COV	0.031		COV	0.031	
σ	17.93536		σ	17.93536	
skew	0.09303		skew	0.09303	
c	0.031		c	0.031	
u	-0.07721		u	-0.04347	
$\Phi_X(x^*)$	0.475349		$\Phi_X(x^*)$	0.488824	
$\Phi_U^{-1}(\Phi_X(x^*))$	-0.06183		$\Phi_U^{-1}(\Phi_X(x^*))$	-0.02802	
$\varphi_U[\Phi_U^{-1}(\Phi_X(x^*))]$	0.39818		$\varphi_U[\Phi_U^{-1}(\Phi_X(x^*))]$	0.398786	
$\varphi_X(x^*)$	0.022259		$\varphi_X(x^*)$	0.02227	
$\boldsymbol{\sigma_X^e}$	17.88813		$\boldsymbol{\sigma_X^e}$	17.90689	
$\boldsymbol{\mu_X^e}$	578.2811		$\boldsymbol{\mu_X^e}$	578.282	

Stellenbosch University http://scholar.sun.ac.za

FORM – Shear about strong axis

				Iteration 1: Strong axis shear						
$g(x_2^*)$	**0**									
$g(x_2^*)$wind	-0.056									
$g(x_2^*)$DL	-0.002									
$g(x_2^*)$LLR	-0.017									
$g(x_2^*)$LLF	-0.017									
$g(x_2^*)$fy	0									
$g(x_2^*)$t	0.141									
$g(x_2^* r_i$	0									
D	-0.40331		$\mathbf{u_1^*}$	2.054238		$\mathbf{x^*_1}$	28	$v_{b,0}$	dg/dx	-0.04
	-0.004			0			0.2	DL		-0.2
	-0.06131			1.803556			0.25	LLR		-1.36
	-0.06136			1.788179			1.5	LLF		-0.226667
	0			-1.61793			550	f_y		0
	0.151453			-0.24826			0.9375	t		3.008
	0			0			2	r_i		0
$\mathbf{D^T}$	-0.40331	-0.004	-0.06131	-0.06136	0	0.151453	0			
						σ_x^e	10.08264		u_x^e	7.287851
			β	**2.472032**			0.02			0.20000
							0.045082			0.16869
							0.270693			1.01595
							17.04591			577.57904
							0.05035			0.95000
	α_1	-0.91771					0.028			2
		-0.0091								
		-0.13951								
		-0.13962								
		0								
		0.344627								
		0								
	$\mathbf{u_2^*}$	-2.26861								
		-0.0225								
		-0.34488								
		-0.34514								
		0								
		0.851928								
		0								
	$\mathbf{x_2^*}$	30.16144	WL							
		0.20045	DL							
		0.18424	LLR							
		1.109378	LLF							
		577.579	fy							
		0.907105	t							
		2	ri							

Stellenbosch University http://scholar.sun.ac.za

				Iteration 2: Strong axis shear						
$g(x_2^*)$	**0**									
$g(x_2^*)$wind	-0.065									
$g(x_2^*)$DL	-0.004									
$g(x_2^*)$LLR	-0.013									
$g(x_2^*)$LLF	-0.013									
$g(x_2^*)$fy	0									
$g(x_2^*)$t	0.143									
$g(x_2^* r_i$	0									
D	-0.46588		u_2^*	2.261196		x^*_2	30.16144	$v_{b,0}$	dg/dx	-0.043101
	-0.00798			0.0225			0.20045	DL		-0.399102
	-0.05137			0.183369			0.18424	LLR		-1.411203
	-0.05136			0.187329			1.109378	LLF		-0.234366
	0			-0.03926			577.579	f_y		0
	0.153847			-0.27805			0.936	t		3.055556
	0			0			2	r_i		0
$\mathbf{D}^T$	-0.46588	-0.00798	-0.05137	-0.05136	0	0.153847	0			
						σ_x^e	10.80885		u_x^e	5.720517
			β	**2.248707**			0.02			0.20000
							0.036403			0.17756
							0.219139			1.06833
							17.90065			578.28177
							0.05035			0.95000
	α_2	-0.9392					0.028			2
		-0.01609								
		-0.10357								
		-0.10354								
		0								
		0.310154								
		0								
	u_3^*	-2.11199								
		-0.03619								
		-0.23289								
		-0.23283								
		0								
		0.697446								
		0								
	x_3^*	28.54868	WL							
		0.200724	DL							
		0.186043	LLR							
		1.119349	LLF							
		578.2818	fy							
		0.914884	t							
		2	ri							

Stellenbosch University http://scholar.sun.ac.za

				Iteration 3: Strong axis shear						
$g(x_2^*)$	**0**									
$g(x_2^*)$wind	-0.062									
$g(x_2^*)$DL	-0.002									
$g(x_2^*)$LLR	-0.014									
$g(x_2^*)$LLF	-0.014									
$g(x_2^*)$fy	0									
$g(x_2^*)$t	0.143									
$g(x_2^*r_i$	0									
D	-0.44606		$\mathbf{u_3^*}$	2.108157		$\mathbf{x^*_3}$	28.54868	$v_{b,0}$	dg/dx	-0.043435
	-0.00399			0.036186			0.200724	DL		-0.199279
	-0.05515			0.232727			0.186043	LLR		-1.505031
	-0.05515			0.232691			1.119349	LLF		-0.250145
	0			-2.4E-05			578.2818	f_y		0
	0.157206			-0.67527			0.916	t		3.122271
	0			0			2	r_i		0
$\mathbf{D^T}$	-0.44606	-0.00399	-0.05515	-0.05515	0	0.157206	0			
						σ_x^e	10.2696		u_x^e	6.898751
			β	**2.23703**			0.02			0.20000
							0.036641			0.17752
							0.220455			1.06805
							17.92243			578.28220
							0.05035			0.95000
	α_3	-0.93054					0.028			2
		-0.00831								
		-0.11504								
		-0.11504								
		0								
		0.327956								
		0								
	$\mathbf{u_4^*}$	-2.08165								
		-0.0186								
		-0.25735								
		-0.25735								
		0								
		0.733648								
		0								
	$\mathbf{x_4^*}$	28.27643	WL							
		0.200372	DL							
		0.186945	LLR							
		1.124786	LLF							
		578.2822	fy							
		0.913061	t							
		2	ri							

				Iteration 4: Strong axis shear						
$g(x_2^*)$	**0**									
$g(x_2^*)$wind	-0.062									
$g(x_2^*)$DL	-0.002									
$g(x_2^*)$LLR	-0.014									
$g(x_2^*)$LLF	-0.014									
$g(x_2^*)$fy	0									
$g(x_2^*)$t	0.143									
$g(x_2^*r_i$	0									
D	-0.44629		$\mathbf{u_4^*}$	2.081527		$\mathbf{x^*_4}$	28.27643	$v_{b,0}$	dg/dx	-0.043853
	-0.00399			0.0186			0.200372	DL		-0.199629
	-0.05506			0.257313			0.186945	LLR		-1.497767
	-0.05506			0.257313			1.124786	LLF		-0.248936
	0			-8.8E-12			578.2822	f_y		0
	0.157723			-0.73486			0.913	t		3.13253
	0			0			2	r_i		0
$\mathbf{D^T}$	-0.44629	-0.00399	-0.05506	-0.05506	0	0.157723	0			
						σ_x^e	10.17706		u_x^e	7.092617
			β	**2.237305**			0.02			0.20000
							0.03676			0.17749
							0.221172			1.06788
							17.92244			578.28220
							0.05035			0.95000
	α_4	-0.93032					0.028			2
		-0.00832								
		-0.11477								
		-0.11477								
		0								
		0.328781								
		0								
	$\mathbf{u_5^*}$	-2.0814								
		-0.01862								
		-0.25678								
		-0.25678								
		0								
		0.735583								
		0								
	$\mathbf{x_5^*}$	28.27516	WL							
		0.200372	DL							
		0.186925	LLR							
		1.124667	LLF							
		578.2822	fy							
		0.912963	t							
		2	ri							

Stellenbosch University http://scholar.sun.ac.za

Live load distribution

	Gamma Dist - applied as Log Normal with lower skewness						
			Iteration 1				
	Roof					**Floor**	
x_1*	0.25	kPa			x_1*	1.5	kPa
μ	0.18	kPa			u	1.083	kPa
COV	0.2				COV	0.2	
σ	0.036	kPa			σ	0.2166	kPa
skew	0.4		E17		skew	0.4	
c	0.132557		F17		c	0.132557	
u	1.944444		I17		u	1.925208	
$\Phi_X(x^*)$	0.964349		L17		$\Phi_X(x^*)$	0.963126	
$\Phi_U^{-1}(\Phi_X(x^*))$	1.803556		J17		$\Phi_U^{-1}(\Phi_X(x^*))$	1.788179	
$\varphi_U[\Phi_U^{-1}(\Phi_X(x^*))]$	0.078446				$\varphi_U[\Phi_U^{-1}(\Phi_X(x^*))]$	0.080642	
$\varphi_X(x^*)$	1.740075		K17		$\varphi_X(x^*)$	0.297911	
σ_X^e	0.045082				σ_X^e	0.270693	
μ_X^e	0.17				μ_X^e	1.02	
			Iteration 2				
	Roof					**Floor**	
x_2*	0.18424	kPa			x_2*	1.109378	kPa
μ	0.18	kPa			u	1.083	kPa
COV	0.2				COV	0.2	
σ	0.036	kPa			σ	0.2166	kPa
skew	0.4		E17		skew	0.4	
c	0.132557		F17		c	0.132557	
u	0.117778		I17		u	0.121783	
$\Phi_X(x^*)$	0.572746		L17		$\Phi_X(x^*)$	0.574299	
$\Phi_U^{-1}(\Phi_X(x^*))$	0.183369		J17		$\Phi_U^{-1}(\Phi_X(x^*))$	0.187329	
$\varphi_U[\Phi_U^{-1}(\Phi_X(x^*))]$	0.392291				$\varphi_U[\Phi_U^{-1}(\Phi_X(x^*))]$	0.392003	
$\varphi_X(x^*)$	10.77636		K17		$\varphi_X(x^*)$	1.788836	
σ_X^e	0.036403				σ_X^e	0.219139	
μ_X^e	0.18				μ_X^e	1.07	

Stellenbosch University http://scholar.sun.ac.za

			Iteration 3				
	Roof					**Floor**	
x_3*	0.186044	kPa			x_3*	1.119355	kPa
μ	0.18	kPa			u	1.083	kPa
COV	0.2				COV	0.2	
σ	0.036	kPa			σ	0.2166	kPa
skew	0.4		E17		skew	0.4	
c	0.132557		F17		c	0.132557	
u	0.167878		I17		u	0.167842	
$\Phi_X(x^*)$	0.592023		L17		$\Phi_X(x^*)$	0.59201	
$\Phi_U^{-1}(\Phi_X(x^*))$	0.232753		J17		$\Phi_U^{-1}(\Phi_X(x^*))$	0.232718	
$\varphi_U[\Phi_U^{-1}(\Phi_X(x^*))]$	0.388281				$\varphi_U[\Phi_U^{-1}(\Phi_X(x^*))]$	0.388284	
$\varphi_X(x^*)$	10.59691		K17		$\varphi_X(x^*)$	1.761282	
$\boldsymbol{\sigma_X^e}$	0.036641				$\boldsymbol{\sigma_X^e}$	0.220456	
$\boldsymbol{\mu_X^e}$	0.18				$\boldsymbol{\mu_X^e}$	1.07	
			Iteration 4				
	Roof					**Floor**	
x_4*	0.186945	kPa			x_4*	1.124788	kPa
μ	0.18	kPa			u	1.083	kPa
COV	0.2				COV	0.2	
σ	0.036	kPa			σ	0.2166	kPa
skew	0.4		E17		skew	0.4	
c	0.132557		F17		c	0.132557	
u	0.192927		I17		u	0.192928	
$\Phi_X(x^*)$	0.601536		L17		$\Phi_X(x^*)$	0.601536	
$\Phi_U^{-1}(\Phi_X(x^*))$	0.257324		J17		$\Phi_U^{-1}(\Phi_X(x^*))$	0.257325	
$\varphi_U[\Phi_U^{-1}(\Phi_X(x^*))]$	0.38595				$\varphi_U[\Phi_U^{-1}(\Phi_X(x^*))]$	0.38595	
$\varphi_X(x^*)$	10.4992		K17		$\varphi_X(x^*)$	1.745018	
$\boldsymbol{\sigma_X^e}$	0.03676				$\boldsymbol{\sigma_X^e}$	0.221173	
$\boldsymbol{\mu_X^e}$	0.18				$\boldsymbol{\mu_X^e}$	1.07	

Stellenbosch University http://scholar.sun.ac.za

Wind load distribution

	Gumbel Dist	
	Iteration 1	
x_1*	28	m/s
μ	14.289	m/s
COV	0.37	
σ	5.28693	m/s
c	0.242589	
x_{mod}	11.91049	
$\Phi_X(x^*)$	0.980024	
$\Phi_U^{-1}(\Phi_X(x^*))$	2.054238	
$\varphi_U[\Phi_U^{-1}(\Phi_X(x^*))]$	0.04837	
$\varphi_X(x^*)$	0.004797	
σ_X^e	10.08264	
μ_X^e	7.287851	
	Iteration 2	
x_1*	30.16144	m/s
μ	14.289	m/s
COV	0.37	
σ	5.28693	m/s
c	0.242589	
x_{mod}	11.91049	
$\Phi_X(x^*)$	0.988126	
$\Phi_U^{-1}(\Phi_X(x^*))$	2.261196	
$\varphi_U[\Phi_U^{-1}(\Phi_X(x^*))]$	0.030948	
$\varphi_X(x^*)$	0.002863	
σ_X^e	10.80885	
μ_X^e	5.720517	

	Iteration 3	
x_3*	28.55128	m/s
μ	14.289	m/s
COV	0.37	
σ	5.28693	m/s
c	0.242589	
x_{mod}	11.91049	
$\Phi_X(x^*)$	0.982502	
$\Phi_U^{-1}(\Phi_X(x^*))$	2.10841	
$\varphi_U[\Phi_U^{-1}(\Phi_X(x^*))]$	0.043212	
$\varphi_X(x^*)$	0.004207	
σ_X^e	10.27048	
μ_X^e	6.896895	
	Iteration 4	
x_4*	28.27726	m/s
μ	14.289	m/s
COV	0.37	
σ	5.28693	m/s
c	0.242589	
x_{mod}	11.91049	
$\Phi_X(x^*)$	0.981311	
$\Phi_U^{-1}(\Phi_X(x^*))$	2.081608	
$\varphi_U[\Phi_U^{-1}(\Phi_X(x^*))]$	0.045708	
$\varphi_X(x^*)$	0.004491	
σ_X^e	10.17734	
μ_X^e	7.09203	

Stellenbosch University http://scholar.sun.ac.za

Yield stress distribution

Log - Normal distribution	
	Iteration 1
x_1*	550
μ	578.56
COV	0.031
σ	17.93536
skew	0.09303
c	0.031
u	-1.59239
$\Phi_X(x^*)$	0.052839
$\Phi_U^{-1}(\Phi_X(x^*))$	-1.61793
$\varphi_U[\Phi_U^{-1}(\Phi_X(x^*))]$	0.107767
$\varphi_X(x^*)$	0.006322
σ_X^e	17.04591
μ_X^e	577.579
	Iteration 2
x_2*	577.579
μ	578.56
COV	0.031
σ	17.93536
skew	0.09303
c	0.031
u	-0.05469
$\Phi_X(x^*)$	0.484343
$\Phi_U^{-1}(\Phi_X(x^*))$	-0.03926
$\varphi_U[\Phi_U^{-1}(\Phi_X(x^*))]$	0.398635
$\varphi_X(x^*)$	0.022269
σ_X^e	17.90065
μ_X^e	578.2818

	Iteration 3
x_3*	578.2818
μ	578.56
COV	0.031
σ	17.93536
skew	0.09303
c	0.031
u	-0.01551
$\Phi_X(x^*)$	0.49999
$\Phi_U^{-1}(\Phi_X(x^*))$	-2.4E-05
$\varphi_U[\Phi_U^{-1}(\Phi_X(x^*))]$	0.398942
$\varphi_X(x^*)$	0.022259
σ_X^e	17.92243
μ_X^e	578.2822
	Iteration 4
x_4*	578.2822
μ	578.56
COV	0.031
σ	17.93536
skew	0.09303
c	0.031
u	-0.01549
$\Phi_X(x^*)$	0.5
$\Phi_U^{-1}(\Phi_X(x^*))$	-8.8E-12
$\varphi_U[\Phi_U^{-1}(\Phi_X(x^*))]$	0.398942
$\varphi_X(x^*)$	0.022259
σ_X^e	17.92244
μ_X^e	578.2822

Stellenbosch University http://scholar.sun.ac.za

FORM – Weak axis shear

				Iteration 1: Weak axis shear						
$g(x_2^*)$	**0**									
$g(x_2^*)$wind	-0.093									
$g(x_2^*)$DL	0									
$g(x_2^*)$LLR	-0.004									
$g(x_2^*)$LLF	-0.004									
$g(x_2^*)$fy	0									
$g(x_2^*)$t	0.141									
$g(x_2^* r_i$	0									
D	-0.66978		**u_1^***	2.054238		**x^*_1**	28	$v_{b,0}$	dg/dx	-0.066429
	0			0			0.2	DL		0
	-0.01443			1.803556			0.25	LLR		-0.32
	-0.01444			1.788179			1.5	LLF		-0.053333
	0			-1.61793			550	f_y		0
	0.189543			-3.99007			0.7491	t		3.764517
	0			0			2	r_i		0
D^T	-0.66978	0	-0.01443	-0.01444	0	0.189543	0			
						σ_x^e	10.08264		**u_x^e**	7.287851
			β	**3.136233**			0.02			0.20000
							0.045082			0.16869
							0.270693			1.01595
							17.04591			577.57904
							0.05035			0.95000
	α_1	-0.9618					0.028			2
		0								
		-0.02072								
		-0.02073								
		0								
		0.272185								
		0								
	u_2^*	-3.01642								
		0								
		-0.06497								
		-0.06502								
		0								
		0.853634								
		0								
	x_2^*	37.70139	WL							
		0.2	DL							
		0.171621	LLR							
		1.033552	LLF							
		577.579	fy							
		0.90702	t							
		2	ri							

				Iteration 2: Weak axis shear						
$g(x_2^*)$	**0**									
$g(x_2^*)$wind	-0.09									
$g(x_2^*)$DL	0									
$g(x_2^*)$LLR	-0.002									
$g(x_2^*)$LLF	-0.002									
$g(x_2^*)$fy	0									
$g(x_2^*)$t	0.148									
$g(x_2^* r_i$	0									
D	-0.62697		$\mathbf{u_2^*}$	2.891678		$\mathbf{x^*_2}$	37.70139	$v_{b,0}$	dg/dx	-0.047744
	0			0			0.2	DL		0
	-0.0081			-0.17145			0.171621	LLR		-0.233071
	-0.00809			-0.16684			1.033552	LLF		-0.038701
	0			-0.03926			577.579	f_y		0
	0.166242			-1.06256			0.8965	t		3.301729
	0			0			2	r_i		0
$\mathbf{D^T}$	-0.62697	0	-0.0081	-0.00809	0	0.166242	0			
						σ_x^e	13.13194		u_x^e	-0.271969
			β	**3.062723**			0.02			0.20000
							0.034738			0.17758
							0.209131			1.06844
							17.90065			578.28177
							0.05035			0.95000
	α_2	-0.96645					0.028			2
		0								
		-0.01248								
		-0.01248								
		0								
		0.256257								
		0								
	$\mathbf{u_3^*}$	-2.95996								
		0								
		-0.03822								
		-0.03821								
		0								
		0.784843								
		0								
	$\mathbf{x_3^*}$	38.59808	WL							
		0.2	DL							
		0.178905	LLR							
		1.076435	LLF							
		578.2818	fy							
		0.910483	t							
		2	ri							

				Iteration 3: Weak axis shear						
$g(x_2^*)$	**0**									
$g(x_2^*)$wind	-0.099									
$g(x_2^*)$DL	0									
$g(x_2^*)$LLR	-0.002									
$g(x_2^*)$LLF	-0.002									
$g(x_2^*)$fy	0									
$g(x_2^*)$t	0.142									
$g(x_2^* r_i$	0									
D	-0.68678		$\mathbf{u_3^*}$	2.959302		$\mathbf{x^*_3}$	38.59808	$v_{b,0}$	dg/dx	-0.051298
	0			0			0.2	DL		0
	-0.00798			0.035375			0.178905	LLR		-0.223583
	-0.00798			0.035485			1.076435	LLF		-0.03716
	0			-2.4E-05			578.2818	f_y		0
	0.157067			-0.78649			0.9104	t		3.119508
	0			0			2	r_i		0
$\mathbf{D^T}$	-0.68678	0	-0.00798	-0.00798	0	0.157067	0			
						σ_x^e	13.3881		u_x^e	-1.021367
			β	**3.060575**			0.02			0.20000
							0.035699			0.17764
							0.214791			1.06881
							17.92243			578.28220
							0.05035			0.95000
	α_3	-0.97471					0.028			2
		0								
		-0.01133								
		-0.01133								
		0								
		0.222916								
		0								
	$\mathbf{u_4^*}$	-2.98316								
		0								
		-0.03467								
		-0.03467								
		0								
		0.68225								
		0								
	$\mathbf{x_4^*}$	38.9175	WL							
		0.2	DL							
		0.17888	LLR							
		1.076259	LLF							
		578.2822	fy							
		0.915649	t							
		2	ri							

				Iteration 4: Weak axis shear						
$g(x_2^*)$	**0**									
$g(x_2^*)$wind	-0.099									
$g(x_2^*)$DL	0									
$g(x_2^*)$LLR	-0.001									
$g(x_2^*)$LLF	-0.001									
$g(x_2^*)$fy	0									
$g(x_2^*)$t	0.141									
$g(x_2^*r_i$	0									
D	-0.68574		u_4^*	2.98308		x^*_4	38.9175	$v_{b,0}$	dg/dx	-0.050877
	0			0			0.2	DL		0
	-0.00399			0.03467			0.17888	LLR		-0.111807
	-0.00399			0.034669			1.076259	LLF		-0.018583
	0			-8.8E-12			578.2822	f_y		0
	0.155126			-0.68918			0.9153	t		3.080957
	0			0			2	r_i		0
$\mathbf{D}^T$	-0.68574	0	-0.00399	-0.00399	0	0.155126	0			
						σ_x^e	13.47841		u_x^e	-1.289688
			β	**3.061918**			0.02			0.20000
							0.035695			0.17764
							0.214768			1.06881
							17.92244			578.28220
							0.05035			0.95000
	α_4	-0.97532					0.028			2
		0								
		-0.00568								
		-0.00568								
		0								
		0.220635								
		0								
	u_5^*	-2.98636								
		0								
		-0.01738								
		-0.01738								
		0								
		0.675567								
		0								
	x_5^*	38.9617	WL							
		0.2	DL							
		0.178263	LLR							
		1.072546	LLF							
		578.2822	fy							
		0.915985	t							
		2	ri							

Stellenbosch University http://scholar.sun.ac.za

Live load distribution

	Gamma Dist - applied as Log Normal with lower skewness						
			Iteration 1				
	Roof					**Floor**	
x_1^*	0.25	kPa			x_1^*	1.5	kPa
μ	0.18	kPa			u	1.083	kPa
COV	0.2				COV	0.2	
σ	0.036	kPa			σ	0.2166	kPa
skew	0.4		E17		skew	0.4	
c	0.132557		F17		c	0.132557	
u	1.944444		I17		u	1.925208	
$\Phi_X(x^*)$	0.964349		L17		$\Phi_X(x^*)$	0.963126	
$\Phi_U^{-1}(\Phi_X(x^*))$	1.803556		J17		$\Phi_U^{-1}(\Phi_X(x^*))$	1.788179	
$\varphi_U[\Phi_U^{-1}(\Phi_X(x^*))]$	0.078446				$\varphi_U[\Phi_U^{-1}(\Phi_X(x^*))]$	0.080642	
$\varphi_X(x^*)$	1.740075		K17		$\varphi_X(x^*)$	0.297911	
$\boldsymbol{\sigma_X^e}$	0.045082				$\boldsymbol{\sigma_X^e}$	0.270693	
$\boldsymbol{\mu_X^e}$	0.17				$\boldsymbol{\mu_X^e}$	1.02	
			Iteration 2				
	Roof					**Floor**	
x_2^*	0.171621	kPa			x_2^*	1.033552	kPa
μ	0.18	kPa			u	1.083	kPa
COV	0.2				COV	0.2	
σ	0.036	kPa			σ	0.2166	kPa
skew	0.4		E17		skew	0.4	
c	0.132557		F17		c	0.132557	
u	-0.232745		I17		u	-0.22829	
$\Phi_X(x^*)$	0.431933		L17		$\Phi_X(x^*)$	0.433749	
$\Phi_U^{-1}(\Phi_X(x^*))$	-0.171454		J17		$\Phi_U^{-1}(\Phi_X(x^*))$	-0.16684	
$\varphi_U[\Phi_U^{-1}(\Phi_X(x^*))]$	0.393121				$\varphi_U[\Phi_U^{-1}(\Phi_X(x^*))]$	0.393428	
$\varphi_X(x^*)$	11.31691		K17		$\varphi_X(x^*)$	1.88125	
$\boldsymbol{\sigma_X^e}$	0.034738				$\boldsymbol{\sigma_X^e}$	0.209131	
$\boldsymbol{\mu_X^e}$	0.18				$\boldsymbol{\mu_X^e}$	1.07	

Stellenbosch University http://scholar.sun.ac.za

			Iteration 3			
	Roof				**Floor**	
x_3*	0.178905	kPa		x_3*	1.076435	kPa
μ	0.18	kPa		u	1.083	kPa
COV	0.2			COV	0.2	
σ	0.036	kPa		σ	0.2166	kPa
skew	0.4		E17	skew	0.4	
c	0.132557		F17	c	0.132557	
u	-0.030421		I17	u	-0.03031	
$\Phi_X(x^*)$	0.514109		L17	$\Phi_X(x^*)$	0.514154	
$\Phi_U^{-1}(\Phi_X(x^*))$	0.035375		J17	$\Phi_U^{-1}(\Phi_X(x^*))$	0.035485	
$\varphi_U[\Phi_U^{-1}(\Phi_X(x^*))]$	0.398693			$\varphi_U[\Phi_U^{-1}(\Phi_X(x^*))]$	0.398691	
$\varphi_X(x^*)$	11.16824		K17	$\varphi_X(x^*)$	1.856182	
$\boldsymbol{\sigma_X^e}$	0.035699			$\boldsymbol{\sigma_X^e}$	0.214791	
$\boldsymbol{\mu_X^e}$	0.18			$\boldsymbol{\mu_X^e}$	1.07	
			Iteration 4			
	Roof				**Floor**	
x_4*	0.17888	kPa		x_4*	1.076259	kPa
μ	0.18	kPa		u	1.083	kPa
COV	0.2			COV	0.2	
σ	0.036	kPa		σ	0.2166	kPa
skew	0.4		E17	skew	0.4	
c	0.132557		F17	c	0.132557	
u	-0.03112		I17	u	-0.03112	
$\Phi_X(x^*)$	0.513828		L17	$\Phi_X(x^*)$	0.513828	
$\Phi_U^{-1}(\Phi_X(x^*))$	0.03467		J17	$\Phi_U^{-1}(\Phi_X(x^*))$	0.034669	
$\varphi_U[\Phi_U^{-1}(\Phi_X(x^*))]$	0.398703			$\varphi_U[\Phi_U^{-1}(\Phi_X(x^*))]$	0.398703	
$\varphi_X(x^*)$	11.16955		K17	$\varphi_X(x^*)$	1.856435	
$\boldsymbol{\sigma_X^e}$	0.035695			$\boldsymbol{\sigma_X^e}$	0.214768	
$\boldsymbol{\mu_X^e}$	0.18			$\boldsymbol{\mu_X^e}$	1.07	

Stellenbosch University http://scholar.sun.ac.za

Wind load distribution

	Gumbel Dist	
	Iteration 1	
x_1*	28	m/s
μ	14.289	m/s
COV	0.37	
σ	5.28693	m/s
c	0.242589	
x_{mod}	11.91049	
$\Phi_X(x^*)$	0.980024	
$\Phi_U^{-1}(\Phi_X(x^*))$	2.054238	
$\varphi_U[\Phi_U^{-1}(\Phi_X(x^*))]$	0.04837	
$\varphi_X(x^*)$	0.004797	
$\boldsymbol{\sigma_X^e}$	10.08264	
$\boldsymbol{\mu_X^e}$	7.287851	
	Iteration 2	
x_1*	37.70139	m/s
μ	14.289	m/s
COV	0.37	
σ	5.28693	m/s
c	0.242589	
x_{mod}	11.91049	
$\Phi_X(x^*)$	0.998084	
$\Phi_U^{-1}(\Phi_X(x^*))$	2.891678	
$\varphi_U[\Phi_U^{-1}(\Phi_X(x^*))]$	0.006098	
$\varphi_X(x^*)$	0.000464	
$\boldsymbol{\sigma_X^e}$	13.13194	
$\boldsymbol{\mu_X^e}$	-0.27197	

	Iteration 3	
x_3*	38.59808	m/s
μ	14.289	m/s
COV	0.37	
σ	5.28693	m/s
c	0.242589	
x_{mod}	11.91049	
$\Phi_X(x^*)$	0.998458	
$\Phi_U^{-1}(\Phi_X(x^*))$	2.959302	
$\varphi_U[\Phi_U^{-1}(\Phi_X(x^*))]$	0.005003	
$\varphi_X(x^*)$	0.000374	
$\boldsymbol{\sigma_X^e}$	13.3881	
$\boldsymbol{\mu_X^e}$	-1.02137	
	Iteration 4	
x_4*	38.9175	m/s
μ	14.289	m/s
COV	0.37	
σ	5.28693	m/s
c	0.242589	
x_{mod}	11.91049	
$\Phi_X(x^*)$	0.998573	
$\Phi_U^{-1}(\Phi_X(x^*))$	2.98308	
$\varphi_U[\Phi_U^{-1}(\Phi_X(x^*))]$	0.004662	
$\varphi_X(x^*)$	0.000346	
$\boldsymbol{\sigma_X^e}$	13.47841	
$\boldsymbol{\mu_X^e}$	-1.28969	

Stellenbosch University http://scholar.sun.ac.za

Yield stress distribution

Log - Normal distribution					
	Iteration 1			**Iteration 3**	
x_1^*	550		x_3^*	578.2818	
μ	578.56		μ	578.56	
COV	0.031		COV	0.031	
σ	17.93536		σ	17.93536	
skew	0.09303		skew	0.09303	
c	0.031		c	0.031	
u	-1.59239		u	-0.01551	
$\Phi_X(x^*)$	0.052839		$\Phi_X(x^*)$	0.49999	
$\Phi_U^{-1}(\Phi_X(x^*))$	-1.61793		$\Phi_U^{-1}(\Phi_X(x^*))$	-2.4E-05	
$\varphi_U[\Phi_U^{-1}(\Phi_X(x^*))]$	0.107767		$\varphi_U[\Phi_U^{-1}(\Phi_X(x^*))]$	0.398942	
$\varphi_X(x^*)$	0.006322		$\varphi_X(x^*)$	0.022259	
$\boldsymbol{\sigma_X^e}$	17.04591		$\boldsymbol{\sigma_X^e}$	17.92243	
$\boldsymbol{\mu_X^e}$	577.579		$\boldsymbol{\mu_X^e}$	578.2822	
	Iteration 2			**Iteration 4**	
x_2^*	577.579		x_4^*	578.2822	
μ	578.56		μ	578.56	
COV	0.031		COV	0.031	
σ	17.93536		σ	17.93536	
skew	0.09303		skew	0.09303	
c	0.031		c	0.031	
u	-0.05469		u	-0.01549	
$\Phi_X(x^*)$	0.484343		$\Phi_X(x^*)$	0.5	
$\Phi_U^{-1}(\Phi_X(x^*))$	-0.03926		$\Phi_U^{-1}(\Phi_X(x^*))$	-8.8E-12	
$\varphi_U[\Phi_U^{-1}(\Phi_X(x^*))]$	0.398635		$\varphi_U[\Phi_U^{-1}(\Phi_X(x^*))]$	0.398942	
$\varphi_X(x^*)$	0.022269		$\varphi_X(x^*)$	0.022259	
$\boldsymbol{\sigma_X^e}$	17.90065		$\boldsymbol{\sigma_X^e}$	17.92244	
$\boldsymbol{\mu_X^e}$	578.2818		$\boldsymbol{\mu_X^e}$	578.2822	

Stellenbosch University http://scholar.sun.ac.za

FORM – Tension

				Iteration 1: Tension					
$g(x_2^*)$	**0**								
$g(x_2^*)$wind	-0.104								
$g(x_2^*)$DL	0								
$g(x_2^*)$LLR	0.001								
$g(x_2^*)$LLF	0.001								
$g(x_2^*)$fy	0.05								
$g(x_2^*)$t	0.038								
$g(x_2^*r_i$	0								
D	-0.749		u_1^*	2.054238		x^*_1	28	$v_{b,0}$	dg/dx	-0.074286
	0			0			0.2	DL		0
	0.003607			1.803556			0.25	LLR		0.08
	0.003609			1.788179			1.5	LLF		0.013333
	0.030993			-1.61793			550	f_u		0.001818
	0.043733			-1.48957			0.875	t		0.868571
	0			0			2	r_i		0
$\mathbf{D}^T$	-0.749	0	0.003607	0.003609	0.0309926	0.043733	0			
						σ_x^e	10.08264		u_x^e	7.287851
			β	**2.185219**			0.02			0.20000
							0.045082			0.16869
							0.270693			1.01595
							17.04591			577.57904
							0.05035			0.95000
	α_1	-0.99743					0.028			2
		0								
		0.004803								
		0.004806								
		0.041272								
		0.058238								
		0								
	u_2^*	-2.17959								
		0								
		0.010495								
		0.010503								
		0.090189								
		0.127263								
		0								
	x_2^*	29.26392	WL							
		0.2	DL							
		0.168219	LLR							
		1.013109	LLF							
		576.0417	fy							
		0.943592	t							
		2	ri							

Stellenbosch University http://scholar.sun.ac.za

				Iteration 2: Tension						
$g(x_2^*)$	**0**									
$g(x_2^*)$wind	-0.103									
$g(x_2^*)$DL	0									
$g(x_2^*)$LLR	0.001									
$g(x_2^*)$LLF	0.001									
$g(x_2^*)$fy	0.05									
$g(x_2^*)$t	0.037									
$g(x_2^* r_i$	0									
D	-0.73988		u_2^*	2.176997		x^*_2	29.26392	$v_{b,0}$	dg/dx	-0.070394
	0			0			0.2	DL		0
	0.004077			-0.27003			0.168219	LLR		0.118893
	0.004075			-0.26523			1.013109	LLF		0.019741
	0.030993			-0.12525			576.0417	f_u		0.001736
	0.039977			-0.3575			0.932	t		0.793991
	0			0			2	r_i		0
$\mathbf{D}^T$	-0.73988	0	0.004077	0.004075	0.0309926	0.039977	0			
						σ_x^e	10.51065		u_x^e	6.382269
			β	**2.199308**			0.02			0.20000
							0.034288			0.17748
							0.206433			1.06786
							17.853			578.27786
							0.05035			0.95000
	α_2	-0.99764					0.028			2
		0								
		0.005497								
		0.005495								
		0.04179								
		0.053905								
		0								
	u_3^*	-2.19412								
		0								
		0.012089								
		0.012085								
		0.091908								
		0.118553								
		0								
	x_3^*	29.4439	WL							
		0.2	DL							
		0.177063	LLR							
		1.065366	LLF							
		576.637	fy							
		0.944031	t							
		2	ri							

Stellenbosch University http://scholar.sun.ac.za

				Iteration 3: Tension						
$g(x_2^*)$	**0**									
$g(x_2^*)$wind	-0.104									
$g(x_2^*)$DL	0									
$g(x_2^*)$LLR	0									
$g(x_2^*)$LLF	0									
$g(x_2^*)$fy	0.05									
$g(x_2^*)$t	0.036									
$g(x_2^* r_i$	0									
D	-0.74675		u_3^*	2.194071		x^*_3	29.4439	$v_{b,0}$	dg/dx	-0.070643
	0			0			0.2	DL		0
	0			-0.01638			0.177063	LLR		0
	0			-0.01622			1.065366	LLF		0
	0.030993			-0.09193			576.637	f_u		0.001734
	0.038281			-0.05958			0.947	t		0.760296
	0			0			2	r_i		0
$\mathbf{D}^T$	-0.74675	0	0	0	0.0309926	0.038281	0			
						σ_x^e	10.57083		u_x^e	6.250748
			β	**2.196169**			0.02			0.20000
							0.035456			0.17764
							0.21333			1.06883
							17.87146			578.27986
							0.05035			0.95000
	α_3	-0.99783					0.028			2
		0								
		0								
		0								
		0.041413								
		0.051152								
		0								
	u_4^*	-2.19141								
		0								
		0								
		0								
		0.09095								
		0.112338								
		0								
	x_4^*	29.41574	WL							
		0.2	DL							
		0.177644	LLR							
		1.068827	LLF							
		576.6544	fy							
		0.944344	t							
		2	ri							

				Iteration 4: Tension						
$g(x_2^*)$	**0**									
$g(x_2^*)$wind	-0.103									
$g(x_2^*)$DL	0									
$g(x_2^*)$LLR	0.001									
$g(x_2^*)$LLF	0.001									
$g(x_2^*)$fy	0.05									
$g(x_2^*)$t	0.036									
$g(x_2^* r_i$	0									
D	-0.73962		u_4^*	2.191406		x^*_4	29.41574	$v_{b,0}$	dg/dx	-0.070031
	0			0			0.2	DL		0
	0.004			-1.8E-05			0.177644	LLR		0.112585
	0.004			-1.7E-05			1.068827	LLF		0.018712
	0.030993			-0.09095			576.6544	f_u		0.001734
	0.038362			-0.0993			0.945	t		0.761905
	0			0			2	r_i		0
D^T	-0.73962	0	0.004	0.004	0.0309926	0.038362	0			
						σ_x^e	10.56142		u_x^e	6.271366
			β	**2.195429**			0.02			0.20000
							0.035532			0.17764
							0.213787			1.06883
							17.872			578.27991
							0.05035			0.95000
	α_4	-0.99776					0.028			2
		0								
		0.005397								
		0.005397								
		0.041809								
		0.05175								
		0								
	u_5^*	-2.1905								
		0								
		0.011848								
		0.011848								
		0.091789								
		0.113614								
		0								
	x_5^*	29.40618	WL							
		0.2	DL							
		0.177224	LLR							
		1.066298	LLF							
		576.6395	fy							
		0.94428	t							
		2	ri							

Stellenbosch University http://scholar.sun.ac.za

Live load distribution

	Gamma Dist - applied as Log Normal with lower skewness					
			Iteration 1			
	Roof				**Floor**	
x_1*	0.25	kPa		x_1*	1.5	kPa
μ	0.18	kPa		u	1.083	kPa
COV	0.2			COV	0.2	
σ	0.036	kPa		σ	0.2166	kPa
skew	0.4			skew	0.4	
c	0.132557			c	0.132557	
u	1.944444			u	1.925208	
$\Phi_X(x^*)$	0.964349			$\Phi_X(x^*)$	0.963126	
$\Phi_U^{-1}(\Phi_X(x^*))$	1.803556			$\Phi_U^{-1}(\Phi_X(x^*))$	1.788179	
$\varphi_U[\Phi_U^{-1}(\Phi_X(x^*))]$	0.078446			$\varphi_U[\Phi_U^{-1}(\Phi_X(x^*))]$	0.080642	
$\varphi_X(x^*)$	1.740075			$\varphi_X(x^*)$	0.297911	
σ_X^e	0.045082			σ_X^e	0.270693	
μ_X^e	0.17			μ_X^e	1.02	
			Iteration 2			
	Roof				**Floor**	
x_2*	0.168219	kPa		x_2*	1.013109	kPa
μ	0.18	kPa		u	1.083	kPa
COV	0.2			COV	0.2	
σ	0.036	kPa		σ	0.2166	kPa
skew	0.4			skew	0.4	
c	0.132557			c	0.132557	
u	-0.327249			u	-0.32267	
$\Phi_X(x^*)$	0.393568			$\Phi_X(x^*)$	0.395417	
$\Phi_U^{-1}(\Phi_X(x^*))$	-0.270031			$\Phi_U^{-1}(\Phi_X(x^*))$	-0.26523	
$\varphi_U[\Phi_U^{-1}(\Phi_X(x^*))]$	0.384659			$\varphi_U[\Phi_U^{-1}(\Phi_X(x^*))]$	0.385154	
$\varphi_X(x^*)$	11.21832			$\varphi_X(x^*)$	1.865757	
σ_X^e	0.034288			σ_X^e	0.206433	
μ_X^e	0.18			μ_X^e	1.07	

Stellenbosch University http://scholar.sun.ac.za

			Iteration 3			
	Roof				**Floor**	
x_3*	0.177063	kPa		x_3*	1.065366	kPa
μ	0.18	kPa		u	1.083	kPa
COV	0.2			COV	0.2	
σ	0.036	kPa		σ	0.2166	kPa
skew	0.4			skew	0.4	
c	0.132557			c	0.132557	
u	-0.08157			u	-0.08141	
$\Phi_X(x^*)$	0.493465			$\Phi_X(x^*)$	0.493529	
$\Phi_U^{-1}(\Phi_X(x^*))$	-0.016383			$\Phi_U^{-1}(\Phi_X(x^*))$	-0.01622	
$\varphi_U[\Phi_U^{-1}(\Phi_X(x^*))]$	0.398889			$\varphi_U[\Phi_U^{-1}(\Phi_X(x^*))]$	0.39889	
$\varphi_X(x^*)$	11.25032			$\varphi_X(x^*)$	1.869824	
$\boldsymbol{\sigma_X^e}$	0.035456			$\boldsymbol{\sigma_X^e}$	0.21333	
$\boldsymbol{\mu_X^e}$	0.18			$\boldsymbol{\mu_X^e}$	1.07	
			Iteration 4			
	Roof				**Floor**	
x_4*	0.177644	kPa		x_4*	1.068827	kPa
μ	0.18	kPa		u	1.083	kPa
COV	0.2			COV	0.2	
σ	0.036	kPa		σ	0.2166	kPa
skew	0.4			skew	0.4	
c	0.132557			c	0.132557	
u	-0.065435			u	-0.06543	
$\Phi_X(x^*)$	0.499993			$\Phi_X(x^*)$	0.499993	
$\Phi_U^{-1}(\Phi_X(x^*))$	-1.77E-05			$\Phi_U^{-1}(\Phi_X(x^*))$	-1.7E-05	
$\varphi_U[\Phi_U^{-1}(\Phi_X(x^*))]$	0.398942			$\varphi_U[\Phi_U^{-1}(\Phi_X(x^*))]$	0.398942	
$\varphi_X(x^*)$	11.22755			$\varphi_X(x^*)$	1.866075	
$\boldsymbol{\sigma_X^e}$	0.035532			$\boldsymbol{\sigma_X^e}$	0.213787	
$\boldsymbol{\mu_X^e}$	0.18			$\boldsymbol{\mu_X^e}$	1.07	

Stellenbosch University http://scholar.sun.ac.za

Wind load distribution

	Gumbel Dist	
	Iteration 1	
x_1*	28	m/s
μ	14.289	m/s
COV	0.37	
σ	5.28693	m/s
c	0.242589	
x_{mod}	11.91049	
$\Phi_X(x^*)$	0.980024	
$\Phi_U^{-1}(\Phi_X(x^*))$	2.054238	
$\varphi_U[\Phi_U^{-1}(\Phi_X(x^*))]$	0.04837	
$\varphi_X(x^*)$	0.004797	
$\boldsymbol{\sigma_X^e}$	10.08264	
$\boldsymbol{\mu_X^e}$	7.287851	
	Iteration 2	
x_1*	29.26392	m/s
μ	14.289	m/s
COV	0.37	
σ	5.28693	m/s
c	0.242589	
x_{mod}	11.91049	
$\Phi_X(x^*)$	0.98526	
$\Phi_U^{-1}(\Phi_X(x^*))$	2.176997	
$\varphi_U[\Phi_U^{-1}(\Phi_X(x^*))]$	0.037306	
$\varphi_X(x^*)$	0.003549	
$\boldsymbol{\sigma_X^e}$	10.51065	
$\boldsymbol{\mu_X^e}$	6.382269	

	Iteration 3	
x_3*	29.4439	m/s
μ	14.289	m/s
COV	0.37	
σ	5.28693	m/s
c	0.242589	
x_{mod}	11.91049	
$\Phi_X(x^*)$	0.985885	
$\Phi_U^{-1}(\Phi_X(x^*))$	2.194071	
$\varphi_U[\Phi_U^{-1}(\Phi_X(x^*))]$	0.03594	
$\varphi_X(x^*)$	0.0034	
$\boldsymbol{\sigma_X^e}$	10.57083	
$\boldsymbol{\mu_X^e}$	6.250748	
	Iteration 4	
x_4*	29.41574	m/s
μ	14.289	m/s
COV	0.37	
σ	5.28693	m/s
c	0.242589	
x_{mod}	11.91049	
$\Phi_X(x^*)$	0.985789	
$\Phi_U^{-1}(\Phi_X(x^*))$	2.191406	
$\varphi_U[\Phi_U^{-1}(\Phi_X(x^*))]$	0.03615	
$\varphi_X(x^*)$	0.003423	
$\boldsymbol{\sigma_X^e}$	10.56142	
$\boldsymbol{\mu_X^e}$	6.271366	

Stellenbosch University http://scholar.sun.ac.za

Yield stress distribution

Log - Normal distribution		
	Iteration 1	
x_1*	550	
μ	578.56	
COV	0.031	
σ	17.93536	
skew	0.09303	
c	0.031	
u	-1.59239	
$\Phi_X(x^*)$	0.052839	
$\Phi_U^{-1}(\Phi_X(x^*))$	-1.61793	
$\varphi_U[\Phi_U^{-1}(\Phi_X(x^*))]$	0.107767	
$\varphi_X(x^*)$	0.006322	
σ_X^e	17.04591	
μ_X^e	577.579	
	Iteration 2	
x_2*	576.0417	
μ	578.56	
COV	0.031	
σ	17.93536	
skew	0.09303	
c	0.031	
u	-0.14041	
$\Phi_X(x^*)$	0.450161	
$\Phi_U^{-1}(\Phi_X(x^*))$	-0.12525	
$\varphi_U[\Phi_U^{-1}(\Phi_X(x^*))]$	0.395825	
$\varphi_X(x^*)$	0.022171	
σ_X^e	17.853	
μ_X^e	578.2779	

	Iteration 3	
x_3*	576.637	
μ	578.56	
COV	0.031	
σ	17.93536	
skew	0.09303	
c	0.031	
u	-0.10722	
$\Phi_X(x^*)$	0.463379	
$\Phi_U^{-1}(\Phi_X(x^*))$	-0.09193	
$\varphi_U[\Phi_U^{-1}(\Phi_X(x^*))]$	0.39726	
$\varphi_X(x^*)$	0.022229	
σ_X^e	17.87146	
μ_X^e	578.2799	
	Iteration 4	
x_4*	576.6544	
μ	578.56	
COV	0.031	
σ	17.93536	
skew	0.09303	
c	0.031	
u	-0.10625	
$\Phi_X(x^*)$	0.463766	
$\Phi_U^{-1}(\Phi_X(x^*))$	-0.09095	
$\varphi_U[\Phi_U^{-1}(\Phi_X(x^*))]$	0.397296	
$\varphi_X(x^*)$	0.02223	
σ_X^e	17.872	
μ_X^e	578.2799	

Stellenbosch University http://scholar.sun.ac.za

FORM – Axial and bending interaction

				Iteration 1: Interaction						
$g(x_2^*)$	**0**									
$g(x_2^*)$wind	-0.121	1.05								
$g(x_2^*)$DL	0	1.05								
$g(x_2^*)$LLR	0	1.05								
$g(x_2^*)$LLF	0	1.05								
$g(x_2^*)$fy	0.029	0.95								
$g(x_2^*)$t	0.063	0.95								
$g(x_2^* r_i$	0	0.95								
D	-0.87143		$\mathbf{u_1^*}$	2.054238		$\mathbf{x^*_1}$	28	$v_{b,0}$	dg/dx	-0.086429
	0			0			0.2	DL		0
	0			1.803556			0.25	LLR		0
	0			1.788179			1.5	LLF		0
	0.017976			-1.61793			550	f_y		0.001055
	0.06678			0			0.95	t		1.326316
	0			0			2	r_i		0
$\mathbf{D^T}$	-0.87143	0	0	0	0.0179757	0.06678	0			
						σ_x^e	10.08264		u_x^e	7.287851
			β	**2.081069**			0.02			0.20000
							0.045082			0.16869
							0.270693			1.01595
							17.04591			577.57904
							0.05035			0.95000
	α_1	-0.99687					0.028			2
		0								
		0								
		0								
		0.020563								
		0.076393								
		0								
	$\mathbf{u_2^*}$	-2.07455								
		0								
		0								
		0								
		0.042793								
		0.158978								
		0								
	$\mathbf{x_2^*}$	28.20476	WL							
		0.2	DL							
		0.168692	LLR							
		1.015952	LLF							
		576.8496	fy							
		0.941995	t							
		2	ri							

Stellenbosch University http://scholar.sun.ac.za

				Iteration 2: Interaction						
$g(x_2^*)$	**0**									
$g(x_2^*)$wind	-0.116									
$g(x_2^*)$DL	0									
$g(x_2^*)$LLR	0									
$g(x_2^*)$LLF	0									
$g(x_2^*)$fy	0.025									
$g(x_2^*)$t	0.061									
$g(x_2^* r_i$	0									
D	-0.83542		u_2^*	2.054238		x^*_2	28	$v_{b,0}$	dg/dx	-0.082857
	0			0			0.2	DL		0
	0			-0.25624			0.168692	LLR		0
	0			-0.25147			1.015952	LLF		0
	0.015496			-0.08003			576.8496	f_y		0.000867
	0.065209			-0.15898			0.941995	t		1.295123
	0			0			2	r_i		0
D^T	-0.83542	0	0	0	0.0154963	0.065209	0			
						σ_x^e	10.08264		u_x^e	7.287851
			β	**2.061508**			0.02			0.20000
							0.034351			0.17749
							0.206808			1.06796
							17.87804			578.28043
							0.05035			0.95000
	α_2	-0.9968					0.028			2
		0								
		0								
		0								
		0.01849								
		0.077806								
		0								
	u_3^*	-2.0549								
		0								
		0								
		0								
		0.038117								
		0.160398								
		0								
	x_3^*	28.00672	WL							
		0.2	DL							
		0.177494	LLR							
		1.067958	LLF							
		577.599	fy							
		0.941924	t							
		2	ri							

Iteration 3: Interaction

$g(x_2^*)$	**0**									
$g(x_2^*)$wind	-0.122									
$g(x_2^*)$DL	0									
$g(x_2^*)$LLR	0									
$g(x_2^*)$LLF	0									
$g(x_2^*)$fy	0.038									
$g(x_2^*)$t	0.074									
$g(x_2^* r_i$	0									
D	-0.87798		u_3^*	2.093644		x^*_3	28.4	$v_{b,0}$	dg/dx	-0.085915
	0			0			0.2	DL		0
	0			-0.00424			0.177494	LLR		0
	0			-0.00408			1.067958	LLF		0
	0.023554			-0.03814			577.599	f_y		0.001316
	0.079113			-0.1604			0.941924	t		1.571252
	0			0			2	r_i		0
D^T	-0.87798	0	0	0	0.0235543	0.079113	0			
						σ_x^e	10.21911		u_x^e	7.004818
			β	**2.09986**			0.02			0.20000
							0.035513			0.17764
							0.213672			1.06883
							17.90127			578.28180
							0.05035			0.95000
	α_3	-0.99561					0.028			2
		0								
		0								
		0								
		0.02671								
		0.089712								
		0								
	u_4^*	-2.09064								
		0								
		0								
		0								
		0.056087								
		0.188382								
		0								
	x_4^*	28.36931	WL							
		0.2	DL							
		0.177645	LLR							
		1.06883	LLF							
		577.2778	fy							
		0.940515	t							
		2	ri							

				Iteration 4: Interaction						
$g(x_2^*)$	**0**									
$g(x_2^*)$wind	-0.12									
$g(x_2^*)$DL	0									
$g(x_2^*)$LLR	0									
$g(x_2^*)$LLF	0									
$g(x_2^*)$fy	0.039									
$g(x_2^*)$t	0.075									
$g(x_2^* r_i$	0									
D	-0.86375		u_4^*	2.083842		x^*_4	28.3	$v_{b,0}$	dg/dx	-0.084806
	0			0			0.2	DL		0
	0			-1.2E-06			0.177645	LLR		0
	0			-1.1E-06			1.06883	LLF		0
	0.024174			-0.05609			577.2778	f_y		0.001351
	0.080302			-0.18838			0.940515	t		1.594871
	0			0			2	r_i		0
$\mathbf{D}^T$	-0.86375	0	0	0	0.0241742	0.080302	0			
						σ_x^e	10.18508		u_x^e	7.075897
			β	**2.093083**			0.02			0.20000
							0.035533			0.17764
							0.213787			1.06883
							17.89131			578.28133
							0.05035			0.95000
	α_4	-0.99532					0.028			2
		0								
		0								
		0								
		0.027856								
		0.092533								
		0								
	u_5^*	-2.08329								
		0								
		0								
		0								
		0.058306								
		0.19368								
		0								
	x_5^*	28.29435	WL							
		0.2	DL							
		0.177645	LLR							
		1.068831	LLF							
		577.2382	fy							
		0.940248	t							
		2	ri							

Stellenbosch University http://scholar.sun.ac.za

Live load distribution

	Gamma Dist - applied as Log Normal with lower skewness					
			Iteration 1			
	Roof				**Floor**	
x_1*	0.25	kPa		x_1*	1.5	kPa
μ	0.18	kPa		u	1.083	kPa
COV	0.2			COV	0.2	
σ	0.036	kPa		σ	0.2166	kPa
skew	0.4			skew	0.4	
c	0.132557			c	0.132557	
u	1.944444			u	1.925208	
$\Phi_X(x^*)$	0.964349			$\Phi_X(x^*)$	0.963126	
$\Phi_U^{-1}(\Phi_X(x^*))$	1.803556			$\Phi_U^{-1}(\Phi_X(x^*))$	1.788179	
$\varphi_U[\Phi_U^{-1}(\Phi_X(x^*))]$	0.078446			$\varphi_U[\Phi_U^{-1}(\Phi_X(x^*))]$	0.080642	
$\varphi_X(x^*)$	1.740075			$\varphi_X(x^*)$	0.297911	
$\boldsymbol{\sigma_X^e}$	0.045082			$\boldsymbol{\sigma_X^e}$	0.270693	
$\boldsymbol{\mu_X^e}$	0.17			$\boldsymbol{\mu_X^e}$	1.02	
			Iteration 2			
	Roof				**Floor**	
x_2*	0.168692	kPa		x_2*	1.015952	kPa
μ	0.18	kPa		u	1.083	kPa
COV	0.2			COV	0.2	
σ	0.036	kPa		σ	0.2166	kPa
skew	0.4			skew	0.4	
c	0.132557			c	0.132557	
u	-0.314106			u	-0.30955	
$\Phi_X(x^*)$	0.398881			$\Phi_X(x^*)$	0.400726	
$\Phi_U^{-1}(\Phi_X(x^*))$	-0.256244			$\Phi_U^{-1}(\Phi_X(x^*))$	-0.25147	
$\varphi_U[\Phi_U^{-1}(\Phi_X(x^*))]$	0.386057			$\varphi_U[\Phi_U^{-1}(\Phi_X(x^*))]$	0.386526	
$\varphi_X(x^*)$	11.23863			$\varphi_X(x^*)$	1.869004	
$\boldsymbol{\sigma_X^e}$	0.034351			$\boldsymbol{\sigma_X^e}$	0.206808	
$\boldsymbol{\mu_X^e}$	0.18			$\boldsymbol{\mu_X^e}$	1.07	

Stellenbosch University http://scholar.sun.ac.za

			Iteration 3			
	Roof				**Floor**	
x_3*	0.177494	kPa		x_3*	1.067958	kPa
μ	0.18	kPa		u	1.083	kPa
COV	0.2			COV	0.2	
σ	0.036	kPa		σ	0.2166	kPa
skew	0.4			skew	0.4	
c	0.132557			c	0.132557	
u	-0.069599			u	-0.06945	
$\Phi_X(x^*)$	0.498309			$\Phi_X(x^*)$	0.498371	
$\Phi_U^{-1}(\Phi_X(x^*))$	-0.004238			$\Phi_U^{-1}(\Phi_X(x^*))$	-0.00408	
$\varphi_U[\Phi_U^{-1}(\Phi_X(x^*))]$	0.398939			$\varphi_U[\Phi_U^{-1}(\Phi_X(x^*))]$	0.398939	
$\varphi_X(x^*)$	11.2337			$\varphi_X(x^*)$	1.867061	
$\boldsymbol{\sigma_X^e}$	0.035513			$\boldsymbol{\sigma_X^e}$	0.213672	
$\boldsymbol{\mu_X^e}$	0.18			$\boldsymbol{\mu_X^e}$	1.07	
			Iteration 4			
	Roof				**Floor**	
x_4*	0.177645	kPa		x_4*	1.06883	kPa
μ	0.18	kPa		u	1.083	kPa
COV	0.2			COV	0.2	
σ	0.036	kPa		σ	0.2166	kPa
skew	0.4			skew	0.4	
c	0.132557			c	0.132557	
u	-0.065419			u	-0.06542	
$\Phi_X(x^*)$	0.5			$\Phi_X(x^*)$	0.5	
$\Phi_U^{-1}(\Phi_X(x^*))$	-1.18E-06			$\Phi_U^{-1}(\Phi_X(x^*))$	-1.1E-06	
$\varphi_U[\Phi_U^{-1}(\Phi_X(x^*))]$	0.398942			$\varphi_U[\Phi_U^{-1}(\Phi_X(x^*))]$	0.398942	
$\varphi_X(x^*)$	11.22752			$\varphi_X(x^*)$	1.866071	
$\boldsymbol{\sigma_X^e}$	0.035533			$\boldsymbol{\sigma_X^e}$	0.213787	
$\boldsymbol{\mu_X^e}$	0.18			$\boldsymbol{\mu_X^e}$	1.07	

Stellenbosch University http://scholar.sun.ac.za

Wind load distribution

	Gumbel Dist	
	Iteration 1	
x_1*	28	m/s
μ	14.289	m/s
COV	0.37	
σ	5.28693	m/s
c	0.242589	
x_{mod}	11.91049	
$\Phi_X(x^*)$	0.980024	
$\Phi_U^{-1}(\Phi_X(x^*))$	2.054238	
$\varphi_U[\Phi_U^{-1}(\Phi_X(x^*))]$	0.04837	
$\varphi_X(x^*)$	0.004797	
$\boldsymbol{\sigma_X^e}$	10.08264	
$\boldsymbol{\mu_X^e}$	7.287851	
	Iteration 2	
x_1*	28	m/s
μ	14.289	m/s
COV	0.37	
σ	5.28693	m/s
c	0.242589	
x_{mod}	11.91049	
$\Phi_X(x^*)$	0.980024	
$\Phi_U^{-1}(\Phi_X(x^*))$	2.054238	
$\varphi_U[\Phi_U^{-1}(\Phi_X(x^*))]$	0.04837	
$\varphi_X(x^*)$	0.004797	
$\boldsymbol{\sigma_X^e}$	10.08264	
$\boldsymbol{\mu_X^e}$	7.287851	

	Iteration 3	
x_3*	28.4	m/s
μ	14.289	m/s
COV	0.37	
σ	5.28693	m/s
c	0.242589	
x_{mod}	11.91049	
$\Phi_X(x^*)$	0.981854	
$\Phi_U^{-1}(\Phi_X(x^*))$	2.093644	
$\varphi_U[\Phi_U^{-1}(\Phi_X(x^*))]$	0.044574	
$\varphi_X(x^*)$	0.004362	
$\boldsymbol{\sigma_X^e}$	10.21911	
$\boldsymbol{\mu_X^e}$	7.004818	
	Iteration 4	
x_4*	28.3	m/s
μ	14.289	m/s
COV	0.37	
σ	5.28693	m/s
c	0.242589	
x_{mod}	11.91049	
$\Phi_X(x^*)$	0.981413	
$\Phi_U^{-1}(\Phi_X(x^*))$	2.083842	
$\varphi_U[\Phi_U^{-1}(\Phi_X(x^*))]$	0.045496	
$\varphi_X(x^*)$	0.004467	
$\boldsymbol{\sigma_X^e}$	10.18508	
$\boldsymbol{\mu_X^e}$	7.075897	

Stellenbosch University http://scholar.sun.ac.za

Yield stress distribution

Log - Normal distribution					
	Iteration 1			**Iteration 3**	
x_1^*	550		x_3^*	578.9648	
μ	578.56		μ	578.56	
COV	0.031		COV	0.031	
σ	17.93536		σ	17.93536	
skew	0.09303		skew	0.09303	
c	0.031		c	0.031	
u	-1.59239		u	0.02257	
$\Phi_X(x^*)$	0.052839		$\Phi_X(x^*)$	0.515182	
$\Phi_U^{-1}(\Phi_X(x^*))$	-1.61793		$\Phi_U^{-1}(\Phi_X(x^*))$	0.038064	
$\varphi_U[\Phi_U^{-1}(\Phi_X(x^*))]$	0.107767		$\varphi_U[\Phi_U^{-1}(\Phi_X(x^*))]$	0.398653	
$\varphi_X(x^*)$	0.006322		$\varphi_X(x^*)$	0.022217	
$\boldsymbol{\sigma_X^e}$	17.04591		$\boldsymbol{\sigma_X^e}$	17.9436	
$\boldsymbol{\mu_X^e}$	577.579		$\boldsymbol{\mu_X^e}$	578.2818	
	Iteration 2			**Iteration 4**	
x_2^*	578.2852		x_4^*	579.1115	
μ	578.56		μ	578.56	
COV	0.031		COV	0.031	
σ	17.93536		σ	17.93536	
skew	0.09303		skew	0.09303	
c	0.031		c	0.031	
u	-0.01532		u	0.030751	
$\Phi_X(x^*)$	0.500066		$\Phi_X(x^*)$	0.518441	
$\Phi_U^{-1}(\Phi_X(x^*))$	0.000166		$\Phi_U^{-1}(\Phi_X(x^*))$	0.04624	
$\varphi_U[\Phi_U^{-1}(\Phi_X(x^*))]$	0.398942		$\varphi_U[\Phi_U^{-1}(\Phi_X(x^*))]$	0.398516	
$\varphi_X(x^*)$	0.022259		$\varphi_X(x^*)$	0.022204	
$\boldsymbol{\sigma_X^e}$	17.92254		$\boldsymbol{\sigma_X^e}$	17.94815	
$\boldsymbol{\mu_X^e}$	578.2822		$\boldsymbol{\mu_X^e}$	578.2816	